

2

Observations: Atmosphere and Surface

Coordinating Lead Authors:

Dennis L. Hartmann (USA), Albert M.G. Klein Tank (Netherlands), Matilde Rusticucci (Argentina)

Lead Authors:

Lisa V. Alexander (Australia), Stefan Brönnimann (Switzerland), Yassine Abdul-Rahman Charabi (Oman), Frank J. Dentener (EU/Netherlands), Edward J. Dlugokencky (USA), David R. Easterling (USA), Alexey Kaplan (USA), Brian J. Soden (USA), Peter W. Thorne (USA/Norway/UK), Martin Wild (Switzerland), Panmao Zhai (China)

Contributing Authors:

Robert Adler (USA), Richard Allan (UK), Robert Allan (UK), Donald Blake (USA), Owen Cooper (USA), Aiguo Dai (USA), Robert Davis (USA), Sean Davis (USA), Markus Donat (Australia), Vitali Fioletov (Canada), Erich Fischer (Switzerland), Leopold Haimberger (Austria), Ben Ho (USA), John Kennedy (UK), Elizabeth Kent (UK), Stefan Kinne (Germany), James Kossin (USA), Norman Loeb (USA), Carl Mears (USA), Christopher Merchant (UK), Steve Montzka (USA), Colin Morice (UK), Cathrine Lund Myhre (Norway), Joel Norris (USA), David Parker (UK), Bill Randel (USA), Andreas Richter (Germany), Matthew Rigby (UK), Ben Santer (USA), Dian Seidel (USA), Tom Smith (USA), David Stephenson (UK), Ryan Teuling (Netherlands), Junhong Wang (USA), Xiaolan Wang (Canada), Ray Weiss (USA), Kate Willett (UK), Simon Wood (UK)

Review Editors:

Jim Hurrell (USA), Jose Marengo (Brazil), Fredolin Tangang (Malaysia), Pedro Viterbo (Portugal)

This chapter should be cited as:

Hartmann, D.L., A.M.G. Klein Tank, M. Rusticucci, L.V. Alexander, S. Brönnimann, Y. Charabi, F.J. Dentener, E.J. Dlugokencky, D.R. Easterling, A. Kaplan, B.J. Soden, P.W. Thorne, M. Wild and P.M. Zhai, 2013: Observations: Atmosphere and Surface. In: *Climate Change 2013: The Physical Science Basis. Contribution of Working Group I to the Fifth Assessment Report of the Intergovernmental Panel on Climate Change* [Stocker, T.F., D. Qin, G.-K. Plattner, M. Tignor, S.K. Allen, J. Boschung, A. Nauels, Y. Xia, V. Bex and P.M. Midgley (eds.)]. Cambridge University Press, Cambridge, United Kingdom and New York, NY, USA.

Table of Contents

Executive Summary	161
2.1 Introduction	164
2.2 Changes in Atmospheric Composition	165
2.2.1 Well-Mixed Greenhouse Gases	165
Box 2.1: Uncertainty in Observational Records	165
2.2.2 Near-Term Climate Forcers	170
2.2.3 Aerosols	174
Box 2.2: Quantifying Changes in the Mean: Trend Models and Estimation	179
2.3 Changes in Radiation Budgets	180
2.3.1 Global Mean Radiation Budget.....	181
2.3.2 Changes in Top of the Atmosphere Radiation Budget.....	182
2.3.3 Changes in Surface Radiation Budget	183
Box 2.3: Global Atmospheric Reanalyses	185
2.4 Changes in Temperature	187
2.4.1 Land Surface Air Temperature	187
2.4.2 Sea Surface Temperature and Marine Air Temperature	190
2.4.3 Global Combined Land and Sea Surface Temperature	192
2.4.4 Upper Air Temperature	194
2.5 Changes in Hydrological Cycle	201
2.5.1 Large-Scale Changes in Precipitation	201
2.5.2 Streamflow and Runoff	204
2.5.3 Evapotranspiration Including Pan Evaporation.....	205
2.5.4 Surface Humidity.....	205
2.5.5 Tropospheric Humidity	206
2.5.6 Clouds.....	208
2.6 Changes in Extreme Events	208
2.6.1 Temperature Extremes	209
2.6.2 Extremes of the Hydrological Cycle.....	213
2.6.3 Tropical Storms	216
2.6.4 Extratropical Storms.....	217
Box 2.4: Extremes Indices	221
2.7 Changes in Atmospheric Circulation and Patterns of Variability	223
2.7.1 Sea Level Pressure.....	223
2.7.2 Surface Wind Speed	224
2.7.3 Upper-Air Winds.....	226
2.7.4 Tropospheric Geopotential Height and Tropopause	226
2.7.5 Tropical Circulation	226
2.7.6 Jets, Storm Tracks and Weather Types	229
2.7.7 Stratospheric Circulation.....	230
2.7.8 Changes in Indices of Climate Variability	230
Box 2.5: Patterns and Indices of Climate Variability	232
References	237
Frequently Asked Questions	
FAQ 2.1 How Do We Know the World Has Warmed?	198
FAQ 2.2 Have There Been Any Changes in Climate Extremes?	218
Supplementary Material	
<i>Supplementary Material is available in online versions of the report.</i>	

Executive Summary

The evidence of climate change from observations of the atmosphere and surface has grown significantly during recent years. At the same time new improved ways of characterizing and quantifying uncertainty have highlighted the challenges that remain for developing long-term global and regional climate quality data records. Currently, the observations of the atmosphere and surface indicate the following changes:

Atmospheric Composition

It is certain that atmospheric burdens of the well-mixed greenhouse gases (GHGs) targeted by the Kyoto Protocol increased from 2005 to 2011. The atmospheric abundance of carbon dioxide (CO_2) was 390.5 ppm (390.3 to 390.7)¹ in 2011; this is 40% greater than in 1750. Atmospheric nitrous oxide (N_2O) was 324.2 ppb (324.0 to 324.4) in 2011 and has increased by 20% since 1750. Average annual increases in CO_2 and N_2O from 2005 to 2011 are comparable to those observed from 1996 to 2005. Atmospheric methane (CH_4) was 1803.2 ppb (1801.2 to 1805.2) in 2011; this is 150% greater than before 1750. CH_4 began increasing in 2007 after remaining nearly constant from 1999 to 2006. Hydrofluorocarbons (HFCs), perfluorocarbons (PFCs), and sulphur hexafluoride (SF_6) all continue to increase relatively rapidly, but their contributions to radiative forcing are less than 1% of the total by well-mixed GHGs. {2.2.1.1}

For ozone-depleting substances (Montreal Protocol gases), it is certain that the global mean abundances of major chlorofluorocarbons (CFCs) are decreasing and HCFCs are increasing. Atmospheric burdens of major CFCs and some halons have decreased since 2005. HCFCs, which are transitional substitutes for CFCs, continue to increase, but the spatial distribution of their emissions is changing. {2.2.1.2}

Because of large variability and relatively short data records, confidence² in stratospheric H_2O vapour trends is low. Near-global satellite measurements of stratospheric water vapour show substantial variability but small net changes for 1992–2011. {2.2.2.1}

It is certain that global stratospheric ozone has declined from pre-1980 values. Most of the decline occurred prior to the mid 1990s; since then ozone has remained nearly constant at about 3.5% below the 1964–1980 level. {2.2.2.2}

Confidence is medium in large-scale increases of tropospheric ozone across the Northern Hemisphere (NH) since the 1970s.

Confidence is low in ozone changes across the Southern Hemisphere (SH) owing to limited measurements. It is *likely*³ that surface ozone trends in eastern North America and Western Europe since 2000 have levelled off or decreased and that surface ozone strongly increased in East Asia since the 1990s. Satellite and surface observations of ozone precursor gases NO_x , CO , and non-methane volatile organic carbons indicate strong regional differences in trends. Most notably NO_2 has *likely* decreased by 30 to 50% in Europe and North America and increased by more than a factor of 2 in Asia since the mid-1990s. {2.2.2.3, 2.2.2.4}

It is very likely that aerosol column amounts have declined over Europe and the eastern USA since the mid 1990s and increased over eastern and southern Asia since 2000. These shifting aerosol regional patterns have been observed by remote sensing of aerosol optical depth (AOD), a measure of total atmospheric aerosol load. Declining aerosol loads over Europe and North America are consistent with ground-based *in situ* monitoring of particulate mass. Confidence in satellite based global average AOD trends is *low*. {2.2.3}

Radiation Budgets

Satellite records of top of the atmosphere radiation fluxes have been substantially extended since AR4, and it is unlikely that significant trends exist in global and tropical radiation budgets since 2000. Interannual variability in the Earth's energy imbalance related to El Niño-Southern Oscillation is consistent with ocean heat content records within observational uncertainty. {2.3.2}

Surface solar radiation likely underwent widespread decadal changes after 1950, with decreases ('dimming') until the 1980s and subsequent increases ('brightening') observed at many land-based sites. There is *medium confidence* for increasing downward thermal and net radiation at land-based observation sites since the early 1990s. {2.3.3}

Temperature

It is certain that Global Mean Surface Temperature has increased since the late 19th century. Each of the past three decades has been successively warmer at the Earth's surface than all the previous decades in the instrumental record, and the first decade of the 21st century has been the warmest. The globally averaged combined land and ocean surface temperature data as calculated by a linear trend, show a warming of 0.85 [0.65 to 1.06] °C, over the period 1880–2012, when multiple independently produced datasets exist, and

¹ Values in parentheses are 90% confidence intervals. Elsewhere in this chapter usually the half-widths of the 90% confidence intervals are provided for the estimated change from the trend method.

² In this Report, the following summary terms are used to describe the available evidence: limited, medium, or robust; and for the degree of agreement: low, medium, or high. A level of confidence is expressed using five qualifiers: very low, low, medium, high, and very high, and typeset in italics, e.g., *medium confidence*. For a given evidence and agreement statement, different confidence levels can be assigned, but increasing levels of evidence and degrees of agreement are correlated with increasing confidence (see Section 1.4 and Box TS.1 for more details).

³ In this Report, the following terms have been used to indicate the assessed likelihood of an outcome or a result: Virtually certain 99–100% probability, Very likely 90–100%, Likely 66–100%, About as likely as not 33–66%, Unlikely 0–33%, Very unlikely 0–10%, Exceptionally unlikely 0–1%. Additional terms (Extremely likely: 95–100%, More likely than not >50–100%, and Extremely unlikely 0–5%) may also be used when appropriate. Assessed likelihood is typeset in italics, e.g., *very likely* (see Section 1.4 and Box TS.1 for more details).

about 0.72°C [0.49°C to 0.89°C] over the period 1951–2012. The total increase between the average of the 1850–1900 period and the 2003–2012 period is 0.78 [0.72 to 0.85] °C and the total increase between the average of the 1850–1900 period and the reference period for projections, 1986–2005, is 0.61 [0.55 to 0.67] °C, based on the single longest dataset available. For the longest period when calculation of regional trends is sufficiently complete (1901–2012), almost the entire globe has experienced surface warming. In addition to robust multi-decadal warming, global mean surface temperature exhibits substantial decadal and interannual variability. Owing to natural variability, trends based on short records are very sensitive to the beginning and end dates and do not in general reflect long-term climate trends. As one example, the rate of warming over the past 15 years (1998–2012; 0.05 [−0.05 to +0.15] °C per decade), which begins with a strong El Niño, is smaller than the rate calculated since 1951 (1951–2012; 0.12 [0.08 to 0.14] °C per decade). Trends for 15-year periods starting in 1995, 1996, and 1997 are 0.13 [0.02 to 0.24], 0.14 [0.03 to 0.24] and 0.07 [−0.02 to 0.18], respectively. Several independently analyzed data records of global and regional land-surface air temperature (LSAT) obtained from station observations are in broad agreement that LSAT has increased. Sea surface temperatures (SSTs) have also increased. Intercomparisons of new SST data records obtained by different measurement methods, including satellite data, have resulted in better understanding of uncertainties and biases in the records. {2.4.1, 2.4.2, 2.4.3; Box 9.2}

It is unlikely that any uncorrected urban heat-island effects and land use change effects have raised the estimated centennial globally averaged LSAT trends by more than 10% of the reported trend. This is an average value; in some regions with rapid development, urban heat island and land use change impacts on regional trends may be substantially larger. {2.4.1.3}

Confidence is medium in reported decreases in observed global diurnal temperature range (DTR), noted as a key uncertainty in the AR4. Several recent analyses of the raw data on which many previous analyses were based point to the potential for biases that differently affect maximum and minimum average temperatures. However, apparent changes in DTR are much smaller than reported changes in average temperatures and therefore it is virtually certain that maximum and minimum temperatures have increased since 1950. {2.4.1.2}

Based on multiple independent analyses of measurements from radiosondes and satellite sensors it is virtually certain that globally the troposphere has warmed and the stratosphere has cooled since the mid-20th century. Despite unanimous agreement on the sign of the trends, substantial disagreement exists among available estimates as to the rate of temperature changes, particularly outside the NH extratropical troposphere, which has been well sampled by radiosondes. Hence there is only medium confidence in the rate of change and its vertical structure in the NH extratropical troposphere and low confidence elsewhere. {2.4.4}

Hydrological Cycle

Confidence in precipitation change averaged over global land areas since 1901 is low for years prior to 1951 and medium afterwards. Averaged over the mid-latitude land areas of the

Northern Hemisphere, precipitation has likely increased since 1901 (medium confidence before and high confidence after 1951). For other latitudinal zones area-averaged long-term positive or negative trends have low confidence due to data quality, data completeness or disagreement amongst available estimates. {2.5.1.1, 2.5.1.2}

It is very likely that global near surface and tropospheric air specific humidity have increased since the 1970s. However, during recent years the near surface moistening over land has abated (medium confidence). As a result, fairly widespread decreases in relative humidity near the surface are observed over the land in recent years. {2.4.4, 2.5.4, 2.5.5}

While trends of cloud cover are consistent between independent data sets in certain regions, substantial ambiguity and therefore low confidence remains in the observations of global-scale cloud variability and trends. {2.5.6}

Extreme Events

It is very likely that the numbers of cold days and nights have decreased and the numbers of warm days and nights have increased globally since about 1950. There is only medium confidence that the length and frequency of warm spells, including heat waves, has increased since the middle of the 20th century mostly owing to lack of data or of studies in Africa and South America. However, it is likely that heatwave frequency has increased during this period in large parts of Europe, Asia and Australia. {2.6.1}

It is likely that since about 1950 the number of heavy precipitation events over land has increased in more regions than it has decreased. Confidence is highest for North America and Europe where there have been likely increases in either the frequency or intensity of heavy precipitation with some seasonal and/or regional variation. It is very likely that there have been trends towards heavier precipitation events in central North America. {2.6.2.1}

Confidence is low for a global-scale observed trend in drought or dryness (lack of rainfall) since the middle of the 20th century, owing to lack of direct observations, methodological uncertainties and geographical inconsistencies in the trends. Based on updated studies, AR4 conclusions regarding global increasing trends in drought since the 1970s were probably overstated. However, this masks important regional changes: the frequency and intensity of drought have likely increased in the Mediterranean and West Africa and likely decreased in central North America and north-west Australia since 1950. {2.6.2.2}

Confidence remains low for long-term (centennial) changes in tropical cyclone activity, after accounting for past changes in observing capabilities. However, it is virtually certain that the frequency and intensity of the strongest tropical cyclones in the North Atlantic has increased since the 1970s. {2.6.3}

Confidence in large-scale trends in storminess or storminess proxies over the last century is low owing to inconsistencies

between studies or lack of long-term data in some parts of the world (particularly in the SH). {2.6.4}

Because of insufficient studies and data quality issues *confidence* is also *low* for trends in small-scale severe weather events such as hail or thunderstorms. {2.6.2.4}

Atmospheric Circulation and Indices of Variability

It is *likely* that circulation features have moved poleward since the 1970s, involving a widening of the tropical belt, a poleward shift of storm tracks and jet streams, and a contraction of the northern polar vortex. Evidence is more robust for the NH. It is *likely* that the Southern Annular Mode has become more positive since the 1950s. {2.7.5, 2.7.6, 2.7.8; Box 2.5}

Large variability on interannual to decadal time scales hampers robust conclusions on long-term changes in atmospheric circulation in many instances. *Confidence is high* that the increase in the northern mid-latitude westerly winds and the North Atlantic Oscillation (NAO) index from the 1950s to the 1990s and the weakening of the Pacific Walker circulation from the late 19th century to the 1990s have been largely offset by recent changes. {2.7.5, 2.7.8, Box 2.5}

Confidence in the existence of long-term changes in remaining aspects of the global circulation is *low* owing to observational limitations or limited understanding. These include surface winds over land, the East Asian summer monsoon circulation, the tropical cold-point tropopause temperature and the strength of the Brewer Dobson circulation. {2.7.2, 2.7.4, 2.7.5, 2.7.7}

2.1 Introduction

This chapter assesses the scientific literature on atmospheric and surface observations since AR4 (IPCC, 2007). The most likely changes in physical climate variables or climate forcing agents are identified based on current knowledge, following the IPCC AR5 uncertainty guidance (Mastrandrea et al., 2011).

As described in AR4 (Trenberth et al., 2007), the climate comprises a variety of space- and timescales: from the diurnal cycle, to interannual variability such as the El Niño–Southern Oscillation (ENSO), to multi-decadal variations. ‘Climate change’ refers to a change in the state of the climate that can be identified by changes in the mean and/or the variability of its properties and that persists for an extended period of time (Annex III: Glossary). In this chapter, climate change is examined for the period with instrumental observations, since about 1850. Change prior to this date is assessed in Chapter 5. The word ‘trend’ is used to designate a long-term movement in a time series that may be regarded, together with the oscillation and random component, as composing the observed values (Annex III: Glossary). Where numerical values are given, they are equivalent linear changes (Box 2.2), though more complex nonlinear changes in the variable will often be clear from the description and plots of the time series.

In recent decades, advances in the global climate observing system have contributed to improved monitoring capabilities. In particular, satellites provide additional observations of climate change, which have been assessed in this and subsequent chapters together with more traditional ground-based and radiosonde observations. Since AR4, substantial developments have occurred including the production of revised data sets, more digital data records, and new data set efforts. New dynamical reanalysis data sets of the global atmosphere have been published (Box 2.3). These various innovations have improved understanding of data issues and uncertainties (Box 2.1).

Developing homogeneous long-term records from these different sources remains a challenge. The longest observational series are land surface air temperatures (LSATs) and sea surface temperatures (SSTs). Like all physical climate system measurements, they suffer from non-climatic artefacts that must be taken into account (Box 2.1). The global combined LSAT and SST remains an important climate change measure for several reasons. Climate sensitivity is typically assessed in the context of global mean surface temperature (GMST) responses to a doubling of CO₂ (Chapter 8) and GMST is thus a key metric in the climate change policy framework. Also, because it extends back in time farther than any other global instrumental series, GMST is key to understanding both the causes of change and the patterns, role and magnitude of natural variability (Chapter 10). Starting at various points in the 20th century, additional observations, including balloon-borne measurements and satellite measurements, and reanalysis products allow analyses of indicators such as atmospheric composition, radiation budgets, hydrological cycle changes, extreme event characterizations and circulation indices. A full understanding of the climate system characteristics and changes requires analyses of all such variables as well as ocean (Chapter 3) and cryosphere (Chapter 4) indicators. Through such a holistic analysis, a clearer and more robust assessment of the changing climate system emerges (FAQ 2.1).

This chapter starts with an assessment of the observations of the abundances of greenhouse gases (GHGs) and of aerosols, the main drivers of climate change (Section 2.2). Global trends in GHGs are indicative of the imbalance between sources and sinks in GHG budgets, and play an important role in emissions verification on a global scale. The radiative forcing (RF) effects of GHGs and aerosols are assessed in Chapter 8. The observed changes in radiation budgets are discussed in Section 2.3. Aerosol–cloud interactions are assessed in Chapter 7. Section 2.4 provides an assessment of observed changes in surface and atmospheric temperature. Observed change in the hydrological cycle, including precipitation and clouds, is assessed in Section 2.5. Changes in variability and extremes (such as cold spells, heat waves, droughts and tropical cyclones) are assessed in Section 2.6. Section 2.7 assesses observed changes in the circulation of the atmosphere and its modes of variability, which help determine seasonal and longer-term anomalies at regional scales (Chapter 14).

Trends have been assessed where possible for multi-decadal periods starting in 1880, 1901 (referred to as long-term trends) and in 1951, 1979 (referred to as short-term trends). The time elapsed since AR4 extends the period for trend calculation from 2005 to 2012 for many variables. The GMST trend since 1998 has also been considered (see also Box 9.2) as well as the trends for sequential 30-year segments of the time series. For many variables derived from satellite data, information is available for 1979–2012 only. In general, trend estimates are more reliable for longer time intervals, and trends computed on short intervals have a large uncertainty. Trends for short intervals are very sensitive to the start and end years. An exception to this is trends in GHGs, whose accurate measurement and long lifetimes make them well-mixed and less susceptible to year-to-year variability, so that trends computed on relatively short intervals are very meaningful for these variables. Where possible, the time interval 1961–1990 has been chosen as the climatological reference period (or normal period) for averaging. This choice enables direct comparisons with AR4, but is different from the present-day climate period (1986–2005) used as a reference in the modelling chapters of AR5 and Annex I: Atlas of Global and Regional Climate Projections.

It is important to note that the question of whether the observed changes are outside the possible range of natural internal climate variability and consistent with the climate effects from changes in atmospheric composition is not addressed in this chapter, but rather in Chapter 10. No attempt has been undertaken to further describe and interpret the observed changes in terms of multi-decadal oscillatory (or low-frequency) variations, (long-term) persistence and/or secular trends (e.g., as in Cohn and Lins, 2005; Koutsoyiannis and Montanari, 2007; Zorita et al., 2008; Lennartz and Bunde, 2009; Mills, 2010; Mann, 2011; Wu et al., 2011; Zhou and Tung, 2012; Tung and Zhou, 2013). In this chapter, the robustness of the observed changes is assessed in relation to various sources of observational uncertainty (Box 2.1). In addition, the reported trend significance and statistical confidence intervals provide an indication of how large the observed trend is compared to the range of observed variability in a given aspect of the climate system (see Box 2.2 for a description of the statistical trend model applied). Unless otherwise stated, 90% confidence intervals are given. The chapter also examines the physical consistency across

different observations, which helps to provide additional confidence in the reported changes. Additional information about data sources and methods is described in the Supplementary Material to Chapter 2.

2.2 Changes in Atmospheric Composition

2.2.1 Well-Mixed Greenhouse Gases

AR4 (Forster et al., 2007; IPCC, 2007) concluded that increasing atmospheric burdens of well-mixed GHGs resulted in a 9% increase in their RF from 1998 to 2005. Since 2005, the atmospheric abundances of many well-mixed GHG increased further, but the burdens of some ozone-depleting substances (ODS) whose production and use were controlled by the Montreal Protocol on Substances that Deplete the Ozone Layer (1987; hereinafter, ‘Montreal Protocol’) decreased.

Based on updated *in situ* observations, this assessment concludes that these trends resulted in a 7.5% increase in RF from GHGs from 2005 to 2011, with carbon dioxide (CO_2) contributing 80%. Of note

is an increase in the average growth rate of atmospheric methane (CH_4) from $\sim 0.5 \text{ ppb yr}^{-1}$ during 1999–2006 to $\sim 6 \text{ ppb yr}^{-1}$ from 2007 through 2011. Current observation networks are sufficient to quantify global annual mean burdens used to calculate RF and to constrain global emission rates (with knowledge of loss rates), but they are not sufficient for accurately estimating regional scale emissions and how they are changing with time.

The globally, annually averaged well-mixed GHG mole fractions reported here are used in Chapter 8 to calculate RF. A direct, inseparable connection exists between observed changes in atmospheric composition and well-mixed GHG emissions and losses (discussed in Chapter 6 for CO_2 , CH_4 , and N_2O). A global GHG budget consists of the total atmospheric burden, total global rate of production or emission (i.e., sources), and the total global rate of destruction or removal (i.e., sinks). Precise, accurate systematic observations from independent globally distributed measurement networks are used to estimate global annual mean well-mixed GHG mole fractions at the Earth’s surface, and these allow estimates of global burdens. Emissions are predominantly from surface sources, which are described in Chapter 6 for CO_2 , CH_4 , and N_2O . Direct

Box 2.1 | Uncertainty in Observational Records

The vast majority of historical (and modern) weather observations were not made explicitly for climate monitoring purposes. Measurements have changed in nature as demands on the data, observing practices and technologies have evolved. These changes almost always alter the characteristics of observational records, changing their mean, their variability or both, such that it is necessary to process the raw measurements before they can be considered useful for assessing the true climate evolution. This is true of all observing techniques that measure physical atmospheric quantities. The uncertainty in observational records encompasses instrumental/recording errors, effects of representation (e.g., exposure, observing frequency or timing), as well as effects due to physical changes in the instrumentation (such as station relocations or new satellites). All further processing steps (transmission, storage, gridding, interpolating, averaging) also have their own particular uncertainties. Because there is no unique, unambiguous, way to identify and account for non-climatic artefacts in the vast majority of records, there must be a degree of uncertainty as to how the climate system has changed. The only exceptions are certain atmospheric composition and flux measurements whose measurements and uncertainties are rigorously tied through an unbroken chain to internationally recognized absolute measurement standards (e.g., the CO_2 record at Mauna Loa; Keeling et al., 1976a).

Uncertainty in data set production can result either from the choice of parameters within a particular analytical framework—parametric uncertainty, or from the choice of overall analytical framework—structural uncertainty. Structural uncertainty is best estimated by having multiple independent groups assess the same data using distinct approaches. More analyses assessed now than in AR4 include published estimates of parametric or structural uncertainty. It is important to note that the literature includes a very broad range of approaches. Great care has been taken in comparing the published uncertainty ranges as they almost always do not constitute a like-for-like comparison. In general, studies that account for multiple potential error sources in a rigorous manner yield larger uncertainty ranges. This yields an apparent paradox in interpretation as one might think that smaller uncertainty ranges should indicate a better product. However, in many cases this would be an incorrect inference as the smaller uncertainty range may instead reflect that the published estimate considered only a subset of the plausible sources of uncertainty. Within the timeseries figures, where this issue would be most acute, such parametric uncertainty estimates are therefore not generally included. Consistent with AR4 HadCRUT4 uncertainties in GMST are included in Figure 2.19, which in addition includes structural uncertainties in GMST.

To conclude, the vast majority of the raw observations used to monitor the state of the climate contain residual non-climatic influences. Removal of these influences cannot be done definitively and neither can the uncertainties be unambiguously assessed. Therefore, care is required in interpreting both data products and their stated uncertainty estimates. Confidence can be built from: redundancy in efforts to create products; data set heritage; and cross-comparisons of variables that would be expected to co-vary for physical reasons, such as LSATs and SSTs around coastlines. Finally, trends are often quoted as a way to synthesize the data into a single number. Uncertainties that arise from such a process and the choice of technique used within this chapter are described in more detail in Box 2.2.

use of observations of well-mixed GHG to model their regional budgets can also play an important role in verifying inventory estimates of emissions (Nisbet and Weiss, 2010).

Systematic measurements of well-mixed GHG in ambient air began at various times during the last six decades, with earlier atmospheric histories being reconstructed from measurements of air stored in air archives and trapped in polar ice cores or in firn. In contrast to the physical meteorological parameters discussed elsewhere in this chapter, measurements of well-mixed GHG are reported relative to standards developed from fundamental SI base units (SI = International System of Units) as dry-air mole fractions, a unit that is conserved with changes in temperature and pressure (Box 2.1). This eliminates dilution by H_2O vapour, which can reach 4% of total atmospheric composition. Here, the following abbreviations are used: ppm = $\mu\text{mol mol}^{-1}$; ppb = nmol mol^{-1} ; and ppt = pmol mol^{-1} . Unless noted otherwise, averages of National Oceanic and Atmospheric Administration (NOAA) and Advanced Global Atmospheric Gases Experiment (AGAGE) annually averaged surface global mean mole fractions is described in Section 2.2.1 (see Supplementary Material 2.SM.2 for further species not listed here).

Table 2.1 summarizes globally, annually averaged well-mixed GHG mole fractions from four independent measurement programs. Sampling strategies and techniques for estimating global means and their uncertainties vary among programs. Differences among measurement programs are relatively small and will not add significantly to uncertainty in RF. Time series of the well-mixed GHG are plotted in Figures 2.1 (CO_2), 2.2 (CH_4), 2.3 (N_2O), and 2.4 (halogen-containing compounds).

2.2.1.1 Kyoto Protocol Gases (Carbon Dioxide, Methane, Nitrous Oxide, Hydrofluorocarbons, Perfluorocarbons and Sulphur Hexafluoride)

2.2.1.1.1 Carbon Dioxide

Precise, accurate systematic measurements of atmospheric CO_2 at Mauna Loa, Hawaii and South Pole were started by C. D. Keeling from Scripps Institution of Oceanography in the late 1950s (Keeling et al., 1976a; Keeling et al., 1976b). The 1750 globally averaged abundance of atmospheric CO_2 based on measurements of air extracted from ice cores and from firn is 278 ± 2 ppm (Etheridge et al., 1996). Globally averaged CO_2 mole fractions since the start of the instrumental record

Table 2.1 | Global annual mean surface dry-air mole fractions and their change since 2005 for well-mixed greenhouse gases (GHGs) from four measurement networks. Units are ppt except where noted. Uncertainties are 90% confidence intervals^a. REs (radiative efficiency) and lifetimes (except CH_4 and N_2O , which are from Prather et al., 2012) are from Chapter 8.

			2011 Global Annual Mean			Global Increase from 2005 to 2011		
Species	Lifetime (yr)	RE ($\text{W m}^{-2} \text{ppb}^{-1}$)	UCI	SIO ^b /AGAGE	NOAA	UCI	SIO ^b /AGAGE	NOAA
CO_2 (ppm)		1.37×10^{-5}		390.48 ± 0.28	390.44 ± 0.16		11.67 ± 0.37	11.66 ± 0.13
CH_4 (ppb)	9.1	3.63×10^{-4}	1798.1 ± 0.6	1803.1 ± 4.8	1803.2 ± 1.2	26.6 ± 0.9	28.9 ± 6.8	28.6 ± 0.9
N_2O (ppb)	131	3.03×10^{-3}		324.0 ± 0.1	324.3 ± 0.1		4.7 ± 0.2	5.24 ± 0.14
SF_6	3200	0.575		7.26 ± 0.02	7.31 ± 0.02		1.65 ± 0.03	1.64 ± 0.01
CF_4	50,000	0.1		79.0 ± 0.1			4.0 ± 0.2	
C_2F_6	10,000	0.26		4.16 ± 0.02			0.50 ± 0.03	
HFC-125	28.2	0.219		9.58 ± 0.04			5.89 ± 0.07	
HFC-134a	13.4	0.159	63.4 ± 0.9	62.4 ± 0.3	63.0 ± 0.6	27.7 ± 1.4	28.2 ± 0.4	28.2 ± 0.1
HFC-143a	47.1	0.159		12.04 ± 0.07			6.39 ± 0.10	
HFC-152a	1.5	0.094		6.4 ± 0.1			3.0 ± 0.2	
HFC-23	222	0.176		24.0 ± 0.3			5.2 ± 0.6	
CFC-11	45	0.263	237.9 ± 0.8	236.9 ± 0.1	238.5 ± 0.2	-13.2 ± 0.8	-12.7 ± 0.2	-13.0 ± 0.1
CFC-12	100	0.32	525.3 ± 0.8	529.5 ± 0.2	527.4 ± 0.4	-12.8 ± 0.8	-13.4 ± 0.3	-14.1 ± 0.1
CFC-113	85	0.3	74.9 ± 0.6	74.29 ± 0.06	74.40 ± 0.04	-4.6 ± 0.8	-4.25 ± 0.08	-4.35 ± 0.02
HCFC-22	11.9	0.2	209.0 ± 1.2	213.4 ± 0.8	213.2 ± 1.2	41.5 ± 1.4	44.6 ± 1.1	44.3 ± 0.2
HCFC-141b	9.2	0.152	20.8 ± 0.5	21.38 ± 0.09	21.4 ± 0.2	3.7 ± 0.5	3.70 ± 0.1	3.76 ± 0.03
HCFC-142b	17.2	0.186	21.0 ± 0.5	21.35 ± 0.06	21.0 ± 0.1	4.9 ± 0.5	5.72 ± 0.09	5.73 ± 0.04
CCl_4	26	0.175	87.8 ± 0.6	85.0 ± 0.1	86.5 ± 0.3	-6.4 ± 0.5	-6.9 ± 0.2	-7.8 ± 0.1
CH_3CCl_3	5	0.069	6.8 ± 0.6	6.3 ± 0.1	6.35 ± 0.07	-14.8 ± 0.5	-11.9 ± 0.2	-12.1 ± 0.1

Notes:

AGAGE = Advanced Global Atmospheric Gases Experiment; NOAA = National Oceanic and Atmospheric Administration, Earth System Research Laboratory, Global Monitoring Division; SIO = Scripps Institution of Oceanography, University of California, San Diego; UCI = University of California, Irvine, Department of Chemistry. HFC-125 = CHF_2CF_3 ; HFC-134a = CH_2FCF_3 ; HFC-143a = CH_3CF_3 ; HFC-152a = CH_3CHF_2 ; HFC-23 = CHF_3 ; CFC-11 = CCl_3F ; CFC-12 = CCl_2F_2 ; CFC-113 = $\text{CClF}_2\text{CCl}_2\text{F}$; HCFC-22 = CHClF_2 ; HCFC-141b = $\text{CH}_3\text{CCl}_2\text{F}$; HCFC-142b = CH_3CClF_2 .

^a Each program uses different methods to estimate uncertainties.

^b SIO reports only CO_2 ; all other values reported in these columns are from AGAGE. SIO CO_2 program and AGAGE are not affiliated with each other.

Budget lifetimes are shown; for CH_4 and N_2O , perturbation lifetimes (12.4 years for CH_4 and 121 years for N_2O) are used to estimate global warming potentials (Chapter 8).

Year 1750 values determined from air extracted from ice cores are below detection limits for all species except CO_2 (278 ± 2 ppm), CH_4 (722 ± 25 ppb), N_2O (270 ± 7 ppb) and CF_4 (34.7 ± 0.2 ppt). Centennial variations up to 10 ppm CO_2 , 40 ppb CH_4 , and 10 ppb occur throughout the late-Holocene (Chapter 6).

are plotted in Figure 2.1. The main features in the contemporary CO₂ record are the long-term increase and the seasonal cycle resulting from photosynthesis and respiration by the terrestrial biosphere, mostly in the Northern Hemisphere (NH). The main contributors to increasing atmospheric CO₂ abundance are fossil fuel combustion and land use change (Section 6.3). Multiple lines of observational evidence indicate that during the past few decades, most of the increasing atmospheric burden of CO₂ is from fossil fuel combustion (Tans, 2009). Since the last year for which the AR4 reported (2005), CO₂ has increased by 11.7 ppm to 390.5 ppm in 2011 (Table 2.1). From 1980 to 2011, the average annual increase in globally averaged CO₂ (from 1 January in one year to 1 January in the next year) was 1.7 ppm yr⁻¹ (1 standard deviation = 0.5 ppm yr⁻¹; 1 ppm globally corresponds to 2.1 PgC increase in the atmospheric burden). Since 2001, CO₂ has increased at 2.0 ppm yr⁻¹ (1 standard deviation = 0.3 ppm yr⁻¹). The CO₂ growth rate varies from year to year; since 1980 the range in annual increase is 0.7 ± 0.1 ppm in 1992 to 2.9 ± 0.1 ppm in 1998. Most of this interannual variability in growth rate is driven by small changes in the balance between photosynthesis and respiration on land, each having global fluxes of ~120 PgC yr⁻¹ (Chapter 6).

2.2.1.1.2 Methane

Globally averaged CH₄ in 1750 was 722 ± 25 ppb (after correction to the NOAA-2004 CH₄ standard scale) (Etheridge et al., 1998; Dlugokencky et al., 2005), although human influences on the global CH₄ budget may have begun thousands of years earlier than this time that is normally considered ‘pre-industrial’ (Ruddiman, 2003; Ferretti et al., 2005; Ruddiman, 2007). In 2011, the global annual mean was 1803 ± 2 ppb. Direct atmospheric measurements of CH₄ of sufficient spatial coverage to calculate global annual means began in 1978 and are plotted through 2011 in Figure 2.2a. This time period is characterized by a decreasing growth rate (Figure 2.2b) from the early 1980s until 1998, stabilization from 1999 to 2006, and an increasing atmospheric burden from 2007 to 2011 (Rigby et al., 2008; Dlugokencky et al.,

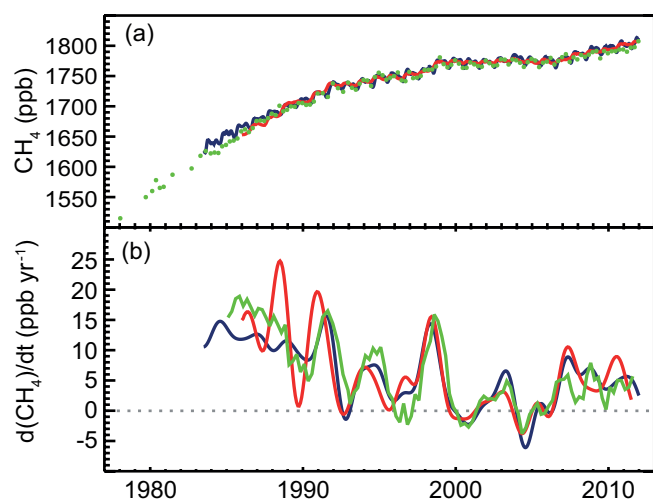


Figure 2.2 | (a) Globally averaged CH₄ dry-air mole fractions from UCI (green; four values per year, except prior to 1984, when they are of lower and varying frequency), AGAGE (red; monthly), and NOAA/ESRL/GMD (blue; quasi-weekly). (b) Instantaneous growth rate for globally averaged atmospheric CH₄ using the same colour code as in (a). Growth rates were calculated as in Figure 2.1.

2009). Assuming no long-term trend in hydroxyl radical (OH) concentration, the observed decrease in CH₄ growth rate from the early 1980s through 2006 indicates an approach to steady state where total global emissions have been approximately constant at ~550 Tg (CH₄) yr⁻¹. Superimposed on the long-term pattern is significant interannual variability; studies of this variability are used to improve understanding of the global CH₄ budget (Chapter 6). The most likely drivers of increased atmospheric CH₄ were anomalously high temperatures in the Arctic in 2007 and greater than average precipitation in the tropics during 2007 and 2008 (Dlugokencky et al., 2009; Bousquet, 2011). Observations of the difference in CH₄ between zonal averages for northern and southern polar regions (53° to 90°) (Dlugokencky et al., 2009, 2011) suggest that, so far, it is unlikely that there has been a permanent measureable increase in Arctic CH₄ emissions from wetlands and shallow sub-sea CH₄ clathrates.

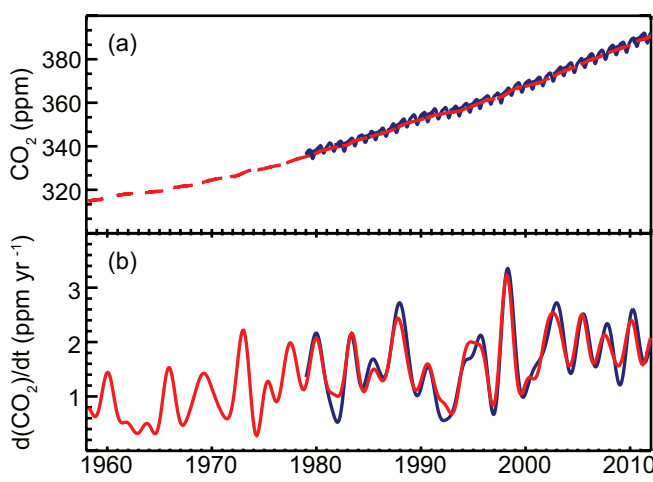


Figure 2.1 | (a) Globally averaged CO₂ dry-air mole fractions from Scripps Institution of Oceanography (SIO) at monthly time resolution based on measurements from Mauna Loa, Hawaii and South Pole (red) and NOAA/ESRL/GMD at quasi-weekly time resolution (blue). SIO values are deseasonalized. (b) Instantaneous growth rates for globally averaged atmospheric CO₂ using the same colour code as in (a). Growth rates are calculated as the time derivative of the deseasonalized global averages (Dlugokencky et al., 1994).

Reaction with the hydroxyl radical (OH) is the main loss process for CH₄ (and for hydrofluorocarbons (HFCs) and hydrochlorofluorocarbons (HCFCs)), and it is the largest term in the global CH₄ budget. Therefore, trends and interannual variability in OH concentration significantly impact our understanding of changes in CH₄ emissions. Methyl chloroform (CH₃CCl₃; Section 2.2.1.2) has been used extensively to estimate globally averaged OH concentrations (e.g., Prinn et al., 2005). AR4 reported no trend in OH from 1979 to 2004, and there is no evidence from this assessment to change that conclusion for 2005 to 2011. Montzka et al. (2011a) exploited the exponential decrease and small emissions in CH₃CCl₃ to show that interannual variations in OH concentration from 1998 to 2007 are 2.3 ± 1.5%, which is consistent with estimates based on CH₄, tetrachloroethene (C₂Cl₄), dichloromethane (CH₂Cl₂), chloromethane (CH₃Cl) and bromomethane (CH₃Br).

2.2.1.1.3 Nitrous Oxide

Globally averaged N₂O in 2011 was 324.2 ppb, an increase of 5.0 ppb over the value reported for 2005 in AR4 (Table 2.1). This is an increase

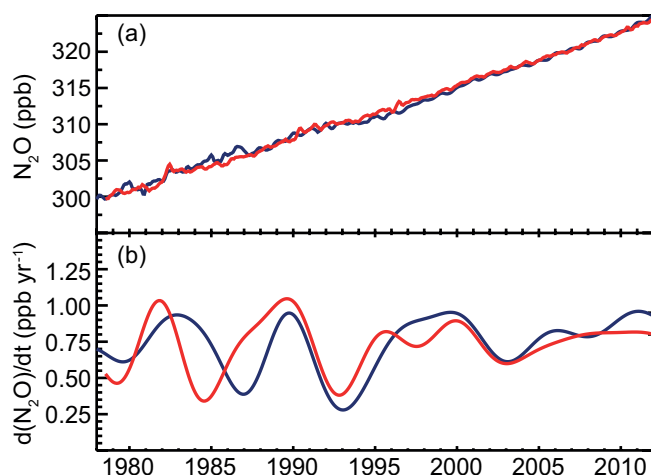


Figure 2.3 | (a) Globally averaged N_2O dry-air mole fractions from AGAGE (red) and NOAA/ESRL/GMD (blue) at monthly resolution. (b) Instantaneous growth rates for globally averaged atmospheric N_2O . Growth rates were calculated as in Figure 2.1.

of 20% over the estimate for 1750 from ice cores, 270 ± 7 ppb (Prather et al., 2012). Measurements of N_2O and its isotopic composition in firn air suggest the increase, at least since the early 1950s, is dominated by emissions from soils treated with synthetic and organic (manure) nitrogen fertilizer (Rockmann and Levin, 2005; Ishijima et al., 2007; Davidson, 2009; Syakila and Kroeze, 2011). Since systematic measurements began in the late 1970s, N_2O has increased at an average rate of ~ 0.75 ppb yr^{-1} (Figure 2.3). Because the atmospheric burden of CFC-12 is decreasing, N_2O has replaced CFC-12 as the third most important well-mixed GHG contributing to RF (Elkins and Dutton, 2011).

Persistent latitudinal gradients in annually averaged N_2O are observed at background surface sites, with maxima in the northern subtropics, values about 1.7 ppb lower in the Antarctic, and values about 0.4 ppb lower in the Arctic (Huang et al., 2008). These persistent gradients contain information about anthropogenic emissions from fertilizer use at northern tropical to mid-latitudes and natural emissions from soils and ocean upwelling regions of the tropics. N_2O time series also contain seasonal variations with peak-to-peak amplitudes of about 1 ppb in high latitudes of the NH and about 0.4 ppb at high southern and tropical latitudes. In the NH, exchange of air between the stratosphere (where N_2O is destroyed by photochemical processes) and troposphere is the dominant contributor to observed seasonal cycles, not seasonality in emissions (Jiang et al., 2007). Nevison et al. (2011) found correlations between the magnitude of detrended N_2O seasonal minima and lower stratospheric temperature, providing evidence for a stratospheric influence on the timing and amplitude of the seasonal cycle at surface monitoring sites. In the Southern Hemisphere (SH), observed seasonal cycles are also affected by stratospheric influx, and by ventilation and thermal out-gassing of N_2O from the oceans.

2.2.1.1.4 Hydrofluorocarbons, Perfluorocarbons, Sulphur Hexafluoride and Nitrogen Trifluoride

The budgets of HFCs, PFCs and SF_6 were recently reviewed in Chapter 1 of the Scientific Assessment of Ozone Depletion: 2010 (Montzka et al., 2011b), so only a brief description is given here. The current atmos-

pheric abundances of these species are summarized in Table 2.1 and plotted in Figure 2.4.

Atmospheric HFC abundances are low and their contribution to RF is small relative to that of the CFCs and HCFCs they replace (less than 1% of the total by well-mixed GHGs; Chapter 8). As they replace CFCs and HCFCs phased out by the Montreal Protocol, however, their contribution to future climate forcing is projected to grow considerably in the absence of controls on global production (Velders et al., 2009).

HFC-134a is a replacement for CFC-12 in automobile air conditioners and is also used in foam blowing applications. In 2011, it reached 62.7 ppt, an increase of 28.2 ppt since 2005. Based on analysis of high-frequency measurements, the largest emissions occur in North America, Europe and East Asia (Stohl et al., 2009).

HFC-23 is a by-product of HCFC-22 production. Direct measurements of HFC-23 in ambient air at five sites began in 2007. The 2005 global annual mean used to calculate the increase since AR4 in Table 2.1, 5.2 ppt, is based on an archive of air collected at Cape Grim, Tasmania (Miller et al., 2010). In 2011, atmospheric HFC-23 was at 24.0 ppt. Its growth rate peaked in 2006 as emissions from developing countries

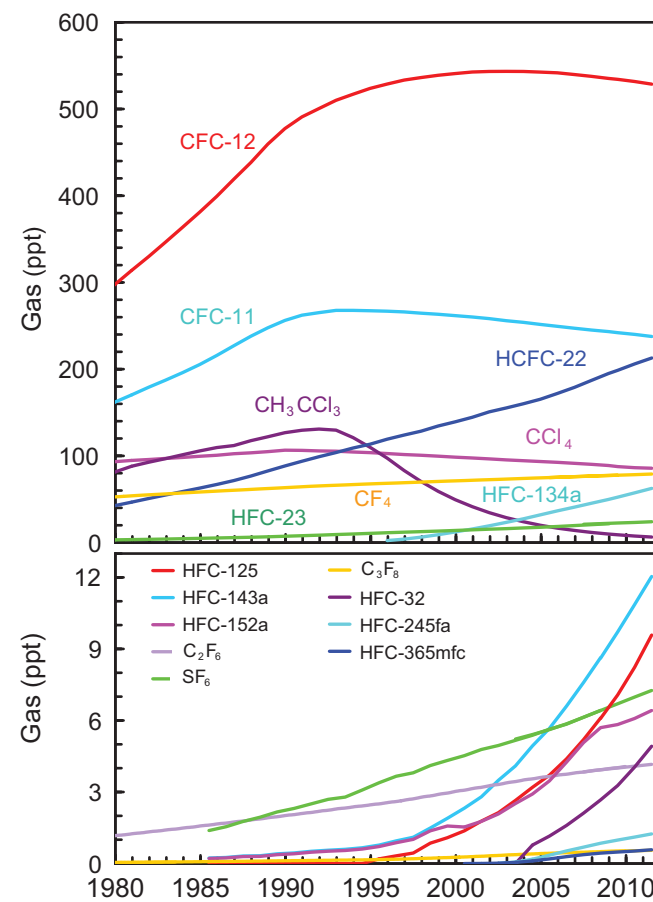


Figure 2.4 | Globally averaged dry-air mole fractions at the Earth's surface of the major halogen-containing well-mixed GHG. These are derived mainly using monthly mean measurements from the AGAGE and NOAA/ESRL/GMD networks. For clarity, only the most abundant chemicals are shown in different compound classes and results from different networks have been combined when both are available.

increased, then declined as emissions were reduced through abatement efforts under the Clean Development Mechanism (CDM) of the UNFCCC. Estimates of total global emissions based on atmospheric observations and bottom-up inventories agree within uncertainties (Miller et al., 2010; Montzka et al., 2010). Currently, the largest emissions of HFC-23 are from East Asia (Yokouchi et al., 2006; Kim et al., 2010; Stohl et al., 2010); developed countries emit less than 20% of the global total. Keller et al. (2011) found that emissions from developed countries may be larger than those reported to the UNFCCC, but their contribution is small. The lifetime of HFC-23 was revised from 270 to 222 years since AR4.

After HFC-134a and HFC-23, the next most abundant HFCs are HFC-143a at 12.04 ppt in 2011, 6.39 ppt greater than in 2005; HFC-125 (O'Doherty et al., 2009) at 9.58 ppt, increasing by 5.89 ppt since 2005; HFC-152a (Greally et al., 2007) at 6.4 ppt with a 3.0 ppt increase since 2005; and HFC-32 at 4.92 ppt in 2011, 3.77 ppt greater than in 2005. Since 2005, all of these were increasing exponentially except for HFC-152a, whose growth rate slowed considerably in about 2007 (Figure 2.4). HFC-152a has a relatively short atmospheric lifetime of 1.5 years, so its growth rate will respond quickly to changes in emissions. Its major uses are as a foam blowing agent and aerosol spray propellant while HFC-143a, HFC-125, and HFC-32 are mainly used in refrigerant blends. The reasons for slower growth in HFC-152a since about 2007 are unclear. Total global emissions of HFC-125 estimated from the observations are within about 20% of emissions reported to the UNFCCC, after accounting for estimates of unreported emissions from East Asia (O'Doherty et al., 2009).

CF_4 and C_2F_6 (PFCs) have lifetimes of 50 kyr and 10 kyr, respectively, and they are emitted as by-products of aluminium production and used in plasma etching of electronics. CF_4 has a natural lithospheric source (Deeds et al., 2008) with a 1750 level determined from Greenland and Antarctic firn air of 34.7 ± 0.2 ppt (Worton et al., 2007; Muhle et al., 2010). In 2011, atmospheric abundances were 79.0 ppt for CF_4 , increasing by 4.0 ppt since 2005, and 4.16 ppt for C_2F_6 , increasing by 0.50 ppt. The sum of emissions of CF_4 reported by aluminium producers and for non-aluminium production in EDGAR (Emission Database for Global Atmospheric Research) v4.0 accounts for only about half of global emissions inferred from atmospheric observations (Muhle et al., 2010). For C_2F_6 , emissions reported to the UNFCCC are also substantially lower than those estimated from atmospheric observations (Muhle et al., 2010).

The main sources of atmospheric SF_6 emissions are electricity distribution systems, magnesium production, and semi-conductor manufacturing. Global annual mean SF_6 in 2011 was 7.29 ppt, increasing by 1.65 ppt since 2005. SF_6 has a lifetime of 3200 years, so its emissions accumulate in the atmosphere and can be estimated directly from its observed rate of increase. Levin et al. (2010) and Rigby et al. (2010) showed that SF_6 emissions decreased after 1995, most likely because of emissions reductions in developed countries, but then increased after 1998. During the past decade, they found that actual SF_6 emissions from developed countries are at least twice the reported values.

NF_3 was added to the list of GHG in the Kyoto Protocol with the Doha Amendment, December, 2012. Arnold et al. (2013) determined 0.59 ppt

for its global annual mean mole fraction in 2008, growing from almost zero in 1978. In 2011, NF_3 was 0.86 ppt, increasing by 0.49 ppt since 2005. These abundances were updated from the first work to quantify NF_3 by Weiss et al. (2008). Initial bottom-up inventories underestimated its emissions; based on the atmospheric observations, NF_3 emissions were 1.18 ± 0.21 Gg in 2011 (Arnold et al., 2013).

In summary, it is certain that atmospheric burdens of well-mixed GHGs targeted by the Kyoto Protocol increased from 2005 to 2011. The atmospheric abundance of CO_2 was 390.5 ± 0.2 ppm in 2011; this is 40% greater than before 1750. Atmospheric N_2O was 324.2 ± 0.2 ppb in 2011 and has increased by 20% since 1750. Average annual increases in CO_2 and N_2O from 2005 to 2011 are comparable to those observed from 1996 to 2005. Atmospheric CH_4 was 1803.2 ± 2.0 ppb in 2011; this is 150% greater than before 1750. CH_4 began increasing in 2007 after remaining nearly constant from 1999 to 2006. HFCs, PFCs, and SF_6 all continue to increase relatively rapidly, but their contributions to RF are less than 1% of the total by well-mixed GHGs (Chapter 8).

2.2.1.2 Ozone-Depleting Substances (Chlorofluorocarbons, Chlorinated Solvents, and Hydrochlorofluorocarbons)

CFC atmospheric abundances are decreasing (Figure 2.4) because of the successful reduction in emissions resulting from the Montreal Protocol. By 2010, emissions from ODSs had been reduced by ~ 11 Pg $\text{CO}_2\text{-eq yr}^{-1}$, which is five to six times the reduction target of the first commitment period (2008–2012) of the Kyoto Protocol ($2 \text{ PgCO}_2\text{-eq yr}^{-1}$) (Velders et al., 2007). These avoided equivalent- CO_2 emissions account for the offsets to RF by stratospheric O_3 depletion caused by ODSs and the use of HFCs as substitutes for them. Recent observations in Arctic and Antarctic firn air further confirm that emissions of CFCs are entirely anthropogenic (Martinerie et al., 2009; Montzka et al., 2011b). CFC-12 has the largest atmospheric abundance and GWP-weighted emissions (which are based on a 100-year time horizon) of the CFCs. Its tropospheric abundance peaked during 2000–2004. Since AR4, its global annual mean mole fraction declined by 13.8 ppt to 528.5 ppt in 2011. CFC-11 continued the decrease that started in the mid-1990s, by 12.9 ppt since 2005. In 2011, CFC-11 was 237.7 ppt. CFC-113 decreased by 4.3 ppt since 2005 to 74.3 ppt in 2011. A discrepancy exists between top-down and bottom-up methods for calculating CFC-11 emissions (Montzka et al., 2011b). Emissions calculated using top-down methods come into agreement with bottom-up estimates when a lifetime of 64 years is used for CFC-11 in place of the accepted value of 45 years; this longer lifetime (64 years) is at the upper end of the range estimated by Douglass et al. (2008) with models that more accurately simulate stratospheric circulation. Future emissions of CFCs will largely come from ‘banks’ (i.e., material residing in existing equipment or stores) rather than current production.

The mean decrease in globally, annually averaged carbon tetrachloride (CCl_4) based on NOAA and AGAGE measurements since 2005 was 7.4 ppt, with an atmospheric abundance of 85.8 ppt in 2011 (Table 2.1). The observed rate of decrease and inter-hemispheric difference of CCl_4 suggest that emissions determined from the observations are on average greater and less variable than bottom-up emission estimates, although large uncertainties in the CCl_4 lifetime result in large uncertainties in the top-down estimates of emissions (Xiao et al., 2010;

Montzka et al., 2011b). CH_3CCl_3 has declined exponentially for about a decade, decreasing by 12.0 ppt since 2005 to 6.3 ppt in 2011.

HCFCs are classified as ‘transitional substitutes’ by the Montreal Protocol. Their global production and use will ultimately be phased out, but their global production is not currently capped and, based on changes in observed spatial gradients, there has likely been a shift in emissions within the NH from regions north of about 30°N to regions south of 30°N (Montzka et al., 2009). Global levels of the three most abundant HCFCs in the atmosphere continue to increase. HCFC-22 increased by 44.5 ppt since 2005 to 213.3 ppt in 2011. Developed country emissions of HCFC-22 are decreasing, and the trend in total global emissions is driven by large increases from south and Southeast Asia (Saikawa et al., 2012). HCFC-141b increased by 3.7 ppt since 2005 to 21.4 ppt in 2011, and for HCFC-142b, the increase was 5.73 ppt to 21.1 ppt in 2011. The rates of increase in these three HCFCs increased since 2004, but the change in HCFC-141b growth rate was smaller and less persistent than for the other two, which approximately doubled from 2004 to 2007 (Montzka et al., 2009).

In summary, for ODS, whose production and consumption are controlled by the Montreal Protocol, it is certain that the global mean abundances of major CFCs are decreasing and HCFCs are increasing. Atmospheric burdens of CFC-11, CFC-12, CFC-113, CCl_4 , CH_3CCl_3 and some halons have decreased since 2005. HCFCs, which are transitional substitutes for CFCs, continue to increase, but the spatial distribution of their emissions is changing.

2.2.2 Near-Term Climate Forcers

This section covers observed trends in stratospheric water vapour; stratospheric and tropospheric ozone (O_3); the O_3 precursor gases, nitrogen dioxide (NO_2) and carbon monoxide (CO); and column and surface aerosol. Since trend estimates from the cited literature are used here, issues such as data records of different length, potential lack of comparability among measurement methods and different trend calculation methods, add to the uncertainty in assessing trends.

2.2.2.1 Stratospheric Water Vapour

Stratospheric H_2O vapour has an important role in the Earth’s radiative balance and in stratospheric chemistry. Increased stratospheric H_2O vapour causes the troposphere to warm and the stratosphere to cool (Manabe and Strickler, 1964; Solomon et al., 2010), and also causes increased rates of stratospheric O_3 loss (Stenke and Grewe, 2005). Water vapour enters the stratosphere through the cold tropical tropopause. As moisture-rich air masses are transported through this region, most water vapour condenses resulting in extremely dry lower stratospheric air. Because tropopause temperature varies seasonally, so does H_2O abundance there. Other contributions include oxidation of methane within the stratosphere, and possibly direct injection of H_2O vapour in overshooting deep convection (Schiller et al., 2009). AR4 reported that stratospheric H_2O vapour showed significant long-term variability and an upward trend over the last half of the 20th century, but no net increase since 1996. This updated assessment finds large interannual variations that have been observed by independent measurement techniques, but no significant net changes since 1996.

The longest continuous time series of stratospheric water vapour abundance is from *in situ* measurements made with frost point hygrometers starting in 1980 over Boulder, USA (40°N, 105°W) (Scherer et al., 2008), with values ranging from 3.5 to 5.5 ppm, depending on altitude. These observations have been complemented by long-term global satellite observations from SAGE II (1984–2005; Stratospheric Aerosol and Gas Experiment II (Chu et al., 1989)), HALOE (1991–2005; HALogen Occultation Experiment (Russell et al., 1993)), Aura MLS (2004–present; Microwave Limb Sounder (Read et al., 2007)) and Envisat MIPAS (2002–2012; Michelson Interferometer for Passive Atmospheric Sounding (Milz et al., 2005; von Clarmann et al., 2009)). Discrepancies in water vapour mixing ratios from these different instruments can be attributed to differences in the vertical resolution of measurements, along with other factors. For example, offsets of up to 0.5 ppm in lower stratospheric water vapour mixing ratios exist between the most current versions of HALOE (v19) and Aura MLS (v3.3) retrievals during their 16-month period of overlap (2004 to 2005), although such biases can be removed to generate long-term records. Since AR4, new studies characterize the uncertainties in measurements from individual types of *in situ* H_2O sensors (Vömel et al., 2007b; Vömel et al., 2007a; Weinstock et al., 2009), but discrepancies between different instruments (50 to 100% at H_2O mixing ratios less than 10 ppm), particularly for high-altitude measurements from aircraft, remain largely unexplained.

Observed anomalies in stratospheric H_2O from the near-global combined HALOE+MLS record (1992–2011) (Figure 2.5) include effects linked to the stratospheric quasi-biennial oscillation (QBO) influence on tropopause temperatures, plus a step-like drop after 2001 (noted in AR4), and an increasing trend since 2005. Variability during 2001–2011 was large yet there was only a small net change from 1992 through 2011. These interannual water vapour variations for the satellite record are closely linked to observed changes in tropical tropopause temperatures (Fueglistaler and Haynes, 2005; Randel et al., 2006; Rosenlof and Reid, 2008; Randel, 2010), providing reasonable understanding of observed changes. The longer record of Boulder balloon measurements (since 1980) has been updated and reanalyzed (Scherer et al., 2008; Hurst et al., 2011), showing deca dal-scale variability and a long-term stratospheric (16 to 26 km) increase of 1.0 ± 0.2 ppm for 1980–2010. Agreement between interannual changes inferred from the Boulder and HALOE+MLS data is good for the period since 1998 but was poor during 1992–1996. About 30% of the positive trend during 1980–2010 determined from frost point hygrometer data (Fujiwara et al., 2010; Hurst et al., 2011) can be explained by increased production of H_2O from CH_4 oxidation (Rohs et al., 2006), but the remainder cannot be explained by changes in tropical tropopause temperatures (Fueglistaler and Haynes, 2005) or other known factors.

In summary, near-global satellite measurements of stratospheric H_2O show substantial variability for 1992–2011, with a step-like decrease after 2000 and increases since 2005. Because of this large variability and relatively short time series, confidence in long-term stratospheric H_2O trends is low. There is good understanding of the relationship between the satellite-derived H_2O variations and tropical tropopause temperature changes. Stratospheric H_2O changes from temporally sparse balloon-borne observations at one location (Boulder, Colorado) are in good agreement with satellite observations from 1998 to the present, but discrepancies exist for changes during 1992–1996. Long-

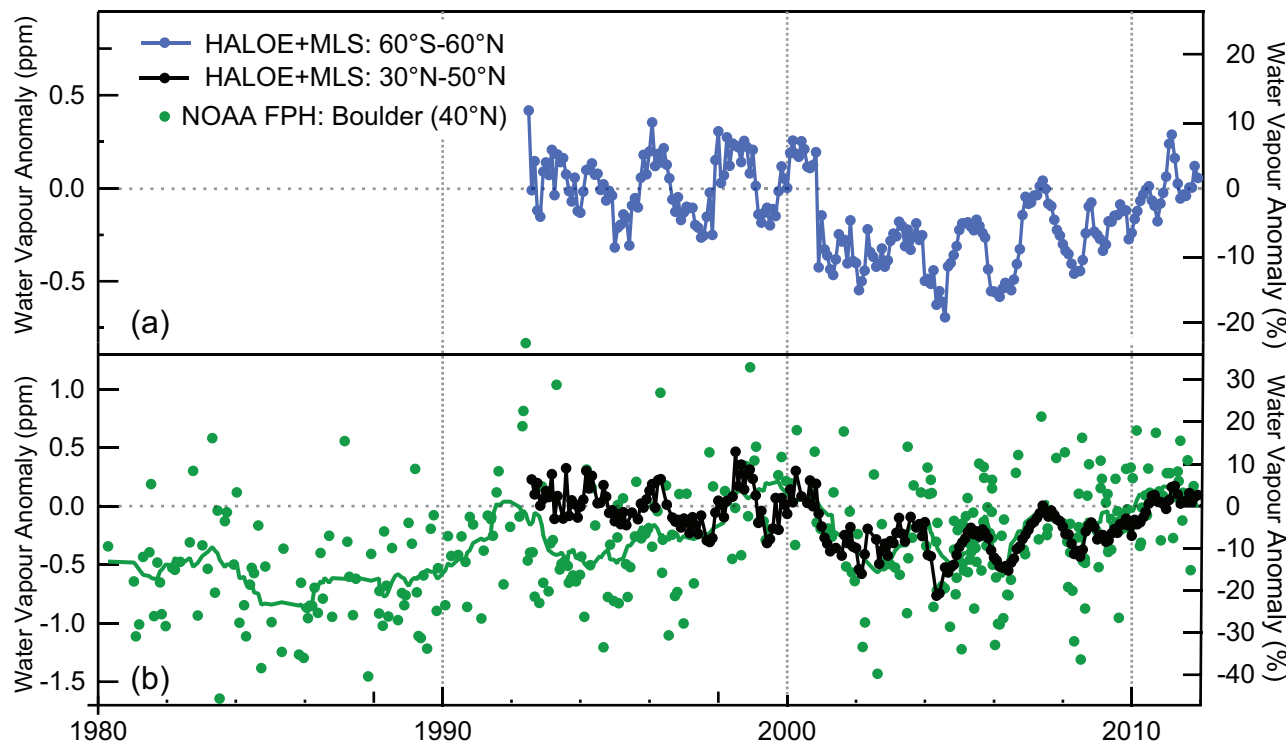


Figure 2.5 | Water vapour anomalies in the lower stratosphere (~16 to 19 km) from satellite sensors and *in situ* measurements normalized to 2000–2011. (a) Monthly mean water vapour anomalies at 83 hPa for 60°S to 60°N (blue) determined from HALOE and MLS satellite sensors. (b) Approximately monthly balloon-borne measurements of stratospheric water vapour from Boulder, Colorado at 40°N (green dots; green curve is 15-point running mean) averaged over 16 to 18 km and monthly means as in (a), but averaged over 30°N to 50°N (black)

term balloon measurements from Boulder indicate a net increase of 1.0 ± 0.2 ppm over 16 to 26 km for 1980–2010, but these long-term increases cannot be fully explained by changes in tropical tropopause temperatures, methane oxidation or other known factors.

2.2.2.2 Stratospheric Ozone

AR4 did not explicitly discuss measured stratospheric ozone trends. For the current assessment report such trends are relevant because they are the basis for revising the RF from $-0.05 \pm 0.10 \text{ W m}^{-2}$ in 1750 to $-0.10 \pm 0.15 \text{ W m}^{-2}$ in 2005 (Section 8.3.3.2). These values strongly depend on the vertical distribution of the stratospheric ozone changes.

Total ozone is a good proxy for stratospheric ozone because tropospheric ozone accounts for only about 10% of the total ozone column. Long-term total ozone changes over various latitudinal belts, derived from Weber et al. (2012), are illustrated in Figure 2.6 (a–d). Annual averaged total column ozone declined during the 1980s and early 1990s and has remained constant for the past decade, about 3.5 and 2.5% below the 1964–1980 average for the entire globe (not shown) and 60°S to 60°N, respectively, with changes occurring mostly outside the tropics, particularly the SH, where the current extratropical (30°S to 60°S) mean values are 6% below the 1964–1980 average, compared to 3.5% for the NH extratropics (Douglass et al., 2011). In the NH, the 1993 minimum of about –6% was caused primarily by ozone loss through heterogeneous reactions on volcanic aerosols from Mt. Pinatubo.

Two altitude regions are mainly responsible for long-term changes in total column ozone (Douglass et al., 2011). In the upper stratosphere (35 to 45 km), there was a strong and statistically significant decline (about 10%) up to the mid-1990s and little change or a slight increase since. The lower stratosphere, between 20 and 25 km over mid-latitudes, also experienced a statistically significant decline (7 to 8%) between 1979 and the mid-1990s, followed by stabilization or a slight (2 to 3%) ozone increase.

Springtime averages of total ozone poleward of 60° latitude in the Arctic and Antarctic are shown in Figure 2.6e. By far the strongest ozone loss in the stratosphere occurs in austral spring over Antarctica (ozone hole) and its impact on SH climate is discussed in Chapters 11, 12 and 14. Interannual variability in polar stratospheric ozone abundance and chemistry is driven by variability in temperature and transport due to year-to-year differences in dynamics. This variability is particularly large in the Arctic, where the most recent large depletion occurred in 2011, when chemical ozone destruction was, for the first time in the observational record, comparable to that in the Antarctic (Manney et al., 2011).

In summary, it is certain that global stratospheric ozone has declined from pre-1980 values. Most of the decline occurred prior to the mid-1990s; since then there has been little net change and ozone has remained nearly constant at about 3.5% below the 1964–1980 level.

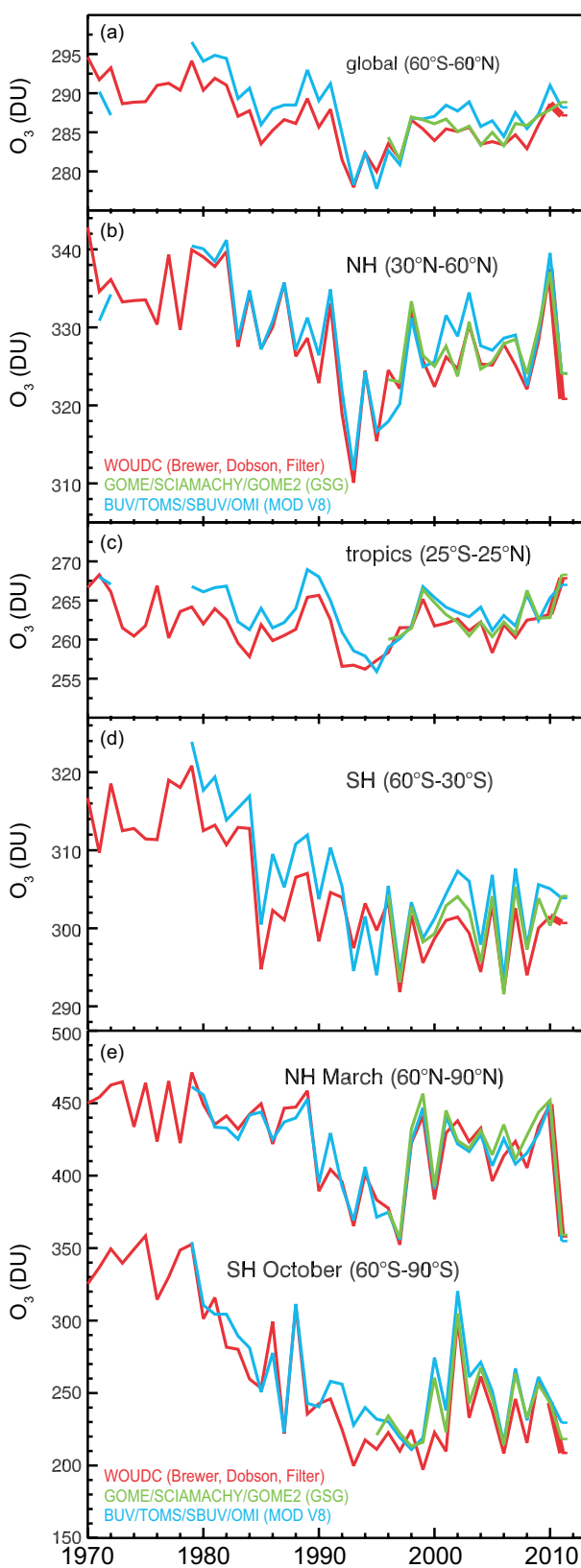


Figure 2.6 | Zonally averaged, annual mean total column ozone in Dobson Units (DU; $1 \text{ DU} = 2.69 \times 10^{16} \text{ O}_3/\text{cm}^2$) from ground-based measurements combining Brewer, Dobson, and filter spectrometer data WOUDC (red), GOME/SCIAMACHY/GOME-2 GSG (green) and merged satellite BUV/TOMS/SBUV/OMI MOD V8 (blue) for (a) Non-Polar Global (60°S to 60°N), (b) NH (30°N to 60°N), (c) Tropics (25°S to 25°N), (d) SH (30°S to 60°S) and (e) March NH Polar (60°N to 90°N) and October SH Polar. (Adapted from Weber et al., 2012; see also for abbreviations.)

2.2.2.3 Tropospheric Ozone

Tropospheric ozone is a short-lived trace gas that either originates in the stratosphere or is produced *in situ* by precursor gases and sunlight (e.g., Monks et al., 2009). An important GHG with an estimated RF of $0.40 \pm 0.20 \text{ W m}^{-2}$ (Chapter 8), tropospheric ozone also impacts human health and vegetation at the surface. Its average atmospheric lifetime of a few weeks produces a global distribution highly variable by season, altitude and location. These characteristics and the paucity of long-term measurements make the assessment of long-term global ozone trends challenging. However, new studies since AR4 provide greater understanding of surface and free tropospheric ozone trends from the 1950s through 2010. An extensive compilation of measured ozone trends is presented in the Supplementary Material, Figure 2.SM.1 and Table 2.SM.2.

The earliest (1876–1910) quantitative ozone observations are limited to Montsouris near Paris where ozone averaged 11 ppb (Volz and Kley, 1988). Semiquantitative ozone measurements from more than 40 locations around the world in the late 1800s and early 1900s range from 5 to 32 ppb with large uncertainty (Pavelin et al., 1999). The low 19th century ozone values cannot be reproduced by most models (Section 8.2.3.1), and this discrepancy is an important factor contributing to uncertainty in RF calculations (Section 8.3.3.1). Limited quantitative measurements from the 1870s to 1950s indicate that surface ozone in Europe increased by more than a factor of 2 compared to observations made at the end of the 20th century (Marenco et al., 1994; Parrish et al., 2012).

Satellite-based tropospheric column ozone retrievals across the tropics and mid-latitudes reveal a greater burden in the NH than in the SH (Ziemke et al., 2011). Tropospheric column ozone trend analyses are few. An analysis by Ziemke et al. (2005) found no trend over the tropical Pacific Ocean but significant positive trends (5 to 9% per decade) in the mid-latitude Pacific of both hemispheres during 1979–2003. Significant positive trends (2 to 9% per decade) were found across broad regions of the tropical South Atlantic, India, southern China, southeast Asia, Indonesia and the tropical regions downwind of China (Beig and Singh, 2007).

Long-term ozone trends at the surface and in the free troposphere (of importance for calculating RF, Chapter 8) can be assessed only from *in situ* measurements at a limited number of sites, leaving large areas such as the tropics and SH sparsely sampled (Table 2.SM.2, Figure 2.7). Nineteen predominantly rural surface sites or regions around the globe have long-term records that stretch back to the 1970s, and in two cases the 1950s (Lelieveld et al., 2004; Parrish et al., 2012; Oltmans et al., 2013). Thirteen of these sites are in the NH, and 11 sites have statistically significant positive trends of 1 to 5 ppb per decade, corresponding to >100% ozone increases since the 1950s and 9 to 55% ozone increases since the 1970s. In the SH, three of six sites have significant trends of approximately 2 ppb per decade and three have insignificant trends. Free tropospheric monitoring since the 1970s is more limited. Significant positive trends since 1971 have been observed using ozone sondes above Western Europe, Japan and coastal Antarctica (rates of increase range from 1 to 3 ppb per decade), but not at all levels (Oltmans et al., 2013). In addition, aircraft have measured

significant upper tropospheric trends in one or more seasons above the north-eastern USA, the North Atlantic Ocean, Europe, the Middle East, northern India, southern China and Japan (Schnadt Poberaj et al., 2009). Insignificant free tropospheric trends were found above the Mid-Atlantic USA (1971–2010) (Oltmans et al., 2013) and in the upper troposphere above the western USA (1975–2001) (Schnadt Poberaj et al., 2009). No site or region showed a significant negative trend.

In recent decades ozone precursor emissions have decreased in Europe and North America and increased in Asia (Granier et al., 2011), impacting ozone production on regional and hemispheric scales (Skeie et al., 2011). Accordingly, 1990–2010 surface ozone trends vary regionally. In Europe ozone generally increased through much of the 1990s but since 2000 ozone has either levelled off or decreased at rural and mountain-top sites, as well as for baseline ozone coming ashore at Mace Head, Ireland (Tarasova et al., 2009; Logan et al., 2012; Parrish et al., 2012; Oltmans et al., 2013). In North America surface ozone has increased in eastern and Arctic Canada, but is unchanged in central and western Canada (Oltmans et al., 2013). Surface ozone has increased in baseline air masses coming ashore along the west coast of the USA (Parrish et al., 2012) and at half of the rural sites in the western USA during spring (Cooper et al., 2012). In the eastern USA surface ozone has decreased strongly in summer, is largely unchanged in spring and has increased in winter (Lefohn et al., 2010; Cooper et al., 2012). East Asian surface ozone is generally increasing (Table 2.SM.2) and at downwind sites ozone is increasing at Mauna Loa, Hawaii but decreasing at Minami Tori Shima in the subtropical western North Pacific (Oltmans et al., 2013). In the SH ozone has increased at the eight available sites, although trends are insignificant at four sites (Helmig et al., 2007; Oltmans et al., 2013).

Owing to methodological changes, free tropospheric ozone observations are most reliable since the mid-1990s. Ozone has decreased above Europe since 1998 (Logan et al., 2012) and is largely unchanged above Japan (Oltmans et al., 2013). Otherwise the remaining regions with measurements (North America, North Pacific Ocean, SH) show a range of positive trends (both significant and insignificant) depending on altitude, with no site having a negative trend at any altitude (Table 2.SM.2).

In summary, there is *medium confidence* from limited measurements in the late 19th through mid-20th century that European surface ozone more than doubled by the end of the 20th century. There is *medium confidence* from more widespread measurements beginning in the 1970s that surface ozone has increased at most (non-urban) sites in the NH (1 to 5 ppb per decade), while there is *low confidence* for ozone increases (2 ppb per decade) in the SH. Since 1990 surface ozone has *likely* increased in East Asia, while surface ozone in the eastern USA and Western Europe has levelled off or is decreasing. Ozone monitoring in the free troposphere since the 1970s is very limited and indicates a weaker rate of increase than at the surface. Satellite instruments can now quantify the present-day tropospheric ozone burden on a near-global basis; significant tropospheric ozone column increases were observed over extended tropical regions of southern Asia, as well as mid-latitude regions of the South and North Pacific Ocean since 1979.

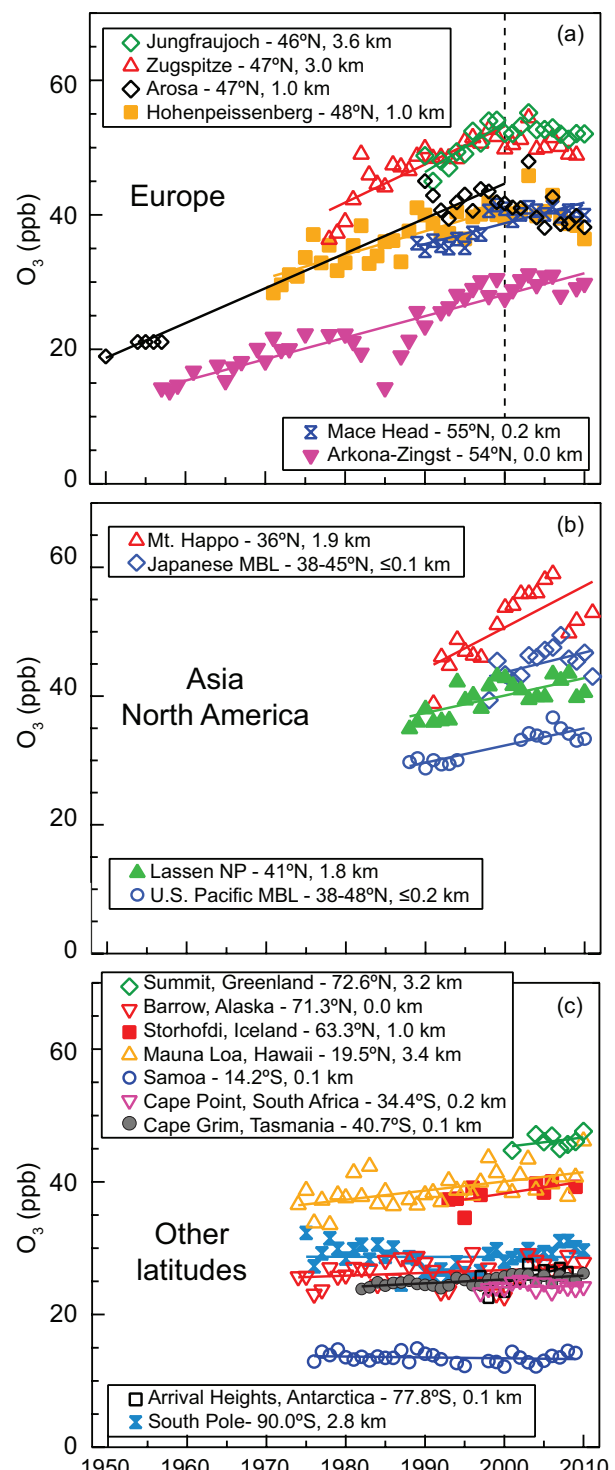


Figure 2.7 | Annual average surface ozone concentrations from regionally representative ozone monitoring sites around the world. (a) Europe. (b) Asia and North America. (c) Remote sites in the Northern and Southern Hemispheres. The station name in the legend is followed by its latitude and elevation. Time series include data from all times of day and trend lines are linear regressions following the method of Parrish et al. (2012). Trend lines are fit through the full time series at each location, except for Jungfraujoch, Zugspitze, Arosa and Hohenpeissenberg where the linear trends end in 2000 (indicated by the dashed vertical line in (a)). Twelve of these 19 sites have significant positive ozone trends (i.e., a trend of zero lies outside the 95% confidence interval); the seven sites with non-significant trends are: Japanese MBL (marine boundary layer), Summit (Greenland), Barrow (Alaska), Storhofdi (Iceland), Samoa (tropical South Pacific Ocean), Cape Point (South Africa) and South Pole (Antarctica).

2.2.2.4 Carbon Monoxide, Non-Methane Volatile Organic Compounds and Nitrogen Dioxide

Emissions of carbon monoxide (CO), non-methane volatile organic compounds (NMVOCs) and NO_x ($\text{NO} + \text{NO}_2$) do not have a direct effect on RF, but affect climate indirectly as precursors to tropospheric O_3 and aerosol formation, and their impacts on OH concentrations and CH_4 lifetime. NMVOCs include aliphatic, aromatic and oxygenated hydrocarbons (e.g., aldehydes, alcohols and organic acids), and have atmospheric lifetimes ranging from hours to months. Global coverage of NMVOC measurements is poor, except for a few compounds. Reports on trends generally indicate declines in a range of NMVOCs in urban and rural regions of North America and Europe on the order of a few percent to more than 10% yr^{-1} . Global ethane levels reported by Simpson et al. (2012) declined by about 21% from 1986 to 2010. Measurements of air extracted from firn suggest that NMVOC concentrations were growing until 1980 and declined afterwards (Aydin et al., 2011; Worton et al., 2012). Satellite retrievals of formaldehyde column abundances from 1997 to 2007 show significant positive trends over northeastern China (4% yr^{-1}) and India (1.6% yr^{-1}), possibly related to strong increases in anthropogenic NMVOC emissions, whereas negative trends of about -3% yr^{-1} are observed over Tokyo, Japan and the northeast USA urban corridor as a result of pollution regulation (De Smedt et al., 2010).

The major sources of atmospheric CO are *in situ* production by oxidation of hydrocarbons (mostly CH_4 and isoprene) and direct emission resulting from incomplete combustion of biomass and fossil fuels. An analysis of MOPITT (Measurements of Pollutants in the Troposphere) and AIRS (Atmospheric Infrared Sounder) satellite data suggest a clear and consistent decline of CO columns for 2002–2010 over a number of polluted regions in Europe, North America and Asia with a global trend of about -1% yr^{-1} (Yurganov et al., 2010; Fortems-Cheiney et al., 2011; Worden et al., 2013). Analysis of satellite data using two more instruments for recent overlapping years shows qualitatively similar decreasing trends (Worden et al., 2013), but the magnitude of trends remains uncertain owing to the presence of instrument biases. Small CO decreases observed in the NOAA and AGAGE networks are consistent with slight declines in global anthropogenic CO emissions over the same time (Supplementary Material 2.SM.2).

Due to its short atmospheric lifetime (approximately hours), NO_x concentrations are highly variable in time and space. AR4 described the potential of satellite observations of NO_2 to verify and improve NO_x emission inventories and their trends and reported strong NO_2 increases by 50% over the industrial areas of China from 1996 to 2004. An extension of this analysis reveals increases between a factor of 1.7 and 3.2 over parts of China, while over Europe and the USA NO_2 has decreased by 30 to 50% between 1996 and 2010 (Hilboll et al., 2013).

Figure 2.8 shows the changes relative to 1996 in satellite-derived tropospheric NO_2 columns, with a strong upward trend over central eastern China and an overall downward trend in Japan, Europe and the USA. NO_2 reductions in the USA are very pronounced after 2004, related to differences in effectiveness of NO_x emission abatements in the USA and also to changes in atmospheric chemistry of NO_x (Russell et al., 2010). Increasingly, satellite data are used to derive trends in anthropogenic

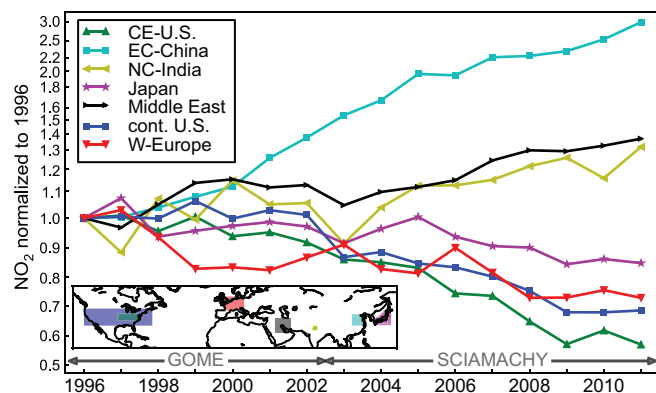


Figure 2.8 | Relative changes in tropospheric NO_2 column amounts (logarithmic scale) in seven selected world regions dominated by high NO_x emissions. Values are normalized for 1996 and derived from the GOME (Global Ozone Monitoring Experiment) instrument from 1996 to 2002 and SCIAMACHY (Scanning Imaging Spectrometer for Atmospheric Cartography) from 2003 to 2011 (Hilboll et al., 2013). The regions are indicated in the map inset.

NO_x emissions, with Castellanos and Boersma (2012) reporting overall increases in global emissions, driven by Asian emission increases of up to 29% yr^{-1} (1996–2006), while moderate decreases up to 7% yr^{-1} (1996–2006) are reported for North America and Europe.

In summary, satellite and surface observations of ozone precursor gases NO_x , CO, and non-methane volatile organic carbons indicate strong regional differences in trends. Most notably, NO_2 has *likely* decreased by 30 to 50% in Europe and North America and increased by more than a factor of 2 in Asia since the mid-1990s.

2.2.3 Aerosols

This section assesses trends in aerosol resulting from both anthropogenic and natural sources. The significance of aerosol changes for global dimming and brightening is discussed in Section 2.3. Chapter 7 provides additional discussion of aerosol properties, while Chapter 8 discusses future RF and the ice-core records that contain information on aerosol changes prior to the 1980s. Chapter 11 assesses air quality–climate change interactions. Because of the short lifetime (days to weeks) of tropospheric aerosol, trends have a strong regional signature. Aerosol from anthropogenic sources (i.e., fossil and biofuel burning) are confined mainly to populated regions in the NH, whereas aerosol from natural sources, such as desert dust, sea salt, volcanoes and the biosphere, are important in both hemispheres and likely dependent on climate and land use change (Carslaw et al., 2010). Owing to interannual variability, long-term trends in aerosols from natural sources are more difficult to identify (Mahowald et al., 2010).

2.2.3.1 Aerosol Optical Depth from Remote Sensing

AOD is a measure of the integrated columnar aerosol load and is an important parameter for evaluating aerosol–radiation interactions. AR4 described early attempts to retrieve AOD from satellites but did not provide estimates of temporal changes in tropospheric aerosols. Little high-accuracy information on AOD changes exists prior to 1995. Better satellite sensors and ground-based sun-photometer networks,

along with improved retrieval methods and methodological intercomparisons, allow assessment of regional AOD trends since about 1995.

AOD sun photometer measurements at two stations in northern Germany, with limited regional representativity, suggest a long-term decline of AOD in Europe since 1986 (Ruckstuhl et al., 2008). Ground-based, cloud-screened solar broadband radiometer measurements provide longer time-records than spectrally selective sun-photometer data, but are less specific for aerosol retrieval. Multi-decadal records over Japan (Kudo et al., 2011) indicate an AOD increase until the mid-1980s, followed by an AOD decrease until the late 1990s and almost constant AOD in the 2000s. Similar broad-band solar radiative flux multi-decadal trends have been observed for urban-industrial regions of Europe and North America (Wild et al., 2005), and were linked to successful measures to reduce sulphate (precursor) emissions since the mid-1980s (Section 2.3). An indirect method to estimate AOD is offered by ground-based visibility observations. These data are more ambiguous to interpret, but records go further back in time than broadband, sun photometer and satellite data. A multi-regional analysis for 1973–2007 (Wang et al., 2009a) shows that prior to the 1990s visibility-derived AOD was relatively constant in most regions analysed (except for positive trends in southern Asia), but after 1990 positive AOD trends were observed over Asia, and parts of South America, Australia and Africa, and mostly negative AOD trends were found over Europe. In North America, a small stepwise decrease of visibility after 1993 was likely related to methodological changes (Wang et al., 2012f).

AOD can be determined most accurately with sun photometers that measure direct solar intensity in the absence of cloud interferences with an absolute uncertainty of single measurements of $\pm 0.01\%$ (Holben et al., 1998). AERONET (AErosol RObotic NETwork) is a global sun photometer network (Holben et al., 1998), with densest coverage over Europe and North America. AERONET AOD temporal trends were examined in independent studies (de Meij et al., 2012; Hsu et al., 2012; Yoon et al., 2012), using different data selection and statistical methods. Hsu et al. (2012) investigated AOD trends at 12 AERONET sites with data coverage of at least 10 years between 1997 and 2010. Yoon et al. (2012) investigated AOD and size trends at 14 AERONET sites with data coverage varying between 4 and 12 years between 1997 and 2009. DeMeij et al. (2012) investigated AOD trends between 2000 and 2009 (550 nm; monthly data) at 62 AERONET sites mostly located in USA and Europe. Each of these studies noted an increase in AOD over East Asia and reductions in North America and Europe. The only dense sun photometer network over southern Asia, ARFINET (Aerosol Radiative Forcing over India NETwork), shows an increase in AOD of about $2\% \text{ yr}^{-1}$ during the last one to two decades (Krishna Moorthy et al., 2013), with an absolute uncertainty of ± 0.02 at 500 nm (Krishna Moorthy et al., 2007). In contrast, negative AOD trends are identified at more than 80% of examined European and North American AERONET sites (de Meij et al., 2012). Decreasing AOD is also observed near the west coast of northern Africa, where aerosol loads are dominated by Saharan dust outflow. Positive AOD trends are found over the Arabian Peninsula, where aerosol is dominated by dust. Inconsistent AOD trends reported for stations in central Africa result from the use of relatively short time series with respect to the large interannual variability caused by wildfires and dust emissions.

Aerosol products from dedicated satellite sensors complement surface-based AOD with better spatial coverage. The quality of the satellite-derived AOD strongly depends on the retrieval's ability to remove scenes contaminated by clouds and to accurately account for reflectivity at the Earth's surface. Due to relatively weak reflectance of incoming sunlight by the sea surface, the typical accuracy of retrieved AOD over oceans (uncertainty of $0.03 + 0.05^* \text{AOD}$; Kahn et al. (2007)) is usually better than over continents (uncertainty of $0.05 + 0.15^* \text{AOD}$, Levy et al. (2010)).

Satellite-based AOD trends at 550 nm over oceans from conservatively cloud-screened MODIS data (Zhang and Reid, 2010) for 2000–2009 are presented in Figure 2.9. Strongly positive AOD trends were observed over the oceans adjacent to southern and eastern Asia. Positive AOD trends are also observed over most tropical oceans. The negative MODIS AOD trends observed over coastal regions of Europe and near the east coast of the USA are in agreement with sun photometer observations and *in situ* measurements (Section 2.2.3.2) of aerosol mass in these regions. These regional changes over oceans are consistent with analyses of AVHRR (Advanced Very High Resolution Radiometer) trends for 1981–2005 (Mishchenko et al., 2007; Cermak et al., 2010; Zhao et al., 2011), except over the Southern Ocean (45°S to 60°S), where negative AOD trends of AVHRR retrievals are neither confirmed by MODIS after 2001 (Zhang and Reid, 2010) nor by ATSR-2 (Along Track Scanning Radiometer) for 1995–2001 (Thomas et al., 2010).

Satellite-based AOD changes for both land and oceans (Figure 2.9b) were examined with re-processed SeaWiFS (Sea-viewing Wide Field-of-view Sensor) AOD data for 1998–2010 (Hsu et al., 2012). A small positive global average AOD trend is reported, which is likely influenced by interannual natural aerosol emissions variability (e.g., related to ENSO or North Atlantic Oscillation (NAO); Box 2.5), and compensating larger positive and negative regional AOD trends. In addition, temporal changes in aerosol composition are ignored in the retrieval algorithms, giving more uncertain trends than suggested by statistical analysis alone (Mishchenko et al., 2012). Thus, confidence is low for global satellite derived AOD trends over these relatively short time periods.

The sign and magnitude of SeaWiFS regional AOD trends over continents are in agreement with most AOD trends by ground-based sun photometer data (see above) and with MODIS trends (Figure 2.9). The strong positive AOD trend over the Arabian Peninsula occurs mainly during spring (MAM) and summer (JJA), during times of dust transport, and is also visible in MODIS data (Figure 2.9). The positive AOD trend over southern and eastern Asia is strongest during the dry seasons (DJF, MAM), when reduced wet deposition allows anthropogenic aerosol to accumulate in the troposphere. AOD over the Saharan outflow region off western Africa displays the strongest seasonal AOD trend differences, with AOD increases only in spring, but strong AOD decreases during the other seasons. SeaWiFS AOD decreases over Europe and the USA and increases over southern and eastern Asia (especially during the dry season) are in agreement with reported temporal trends in anthropogenic emissions, and surface observations (Section 2.2.3.2).

In summary, based on satellite- and surface-based remote sensing it is very *likely* that AOD has decreased over Europe and the eastern

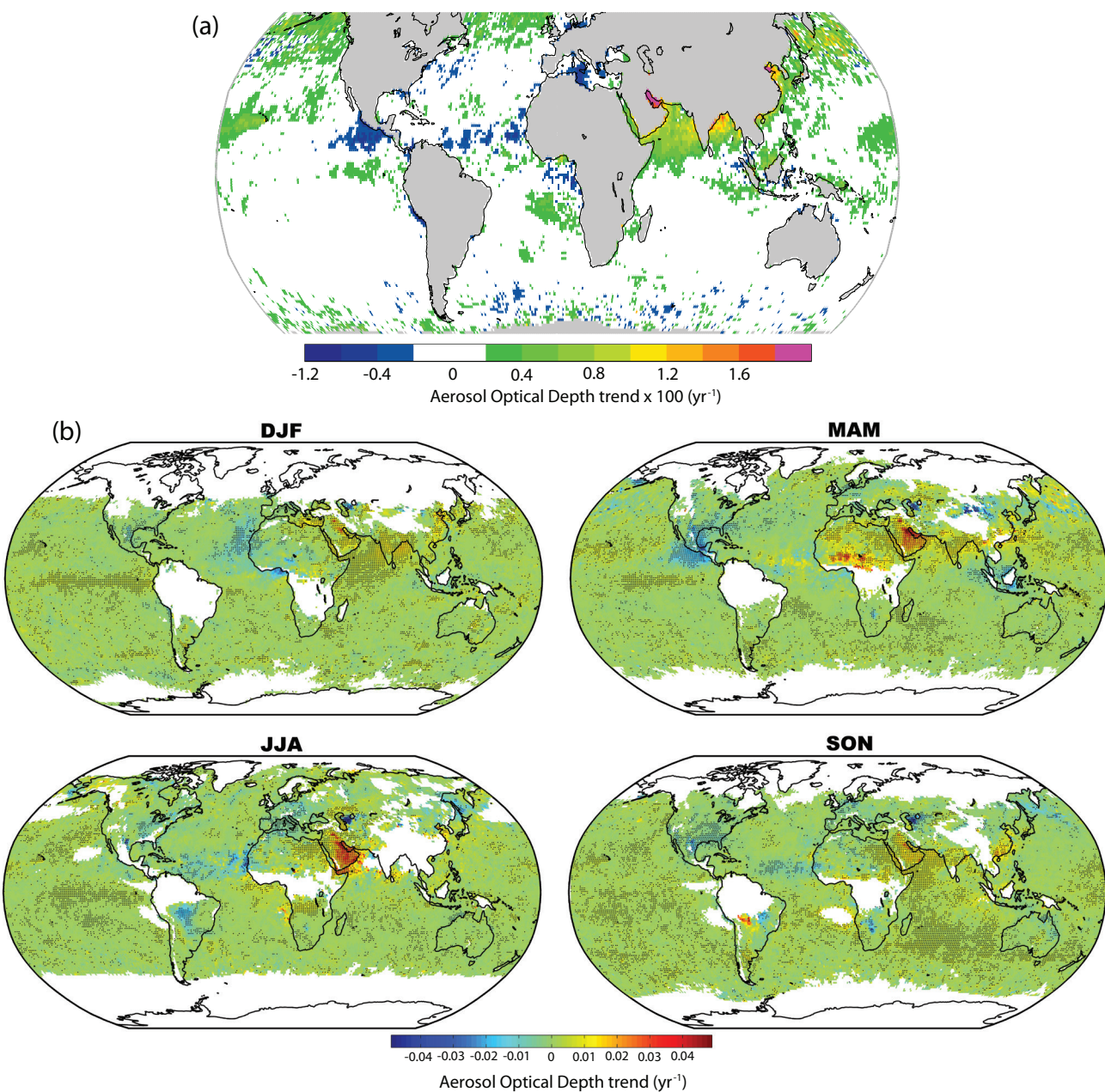


Figure 2.9 | (a) Annual average aerosol optical depth (AOD) trends at $0.55\text{ }\mu\text{m}$ for 2000–2009, based on de-seasonalized, conservatively cloud-screened MODIS aerosol data over oceans (Zhang and Reid, 2010). Negative AOD trends off Mexico are due to enhanced volcanic activity at the beginning of the record. Most non-zero trends are significant (i.e., a trend of zero lies outside the 95% confidence interval). (b) Seasonal average AOD trends at $0.55\text{ }\mu\text{m}$ for 1998–2010 using SeaWiFS data (Hsu et al., 2012). White areas indicate incomplete or missing data. Black dots indicate significant trends (i.e., a trend of zero lies outside the 95% confidence interval).

USA since the mid 1990s and increased over eastern and southern Asia since 2000. In the 2000s dust-related AOD has been increasing over the Arabian Peninsula and decreasing over the North Atlantic Ocean. Aerosol trends over other regions are less strong or not significant during this period owing to relative strong interannual variability. Overall, *confidence* in satellite-based global average AOD trends is *low*.

2.2.3.2 *In Situ* Surface Aerosol Measurements

AR4 did not report trends in long-term surface-based *in situ* measurements of particulate matter, its components or its properties. This section summarizes reported trends of PM_{10} , $\text{PM}_{2.5}$ (particulate matter

with aerodynamic diameters <10 and $<2.5\text{ }\mu\text{m}$, respectively), sulphate and equivalent black carbon/elemental carbon, from regionally representative measurement networks. An overview of current networks and definitions pertinent to aerosol measurements is given in Supplementary Material 2.SM.2.3. Studies reporting trends representative of regional changes are presented in Table 2.2. Long-term data are almost entirely from North America and Europe, whereas a few individual studies on aerosol trends in India and China are reported in Supplementary Material 2.SM.2.3. Figure 2.10 gives an overview of observed PM_{10} , $\text{PM}_{2.5}$, and sulphate trends in North America and Europe for 1990–2009 and 2000–2009.

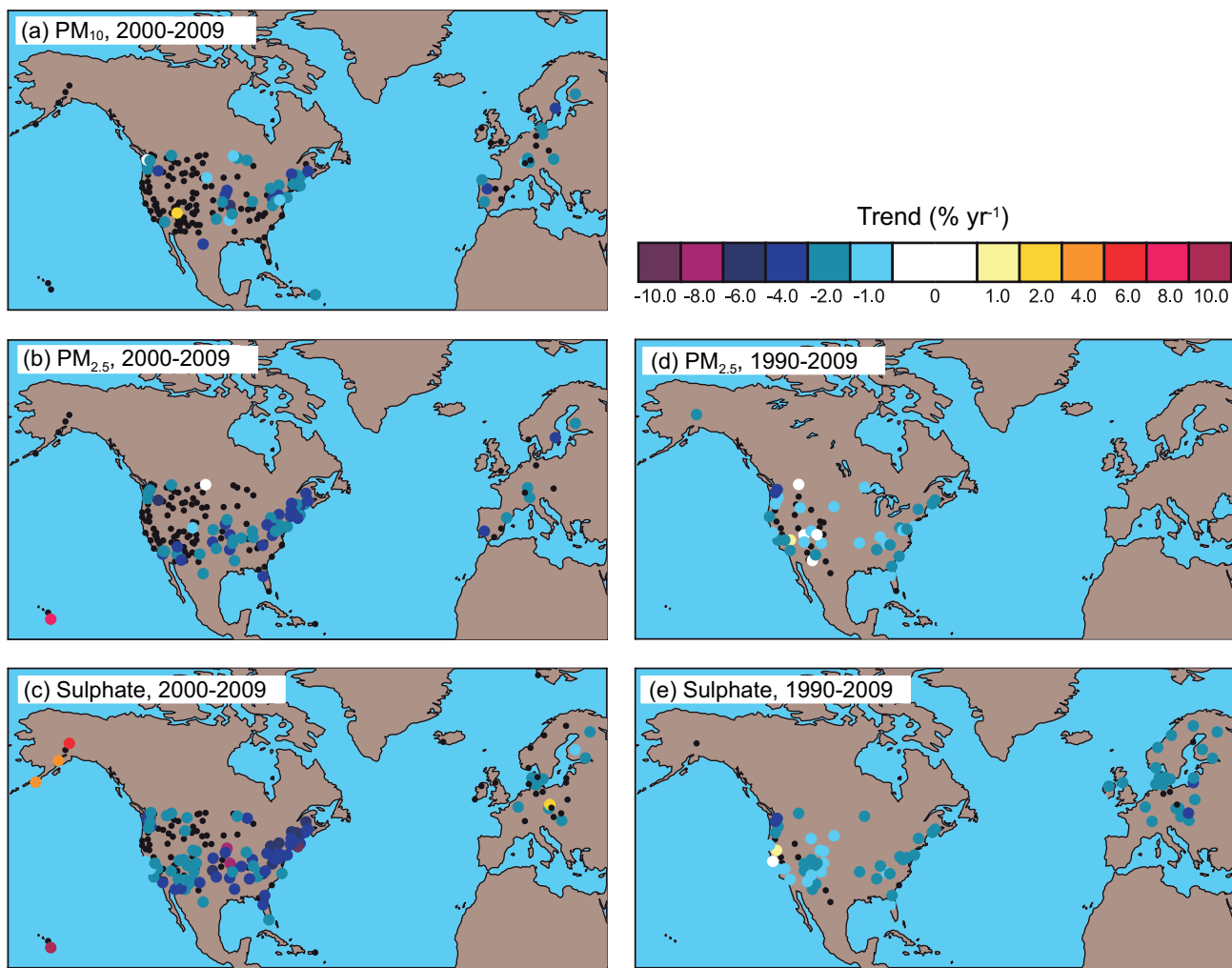


Figure 2.10 | Trends in particulate matter (PM_{10} and $\text{PM}_{2.5}$ with aerodynamic diameters <10 and $<2.5\text{ }\mu\text{m}$, respectively) and sulphate in Europe and USA for two overlapping periods 2000–2009 (a, b, c) and 1990–2009 (d, e). The trends are based on measurements from the EMEP (Torseth et al., 2012) and IMPROVE (Hand et al., 2011) networks in Europe and USA, respectively. Sites with significant trends (i.e., a trend of zero lies outside the 95% confidence interval) are shown in colour; black dots indicate sites with non-significant trends.

In Europe, strong downward trends are observed for PM_{10} , $\text{PM}_{2.5}$ and sulphate from the rural stations in the EMEP (European Monitoring and Evaluation Programme) network. For 2000–2009, $\text{PM}_{2.5}$ shows an average reduction of $3.9\% \text{ yr}^{-1}$ for the six stations with significant trends, while trends are not significant at seven other stations. Over 2000–2009, PM_{10} at 12 (out of 24) sites shows significant downward trend of on average $2.6\% \text{ yr}^{-1}$. Similarly sulphate strongly decreased at $3.1\% \text{ yr}^{-1}$ from 1990 to 2009 with 26 of 30 sites having significant reductions. The largest decrease occurred before 2000, while for 2000–2009, the trends were weaker and less robust. This is consistent with reported emission reductions of 65% from 1990 to 2000 and 28% from 2001 to 2009 (Yttri et al., 2011; Torseth et al., 2012). Model analysis (Pozzoli et al., 2011) attributed the trends in large part to emission changes.

In the USA, the largest reductions in PM and sulphate are observed in the 2000s, rather than the 1990s as in Europe. IMPROVE (U.S. Interagency Monitoring of Protected Visual Environments Network) $\text{PM}_{2.5}$ measurements (Hand et al., 2011) show significant downward trends averaging $4.0\% \text{ yr}^{-1}$ for 2000–2009 at sites with significant trends,

and $2.1\% \text{ yr}^{-1}$ at all sites, and PM_{10} decreases of $3.1\% \text{ yr}^{-1}$ for 2000–2009. Declines of $\text{PM}_{2.5}$ and SO_4^{2-} in Canada are very similar (Hidy and Pennell, 2010), with annual mean $\text{PM}_{2.5}$ at urban measurement sites decreasing by $3.6\% \text{ yr}^{-1}$ during 1985–2006 (Canada, 2012).

In the eastern and southwestern USA, IMPROVE data show strong sulphate declines, which range from 2 to $6\% \text{ yr}^{-1}$, with an average of $2.3\% \text{ yr}^{-1}$ for the sites with significant negative trends for 1990–2009. However, four IMPROVE sites show strong SO_4^{2-} increases from 2000 to 2009, amounting to $11.9\% \text{ yr}^{-1}$, at Hawaii (1225 m above sea level), and 4 to $7\% \text{ yr}^{-1}$ at three sites in southwest Alaska.

A recent study on long-term trends in aerosol optical properties from 24 globally distributed background sites (Collaud Coen et al., 2013) reported statistically significant trends at 16 locations, but the sign and magnitude of the trends varied largely with the aerosol property considered and geographical region (Table 2.3). Among the sites, this study reported strong increases in absorption and scattering coefficients in the free troposphere at Mauna Loa, Hawaii (3400 m above sea level), which is a regional feature also evident in the satellite-based AOD

Table 2.2 | Trend estimates for various aerosol variables reported in the literature, using data sets with at least 10 years of measurements. Unless otherwise noted, trends of individual stations were reported in % yr⁻¹, and 95% confidence intervals. The standard deviation (in parentheses) is determined from the individual trends of a set of regional stations.

Aerosol variable	Trend, % yr ⁻¹ (1 σ , standard deviation)	Period	Reference	Comments
Europe				
PM_{2.5}	−2.9 (1.31) −3.9 (0.87) ^b	2000–2009	(Adapted from Torseth et al., 2012) Regional background sites	13 sites available, 6 sites show statistically significant results. Average change was −0.37 and −0.52 ^b mg m ^{−3} yr ^{−1} .
PM₁₀	−1.9 (1.43) −2.6 (1.19) ^b	2000–2009		24 sites available, 12 sites show statistically significant results. Average change was −0.29 and −0.40 ^b mg m ^{−3} yr ^{−1} .
SO₄^{2−}	−3.0 (0.82) −3.1 (0.72) ^b	1990–2009		30 sites available, 26 sites show statistically significant results. Average change was −0.04 and −0.04 ^b mg m ^{−3} yr ^{−1} .
SO₄^{2−}	−1.5 (1.41) −2.0 (1.8) ^b	2000–2009		30 sites available, 10 sites show statistically significant results. Average change was −0.01 and −0.01 ^b mg m ^{−3} yr ^{−1} .
PM₁₀	−1.9	1991–2008	(Barmpadimos et al., 2012) Rural and urban sites	10 sites in Switzerland. The trend is adjusted for change in meteorology—unadjusted data did not differ strongly. The average change was −0.51 mg m ^{−3} yr ^{−1} .
USA				
PM_{2.5}	−2.1 (2.08) −4.0 (1.01) ^b	2000–2009	Adapted from (Hand et al., 2011) Regional background sites	153 sites available, 52 sites show statistically significant negative results. Only 1 site shows statistically positive trend.
PM_{2.5}	−1.5 (1.25) −2.1 (0.97) ^b	1990–2009		153 sites available, 39 sites show statistically significant results.
PM₁₀	−1.7 (2.00) −3.1 (1.65) ^b	2000–2009		154 sites available, 37 sites show statistically significant results.
SO₄^{2−}	−3.0 (2.86) −3.0 (0.62) ^b	2000–2009		154 sites available, 83 sites show statistically significant negative results. 4 sites showed statistical positive trend.
SO₄^{2−}	−2.0 (1.07) −2.3 (0.85) ^b	1990–2009		103 sites available, 41 sites show statistically significant results.
Total Carbon	−2.5 to −7.5	1989–2008	(Hand et al., 2011) Regional background sites	The trend interval includes about 50 sites mainly located along the East and West Coasts of the USA; fewer sites were situated in the central part of the continent.
Arctic				
EBC^a	−3.8 (0.7) ^c	1989–2008	(Hirdman et al., 2010)	Alert, Canada 62.3°W 82.5°N
SO₄^{2−}	−3.0 (0.6) ^c	1985–2006		
EBC^a	Not sig. ^c	1998–2008		Barrow, Alaska, 156.6°W 71.3° N
SO₄^{2−}	Not sig. ^c	1997–2008		
EBC^a	−9.0 (5.0) ^c	2002–2009		Zeppelin, Svalbard, 11.9°E 78.9° N
SO₄^{2−}	−1.9 (1.7) ^c	1990–2008		

Notes:

^a Equivalent black carbon.

^b Trend numbers indicated refer to the subset of stations with significant changes over time—generally in regions strongly influenced by anthropogenic emissions (Figure 2.10).

^c Trend values significant at 1% level.

trends (illustrated in Figure 2.9). Possible explanations for these changes include the influence of increasing Asian emissions and changes in clouds and removal processes. More and longer Asian time series, coupled with transport analyses, are needed to corroborate these findings. Aerosol number concentrations (Asmi et al., 2013) are declining significantly at most sites in Europe, North America, the Pacific and the Caribbean, but increasing at South Pole based on a study of 17 globally distributed remote sites.

Total carbon (= light absorbing carbon + organic carbon) measurements indicate highly significant downward trends between 2.5 and 7.5% yr⁻¹ along the east and west coasts of the USA, and smaller and less significant trends in other regions of the USA from 1989 to 2008 (Hand et al., 2011; Murphy et al., 2011).

In Europe, Torseth et al. (2012) suggest a slight reduction in elemental carbon concentrations at two stations from 2001 to 2009, subject to

large interannual variability. Collaud Coen et al. (2013) reported consistent negative trends in the aerosol absorption coefficient at stations in the continental USA, Arctic and Antarctica, but mostly insignificant trends in Europe over the last decade.

In the Arctic, changes in aerosol impact the atmosphere's radiative balance as well as snow and ice albedo. Similar to Europe and the USA, Hirdman et al. (2010) reported downward trends in equivalent black carbon and SO₄²⁻ for two out of total three Arctic stations and attributed them to emission changes.

In summary, declining AOD in Europe and North America is corroborated by very likely downward trends in ground-based *in situ* particulate matter measurements since the mid-1980s. Robust evidence from around 200 regional background sites with *in situ* ground based aerosol measurements indicate downward trends in the last two decades of PM_{2.5} in parts of Europe (2 to 6% yr⁻¹) and the USA (1 to 2.5% yr⁻¹),

Table 2.3 | Summary table of aerosol optical property trends reported in the literature, using data sets with at least 10 years of measurements. Otherwise as in Table 2.2.

Region	Trend, % yr ⁻¹ (1σ, standard deviation)	Period	Reference	Comments
Scattering coefficient				
Europe (4/1)	+0.6 (1.9) +2.7 ^a	2001–2010	Adapted from (Collaud Coen et al., 2013) Regional background sites	Trend study including 24 regional background sites with more than 10 years of observations. Regional averages for last 10 years are included here. Values in parenthesis show total number of sites/number of sites with significant trend.
USA (14/10)	-2.0 (2.5) -2.9 (2.4) ^a			
Mauna Loa (1/1)	+2.7			
Arctic (1/0)	+2.4			
Antarctica (1/0)	+2.5			
Absorption coefficient				
Europe (3/0)	+0.3 (0.4)	2001–2010	Adapted from (Collaud Coen et al., 2013) Regional background sites	Trend study of aerosol optical properties including 24 regional background sites with more than 10 years of observations. Regional averages for last 10 years are included here. Values in parenthesis show total number of sites and number of sites with significant trend.
USA (1/1)	-2.0			
Mauna Loa (1/1)	+9.0			
Arctic (1/1)	-6.5			
Antarctica (1/1)	-0.1			
Particle number concentration				
Europe (4/2)	-0.9 (1.8) -2.3 (1.0) ^a	2001–2010	Adapted from (Asmi et al., 2013) Regional background sites	Trend study of particle number concentration (N) and size distribution including 17 regional background sites. Regional averages of particle number concentration for last 10 years are included here. Values in parentheses show total number of sites and number of sites with significant trend.
North America and Caribbean (3/3)	-5.3 (2.8) -6.6 (1.1) ^a			
Mauna Loa (1/1)	-3.5			
Arctic (1/0)	-1.3			
Antarctica (2/2)	+2.7 (1.4)			

Notes:

^a Trend numbers indicated refer to the subset of stations with significant changes over time—generally in regions strongly influenced by anthropogenic emissions (Figure 2.10).

Box 2.2 | Quantifying Changes in the Mean: Trend Models and Estimation

Many statistical methods exist for estimating trends in environmental time series (see Chandler and Scott, 2011 for a review). The assessment of long-term changes in historical climate data requires trend models that are transparent and robust, and that can provide credible uncertainty estimates.

Linear Trends

Historical climate trends are frequently described and quantified by estimating the linear component of the change over time (e.g., AR4). Such linear trend modelling has broad acceptance and understanding based on its frequent and widespread use in the published research assessed in this report, and its strengths and weaknesses are well known (von Storch and Zwiers, 1999; Wilks, 2006). Challenges exist in assessing the uncertainty in the trend and its dependence on the assumptions about the sampling distribution (Gaussian or otherwise), uncertainty in the data, dependency models for the residuals about the trend line, and treating their serial correlation (Von Storch, 1999; Santer et al., 2008).

The quantification and visualization of temporal changes are assessed in this chapter using a linear trend model that allows for first-order autocorrelation in the residuals (Santer et al., 2008; Supplementary Material 2.SM.3). Trend slopes in such a model are the same as ordinary least squares trends; uncertainties are computed using an approximate method. The 90% confidence interval quoted is solely that arising from sampling uncertainty in estimating the trend. Structural uncertainties, to the extent sampled, are apparent from the range of estimates from different data sets. Parametric and other remaining uncertainties (Box 2.1), for which estimates are provided with some data sets, are not included in the trend estimates shown here, so that the same method can be applied to all data sets considered.

Nonlinear Trends

There is no *a priori* physical reason why the long-term trend in climate variables should be linear in time. Climatic time series often have trends for which a straight line is not a good approximation (e.g., Seidel and Lanzante, 2004). The residuals from a linear fit in time often do not follow a simple autoregressive or moving average process, and linear trend estimates can easily change when recalculated (*continued on next page*)

Box 2.2 (continued)

for shorter or longer time periods or when new data are added. When linear trends for two parts of a longer time series are calculated separately, the trends calculated for two shorter periods may be very different (even in sign) from the trend in the full period, if the time series exhibits significant nonlinear behavior in time (Box 2.2, Table 1).

Many methods have been developed for estimating the long-term change in a time series without assuming that the change is linear in time (e.g., Wu et al., 2007; Craigmire and Guttorm, 2011). Box 2.2, Figure 1 shows the linear least squares and a nonlinear trend fit to the GMST values from the HadCRUT4 data set (Section 2.4.3). The nonlinear trend is obtained by fitting a smoothing spline trend (Wood, 2006; Scinocca et al., 2010) while allowing for first-order autocorrelation in the residuals (Supplementary Material 2.SM.3). The results indicate that there are significant departures from linearity in the trend estimated this way.

Box 2.2, Table 1 shows estimates of the change in the GMST from the two methods. The methods give similar estimates with 90% confidence intervals that overlap one another. Smoothing methods that do not assume the trend is linear can provide useful information on the structure of change that is not as well treated with linear fits. The linear trend fit is used in this chapter because it can be applied consistently to all the data sets, is relatively simple, transparent and easily comprehended, and is frequently used in the published research assessed here.

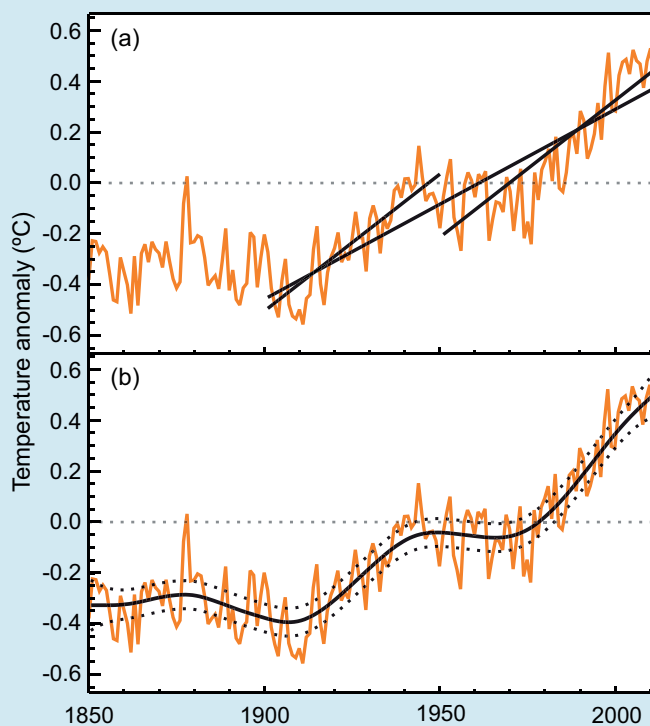
Box 2.2, Table 1 | Estimates of the mean change in global mean surface temperature (GMST) between 1901 and 2012, 1901 and 1950, and 1951 and 2012, obtained from the linear (least squares) and nonlinear (smoothing spline) trend models. Half-widths of the 90% confidence intervals are also provided for the estimated changes from the two trend methods.

Method	Trends in °C per decade		
	1901–2012	1901–1950	1951–2012
Least squares	0.075 ± 0.013	0.107 ± 0.026	0.106 ± 0.027
Smoothing spline	0.081 ± 0.010	0.070 ± 0.016	0.090 ± 0.018

and also for SO_4^{2-} (2 to 5% yr^{-1}). The strongest decreases were in the 1990s in Europe and in the 2000s in the USA. There is robust evidence for downward trends of light absorbing aerosol in the USA and the Arctic, while elsewhere in the world *in situ* time series are lacking or not long enough to reach statistical significance.

2.3 Changes in Radiation Budgets

The radiation budget of the Earth is a central element of the climate system. On average, radiative processes warm the surface and cool the atmosphere, which is balanced by the hydrological cycle and sensible



Box 2.2, Figure 1 | (a) Global mean surface temperature (GMST) anomalies relative to a 1961–1990 climatology based on HadCRUT4 annual data. The straight black lines are least squares trends for 1901–2012, 1901–1950 and 1951–2012. (b) Same data as in (a), with smoothing spline (solid curve) and the 90% confidence interval on the smooth curve (dashed lines). Note that the (strongly overlapping) 90% confidence intervals for the least square lines in (a) are omitted for clarity. See Figure 2.20 for the other two GMST data products.

heating. Spatial and temporal energy imbalances due to radiation and latent heating produce the general circulation of the atmosphere and oceans. Anthropogenic influence on climate occurs primarily through perturbations of the components of the Earth radiation budget.

The radiation budget at the top of the atmosphere (TOA) includes the absorption of solar radiation by the Earth, determined as the difference between the incident and reflected solar radiation at the TOA, as well as the thermal outgoing radiation emitted to space. The surface radiation budget takes into account the solar fluxes absorbed at the Earth's surface, as well as the upward and downward thermal radiative fluxes emitted by the surface and atmosphere, respectively. In view of new

observational evidence since AR4, the mean state as well as multi-decadal changes of the surface and TOA radiation budgets are assessed in the following.

2.3.1 Global Mean Radiation Budget

Since AR4, knowledge on the magnitude of the radiative energy fluxes in the climate system has improved, requiring an update of the global annual mean energy balance diagram (Figure 2.11). Energy exchanges between Sun, Earth and Space are observed from space-borne platforms such as the Clouds and the Earth's Radiant Energy System (CERES, Wielicki et al., 1996) and the Solar Radiation and Climate Experiment (SORCE, Kopp and Lawrence, 2005) which began data collection in 2000 and 2003, respectively. The total solar irradiance (TSI) incident at the TOA is now much better known, with the SORCE Total Irradiance Monitor (TIM) instrument reporting uncertainties as low as 0.035%, compared to 0.1% for other TSI instruments (Kopp et al., 2005). During the 2008 solar minimum, SORCE/TIM observed a solar irradiance of $1360.8 \pm 0.5 \text{ W m}^{-2}$ compared to $1365.5 \pm 1.3 \text{ W m}^{-2}$ for instruments launched prior to SORCE and still operating in 2008 (Section 8.4.1.1). Kopp and Lean (2011) conclude that the SORCE/TIM value of TSI is the most credible value because it is validated by a National Institute of Standards and Technology calibrated cryogenic radiometer. This revised TSI estimate corresponds to a solar irradiance close to 340 W m^{-2} globally averaged over the Earth's sphere (Figure 2.11).

The estimate for the reflected solar radiation at the TOA in Figure 2.11, 100 W m^{-2} , is a rounded value based on the CERES Energy Balanced and Filled (EBAF) satellite data product (Loeb et al., 2009, 2012b) for the period 2001–2010. This data set adjusts the solar and thermal TOA fluxes within their range of uncertainty to be consistent with independent estimates of the global heating rate based on *in situ* ocean observations (Loeb et al., 2012b). This leaves 240 W m^{-2} of solar radiation absorbed by the Earth, which is nearly balanced by thermal emission to space of about 239 W m^{-2} (based on CERES EBAF), considering a global heat storage of 0.6 W m^{-2} (imbalance term in Figure 2.11) based on Argo data from 2005 to 2010 (Hansen et al., 2011; Loeb et al., 2012b; Box 3.1). The stated uncertainty in the solar reflected TOA fluxes from CERES due to uncertainty in absolute calibration alone is about 2% (2-sigma), or equivalently 2 W m^{-2} (Loeb et al., 2009). The uncertainty of the outgoing thermal flux at the TOA as measured by CERES due to calibration is $\sim 3.7 \text{ W m}^{-2}$ (2σ). In addition to this, there is uncertainty in removing the influence of instrument spectral response on measured radiance, in radiance-to-flux conversion, and in time-space averaging, which adds up to another 1 W m^{-2} (Loeb et al., 2009).

The components of the radiation budget at the surface are generally more uncertain than their counterparts at the TOA because they cannot be directly measured by passive satellite sensors and surface measurements are not always regionally or globally representative. Since AR4, new estimates for the downward thermal infrared (IR) radiation at

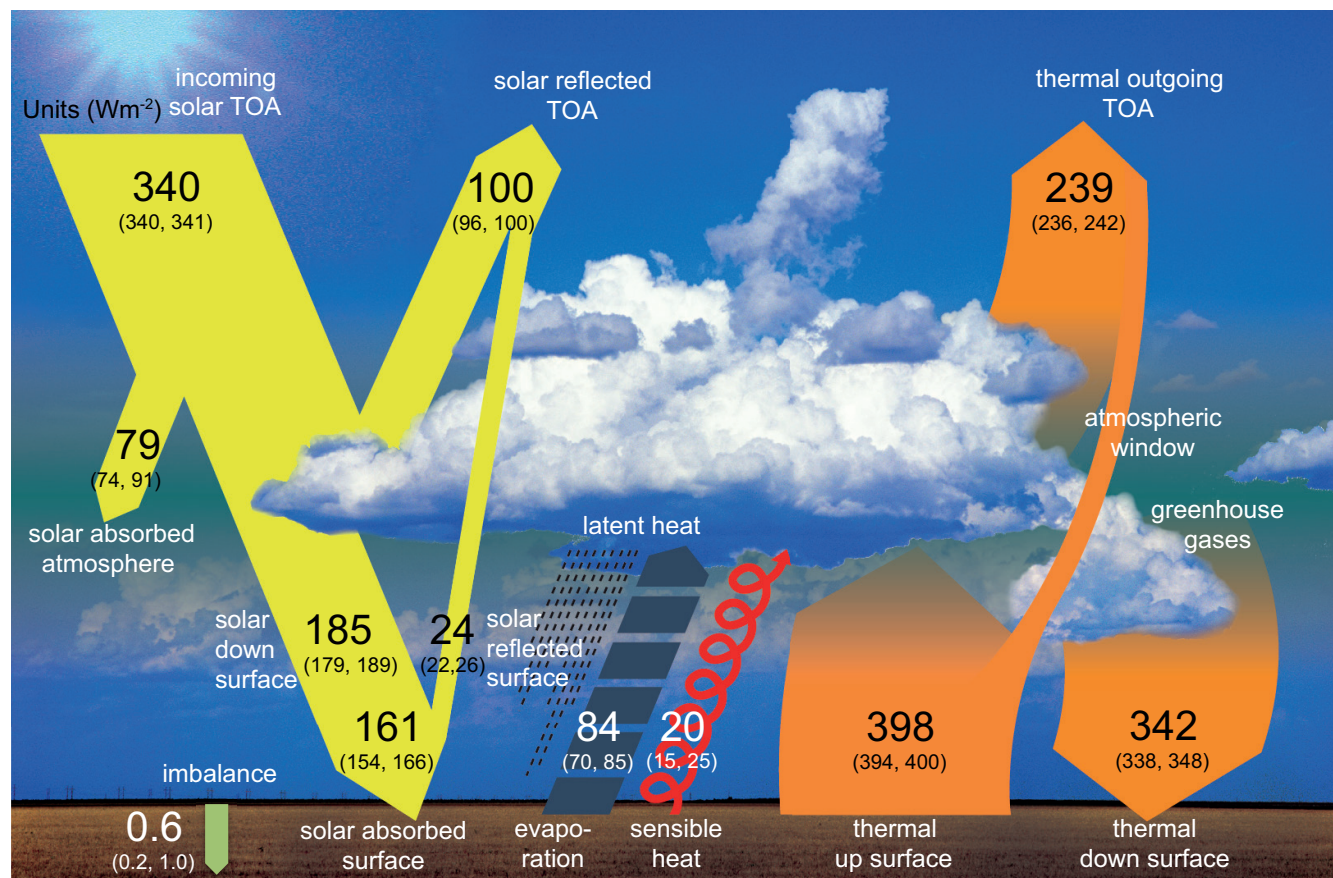


Figure 2.11: | Global mean energy budget under present-day climate conditions. Numbers state magnitudes of the individual energy fluxes in W m^{-2} , adjusted within their uncertainty ranges to close the energy budgets. Numbers in parentheses attached to the energy fluxes cover the range of values in line with observational constraints. (Adapted from Wild et al., 2013.)

the surface have been established that incorporate critical information on cloud base heights from space-borne radar and lidar instruments (L'Ecuyer et al., 2008; Stephens et al., 2012a; Kato et al., 2013). In line with studies based on direct surface radiation measurements (Wild et al., 1998, 2013) these studies propose higher values of global mean downward thermal radiation than presented in previous IPCC assessments and typically found in climate models, exceeding 340 W m^{-2} (Figure 2.11). This aligns with the downward thermal radiation in the ERA-Interim and ERA-40 reanalyses (Box 2.3), of 341 and 344 W m^{-2} , respectively (Berrisford et al., 2011). Estimates of global mean downward thermal radiation computed as a residual of the other terms of the surface energy budget (Kiehl and Trenberth, 1997; Trenberth et al., 2009) are lower (324 to 333 W m^{-2}), highlighting remaining uncertainties in estimates of both radiative and non-radiative components of the surface energy budget.

2

Estimates of absorbed solar radiation at the Earth's surface include considerable uncertainty. Published global mean values inferred from satellite retrievals, reanalyses and climate models range from below 160 W m^{-2} to above 170 W m^{-2} . Recent studies taking into account surface observations as well as updated spectroscopic parameters and continuum absorption for water vapor favour values towards the lower bound of this range, near 160 W m^{-2} , and an atmospheric solar absorption around 80 W m^{-2} (Figure 2.11) (Kim and Ramanathan, 2008; Trenberth et al., 2009; Kim and Ramanathan, 2012; Trenberth and Fasullo, 2012b; Wild et al., 2013). The ERA-Interim and ERA-40 reanalyses further support an atmospheric solar absorption of this magnitude (Berrisford et al., 2011). Latest satellite-derived estimates constrained by CERES now also come close to these values (Kato et al., in press). Recent independently derived surface radiation estimates favour therefore a global mean surface absorbed solar flux near 160 W m^{-2} and a downward thermal flux slightly above 340 W m^{-2} , respectively (Figure 2.11).

The global mean latent heat flux is required to exceed 80 W m^{-2} to close the surface energy balance in Figure 2.11, and comes close to the 85 W m^{-2} considered as upper limit by Trenberth and Fasullo (2012b) in view of current uncertainties in precipitation retrieval in the Global Precipitation Climatology Project (GPCP, Adler et al., 2012) (the latent heat flux corresponds to the energy equivalent of evaporation, which globally equals precipitation; thus its magnitude may be constrained by global precipitation estimates). This upper limit has recently been challenged by Stephens et al. (2012b). The emerging debate reflects potential remaining deficiencies in the quantification of the radiative and non-radiative energy balance components and associated uncertainty ranges, as well as in the consistent representation of the global mean energy and water budgets (Stephens et al., 2012b; Trenberth and Fasullo, 2012b; Wild et al., 2013). Relative uncertainty in the globally averaged sensible heat flux estimate remains high owing to the very limited direct observational constraints (Trenberth et al., 2009; Stephens et al., 2012b).

In summary, newly available observations from both space-borne and surface-based platforms allow a better quantification of the Global Energy Budget, even though notable uncertainties remain, particularly in the estimation of the non-radiative surface energy balance components.

2.3.2 Changes in Top of the Atmosphere Radiation Budget

While the previous section emphasized the temporally-averaged state of the radiation budget, the focus in the following is on the temporal (multi-decadal) changes of its components. Variations in TSI are discussed in Section 8.4.1. AR4 reported large changes in tropical TOA radiation between the 1980s and 1990s based on observations from the Earth Radiation Budget Satellite (ERBS) (Wielicki et al., 2002; Wong et al., 2006). Although the robust nature of the large decadal changes in tropical radiation remains to be established, several studies have suggested links to changes in atmospheric circulation (Allan and Slingo, 2002; Chen et al., 2002; Clement and Soden, 2005; Merrifield, 2011) (Section 2.7).

Since AR4, CERES enabled the extension of satellite records of TOA fluxes into the 2000s (Loeb et al., 2012b). The extended records from CERES suggest no noticeable trends in either the tropical or global radiation budget during the first decade of the 21st century (e.g., Andronova et al., 2009; Harries and Belotti, 2010; Loeb et al., 2012a, 2012b). Comparisons between ERBS/CERES thermal radiation and that derived from the NOAA High Resolution Infrared Radiation Sounder (HIRS) (Lee et al., 2007) show good agreement until approximately 1998, corroborating the rise of 0.7 W m^{-2} between the 1980s and 1990s reported in AR4. Thereafter the HIRS thermal fluxes show much higher values, likely due to changes in the channels used for HIRS/3 instruments launched after October 1998 compared to earlier HIRS instruments (Lee et al., 2007).

On a global scale, interannual variations in net TOA radiation and ocean heating rate (OHR) should correspond, as oceans have a much larger effective heat capacity than land and atmosphere, and therefore serve as the main reservoir for heat added to the Earth–atmosphere system (Box 3.1). Wong et al. (2006) showed that interannual variations in these two data sources are in good agreement for 1992–2003. In the ensuing 5 years, however, Trenberth and Fasullo (2010) note that the two diverge with ocean *in situ* measurements (Levitus et al., 2009), indicating a decline in OHR, in contrast to expectations from the observed net TOA radiation. The divergence after 2004 is referred to as "missing energy" by Trenberth and Fasullo (2012b), who further argue that the main sink of the missing energy likely occurs at ocean depths below 275 m. Loeb et al. (2012b) compared interannual variations in CERES net radiation with OHRs derived from three independent ocean heat content anomaly analyses and included an error analysis of both CERES and the OHRs. They conclude that the apparent decline in OHR is not statistically robust and that differences between interannual variations in OHR and satellite net TOA flux are within the uncertainty of the measurements (Figure 2.12). They further note that between January 2001 and December 2012, the Earth has been steadily accumulating energy at a rate of $0.50 \pm 0.43 \text{ W m}^{-2}$ (90% CI). Hansen et al. (2011) obtained a similar value for 2005–2010 using an independent analysis of the ocean heat content anomaly data (von Schuckmann and Le Traon, 2011). The variability in the Earth's energy imbalance is strongly influenced by ocean circulation changes relating to the ENSO (Box 2.5); during cooler La Niña years (e.g., 2009) less thermal radiation is emitted and the climate system gains heat while the reverse is true for warmer El Niño years (e.g., 2010) (Figure 2.12).

In summary, satellite records of TOA radiation fluxes have been substantially extended since AR4. It is *unlikely* that significant trends exist in global and tropical radiation budgets since 2000. Interannual variability in the Earth's energy imbalance related to ENSO is consistent with ocean heat content records within observational uncertainty.

2.3.3 Changes in Surface Radiation Budget

2.3.3.1 Surface Solar Radiation

Changes in radiative fluxes at the surface can be traced further back in time than the satellite-based TOA fluxes, although only at selected terrestrial locations where long-term records exist. Monitoring of radiative fluxes from land-based stations began on a widespread basis in the mid-20th century, predominantly measuring the downward solar component, also known as global radiation or surface solar radiation (SSR).

AR4 reported on the first indications for substantial decadal changes in observational records of SSR. Specifically, a decline of SSR from the beginning of widespread measurements in the 1950s until the mid-1980s has been observed at many land-based sites (popularly known as 'global dimming'; Stanhill and Cohen, 2001; Liepert, 2002), as well as a partial recovery from the 1980s onward ('brightening'; Wild et al., 2005) (see the longest available SSR series of Stockholm, Sweden, in Figure 2.13 as an illustrative example).

Since AR4, numerous studies have substantiated the findings of significant decadal SSR changes observed both at worldwide distributed terrestrial sites (Dutton et al., 2006; Wild et al., 2008; Gilgen et al., 2009; Ohmura, 2009; Wild, 2009 and references therein) as well as in specific regions. In Europe, Norris and Wild (2007) noted a dimming between 1971 and 1986 of 2.0 to 3.1 W m⁻² per decade and subsequent brightening of 1.1 to 1.4 W m⁻² per decade from 1987 to 2002 in a pan-European time series comprising 75 sites. Similar tendencies were found at sites in northern Europe (Stjern et al., 2009), Estonia (Russak, 2009) and Moscow (Abakumova et al., 2008). Chiachio and Wild (2010) pointed out that dimming and subsequent brightening in Europe is seen mainly in spring and summer. Brightening in Europe from the 1980s onward was further documented at sites in Switzerland, Germany, France, the Benelux, Greece, Eastern Europe and the Iberian Peninsula (Ruckstuhl et al., 2008; Wild et al., 2009; Zerefos et al., 2009; Sanchez-Lorenzo et al., 2013). Concurrent brightening of 2 to 8 W m⁻² per decade was also noted at continental sites in the USA (Long et al., 2009; Riihimaki et al., 2009; Augustine and Dutton, 2013). The general pattern of dimming and consecutive brightening was further found at numerous sites in Japan (Norris and Wild, 2009; Ohmura, 2009; Kudo et al., 2011) and in the SH in New Zealand (Liley, 2009). Analyses of observations from sites in China confirmed strong declines in SSR from the 1960s to 1980s on the order of 2 to 8 W m⁻² per decade, which also did not persist in the 1990s (Che et al., 2005; Liang and Xia, 2005; Qian et al., 2006; Shi et al., 2008; Norris and Wild, 2009; Xia, 2010a). On the other hand, persistent dimming since the mid-20th

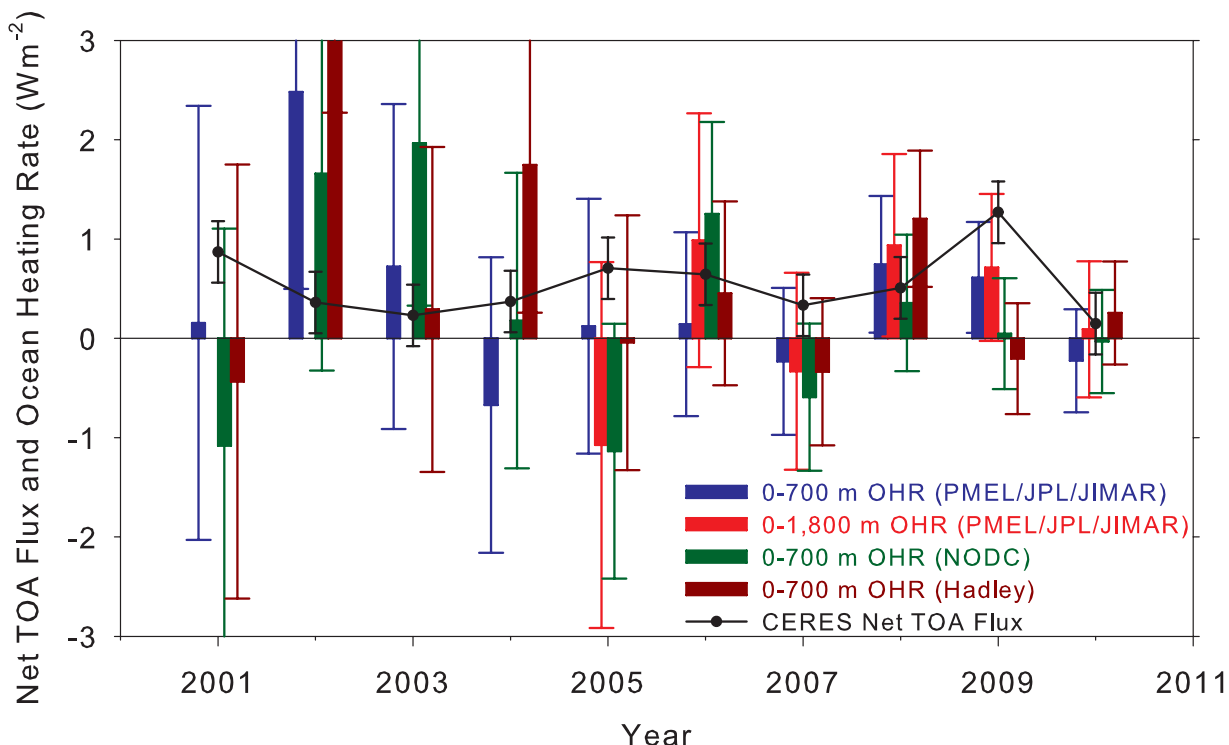


Figure 2.12 | Comparison of net top of the atmosphere (TOA) flux and upper ocean heating rates (OHRs). Global annual average (July to June) net TOA flux from CERES observations (based on the EBAF-TOA_Ed2.6r product) (black line) and 0–700 (blue) and 0–1,800 m (red) OHR from the Pacific Marine Environmental Laboratory/Jet Propulsion Laboratory/Joint Institute for Marine and Atmospheric Research (PMEL/JPL/JIMAR), 0–700 m OHR from the National Oceanic Data Center (NODC) (green; Levitus et al., 2009), and 0–700 m OHR from the Hadley Center (brown; Palmer et al., 2007). The length of the coloured bars corresponds to the magnitude of OHR. Thin vertical lines are error bars, corresponding to the magnitude of uncertainties. Uncertainties for all annual OHR are given at one standard error derived from ocean heat content anomaly uncertainties (Lyman et al., 2010). CERES net TOA flux uncertainties are given at the 90% confidence level determined following Loeb et al. (2012b). (Adapted from Loeb et al., 2012b.)

century with no evidence for a trend reversal was noted at sites in India (Wild et al., 2005; Kumari et al., 2007; Kumari and Goswami, 2010; Soni et al., 2012) and in the Canadian Prairie (Cutforth and Judiesch, 2007). Updates on latest SSR changes observed since 2000 provide a less coherent picture (Wild, 2012). They suggest a continuation of brightening at sites in Europe, USA, and parts of Asia, a levelling off at sites in Japan and Antarctica, and indications for a renewed dimming in parts of China (Wild et al., 2009; Xia, 2010a).

The longest observational SSR records, extending back to the 1920s and 1930s at a few sites in Europe, further indicate some brightening during the first half of the 20th century, known as ‘early brightening’ (cf. Figure 2.13) (Ohmura, 2009; Wild, 2009). This suggests that the decline in SSR, at least in Europe, was confined to a period between the 1950s and 1980s.

2

A number of issues remain, such as the quality and representativeness of some of the SSR data as well as the large-scale significance of the phenomenon (Wild, 2012). The historic radiation records are of variable quality and rigorous quality control is necessary to avoid spurious trends (Dutton et al., 2006; Shi et al., 2008; Gilgen et al., 2009; Tang et al., 2011; Wang et al., 2012e; Sanchez-Lorenzo et al., 2013). Since the mid-1990s, high-quality data are becoming increasingly available from new sites of the Baseline Surface Radiation Network (BSRN) and Atmospheric Radiation Measurement (ARM) Program, which allow the determination of SSR variations with unprecedented accuracy (Ohmura et al., 1998). Alpert et al. (2005) and Alpert and Kishcha (2008) argued that the observed SSR decline between 1960 and 1990 was larger in densely populated than in rural areas. The magnitude of this ‘urbanization effect’ in the radiation data is not yet well quantified. Dimming and brightening is, however, also notable at remote and rural sites (Dutton et al., 2006; Karnieli et al., 2009; Liley, 2009; Russak, 2009; Wild, 2009; Wang et al., 2012d).

Globally complete satellite estimates have been available since the early 1980s (Hatzianastassiou et al., 2005; Pinker et al., 2005; Hinkelmann et al., 2009). Because satellites do not directly measure the surface fluxes, they have to be inferred from measurable TOA signals using empirical or physical models to remove atmospheric perturbations. Available satellite-derived products qualitatively agree on a brightening from the mid-1980s to 2000 averaged globally as well as over oceans, on the order of 2 to 3 W m⁻² per decade (Hatzianastassiou et al., 2005; Pinker et al., 2005; Hinkelmann et al., 2009). Averaged over land, however, trends are positive or negative depending on the respective satellite product (Wild, 2009). Knowledge of the decadal variation of aerosol burdens and optical properties, required in satellite retrievals of SSR and considered relevant for dimming/brightening particularly over land, is very limited (Section 2.2.3). Extensions of satellite-derived SSR beyond 2000 indicate tendencies towards a renewed dimming at the beginning of the new millennium (Hinkelmann et al., 2009; Hatzianastassiou et al., 2012).

Reconstructions of SSR changes from more widely measured meteorological variables can help to increase their spatial and temporal coverage. Multi-decadal SSR changes have been related to observed changes in sunshine duration, atmospheric visibility, diurnal temperature range (DTR; Section 2.4.1.2) and pan evaporation (Section 2.5.3).

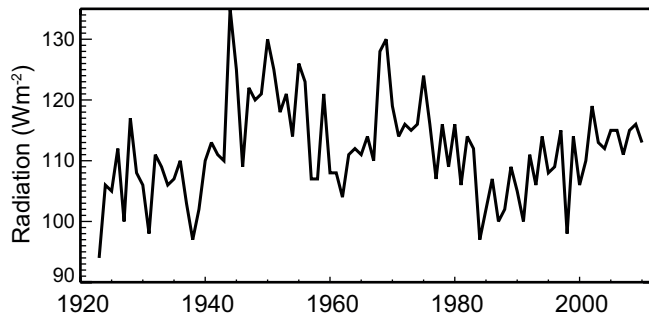


Figure 2.13 | Annual mean Surface Solar Radiation (SSR) as observed at Stockholm, Sweden, from 1923 to 2010. Stockholm has the longest SSR record available worldwide. (Updated from Wild (2009) and Ohmura (2009).)

Overall, these proxies provide independent evidence for the existence of large-scale multi-decadal variations in SSR. Specifically, widespread observations of declines in pan evaporation from the 1950s to the 1980s were related to SSR dimming amongst other factors (Roderick and Farquhar, 2002). The observed decline in DTR over global land surfaces from the 1950s to the 1980s (Section 2.4.1.2), and its stabilisation thereafter fits to a large-scale dimming and subsequent brightening, respectively (Wild et al., 2007). Widespread brightening after 1980 is further supported by reconstructions from sunshine duration records (Wang et al., 2012e). Over Europe, SSR dimming and subsequent brightening is consistent with concurrent declines and increases in sunshine duration (Sanchez-Lorenzo et al., 2008), evaporation in energy limited environments (Teuling et al., 2009), visibility records (Vautard et al., 2009; Wang et al., 2009b) and DTR (Makowski et al., 2009). The early brightening in the 1930s and 1940s seen in a few European SSR records is in line with corresponding changes in sunshine duration and DTR (Sanchez-Lorenzo et al., 2008; Wild, 2009; Sanchez-Lorenzo and Wild, 2012). In China, the levelling off in SSR in the 1990s after decades of decline coincides with similar tendencies in the pan evaporation records, sunshine duration and DTR (Liu et al., 2004a; Liu et al., 2004b; Qian et al., 2006; Ding et al., 2007; Wang et al., 2012d). Dimming up to the 1980s and subsequent brightening is also indicated in a set of 237 sunshine duration records in South America (Raichijk, 2011).

2.3.3.2 Surface Thermal and Net Radiation

Thermal radiation, also known as longwave, terrestrial or far-IR radiation is sensitive to changes in atmospheric GHGs, temperature and humidity. Long-term measurements of the thermal surface components as well as surface net radiation are available at far fewer sites than SSR. Downward thermal radiation observations started to become available during the early 1990s at a limited number of globally distributed terrestrial sites. From these records, Wild et al. (2008) determined an overall increase of 2.6 W m⁻² per decade over the 1990s, in line with model projections and the expectations of an increasing greenhouse effect. Wang and Liang (2009) inferred an increase in downward thermal radiation of 2.2 W m⁻² per decade over the period 1973–2008 from globally available terrestrial observations of temperature, humidity and cloud fraction. Prata (2008) estimated a slightly lower increase of 1.7 W m⁻² per decade for clear sky conditions over the earlier period 1964–1990, based on observed temperature and

humidity profiles from globally distributed land-based radiosonde stations and radiative transfer calculations. Philipona et al. (2004; 2005) and Wacker et al. (2011) noted increasing downward thermal fluxes recorded in the Swiss Alpine Surface Radiation Budget (ASRB) network since the mid-1990s, corroborating an increasing greenhouse effect. For mainland Europe, Philipona et al. (2009) estimated an increase of downward thermal radiation of 2.4 to 2.7 W m⁻² per decade for the period 1981–2005.

There is limited observational information on changes in surface net radiation, in large part because measurements of upward fluxes at the surface are made at only a few sites and are not spatially representative. Wild et al. (2004, 2008) inferred a decline in land surface net radiation on the order of 2 W m⁻² per decade from the 1960s to the 1980s, and an increase at a similar rate from the 1980s to 2000, based on estimated changes of the individual radiative components that constitute the surface net radiation. Philipona et al. (2009) estimated an increase in surface net radiation of 1.3 to 2 W m⁻² per decade for central Europe and the Alps between 1981 and 2005.

2.3.3.3 Implications from Observed Changes in Related Climate Elements

The observed multi-decadal SSR variations cannot be explained by changes in TSI, which are an order of magnitude smaller (Willson and Mordvinov, 2003). They therefore have to originate from alterations in the transparency of the atmosphere, which depends on the presence of clouds, aerosols and radiatively active gases (Kvalevag and Myhre, 2007; Kim and Ramanathan, 2008). Cloud cover changes (Section 2.5.7) effectively modulate SSR on an interannual basis, but their contribution to the longer-term SSR trends is ambiguous. Although cloud cover changes were found to explain the trends in some areas (e.g., Liley, 2009), this is not always the case, particularly in relatively polluted regions (Qian et al., 2006; Norris and Wild, 2007, 2009; Wild, 2009; Kudo et al., 2012). SSR dimming and brightening has also been observed under cloudless atmospheres at various locations, pointing to a prominent role of atmospheric aerosols (Wild et al., 2005; Qian et al., 2007; Ruckstuhl et al., 2008; Sanchez-Lorenzo et al., 2009; Wang et al., 2009b; Zerefos et al., 2009).

Box 2.3 | Global Atmospheric Reanalyses

Dynamical reanalyses are increasingly used for assessing weather and climate phenomena. Given their more frequent use in this assessment compared to AR4, their characteristics are described in more detail here.

Reanalyses are distinct from, but complement, more ‘traditional’ statistical approaches to assessing the raw observations. They aim to produce continuous reconstructions of past atmospheric states that are consistent with all observations as well as with atmospheric physics as represented in a numerical weather prediction model, a process termed data assimilation. Unlike real-world observations, reanalyses are uniform in space and time and provide non-observable variables (e.g., potential vorticity).

Several groups are actively pursuing reanalysis development at the global scale, and many of these have produced several generations of reanalyses products (Box 2.3, Table 1). Since the first generation of reanalyses produced in the 1990s, substantial development has taken place. The NASA Modern-Era Retrospective Analysis for Research and Applications (MERRA) and ERA-Interim reanalyses show improved tropical precipitation and hence better represent the global hydrological cycle (Dee et al., 2011b). The NCEP/CFSR reanalysis (*continued on next page*)

Box 2.3, Table 1 | Overview of global dynamical reanalysis data sets (ranked by start year; the period extends to present if no end year is provided). A further description of reanalyses and their technical derivation is given in pp. S33–35 of Blunden et al. (2011). Approximate resolution is calculated as 1000 km * 20/N (with N denoting the spectral truncation, Laprise, 1992).

Institution	Reanalysis	Period	Approximate Resolution at Equator	Reference
Cooperative Institute for Research in Environmental Sciences (CIRES), National Oceanic and Atmospheric Administration (NOAA), USA	20th Century Reanalysis, Vers. 2 (20CR)	1871–2010	320 km	Compo et al. (2011)
National Centers for Environmental Prediction (NCEP) and National Center for Atmospheric Research (NCAR), USA	NCEP/NCAR R1 (NNR)	1948–	320 km	Kistler et al. (2001)
European Centre for Medium-Range Weather Forecasts (ECMWF)	ERA-40	1957–2002	125 km	Uppala et al. (2005)
Japan Meteorological Agency (JMA)	JRA-55	1958–	60 km	Ebita et al. (2011)
National Centers for Environmental Prediction (NCEP), US Department of Energy, USA	NCEP/DOE R2	1979–	320 km	Kanamitsu et al. (2002)
Japan Meteorological Agency (JMA)	JRA-25	1979–	190 km	Onogi et al. (2007)
National Aeronautics and Space Administration (NASA), USA	MERRA	1979–	75 km	Rienecker et al. (2011)
European Centre for Medium-Range Weather Forecasts (ECMWF)	ERA-Interim	1979–	80 km	Dee et al. (2011b)
National Centers for Environmental Prediction (NCEP), USA	CFSR	1979–	50 km	Saha et al. (2010)

Box 2.3 (continued)

uses a coupled ocean–atmosphere–land–sea–ice model (Saha et al., 2010). The 20th Century Reanalyses (20CR, Compo et al., 2011) is a 56-member ensemble and covers 140 years by assimilating only surface and sea level pressure (SLP) information. This variety of groups and approaches provides some indication of the robustness of reanalyses when compared. In addition to the global reanalyses, several regional reanalyses exist or are currently being produced.

Reanalyses products provide invaluable information on time scales ranging from daily to interannual variability. However, they may often be unable to characterize long-term trends (Trenberth et al., 2011). Although reanalyses projects by definition use a ‘frozen’ assimilation system, there are many other sources of potential errors. In addition to model biases, changes in the observational systems (e.g., coverage, introduction of satellite data) and time-dependent errors in the underlying observations or in the boundary conditions lead to step changes in time, even in latest generation reanalyses (Bosilovich et al., 2011).

Errors of this sort were ubiquitous in early generation reanalyses and rendered them of limited value for trend characterization (Thorne and Vose, 2010). Subsequent products have improved and uncertainties are better understood (Dee et al., 2011a), but artefacts are still present. As a consequence, trend adequacy depends on the variable under consideration, the time period and the region of interest. For example, surface air temperature and humidity trends over land in the ERA-Interim reanalysis compare well with observations (Simmons et al., 2010), but polar tropospheric temperature trends in ERA-40 disagree with trends derived from radiosonde and satellite observations (Bitz and Fu, 2008; Grant et al., 2008; Graversen et al., 2008; Thorne, 2008; Screen and Simmonds, 2011) owing to problems that were resolved in ERA-Interim (Dee et al., 2011a).

Studies based on reanalyses are used cautiously in AR5 and known inadequacies are pointed out and referenced. Later generation reanalyses are preferred where possible; however, literature based on these new products is still sparse.

Aerosols can directly attenuate SSR by scattering and absorbing solar radiation, or indirectly, through their ability to act as cloud condensation nuclei, thereby changing cloud reflectivity and lifetime (Chapter 7). SSR dimming and brightening is often reconcilable with trends in anthropogenic emission histories and atmospheric aerosol loadings (Stern, 2006; Streets et al., 2006; Mishchenko et al., 2007; Ruckstuhl et al., 2008; Ohvrii et al., 2009; Russak, 2009; Streets et al., 2009; Cermak et al., 2010; Wild, 2012). Recent trends in aerosol optical depth derived from satellites indicate a decline in Europe since 2000 (Section 2.2.3), in line with evidence from SSR observations. However, direct aerosol effects alone may not be able to account for the full extent of the observed SSR changes in remote regions with low pollution levels (Dutton and Bodhaine, 2001; Schwartz, 2005). Aerosol indirect effects have not yet been well quantified, but have the potential to amplify aerosol-induced SSR trends, particularly in relatively pristine environments, such as over oceans (Wild, 2012).

SSR trends are also qualitatively in line with observed multi-decadal surface warming trends (Chapter 10), with generally smaller warming rates during phases of declining SSR, and larger warming rates in phases of increasing SSR (Wild et al., 2007). This is seen more pronounced for the relatively polluted NH than the more pristine SH (Wild, 2012). For Europe, Vautard et al. (2009) found that a decline in the frequency of low-visibility conditions such as fog, mist and haze over the past 30 years and associated SSR increase may be responsible for 10 to 20% of Europe’s recent daytime warming, and 50% of Eastern European warming. Philipona (2012) noted that both warming and brightening are weaker in the European Alps compared to the surrounding lowlands with stronger aerosol declines since 1981.

Reanalyses and observationally based methods have been used to show that increased atmospheric moisture with warming (Willett et al., 2008; Section 2.5) enhances thermal radiative emission of the atmosphere to the surface, leading to reduced net thermal cooling of the surface (Prata, 2008; Allan, 2009; Philipona et al., 2009; Wang and Liang, 2009).

In summary, the evidence for widespread multi-decadal variations in solar radiation incident on land surfaces has been substantiated since AR4, with many of the observational records showing a decline from the 1950s to the 1980s (‘dimming’), and a partial recovery thereafter (‘brightening’). *Confidence* in these changes is *high* in regions with high station densities such as over Europe and parts of Asia. These *likely* changes are generally supported by observed changes in related, but more widely measured variables, such as sunshine duration, DTR and hydrological quantities, and are often in line with aerosol emission patterns. Over some remote land areas and over the oceans, *confidence* is *low* owing to the lack of direct observations, which hamper a truly global assessment. Satellite-derived SSR fluxes support the existence of brightening also over oceans, but are less consistent over land surface where direct aerosol effects become more important. There are also indications for increasing downward thermal and net radiation at terrestrial stations since the early 1990s with *medium confidence*.

2.4 Changes in Temperature

2.4.1 Land Surface Air Temperature

2.4.1.1 Large-Scale Records and Their Uncertainties

AR4 concluded global land-surface air temperature (LSAT) had increased over the instrumental period of record, with the warming rate approximately double that reported over the oceans since 1979. Since AR4, substantial developments have occurred including the production of revised data sets, more digital data records, and new data set efforts. These innovations have improved understanding of data issues and uncertainties, allowing better quantification of regional changes. This reinforces confidence in the reported globally averaged LSAT time series behaviour.

Global Historical Climatology Network Version 3 (GHCNv3) incorporates many improvements (Lawrimore et al., 2011) but was found to be virtually indistinguishable at the global mean from version 2 (used in AR4). Goddard Institute of Space Studies (GISS) continues to provide an estimate based upon primarily GHCN, accounting for urban impacts through nightlights adjustments (Hansen et al., 2010). CRUTEM4 (Jones et al., 2012) incorporates additional station series and also newly homogenized versions of many individual station records. A new data product from a group based predominantly at Berkeley (Rohde et al., 2013a) uses a method that is substantially distinct from earlier efforts (further details on all the data sets and data availability are given in Supplementary Material 2.SM.4). Despite the range of approaches, the long-term variations and trends broadly agree among these various LSAT estimates, particularly after 1900. Global LSAT has increased (Figure 2.14, Table 2.4).

Since AR4, various theoretical challenges have been raised over the verity of global LSAT records (Pielke et al., 2007). Globally, sampling and methodological independence has been assessed through sub-sampling (Parker et al., 2009; Jones et al., 2012), creation of an entirely new and structurally distinct product (Rohde et al., 2013b) and a complete reprocessing of GHCN (Lawrimore et al., 2011). None of these yielded more than minor perturbations to the global LSAT records since 1900. Willett et al. (2008) and Peterson et al. (2011) explicitly showed that changes in specific and relative humidity (Section 2.5) were physically consistent with reported temperature trends, a result replicated in the ERA reanalyses (Simmons et al., 2010). Various investigators (Onogi et al., 2007; Simmons et al., 2010; Parker, 2011; Vose et al., 2012a) showed that LSAT estimates from modern reanalyses were in quantitative agreement with observed products.

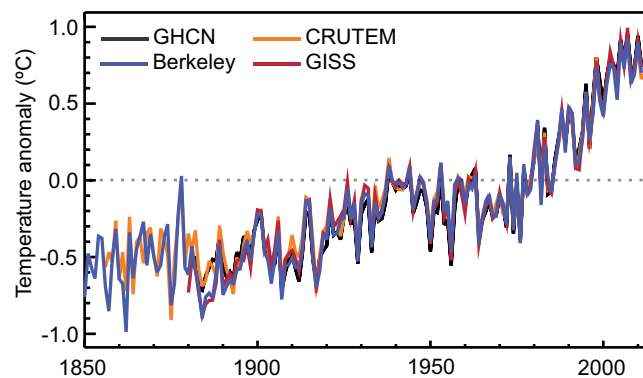


Figure 2.14 | Global annual average land-surface air temperature (LSAT) anomalies relative to a 1961–1990 climatology from the latest versions of four different data sets (Berkeley, CRUTEM, GHCN and GISS).

Particular controversy since AR4 has surrounded the LSAT record over the United States, focussed on siting quality of stations in the US Historical Climatology Network (USHCN) and implications for long-term trends. Most sites exhibit poor current siting as assessed against official WMO siting guidance, and may be expected to suffer potentially large siting-induced absolute biases (Fall et al., 2011). However, overall biases for the network since the 1980s are *likely* dominated by instrument type (owing to replacement of Stevenson screens with maximum minimum temperature systems (MMTS) in the 1980s at the majority of sites), rather than siting biases (Menne et al., 2010; Williams et al., 2012). A new automated homogeneity assessment approach (also used in GHCNv3, Menne and Williams, 2009) was developed that has been shown to perform as well or better than other contemporary approaches (Venema et al., 2012). This homogenization procedure *likely* removes much of the bias related to the network-wide changes in the 1980s (Menne et al., 2010; Fall et al., 2011; Williams et al., 2012). Williams et al. (2012) produced an ensemble of data set realizations using perturbed settings of this procedure and concluded through assessment against plausible test cases that there existed a propensity to under-estimate adjustments. This propensity is critically dependent upon the (unknown) nature of the inhomogeneities in the raw data records. Their homogenization increases both minimum temperature and maximum temperature centennial-time-scale USA average LSAT trends. Since 1979 these adjusted data agree with a range of reanalysis products whereas the raw records do not (Fall et al., 2010; Vose et al., 2012a).

Regional analyses of LSAT have not been limited to the United States. Various national and regional studies have undertaken assessments for Europe (Winkler, 2009; Bohm et al., 2010; Tietavainen et al., 2010; van

Table 2.4: | Trend estimates and 90% confidence intervals (Box 2.2) for LSAT global average values over five common periods.

Data Set	Trends in °C per decade				
	1880–2012	1901–2012	1901–1950	1951–2012	1979–2012
CRUTEM4.1.1.0 (Jones et al., 2012)	0.086 ± 0.015	0.095 ± 0.020	0.097 ± 0.029	0.175 ± 0.037	0.254 ± 0.050
GHCNv3.2.0 (Lawrimore et al., 2011)	0.094 ± 0.016	0.107 ± 0.020	0.100 ± 0.033	0.197 ± 0.031	0.273 ± 0.047
GISS (Hansen et al., 2010)	0.095 ± 0.015	0.099 ± 0.020	0.098 ± 0.032	0.188 ± 0.032	0.267 ± 0.054
Berkeley (Rohde et al., 2013)	0.094 ± 0.013	0.101 ± 0.017	0.111 ± 0.034	0.175 ± 0.029	0.254 ± 0.049

der Schrier et al., 2011), China (Li et al., 2009; Zhen and Zhong-Wei, 2009; Li et al., 2010a; Tang et al., 2010), India (Jain and Kumar, 2012), Australia (Trewin, 2012), Canada (Vincent et al., 2012), South America, (Falvey and Garreaud, 2009) and East Africa (Christy et al., 2009). These analyses have used a range of methodologies and, in many cases, more data and metadata than available to the global analyses. Despite the range of analysis techniques they are generally in broad agreement with the global products in characterizing the long-term changes in mean temperatures. This includes some regions, such as the Pacific coast of South America, that have exhibited recent cooling (Falvey and Garreaud, 2009). Of specific importance for the early global records, large ($>1^{\circ}\text{C}$) summer time warm bias adjustments for many European 19th century and early 20th century records were revisited and broadly confirmed by a range of approaches (Bohm et al., 2010; Brunet et al., 2011).

Since AR4 efforts have also been made to interpolate Antarctic records from the sparse, predominantly coastal ground-based network (Chapman and Walsh, 2007; Monaghan et al., 2008; Steig et al., 2009; O'Donnell et al., 2011). Although these agree that Antarctica as a whole has warmed since the late 1950s, substantial multi-annual to multi-decadal variability and uncertainties in reconstructed magnitude and spatial trend structure yield only *low confidence* in the details of pan-Antarctic regional LSAT changes.

In summary, it is certain that globally averaged LSAT has risen since the late 19th century and that this warming has been particularly marked since the 1970s. Several independently analyzed global and regional LSAT data products support this conclusion. There is *low confidence* in changes prior to 1880 owing to the reduced number of estimates, non-standardized measurement techniques, the greater spread among the estimates and particularly the greatly reduced observational sampling. *Confidence* is also *low* in the spatial detail and magnitude of LSAT trends in sparsely sampled regions such as Antarctica. Since AR4 significant efforts have been undertaken to identify and adjust for data issues and new estimates have been produced. These innovations have further strengthened overall understanding of the global LSAT records.

2.4.1.2 Diurnal Temperature Range

In AR4 diurnal temperature range (DTR) was found, globally, to have narrowed since 1950, with minimum daily temperatures increasing faster than maximum daily temperatures. However, significant multi-decadal variability was highlighted including a recent period from 1997 to 2004 of no change, as both maximum and minimum temperatures rose at similar rates. The Technical Summary of AR4 highlighted changes in DTR and their causes as a key uncertainty. Since AR4, uncertainties in DTR and its physical interpretation have become even more apparent.

No dedicated global analysis of DTR has been undertaken subsequent to Vose et al. (2005a), although global behaviour has been discussed in two broader ranging analyses. Rohde et al. (2012) and Wild et al. (2007) note an apparent reversal since the mid-1980s; with DTR subsequently increasing. This decline and subsequent increase in DTR over global land surfaces is qualitatively consistent with the dimming and subsequent brightening noted in Section 2.3.3.1. Donat et al. (2013c)

using HadEX2 (Section 2.6) find significant decreasing DTR trends in more than half of the land areas assessed but less than 10% of land with significant increases since 1951. Available trend estimates ($-0.04 \pm 0.01^{\circ}\text{C}$ per decade over 1950–2011 (Rohde et al., 2013b) and -0.066°C per decade over 1950–2004 (Vose et al., 2005a)) are much smaller than global mean LSAT average temperature trends over 1951–2012 (Table 2.4). It therefore logically follows that globally averaged maximum and minimum temperatures over land have both increased by in excess of 0.1°C per decade since 1950.

Regionally, Makowski et al. (2008) found that DTR behaviour in Europe over 1950 to 2005 changed from a decrease to an increase in the 1970s in Western Europe and in the 1980s in Eastern Europe. Sen Roy and Balling (2005) found significant increases in both maximum and minimum temperatures for India, but little change in DTR over 1931–2002. Christy et al. (2009) reported that for East Africa there has been no pause in the narrowing of DTR in recent decades. Zhou and Ren (2011) reported a significant decrease in DTR over mainland China of -0.15°C per decade during 1961–2008.

Various investigators (e.g., Christy et al. (2009), Pielke and Matsui (2005), Zhou and Ren (2011)) have raised doubts about the physical interpretation of minimum temperature trends, hypothesizing that microclimate and local atmospheric composition impacts are more apparent because the dynamical mixing at night is much reduced. Parker (2006) investigated this issue arguing that if data were affected in this way, then a trend difference would be expected between calm and windy nights. However, he found no such minimum temperature differences on a global average basis. Using more complex boundary layer modelling techniques, Steeneveld et al. (2011) and McNider et al. (2012) showed much lower sensitivity to windspeed variations than posited by Pielke and Matsui but both concluded that boundary layer understanding was key to understanding the minimum temperature changes. Data analysis and long-term side-by-side instrumentation field studies show that real non-climatic data artefacts certainly affect maximum and minimum differently in the raw records for both recent (Fall et al., 2011; Williams et al., 2012) and older (Bohm et al., 2010; Brunet et al., 2011) records. Hence there could be issues over interpretation of apparent DTR trends and variability in many regions (Christy et al., 2006, 2009; Fall et al., 2011; Zhou and Ren, 2011; Williams et al., 2012), particularly when accompanied by regional-scale land-use/land-cover (LULC) changes (Christy et al., 2006).

In summary, *confidence* is *medium* in reported decreases in observed global DTR, noted as a key uncertainty in AR4. Several recent analyses of the raw data on which many previous analyses were based point to the potential for biases that differently affect maximum and minimum average temperatures. However, apparent changes in DTR are much smaller than reported changes in average temperatures and therefore it is *virtually certain* that maximum and minimum temperatures have increased since 1950.

2.4.1.3 Land Use Change and Urban Heat Island Effects

In AR4 Urban Heat Island (UHI) effects were concluded to be real local phenomena with negligible impact on large-scale trends. UHI and land-use land-cover change (LULC) effects arise mainly because the

modified surface affects the storage and transfer of heat, water and airflow. For single discrete locations these impacts may dominate all other factors.

Regionally, most attention has focused on China. A variety of investigations have used methods as diverse as SST comparisons (e.g., Jones et al., 2008), urban minus rural (e.g., Ren et al., 2008; Yang et al., 2011), satellite observations (Ren and Ren, 2011) and observations minus reanalysis (e.g., Hu et al., 2010; Yang et al., 2011). Interpretation is complicated because often studies have used distinct versions of station series. For example, the effect in Beijing is estimated at 80% (Ren et al., 2007) or 40% (Yan et al., 2010) of the observed trend depending on data corrections applied. A representative sample of these studies suggest the effect of UHI and LULC is approximately 20% of the trend in Eastern China as a whole and of the order 0.1°C per decade nationally (Table 1 in Yang et al., 2011) over the last 30 years, but with very substantial uncertainties. These effects have *likely* been partially or completely accounted for in many homogenized series (e.g., Li et al., 2010b; Yan et al., 2010). Fujibe (2009) ascribes about 25% of Japanese warming trends in 1979–2006 to UHI effects. Das et al. (2011) confirmed that many Japanese sites have experienced UHI warming but that rural stations show unaffected behaviour when compared to nearby SSTs.

There is an important distinction to be made between UHI trend effects in regions underseeing rapid development and those that have been developed for a long time. Jones and Lister (2009) and Wilby et al. (2011) using data from London (UK) concluded that some sites that have always been urban and where the UHI has not grown in magnitude will exhibit regionally indicative trends that agree with nearby rural locations and that in such cases the time series may exhibit multi-decadal trends driven primarily by synoptic variations. A lack of obvious time-varying UHI influences was also noted for Sydney, Melbourne and Hobart in Australia by Trewin (2012). The impacts of urbanization also will be dependent on the natural LULC characteristics that they replace. Zhang et al. (2010) found no evidence for urban influences in the desert North West region of China despite rapid urbanization.

Global adjusted data sets *likely* account for much of the UHI effect present in the raw data. For the US network, Hausfather et al. (2013) showed that the adjustments method used in GHCNv3 removed much of an apparent systematic difference between urban and rural locations, concluding that this arose from adjustment of biased urban location data. Globally, Hansen et al. (2010) used satellite-based nightlight radiances to estimate the worldwide influence on LSAT of local urban development. Adjustments reduced the global 1900–2009 temperature change (averaged over land and ocean) only from 0.71°C to 0.70°C . Wickham et al. (2013) also used satellite data and found that urban locations in the Berkeley data set exhibited even less warming than rural stations, although not statistically significantly so, over 1950 to 2010.

Studies of the broader effects of LULC since AR4 have tended to focus on the effects of irrigation on temperatures, with a large number of studies in the Californian central belt (Christy et al., 2006; Kueppers et al., 2007; Bonfils et al., 2008; Lo and Famiglietti, 2013). They find cooler average temperatures and a marked reduction in DTR in areas of active irrigation and ascribe this to increased humidity; effectively a repar-

titioning of moist and dry energy terms. Reanalyses have also been used to estimate the LULC signature in LSAT trends. Fall et al. (2010) found that the North American Regional Reanalysis generated overall surface air temperature trends for 1979–2003 similar to observed records. Observations-minus-reanalysis trends were most positive for barren and urban areas, in accord with the results of Lim et al. (2008) using the NCEP/NCAR and ERA-40 reanalyses, and negative in agricultural areas.

McKittrick and Michaels (2004) and de Laat and Maurellis (2006) assessed regression of trends with national socioeconomic and geographical indicators, concluding that UHI and related LULC have caused much of the observed LSAT warming. AR4 concluded that this correlation ceases to be statistically significant if one takes into account the fact that the locations of greatest socioeconomic development are also those that have been most warmed by atmospheric circulation changes but provided no explicit evidence for this overall assessment result. Subsequently McKittrick and Michaels (2007) concluded that about half the reported warming trend in global-average land surface air temperature in 1980–2002 resulted from local land surface changes and faults in the observations. Schmidt (2009) undertook a quantitative analysis that supported AR4 conclusions that much of the reported correlation largely arose due to naturally occurring climate variability and model over-fitting and was not robust. Taking these factors into account, modified analyses by McKittrick (2010) and McKittrick and Nierenberg (2010) still yielded significant evidence for such contamination of the record.

In marked contrast to regression based studies, several studies have shown the methodologically diverse set of modern reanalysis products and the various LSAT records at global and regional levels to be similar since at least the mid-20th century (Simmons et al., 2010; Parker, 2011; Ferguson and Villarini, 2012; Jones et al., 2012; Vose et al., 2012a). These reanalyses do not directly assimilate the LSAT measurements but rather infer LSAT estimates from an observational constraint provided by much of the rest of the global observing system, thus representing an independent estimate. A hypothesized residual significant warming artefact argued for by regression-based analyses is therefore physically inconsistent with many other components of the global observing system according to a broad range of state-of-the-art data assimilation models (Box 2.3). Further, Efthymiadis and Jones (2010) estimated an absolute upper limit on urban influence globally of 0.02°C per decade, or about 15% of the total LSAT trends, in 1951–2009 from trends of coastal land and SST.

In summary, it is indisputable that UHI and LULC are real influences on raw temperature measurements. At question is the extent to which they remain in the global products (as residual biases in broader regionally representative change estimates). Based primarily on the range of urban minus rural adjusted data set comparisons and the degree of agreement of these products with a broad range of reanalysis products, it is *unlikely* that any uncorrected urban heat-island effects and LULC change effects have raised the estimated centennial globally averaged LSAT trends by more than 10% of the reported trend (*high confidence*, based on robust evidence and high agreement). This is an average value; in some regions with rapid development, UHI and LULC change impacts on regional trends may be substantially larger.

2.4.2 Sea Surface Temperature and Marine Air Temperature

AR4 concluded that ‘recent’ warming (since the 1950s) is strongly evident at all latitudes in SST over each ocean. Prominent spatio-temporal structures including the ENSO and decadal variability patterns in the Pacific Ocean (Box 2.5) and a hemispheric asymmetry in the Atlantic Ocean were highlighted as contributors to the regional differences in surface warming rates, which in turn affect atmospheric circulation. Since AR4 the availability of metadata has increased, data completeness has improved and a number of new SST products have been produced. Intercomparisons of data obtained by different measurement methods, including satellite data, have resulted in better understanding of errors and biases in the record.

2

2.4.2.1 Advances in Assembling Data Sets and in Understanding Data Errors

2.4.2.1.1 *In situ* data records

Historically, most SST observations were obtained from moving ships. Buoy measurements comprise a significant and increasing fraction of *in situ* SST measurements from the 1980s onward (Figure 2.15). Improvements in the understanding of uncertainty have been expedited by the use of metadata (Kent et al., 2007) and the recovery of

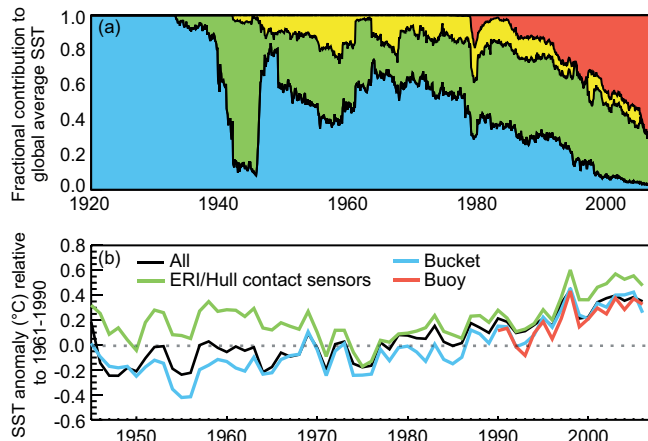


Figure 2.15 | Temporal changes in the prevalence of different measurement methods in the International Comprehensive Ocean-Atmosphere Data Set (ICOADS). (a) Fractional contributions of observations made by different measurement methods: bucket observations (blue), engine room intake (ERI) and hull contact sensor observations (green), moored and drifting buoys (red), and unknown (yellow). (b) Global annual average sea surface temperature (SST) anomalies based on different kinds of data: ERI and hull contact sensor (green), bucket (blue), buoy (red), and all (black). Averages are computed over all $5^\circ \times 5^\circ$ grid boxes where both ERI/hull and bucket measurements, but not necessarily buoy data, were available. (Adapted from Kennedy et al., 2011a.)

Table 2.5 | Trend estimates and 90% confidence intervals (Box 2.2) for two subsequent versions of the HadSST data set over five common periods. HadSST2 has been used in AR4; HadSST3 is used in this chapter.

Data Set	Trends in °C per decade				
	1880–2012	1901–2012	1901–1950	1951–2012	1979–2012
HadSST3 (Kennedy et al., 2011a)	0.054 ± 0.012	0.067 ± 0.013	0.117 ± 0.028	0.074 ± 0.027	0.124 ± 0.030
HadSST2 (Rayner et al., 2006)	0.051 ± 0.015	0.069 ± 0.012	0.084 ± 0.055	0.098 ± 0.017	0.121 ± 0.033

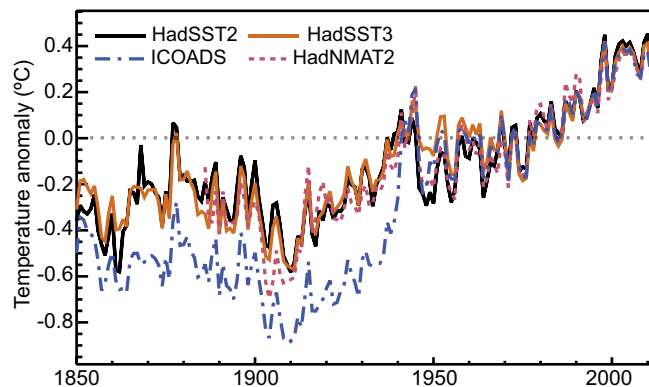


Figure 2.16 | Global annual average sea surface temperature (SST) and Night Marine Air Temperature (NMAT) relative to a 1961–1990 climatology from gridded data sets of SST observations (HadSST2 and its successor HadSST3), the raw SST measurement archive (ICOADS, v2.5) and night marine air temperatures data set HadNMAT2 (Kent et al., 2013). HadSST2 and HadSST3 both are based on SST observations from versions of the ICOADS data set, but differ in degree of measurement bias correction.

observer instructions and other related documents. Early data were systematically cold biased because they were made using canvas or wooden buckets that, on average, lost heat to the air before the measurements were taken. This effect has long been recognized (Brooks, 1926), and prior to AR4 represented the only artefact adjusted in gridded SST products, such as HadSST2 (Rayner et al., 2006) and ERSST (Smith et al., 2005, 2008), which were based on ‘bucket correction’ methods by Folland and Parker (1995) and Smith and Reynolds (2002), respectively. The adjustments, made using ship observations of Night Marine Air Temperature (NMAT) and other sources, had a striking effect on the SST global mean estimates: note the difference in 1850–1941 between HadSST2 and International Comprehensive Ocean-Atmosphere Data Set (ICOADS) curves in Figure 2.16 (a brief description of SST and NMAT data sets and their methods is given in Supplementary Material 2.SM.4.3).

Buckets of improved design and measurement methods with smaller, on average, biases came into use after 1941 (Figure 2.15, top); average biases were reduced further in recent decades, but not eliminated (Figure 2.15, bottom). Increasing density of SST observations made possible the identification (Reynolds et al., 2002, 2010; Kennedy et al., 2012) and partial correction of more recent period biases (Kennedy et al., 2011a). In particular, it is hypothesized that the proximity of the hot engine often biases engine room intake (ERI) measurements warm (Kent et al., 2010). Because of the prevalence of the ERI measurements among SST data from ships, the ship SSTs are biased warm by 0.12°C to 0.18°C on average compared to the buoy data (Reynolds et al., 2010; Kennedy et al., 2011a, 2012). An assessment of the potential impact of modern biases can be ascertained by considering the difference

between HadSST3 (bias corrections applied throughout) and HadSST2 (bucket corrections only) global means (Figure 2.16): it is particularly prominent in 1945–1970 period, when rapid changes in prevalence of ERI and bucket measurements during and after the World War II affect HadSST2 owing to the uncorrected measurement biases (Thompson et al., 2008), while these are corrected in HadSST3. Nevertheless, for periods longer than a century the effect of HadSST3-HadSST2 differences on linear trend slopes is small relative to the trend uncertainty (Table 2.5). Some degree of independent check on the validity of HadSST3 adjustments comes from a comparison to sub-surface temperature data (Gouretski et al., 2012) (see Section 3.2).

The traditional approach to modeling random error of *in situ* SST data assumed the independence of individual measurements. Kent and Berry (2008) identified the need to account for error correlation for measurements from the same “platform” (i.e., an individual ship or buoy), while measurement errors from different platforms remain independent.. Kennedy et al. (2011b) achieved that by introducing platform-dependent biases, which are constant within the same platform, but change randomly from one platform to another. Accounting for such correlated errors in HadSST3 resulted in estimated error for global and hemispheric monthly means that are more than twice the estimates given by HadSST2. The uncertainty in many, but not all, components of the HadSST3 product is represented by the ensemble of its realizations (Figure 2.17).

Data sets of marine air temperatures (MATs) have traditionally been restricted to nighttime series only (NMAT data sets) due to the direct solar heating effect on the daytime measurements, although corrected daytime MAT records for 1973–present are already available (Berry and Kent, 2009). Other major biases, affecting both nighttime and daytime MAT are due to increasing deck height with the general increase in the size of ships over time and non-standard measurement practices. Recently these biases were re-examined and explicit uncertainty calculation undertaken for NMAT by Kent et al. (2013), resulting in the HadNMAT2 data set.

2.4.2.1.2 Satellite SST data records

Satellite SST data sets are based on measuring electromagnetic radiation that left the ocean surface and got transmitted through the atmosphere. Because of the complexity of processes involved, the majority of such data has to be calibrated on the basis of *in situ* observations. The resulting data sets, however, provide a description of global SST fields with a level of spatial detail unachievable by *in situ* data only. The principal IR sensor is the Advanced Very High Resolution Radiometer (AVHRR). Since AR4, the AVHRR time series has been reprocessed consistently back to March 1981 (Casey et al., 2010) to create the AVHRR Pathfinder v5.2 data set. Passive microwave data sets of SST are available since 1997 equatorward of 40° and near-globally since 2002 (Wentz et al., 2000; Gentemann et al., 2004). They are generally less accurate than IR-based SST data sets, but their superior coverage in areas of persistent cloudiness provides SST estimates where the IR record has none (Reynolds et al., 2010).

The (Advanced) Along Track Scanning Radiometer (A)ATSR) series of three sensors was designed for climate monitoring of SST; their com-

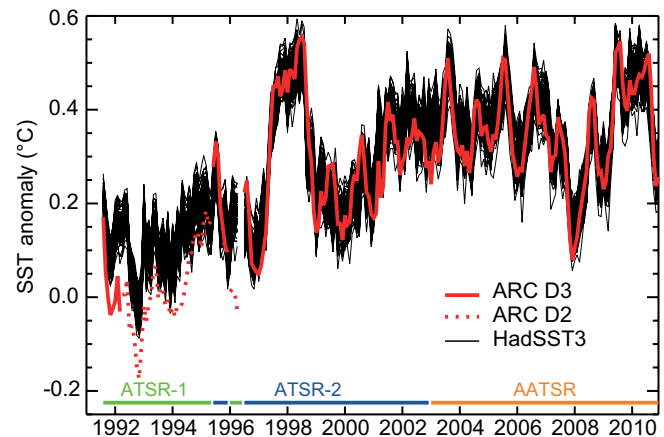


Figure 2.17 | Global monthly mean sea surface temperature (SST) anomalies relative to a 1961–1990 climatology from satellites (ATSRs) and *in situ* records (HadSST3). Black lines: the 100-member HadSST3 ensemble. Red lines: ATSR-based nighttime subsurface temperature at 0.2 m depth ($SST_{0.2m}$) estimates from the ATSR Reprocessing for Climate (ARC) project. Retrievals based on three spectral channels (D3, solid line) are more accurate than retrievals based on only two (D2, dotted line). Contributions of the three different ATSR missions to the curve shown are indicated at the bottom. The *in situ* and satellite records were co-located within $5^\circ \times 5^\circ$ monthly grid boxes: only those where both data sets had data for the same month were used in the comparison. (Adapted from Merchant et al. 2012.)

bined record starts in August 1991 and exceeds two decades (it stopped with the demise of the ENVISAT platform in 2012). The (A) ATSRs are ‘dual-view’ IR radiometers intended to allow atmospheric effects removal without the use of *in situ* observations. Since AR4, (A)ATSR observations have been reprocessed with new estimation techniques (Embry and Merchant, 2011). The resulting SST products seem to be more accurate than many *in situ* observations (Embry et al., 2011). In terms of monthly global means, the agreement is illustrated in Figure 2.17. By analyzing (A)ATSR and *in situ* data together, Kennedy et al. (2012) verified and extended existing models for biases and random errors of *in situ* data.

2.4.2.2 Interpolated SST Products and Trends

SST data sets form a major part of global surface temperature analyses considered in this assessment report. To use an SST data set as a boundary condition for atmospheric reanalyses products (Box 2.3) or in atmosphere-only climate simulations (considered in Chapter 9 onwards), gridded data sets with complete coverage over the global ocean are typically needed. These are usually based on a special form of kriging (optimal interpolation) procedure that retains large-scale correlation structures and can accommodate very sparse data coverage. For the pre-satellite era (generally, before October 1981) only *in situ* data are used; for the latter period some products also use AVHRR data. Figure 2.18 compares interpolated SST data sets that extend back to the 19th century with the uninterpolated HadSST3 and HadNMAT2 products. Linear trend estimates for global mean SSTs from those products updated through 2012 are presented in Table 2.6. Differences between the trends from different data sets are larger when the calculation period is shorter (1979–2012) or has lower quality data (1901–1950); these are due mainly to different data coverage of underlying observational data sets and bias correction methods used in these products.

Table 2.6 | Trend estimates and 90% confidence intervals (Box 2.2) for interpolated SST data sets (uninterpolated state-of-the-art HadSST3 data set is included for comparison). Dash indicates not enough data available for trend calculation.

Data Set	Trends in °C per decade				
	1880–2012	1901–2012	1901–1950	1951–2012	1979–2012
HadISST (Rayner et al., 2003)	0.042 ± 0.007	0.052 ± 0.007	0.067 ± 0.024	0.064 ± 0.015	0.072 ± 0.024
COBE-SST (Ishii et al., 2005)	–	0.058 ± 0.007	0.066 ± 0.032	0.071 ± 0.014	0.073 ± 0.020
ERSSTv3b (Smith et al., 2008)	0.054 ± 0.015	0.071 ± 0.011	0.097 ± 0.050	0.088 ± 0.017	0.105 ± 0.031
HadSST3 (Kennedy et al., 2011a)	0.054 ± 0.012	0.067 ± 0.013	0.117 ± 0.028	0.074 ± 0.027	0.124 ± 0.030

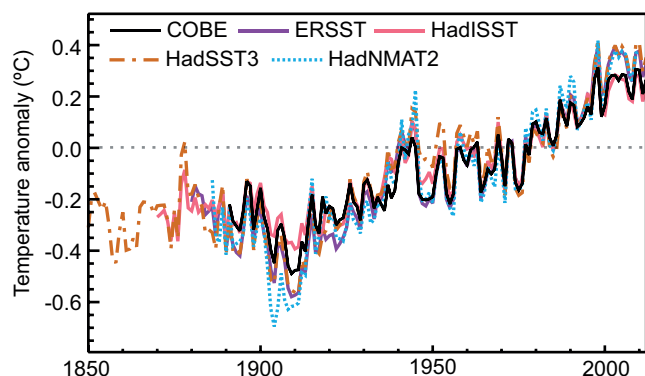


Figure 2.18 | Global annual average sea surface temperature (SST) and Night Marine Air Temperature (NMAT) relative to a 1961–1990 climatology from state of the art data sets. Spatially interpolated products are shown by solid lines; non-interpolated products by dashed lines.

In summary, it is certain that global average sea surface temperatures (SSTs) have increased since the beginning of the 20th century. Since AR4, major improvements in availability of metadata and data completeness have been made, and a number of new global SST records have been produced. Intercomparisons of new SST data records obtained by different measurement methods, including satellite data, have resulted in better understanding of uncertainties and biases in the records. Although these innovations have helped highlight and quantify uncertainties and affect our understanding of the character of changes since the mid-20th century, they do not alter the conclusion that global SSTs have increased both since the 1950s and since the late 19th century.

2.4.3 Global Combined Land and Sea Surface Temperature

AR4 concluded that the GMST had increased, with the last 50 years increasing at almost double the rate of the last 100 years. Subsequent developments in LSAT and SST have led to better understanding of the data and their uncertainties as discussed in preceding sections. This improved understanding has led to revised global products.

Changes have been made to all three GMST data sets that were used in AR4 (Hansen et al., 2010; Morice et al., 2012; Vose et al., 2012b). These are now in somewhat better agreement with each other over recent years, in large part because HadCRUT4 now better samples the NH high latitude land regions (Jones et al., 2012; Morice et al., 2012) which comparisons to reanalyses had shown led to a propensity for HadCRUT3 to underestimate recent warming (Simmons et al., 2010).

Starting in the 1980s each decade has been significantly warmer at the Earth's surface than any preceding decade since the 1850s in HadCRUT4, a data set that explicitly quantifies a large number of sources of uncertainty (Figure 2.19). Each of the last three decades is also the warmest in the other two GMST data sets, but these have substantially less mature and complete uncertainty estimates, precluding such an assessment of significance of their decadal differences. The GISS and MLOST data sets fall outside the 90% CI of HadCRUT4 for several decades in the 20th century (Figure 2.19). These decadal differences could reflect residual biases in one or more data set, an incomplete treatment of uncertainties in HadCRUT4.1 or a combination of these effects (Box 2.1). The data sets utilize different LSAT (Section 2.4.1) and SST (Section 2.4.2) component records (Supplementary Material 2.SM.4.3.4) that in the case of SST differ somewhat in their multi-decadal trend behaviour (Table 2.6 compare HadSST3 and ERSSTv3b).

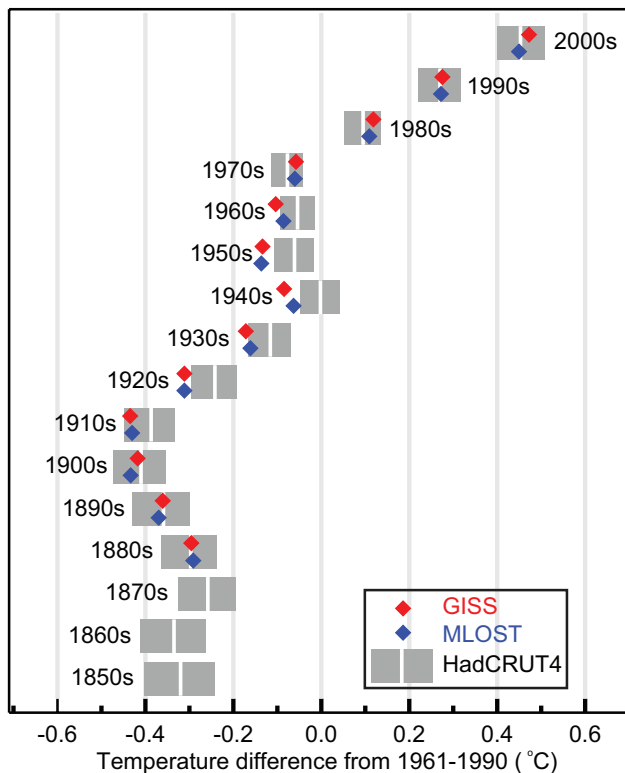


Figure 2.19 | Decadal global mean surface temperature (GMST) anomalies (white vertical lines in grey blocks) and their uncertainties (90% confidence intervals as grey blocks) based upon the land-surface air temperature (LSAT) and sea surface temperature (SST) combined HadCRUT4 (v4.1.1.0) ensemble (Morice et al., 2012). Anomalies are relative to a 1961–1990 climatology. 1850s indicates the period 1850–1859, and so on. NCDC MLOST and GISS data set best-estimates are also shown.

All ten of the warmest years have occurred since 1997, with 2010 and 2005 effectively tied for the warmest year on record in all three products. However, uncertainties on individual annual values are sufficiently large that the ten warmest years are statistically indistinguishable from one another. The global-mean trends are significant for all data sets and multi-decadal periods considered in Table 2.7. Using HadCRUT4 and its uncertainty estimates, the warming from 1850–1900 to 1986–2005 (reference period for the modelling chapters and Annex I) is $0.61 [0.55 \text{ to } 0.67] \text{ }^{\circ}\text{C}$ (90% confidence interval), and the warming from 1850–1900 to 2003–2012 (the most recent decade) is $0.78 [0.72 \text{ to } 0.85] \text{ }^{\circ}\text{C}$ (Supplementary Material 2.SM.4.3.3).

Differences between data sets are much smaller than both interannual variability and the long-term trend (Figure 2.20). Since 1901 almost the whole globe has experienced surface warming (Figure 2.21). Warming has not been linear; most warming occurred in two periods: around 1900 to around 1940 and around 1970 onwards (Figure 2.22). Shorter periods are noisier and so proportionately less of the sampled globe exhibits statistically significant trends at the grid box level (Figure 2.22). The two periods of global mean warming exhibit very distinct spatial signatures. The early 20th century warming was largely a NH mid- to high-latitude phenomenon, whereas the more recent warming is more global in nature. These distinctions may yield important information as to causes (Chapter 10). Differences between data sets are larger in earlier periods (Figures 2.19, 2.20), particularly prior to the 1950s when observational sampling is much more geographically incomplete (and many of the well sampled areas may have been globally unrepresentative (Brönnimann, 2009)), data errors and subsequent methodological impacts are larger (Thompson et al., 2008), and different ways of accounting for data void regions are more important (Vose et al., 2005b).

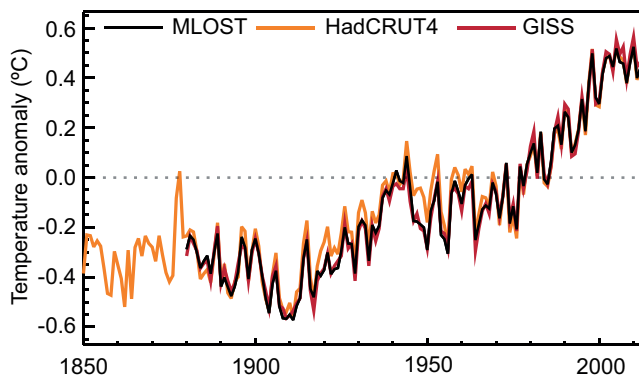


Figure 2.20 | Annual global mean surface temperature (GMST) anomalies relative to a 1961–1990 climatology from the latest version of the three combined land-surface air temperature (LSAT) and sea surface temperature (SST) data sets (HadCRUT4, GISS and NCDC MLOST). Published data set uncertainties are not included for reasons discussed in Box 2.1.

Table 2.7 | Same as Table 2.4, but for global mean surface temperature (GMST) over five common periods.

Data Set	Trends in °C per decade				
	1880–2012	1901–2012	1901–1950	1951–2012	1979–2012
HadCRUT4 (Morice et al., 2012)	0.062 ± 0.012	0.075 ± 0.013	0.107 ± 0.026	0.106 ± 0.027	0.155 ± 0.033
NCDC MLOST (Vose et al., 2012b)	0.064 ± 0.015	0.081 ± 0.013	0.097 ± 0.040	0.118 ± 0.021	0.151 ± 0.037
GISS (Hansen et al., 2010)	0.065 ± 0.015	0.083 ± 0.013	0.090 ± 0.034	0.124 ± 0.020	0.161 ± 0.033

Much interest has focussed on the period since 1998 and an observed reduction in warming trend, most marked in NH winter (Cohen et al., 2012). Various investigators have pointed out the limitations of such short-term trend analysis in the presence of auto-correlated series variability and that several other similar length phases of no warming exist in all the observational records and in climate model simulations

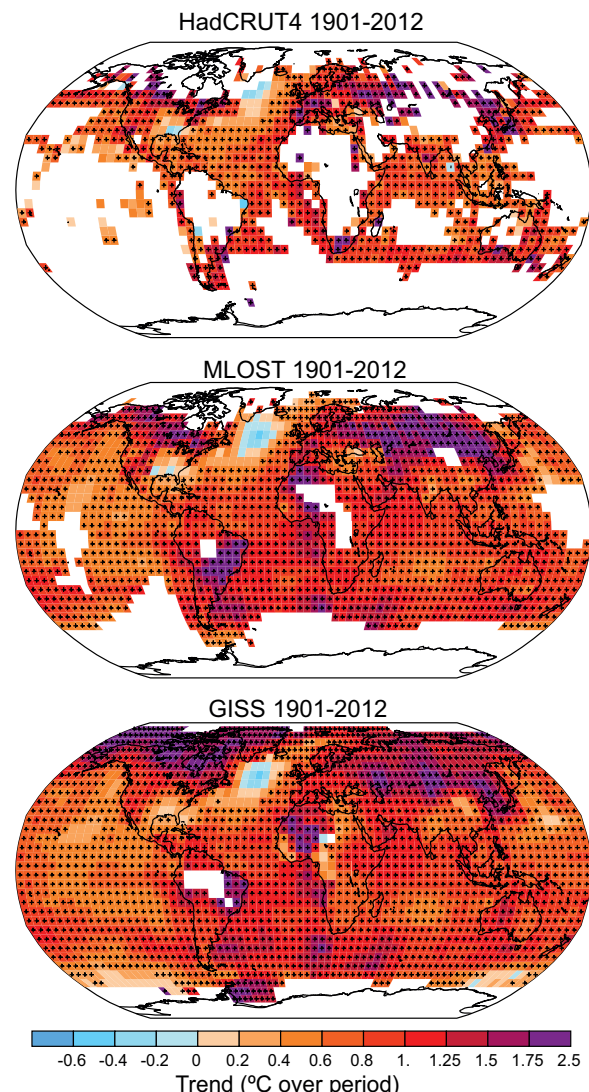


Figure 2.21 | Trends in surface temperature from the three data sets of Figure 2.20 for 1901–2012. White areas indicate incomplete or missing data. Trends have been calculated only for those grid boxes with greater than 70% complete records and more than 20% data availability in first and last decile of the period. Black plus signs (+) indicate grid boxes where trends are significant (i.e., a trend of zero lies outside the 90% confidence interval). Differences in coverage primarily reflect the degree of interpolation to account for data void regions undertaken by the data set providers ranging from none beyond grid box averaging (HadCRUT4) to substantial (GISS).

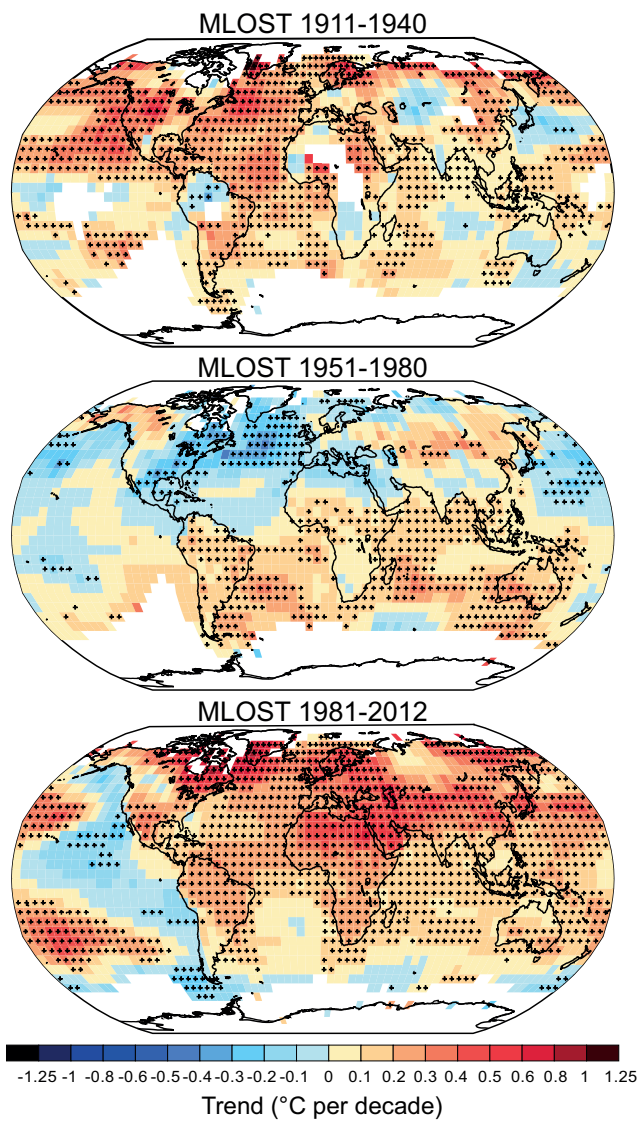


Figure 2.22 | Trends in surface temperature from NCDC MLOST for three non-consecutive shorter periods (1911–1940; 1951–1980; 1981–2012). White areas indicate incomplete or missing data. Trends and significance have been calculated as in Figure 2.21.

(Easterling and Wehner, 2009; Peterson et al., 2009; Liebmann et al., 2010; Foster and Rahmstorf, 2011; Santer et al., 2011). This issue is discussed in the context of model behaviour, forcings and natural variability in Box 9.2 and Section 10.3.1. Regardless, all global combined LSAT and SST data sets exhibit a statistically non-significant warming trend over 1998–2012 ($0.042^{\circ}\text{C} \pm 0.093^{\circ}\text{C}$ per decade (HadCRUT4); $0.037^{\circ}\text{C} \pm 0.085^{\circ}\text{C}$ per decade (NCDC MLOST); $0.069^{\circ}\text{C} \pm 0.082^{\circ}\text{C}$ per decade (GISS)). An average of the trends from these three data sets yields an estimated change for the 1998–2012 period of $0.05 [-0.05 \text{ to } +0.15]^{\circ}\text{C}$ per decade. Trends of this short length are very sensitive to the precise period selection with trends calculated in the same manner for the 15-year periods starting in 1995, 1996, and 1997 being $0.13 [0.02 \text{ to } 0.24]$, $0.14 [0.03 \text{ to } 0.24]$ and $0.07 [-0.02 \text{ to } 0.18]$ (all $^{\circ}\text{C}$ per decade), respectively.

In summary, it is certain that globally averaged near surface temperatures have increased since the late 19th century. Each of the past

three decades has been warmer than all the previous decades in the instrumental record, and the decade of the 2000s has been the warmest. The globally averaged combined land and ocean surface temperature data as calculated by a linear trend, show a warming of $0.85 [0.65 \text{ to } 1.06]^{\circ}\text{C}$, over the period 1880–2012, when multiple independently produced datasets exist, about $0.89^{\circ}\text{C} [0.69 \text{ to } 1.08]^{\circ}\text{C}$ over the period 1901–2012, and about $0.72 [0.49 \text{ to } 0.89]^{\circ}\text{C}$ over the period 1951–2012. The total increase between the average of the 1850–1900 period and the 2003–2012 period is $0.78 [0.72 \text{ to } 0.85]^{\circ}\text{C}$ and the total increase between the average of the 1850–1900 period and the reference period for projections 1986–2005 is $0.61 [0.55 \text{ to } 0.67]^{\circ}\text{C}$, based on the single longest dataset available. For the longest period when calculation of regional trends is sufficiently complete (1901–2012), almost the entire globe has experienced surface warming. In addition to robust multi-decadal warming, global mean surface temperature exhibits substantial decadal and interannual variability. Owing to natural variability, trends based on short records are very sensitive to the beginning and end dates and do not in general reflect long-term climate trends. As one example, the rate of warming over the past 15 years (1998–2012; $0.05 [-0.05 \text{ to } +0.15]^{\circ}\text{C}$ per decade), which begins with a strong El Niño, is smaller than the rate calculated since 1951 (1951–2012; $0.12 [0.08 \text{ to } 0.14]^{\circ}\text{C}$ per decade). Trends for 15-year periods starting in 1995, 1996, and 1997 are $0.13 [0.02 \text{ to } 0.24]$, $0.14 [0.03 \text{ to } 0.24]$ and $0.07 [-0.02 \text{ to } 0.18]$, respectively..

2.4.4 Upper Air Temperature

AR4 summarized that globally the troposphere had warmed at a rate greater than the GMST over the radiosonde record, while over the shorter satellite era the GMST and tropospheric warming rates were indistinguishable. Trends in the tropics were more uncertain than global trends although even this region was concluded to be warming. Globally, the stratosphere was reported to be cooling over the satellite era starting in 1979. New advances since AR4 have highlighted the substantial degree of uncertainty in both satellite and balloon-borne radiosonde records and led to some revisions and improvements in existing products and the creation of a number of new data products.

2.4.4.1 Advances in Multi-Decadal Observational Records

The major global radiosonde records extend back to 1958, with temperatures, measured as the balloon ascends, reported at mandatory pressure levels. Satellites have monitored tropospheric and lower stratospheric temperature trends since late 1978 through the Microwave Sounding Unit (MSU) and its follow-on Advanced Microwave Sounding Unit (AMSU) since 1998. These measures of upwelling radiation represent bulk (volume averaged) atmospheric temperature (Figure 2.23). The ‘Mid-Tropospheric’ (MT) MSU channel that most directly corresponds to the troposphere has 10 to 15% of its signal from both the skin temperature of the Earth’s surface and the stratosphere. Two alternative approaches have been suggested for removing the stratospheric component based on differencing of view angles (LT) and statistical recombination (*G) with the ‘Lower Stratosphere’ (LS) channel (Spencer and Christy, 1992; Fu et al., 2004). The MSU satellite series also included a Stratospheric Sounding Unit (SSU) that measured at higher altitudes (Seidel et al., 2011).

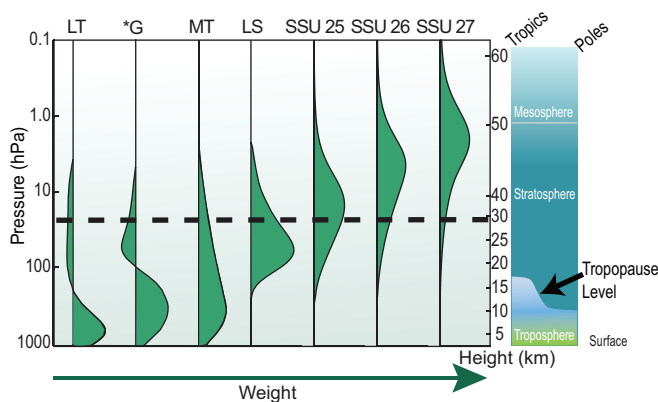


Figure 2.23 | Vertical weighting functions for those satellite temperature retrievals discussed in this chapter (modified from Seidel et al. (2011)). The dashed line indicates the typical maximum altitude achieved in the historical radiosonde record. The three SSU channels are denoted by the designated names 25, 26 and 27. LS (Lower Stratosphere) and MT (Mid Troposphere) are two direct MSU measures and LT (Lower Troposphere) and *G (Global Troposphere) are derived quantities from one or more of these that attempt to remove the stratospheric component from MT.

At the time of AR4 there were only two ‘global’ radiosonde data sets that included treatment of homogeneity issues: RATPAC (Free et al., 2005) and HadAT (Thorne et al., 2005). Three additional estimates have appeared since AR4 based on novel and distinct approaches. A group at the University of Vienna have produced RAOBCORE and RICH (Haimberger, 2007; Haimberger et al., 2008, 2012) using ERA reanalysis products (Box 2.3). Sherwood and colleagues developed an iterative universal kriging approach for radiosonde data to create IUK (Sherwood et al., 2008) and concluded that non-climatic data issues leading to spurious cooling remained in the deep tropics even after homogenization. The HadAT group created an automated version, undertook systematic experimentation and concluded that the parametric uncertainty (Box 2.1) was of the same order of magnitude as the apparent climate signal (McCarthy et al., 2008; Titchner et al., 2009; Thorne et al., 2011). A similar ensemble approach has also been applied to the RICH product (Haimberger et al., 2012). These various ensembles and new products exhibit more tropospheric warming / less stratospheric cooling than pre-existing products at all levels. Globally the radiosonde records all imply the troposphere has warmed and the stratosphere cooled since 1958 but with uncertainty that grows with height and is much greater outside the better-sampled NH extra-tropics (Thorne et al., 2011; Haimberger et al., 2012), where it is of the order 0.1°C per decade.

For MSU, AR4 considered estimates produced from three groups: UAH (University of Alabama in Huntsville); RSS (Remote Sensing Systems) and VG2 (now no longer updated). A new product has been created by NOAA labelled STAR, using a fundamentally distinct approach for the critical inter-satellite warm target calibration step (Zou et al., 2006a). STAR exhibits more warming/less cooling at all levels than UAH and RSS. For MT and LS, Zou and Wang (2010) concluded that this does not relate primarily to use of their inter-satellite calibration technique but rather differences in other processing steps. RSS also produced a parametric uncertainty ensemble (Box 2.1) employing a Monte Carlo approach allowing methodological inter-dependencies to be fully expressed (Mears et al., 2011). For large-scale trends dominant

effects were inter-satellite offset determinations and, for tropospheric channels, diurnal drift. Uncertainties were concluded to be of the order 0.1°C per decade at the global mean for both tropospheric channels (where it is of comparable magnitude to the long-term trends) and the stratospheric channel.

SSU provides the only long-term near-global temperature data above the lower stratosphere, with the series terminating in 2006. Some AMSU-A channels have replaced this capability and efforts to understand the effect of changed measurement properties have been undertaken (Kobayashi et al., 2009). Until recently only one SSU data set existed (Nash and Edge, 1989), updated by Randel et al. (2009). Liu and Weng (2009) have produced an intermediate analysis for Channels 25 and 26 (but not Channel 27). Wang et al. (2012g), building on insights from several of these recent studies, have produced a more complete analysis. Differences between the independent estimates are much larger than differences between MSU records or radiosonde records at lower levels, with substantial inter-decadal time series behaviour departures, zonal trend structure, and global trend differences of the order 0.5°C per decade (Seidel et al., 2011; Thompson et al., 2012; Wang et al., 2012g). Although all SSU data sets agree that the stratosphere is cooling, there is therefore *low confidence* in the details above the lower stratosphere.

In summary, many new data sets have been produced since AR4 from radiosondes and satellites with renewed interest in satellite measurements above the lower stratosphere. Several studies have attempted to quantify the parametric uncertainty (Box 2.1) more rigorously. These various data sets and analyses have served to highlight the degree of uncertainty in the data and derived products.

2.4.4.2 Intercomparisons of Various Long-Term Radiosonde and MSU Products

Since AR4 there have been a large number of intercomparisons between radiosonde and MSU data sets. Interpretation is complicated, as most studies considered data set versions that have since been superseded. Several studies compared UAH and RSS products to local, regional or global raw/homogenized radiosonde data (Christy and Norris, 2006, 2009; Christy et al., 2007, 2010, 2011; Randall and Herman, 2008; Mears et al., 2012; Po-Chedley and Fu, 2012). Early studies focussed on the time of transition from NOAA-11 to NOAA-12 (early 1990s) which indicated an apparent issue in RSS. Christy et al. (2007) noted that this coincided with the Mt Pinatubo eruption and that RSS was the only product, either surface or tropospheric, that exhibited tropical warming immediately after the eruption when cooling would be expected. Using reanalysis data Bengtsson and Hodges (2011) also found evidence of a potential jump in RSS in 1993 over the tropical oceans. Mears et al. (2012) cautioned that an El Niño event quasi-simultaneous with Pinatubo complicates interpretation. They also highlighted several other periods of disagreement between radiosonde records and MSU records. All MSU records were most uncertain when satellite orbits are drifting rapidly (Christy and Norris, 2006, 2009). Mears et al. (2011) found that trend differences between RSS and other data sets could not be explained in many cases by parametric uncertainties in RSS alone. It was repeatedly cautioned that there were potential common biases (of varying magnitude) between the different MSU

records or between the different radiosonde records which complicate intercomparisons (Christy and Norris, 2006, 2009; Mears et al., 2012).

In summary, assessment of the large body of studies comparing various long-term radiosonde and MSU products since AR4 is hampered by data set version changes, and inherent data uncertainties. These factors substantially limit the ability to draw robust and consistent inferences from such studies about the true long-term trends or the value of different data products.

2.4.4.3 Additional Evidence from Other Technologies and Approaches

Global Positioning System (GPS) radio occultation (RO) currently represents the only self-calibrated SI traceable raw satellite measurements (Anthes et al., 2008; Anthes, 2011). The fundamental observation is time delay of the occulted signal's phase traversing the atmosphere. The time delay is a function of several atmospheric physical state variables. Subsequent analysis converts the time delay to temperature and other parameters, which inevitably adds some degree of uncertainty to the derived temperature data. Intercomparisons of GPS-RO products show that differences are largest for derived geophysical parameters (including temperature), but are still small relative to other observing technologies (Ho et al., 2012). Comparisons to MSU and radiosondes (Kuo et al., 2005; Ho et al., 2007, 2009a, 2009b; He et al., 2009; Baringer et al., 2010; Sun et al., 2010; Ladstadter et al., 2011) show substantive agreement in interannual behaviour, but also some multi-year drifts that require further examination before this additional data source can usefully arbitrate between different MSU and radiosonde trend estimates.

Atmospheric winds are driven by thermal gradients. Radiosonde winds are far less affected by time-varying biases than their temperatures (Gruber and Haimberger, 2008; Sherwood et al., 2008; Section 2.7.3). Allen and Sherwood (2007) initially used radiosonde wind to infer temperatures within the Tropical West Pacific warm pool region, then extended this to a global analysis (Allen and Sherwood, 2008) yielding a distinct tropical upper tropospheric warming trend maximum within the vertical profile, but with large uncertainty. Winds can only quantify relative changes and require an initialization (location and trend at that location) (Allen and Sherwood, 2008). The large uncertainty range was predominantly driven by this initialization choice, a finding later confirmed by Christy et al. (2010), who in addition questioned the stability given the sparse geographical sampling, particularly in the tropics, and possible systematic sampling effects amongst other potential issues. Initializing closer to the tropics tended to reduce or remove the appearance of a tropical upper tropospheric warming trend maximum (Allen and Sherwood, 2008; Christy et al., 2010). There is only *low confidence* in trends inferred from 'thermal winds' given the relative immaturity of the analyses and their large uncertainties.

In summary, new technologies and approaches have emerged since AR4. However, these new technologies and approaches either constitute too short a record or are too immature to inform assessments of long-term trends at the present time.

2.4.4.4 Synthesis of Free Atmosphere Temperature Estimates

Global-mean lower tropospheric temperatures have increased since the mid-20th century (Figure 2.24, bottom). Structural uncertainties (Box 2.1) are larger than at the surface but it can still be concluded that globally the troposphere has warmed (Table 2.8). On top of this long-term trend are superimposed short-term variations that are highly correlated with those at the surface but of somewhat greater amplitude. Global mean lower stratospheric temperatures have decreased since the mid-20th century punctuated by short-lived warming events associated with explosive volcanic activity (Figure 2.24a). However, since the mid-1990s little net change has occurred. Cooling rates are on average greater from radiosonde data sets than MSU data sets. This *very likely* relates to widely recognized cooling biases in radiosondes (Mears et al., 2006) which all data set producers explicitly caution are *likely* to remain to some extent in their final products (Free and Seidel, 2007; Haimberger et al., 2008; Sherwood et al., 2008; Thorne et al., 2011).

In comparison to the surface (Figure 2.22), tropospheric layers exhibit smoother geographic trends (Figure 2.25) with warming dominating cooling north of approximately 45°S and greatest warming in high northern latitudes. The lower stratosphere cooled almost everywhere but this cooling exhibits substantial large-scale structure. Cooling is greatest in the highest southern latitudes and smallest in high northern latitudes. There are also secondary stratospheric cooling maxima in the mid-latitude regions of each hemisphere.

Available global and regional trends from radiosondes since 1958 (Figure 2.26) show agreement that the troposphere has warmed and the stratosphere cooled. While there is little ambiguity in the sign of the changes, the rate and vertical structure of change are distinctly data set dependent, particularly in the stratosphere. Differences are greatest in the tropics and SH extra-tropics where the historical radiosonde data coverage is poorest. Not shown in the figure for clarity are estimates of parametric data set uncertainties or trend-fit uncertainties—both of which are of the order of at least 0.1°C per decade (Section 2.4.4.1).

Differences in trends between available radiosonde data sets are greater during the satellite era than for the full radiosonde period of record in all regions and at most levels (Figure 2.27; cf. Figure 2.26). The RAOBCORE product exhibits greater vertical trend gradients than other data sets and it has been posited that this relates to its dependency on reanalysis fields (Sakamoto and Christy, 2009; Christy et al., 2010). MSU trend estimates in the troposphere are generally bracketed by the radiosonde range. In the stratosphere MSU deep layer estimates tend to show slightly less cooling. Over both 1958–2011 and 1979–2011 there is some evidence in the radiosonde products taken as a whole that the tropical tropospheric trends increase with height. But the magnitude and the structure is highly data set dependent.

In summary, based on multiple independent analyses of measurements from radiosondes and satellite sensors it is *virtually certain* that globally the troposphere has warmed and the stratosphere has cooled since the mid-20th century. Despite unanimous agreement on the sign of the trends, substantial disagreement exists among available estimates as to the rate of temperature changes, particularly outside the NH extra-tropical troposphere, which has been well sampled by radiosondes.

Table 2.8 | Trend estimates and 90% confidence intervals (Box 2.2) for radiosonde and MSU data set global average values over the radiosonde (1958–2012) and satellite periods (1979–2012). LT indicates Lower Troposphere, MT indicates Mid Troposphere and LS indicates Lower Stratosphere (Figure 2.23. Satellite records start only in 1979 and STAR do not produce an LT product.

Data Set	Trends in °C per decade					
	1958–2012			1979–2012		
	LT	MT	LS	LT	MT	LS
HadAT2 (Thorne et al., 2005)	0.159 ± 0.038	0.095 ± 0.034	-0.339 ± 0.086	0.162 ± 0.047	0.079 ± 0.057	-0.436 ± 0.204
RAOB CORE 1.5 (Haimberger et al., 2012)	0.156 ± 0.031	0.109 ± 0.029	-0.186 ± 0.087	0.139 ± 0.049	0.079 ± 0.054	-0.266 ± 0.227
RICH-obs (Haimberger et al., 2012)	0.162 ± 0.031	0.102 ± 0.029	-0.285 ± 0.087	0.158 ± 0.046	0.081 ± 0.052	-0.331 ± 0.241
RICH-tau (Haimberger et al., 2012)	0.168 ± 0.032	0.111 ± 0.030	-0.280 ± 0.085	0.160 ± 0.046	0.083 ± 0.052	-0.345 ± 0.238
RATPAC (Free et al., 2005)	0.136 ± 0.028	0.076 ± 0.028	-0.338 ± 0.092	0.128 ± 0.044	0.039 ± 0.051	-0.468 ± 0.225
UAH (Christy et al., 2003)				0.138 ± 0.043	0.043 ± 0.042	-0.372 ± 0.201
RSS (Mears and Wentz, 2009a, 2009b)				0.131 ± 0.045	0.079 ± 0.043	-0.268 ± 0.177
STAR (Zou and Wang, 2011)					0.123 ± 0.047	-0.320 ± 0.175

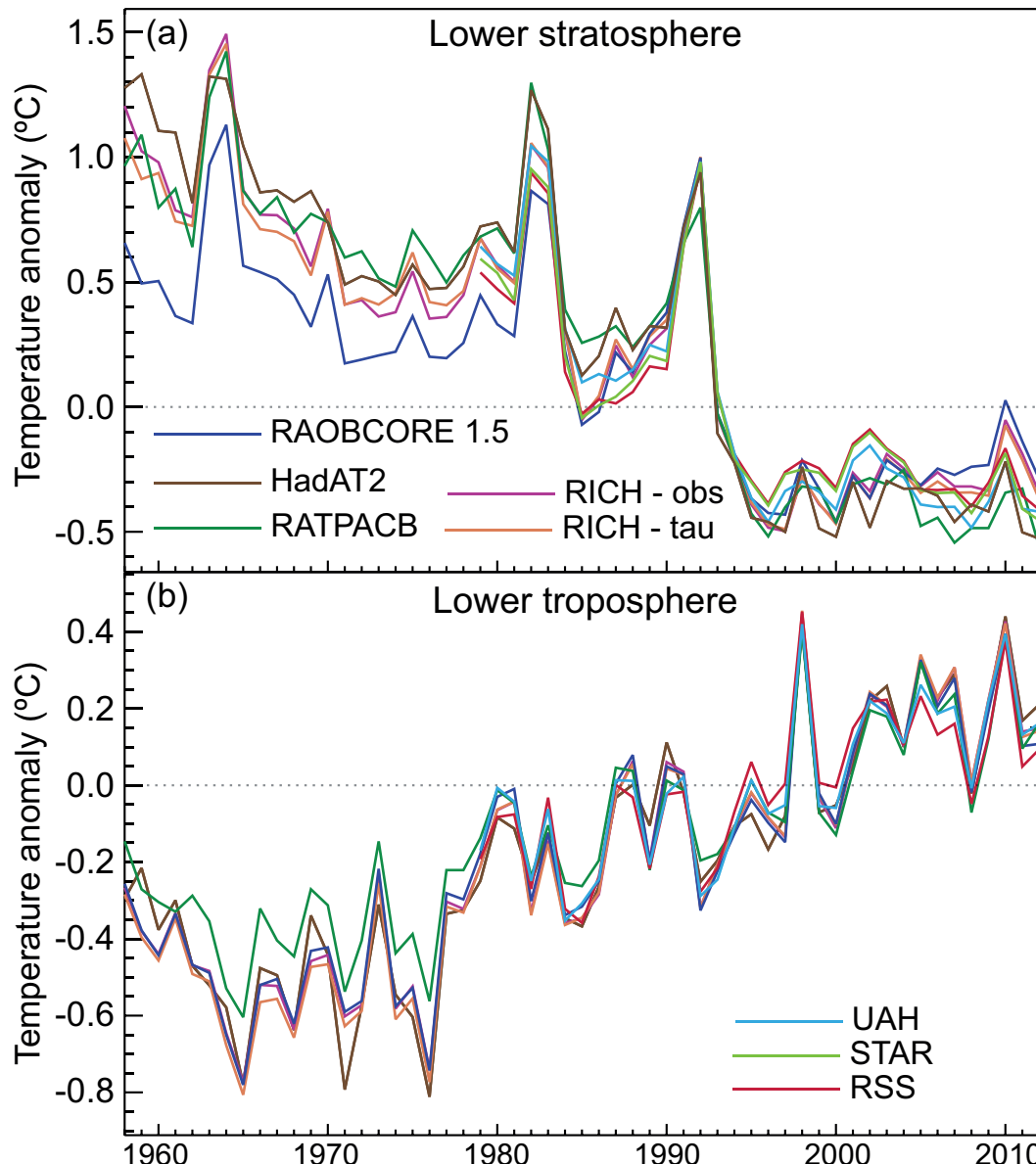


Figure 2.24 | Global annual average lower stratospheric (top) and lower tropospheric (bottom) temperature anomalies relative to a 1981–2010 climatology from different data sets. STAR does not produce a lower tropospheric temperature product. Note that the y-axis resolution differs between the two panels.

Frequently Asked Questions

FAQ 2.1 | How Do We Know the World Has Warmed?

Evidence for a warming world comes from multiple independent climate indicators, from high up in the atmosphere to the depths of the oceans. They include changes in surface, atmospheric and oceanic temperatures; glaciers; snow cover; sea ice; sea level and atmospheric water vapour. Scientists from all over the world have independently verified this evidence many times. That the world has warmed since the 19th century is unequivocal.

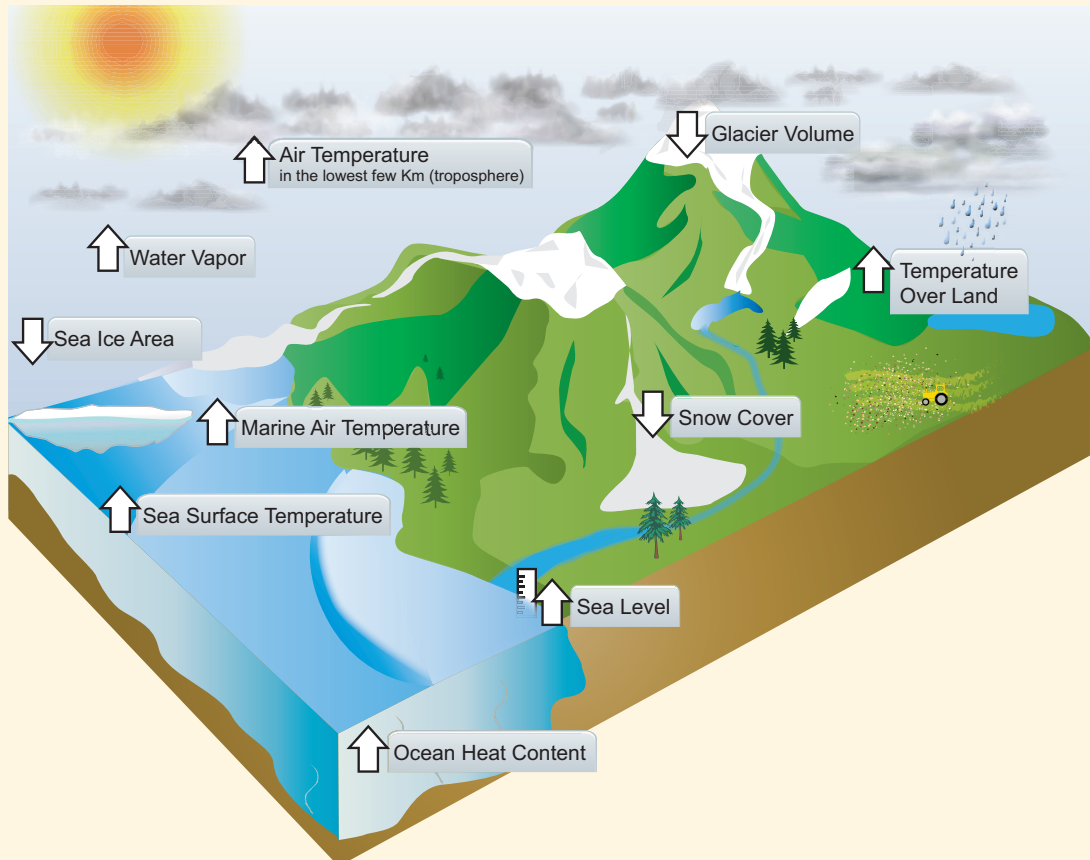
Discussion about climate warming often centres on potential residual biases in temperature records from land-based weather stations. These records are very important, but they only represent one indicator of changes in the climate system. Broader evidence for a warming world comes from a wide range of independent physically consistent measurements of many other, strongly interlinked, elements of the climate system (FAQ 2.1, Figure 1).

2

A rise in global average surface temperatures is the best-known indicator of climate change. Although each year and even decade is not always warmer than the last, global surface temperatures have warmed substantially since 1900.

Warming land temperatures correspond closely with the observed warming trend over the oceans. Warming oceanic air temperatures, measured from aboard ships, and temperatures of the sea surface itself also coincide, as borne out by many independent analyses.

The atmosphere and ocean are both fluid bodies, so warming at the surface should also be seen in the lower atmosphere, and deeper down into the upper oceans, and observations confirm that this is indeed the case. Analyses of measurements made by weather balloon radiosondes and satellites consistently show warming of the troposphere, the active weather layer of the atmosphere. More than 90% of the excess energy absorbed by the climate system since at least the 1970s has been stored in the oceans as can be seen from global records of ocean heat content going back to the 1950s. (*continued on next page*)



FAQ 2.1, Figure 1 | Independent analyses of many components of the climate system that would be expected to change in a warming world exhibit trends consistent with warming (arrow direction denotes the sign of the change), as shown in FAQ 2.1, Figure 2.

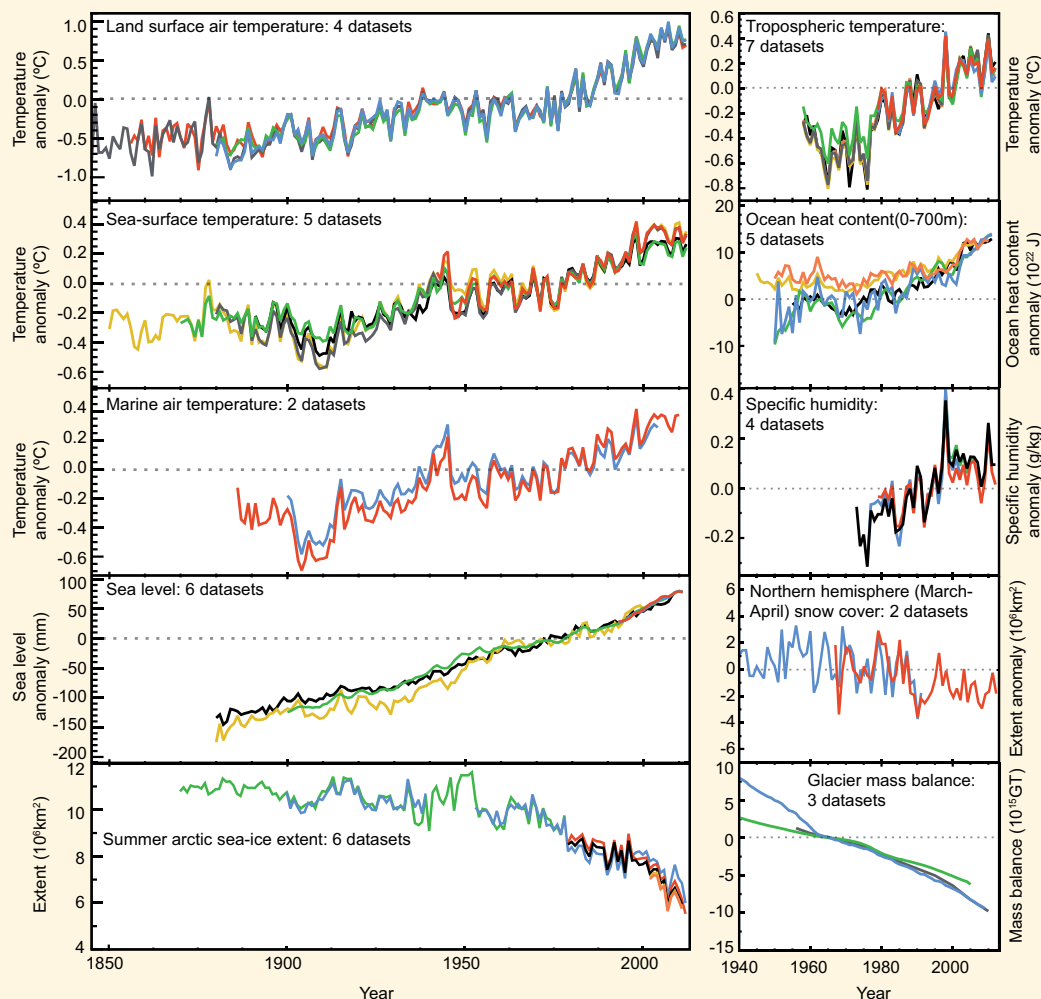
FAQ 2.1 (continued)

As the oceans warm, the water itself expands. This expansion is one of the main drivers of the independently observed rise in sea levels over the past century. Melting of glaciers and ice sheets also contribute, as do changes in storage and usage of water on land.

A warmer world is also a moister one, because warmer air can hold more water vapour. Global analyses show that specific humidity, which measures the amount of water vapour in the atmosphere, has increased over both the land and the oceans.

The frozen parts of the planet—known collectively as the cryosphere—affect, and are affected by, local changes in temperature. The amount of ice contained in glaciers globally has been declining every year for more than 20 years, and the lost mass contributes, in part, to the observed rise in sea level. Snow cover is sensitive to changes in temperature, particularly during the spring, when snow starts to melt. Spring snow cover has shrunk across the NH since the 1950s. Substantial losses in Arctic sea ice have been observed since satellite records began, particularly at the time of the minimum extent, which occurs in September at the end of the annual melt season. By contrast, the increase in Antarctic sea ice has been smaller.

Individually, any single analysis might be unconvincing, but analysis of these different indicators and independent data sets has led many independent research groups to *all* reach the same conclusion. From the deep oceans to the top of the troposphere, the evidence of warmer air and oceans, of melting ice and rising seas all points unequivocally to one thing: the world has warmed since the late 19th century (FAQ 2.1, Figure 2).



FAQ 2.1, Figure 2 | Multiple independent indicators of a changing global climate. Each line represents an independently derived estimate of change in the climate element. In each panel all data sets have been normalized to a common period of record. A full detailing of which source data sets go into which panel is given in the Supplementary Material 2.SM.5.

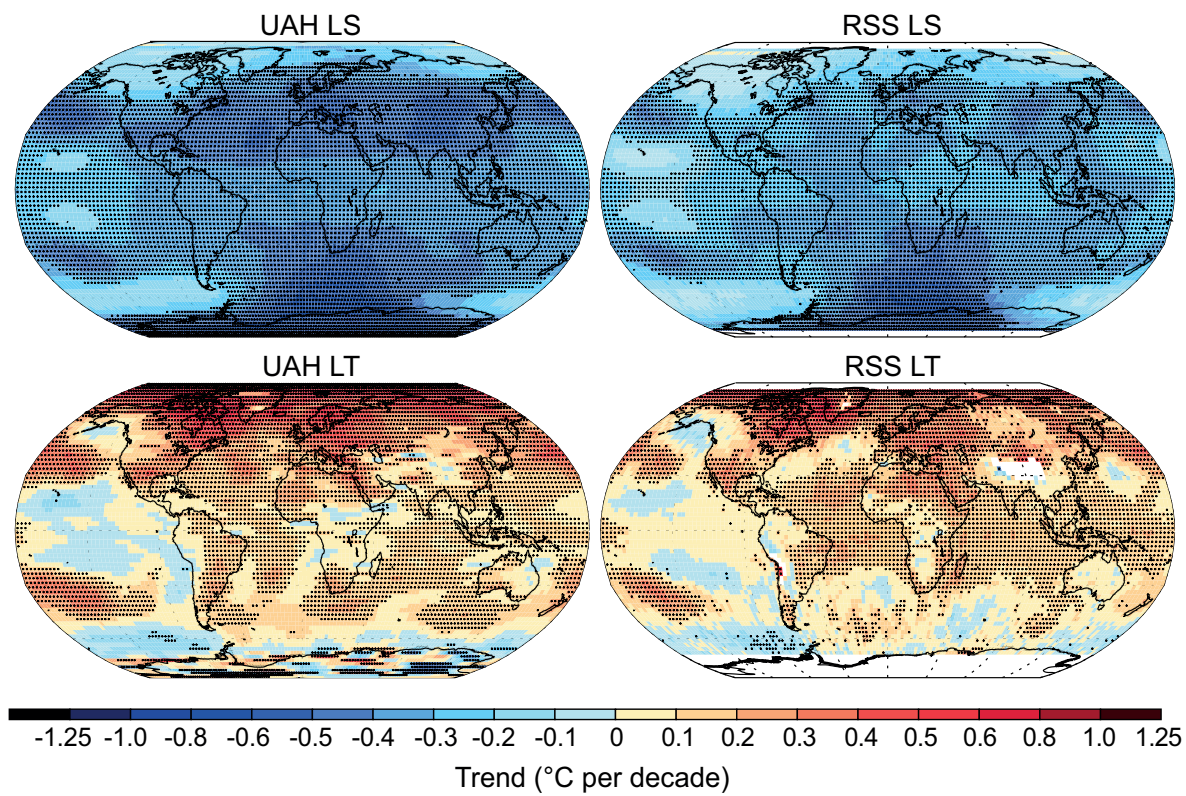


Figure 2.25 | Trends in MSU upper air temperature over 1979–2012 from UAH (left-hand panels) and RSS (right-hand panels) and for LS (top row) and LT (bottom row). Data are temporally complete within the sampled domains for each data set. White areas indicate incomplete or missing data. Black plus signs (+) indicate grid boxes where trends are significant (i.e., a trend of zero lies outside the 90% confidence interval).

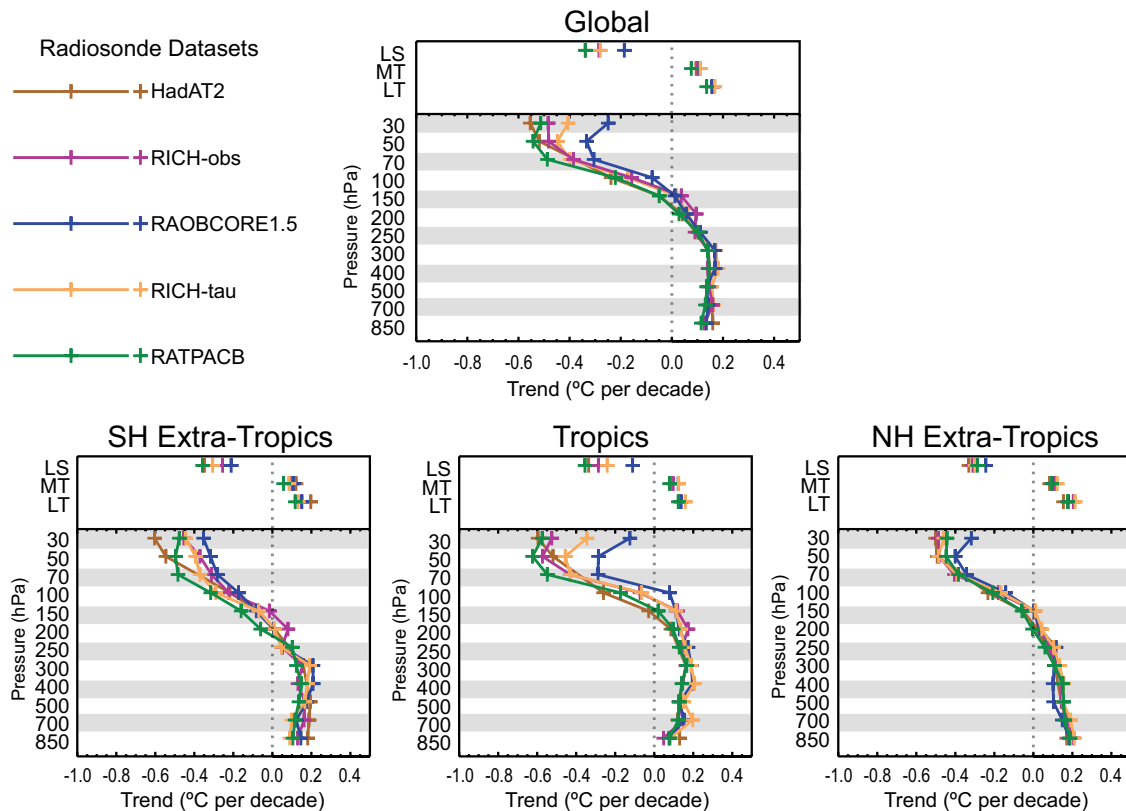


Figure 2.26 | Trends in upper air temperature for all available radiosonde data products that contain records for 1958–2012 for the globe (top) and tropics (20°N to 20°S) and extra-tropics (bottom). The bottom panel trace in each case is for trends on distinct pressure levels. Note that the pressure axis is not linear. The top panel points show MSU layer equivalent measure trends. MSU layer equivalents have been processed using the method of Thorne et al. (2005). No attempts have been made to sub-sample to a common data mask.

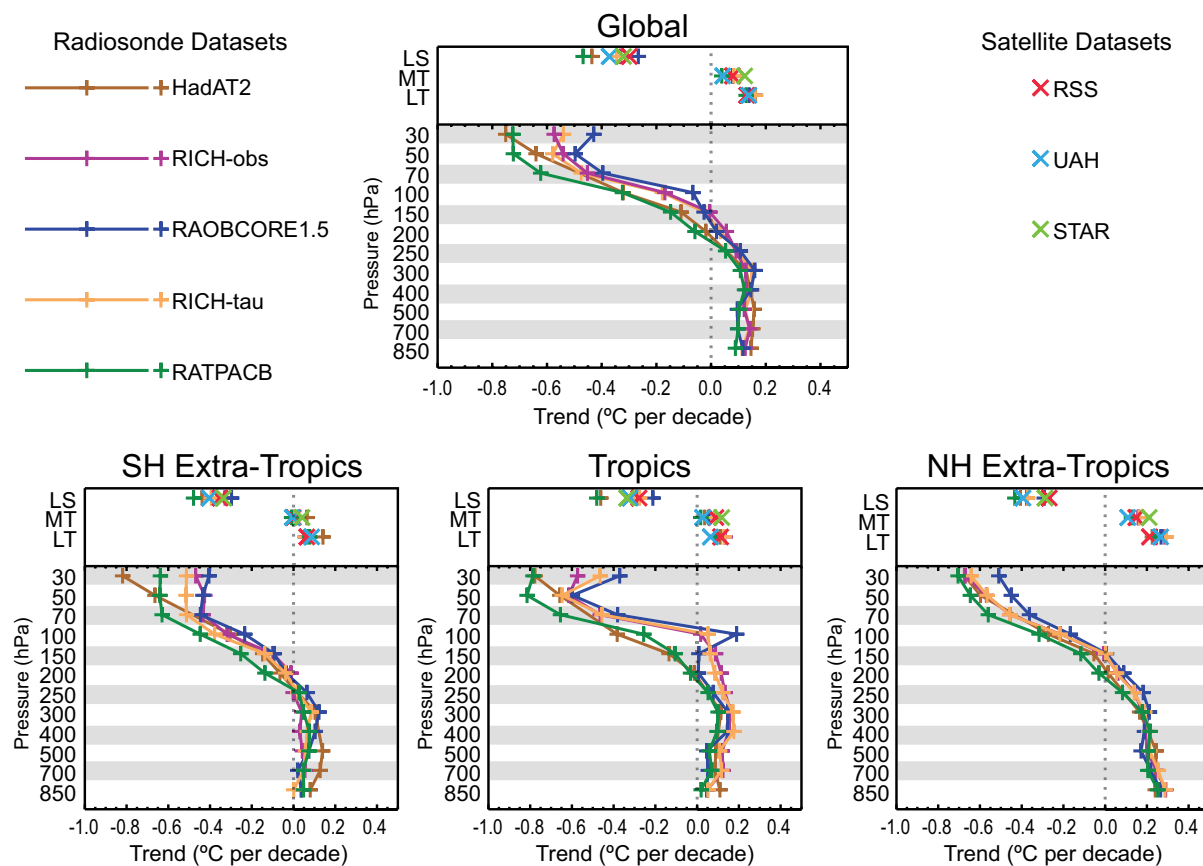


Figure 2.27 | As Figure 2.26 except for the satellite era 1979–2012 period and including MSU products (RSS, STAR and UAH).

Hence there is only *medium confidence* in the rate of change and its vertical structure in the NH extratropical troposphere and *low confidence* elsewhere.

2.5 Changes in Hydrological Cycle

This section covers the main aspects of the hydrological cycle, including large-scale average precipitation, stream flow and runoff, soil moisture, atmospheric water vapour, and clouds. Meteorological drought is assessed in Section 2.6. Ocean precipitation changes are assessed in Section 3.4.3 and changes in the area covered by snow in Section 4.5.

2.5.1 Large-Scale Changes in Precipitation

2.5.1.1 Global Land Areas

AR4 concluded that precipitation has generally increased over land north of 30°N over the period 1900–2005 but downward trends dominate the tropics since the 1970s. AR4 included analysis of both the GHCN (Vose et al., 1992) and CRU (Mitchell and Jones, 2005) gauge-based precipitation data sets for the globally averaged annual precipitation over land. For both data sets the overall linear trend from 1900 to 2005 (1901–2002 for CRU) was positive but not statistically significant (Table 3.4 from AR4). Other periods covered in AR4 (1951–2005 and 1979–2005) showed a mix of negative and positive trends depending on the data set.

Since AR4, existing data sets have been updated and a new data set developed. Figure 2.28 shows the century-scale variations and trends on globally and zonally averaged annual precipitation using five data sets: GHCN V2 (updated through 2011; Vose et al., 1992), Global Precipitation Climatology Project V2.2 (GPCP) combined raingauge–satellite product (Adler et al., 2003), CRUTS 3.10.01 (updated from Mitchell and Jones, 2005), Global Precipitation Climatology Centre V6 (GPCC) data set (Becker et al., 2013) and a reconstructed data set by Smith et al. (2012). Each data product incorporates a different number of station series for each region. The Smith et al. product is a statistical reconstruction using Empirical Orthogonal Functions, similar to the NCDC MLOST global temperature product (Section 2.4.3) that does provide coverage for most of the global surface area although only land is included here. The data sets based on *in situ* observations only start in 1901, but the Smith et al. data set ends in 2008, while the other three data sets contain data until at least 2010.

For the longest common period of record (1901–2008) all datasets exhibit increases in globally averaged precipitation, with three of the four showing statistically significant changes (Table 2.9). However, there is a factor of almost three spread in the magnitude of the change which serves to create *low confidence*. Global trends for the shorter period (1951–2008) show a mix of statistically non-significant positive and negative trends amongst the four data sets with the infilled Smith et al. (2012) analysis showing increases and the remainder decreases. These differences among data sets indicate that long-term increases

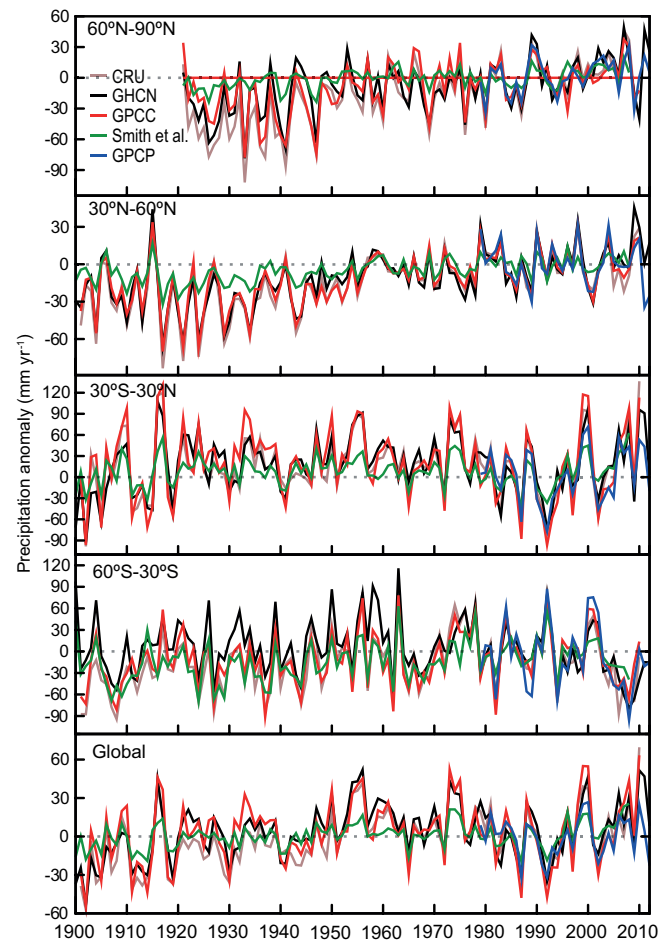


Figure 2.28 | Annual precipitation anomalies averaged over land areas for four latitudinal bands and the globe from five global precipitation data sets relative to a 1981–2000 climatology.

in global precipitation discussed in AR4 are uncertain, owing in part to issues in data coverage in the early part of the 20th century (Wan et al., 2013).

In summary, *confidence* in precipitation change averaged over global land areas is *low* for the years prior to 1950 and *medium* afterwards because of insufficient data, particularly in the earlier part of the record. Available globally incomplete records show mixed and non-significant long-term trends in reported global mean changes. Further, when virtually all the land area is filled in using a reconstruction method, the resulting time series shows less change in land-based precipitation since 1900.

Table 2.9 | Trend estimates and 90% confidence intervals (Box 2.2) for annual precipitation for each time series in Figure 2.28 over two common periods of record.

Data Set	Area	Trends in mm yr^{-1} per decade	
		1901–2008	1951–2008
CRU TS 3.10.01 (updated from Mitchell and Jones, 2005)	Global	2.77 ± 1.46	-2.12 ± 3.52
GHCN V2 (updated through 2011; Vose et al., 1992)	Global	2.08 ± 1.66	-2.77 ± 3.92
GPCC V6 (Becker et al., 2013)	Global	1.48 ± 1.65	-1.54 ± 4.50
Smith et al. (2012)	Global	1.01 ± 0.64	0.68 ± 2.07

2.5.1.2 Spatial Variability of Observed Trends

The latitude band plots in Figure 2.28 suggest that precipitation over tropical land areas (30°S to 30°N) has increased over the last decade reversing the drying trend that occurred from the mid-1970s to mid-1990s. As a result the period 1951–2008 shows no significant overall trend in tropical land precipitation in any of the datasets (Table 2.10). Longer term trends (1901–2008) in the tropics, shown in Table 2.10, are also non-significant for each of the four data sets. The mid-latitudes of the NH (30°N to 60°N) show an overall increase in precipitation from 1901 to 2008 with statistically significant trends for each data set. For the shorter period (1951–2008) the trends are also positive but non-significant for three of the four data sets. For the high latitudes of the NH (60°N to 90°N) where data completeness permits trend calculations solely for the 1951–2008 period, all datasets show increases but there is a wide range of magnitudes and the infilled Smith et al. series shows small and insignificant trends (Table 2.10). Fewer data from high latitude stations make these trends less certain and yield *low confidence* in resulting zonal band average estimates. In the mid-latitudes of the SH (60°S to 30°S) there is limited evidence of long-term increases with three data sets showing significant trends for the 1901–2008 period but GHCN having negative trends that are not significant. For the 1951–2008 period changes in SH mid-latitude precipitation are less certain, with one data set showing a significant trend towards drying, two showing non-significant drying trends and the final dataset suggesting increases in precipitation. All data sets show an abrupt decline in SH mid-latitude precipitation in the early 2000s (Figure 2.28) consistent with enhanced drying that has very recently recovered. These results for latitudinal changes are broadly consistent with the global satellite observations for the 1979–2008 period (Allan et al., 2010) and land-based gauge measurements for the 1950–1999 period (Zhang et al., 2007a).

In AR4, maps of observed trends of annual precipitation for 1901–2005 were calculated using GHCN interpolated to a $5^{\circ} \times 5^{\circ}$ latitude/longitude grid. Trends (in percent per decade) were calculated for each grid box and showed statistically significant changes, particularly increases in eastern and northwestern North America, parts of Europe and Russia, southern South America and Australia, declines in the Sahel region of Africa, and a few scattered declines elsewhere.

Figure 2.29 shows the spatial variability of long-term trends (1901–2010) and more recent trends (1951–2010) over land in annual precipitation using the CRU, GHCN and GPCC data sets. The trends are computed from land-only grid box time series using each native data set grid resolution. The patterns of these absolute trends (in mm yr^{-1} per decade) are broadly similar to the trends (in percent per decade) relative

Table 2.10 | Trend estimates and 90% confidence intervals (Box 2.2) for annual precipitation for each time series in Figure 2.28 over two periods. Dashes indicate not enough data available for trend calculation. For the latitudinal band 90°S to 60°S not enough data exist for each product in either period.

Data Set	Area	Trends in mm yr^{-1} per decade	
		1901–2008	1951–2008
CRU TS 3.10.01 (updated from Mitchell and Jones, 2005)	60°N–90°N	–	5.82 ± 2.72
	30°N–60°N	3.82 ± 1.14	1.13 ± 2.01
	30°S–30°N	0.89 ± 2.89	-4.22 ± 8.27
	60°S–30°S	3.88 ± 2.28	-3.73 ± 5.94
GHCN V2 (updated through 2011; Vose et al., 1992)	60°N–90°N	–	4.52 ± 2.64
	30°N–60°N	3.23 ± 1.10	1.39 ± 1.98
	30°S–30°N	1.01 ± 3.00	-5.15 ± 7.28
	60°S–30°S	-0.57 ± 2.27	-8.01 ± 5.63
GPCC V6 (Becker et al., 2013)	60°N–90°N	–	2.69 ± 2.54
	30°N–60°N	3.14 ± 1.05	1.50 ± 1.93
	30°S–30°N	-0.48 ± 3.35	-4.16 ± 9.65
	60°S–30°S	2.40 ± 2.01	-0.51 ± 5.45
Smith et al. (2012)	60°N–90°N	–	0.63 ± 1.27
	30°N–60°N	1.44 ± 0.50	0.97 ± 0.88
	30°S–30°N	0.43 ± 1.48	0.67 ± 4.75
	60°S–30°S	2.94 ± 1.40	0.78 ± 3.31

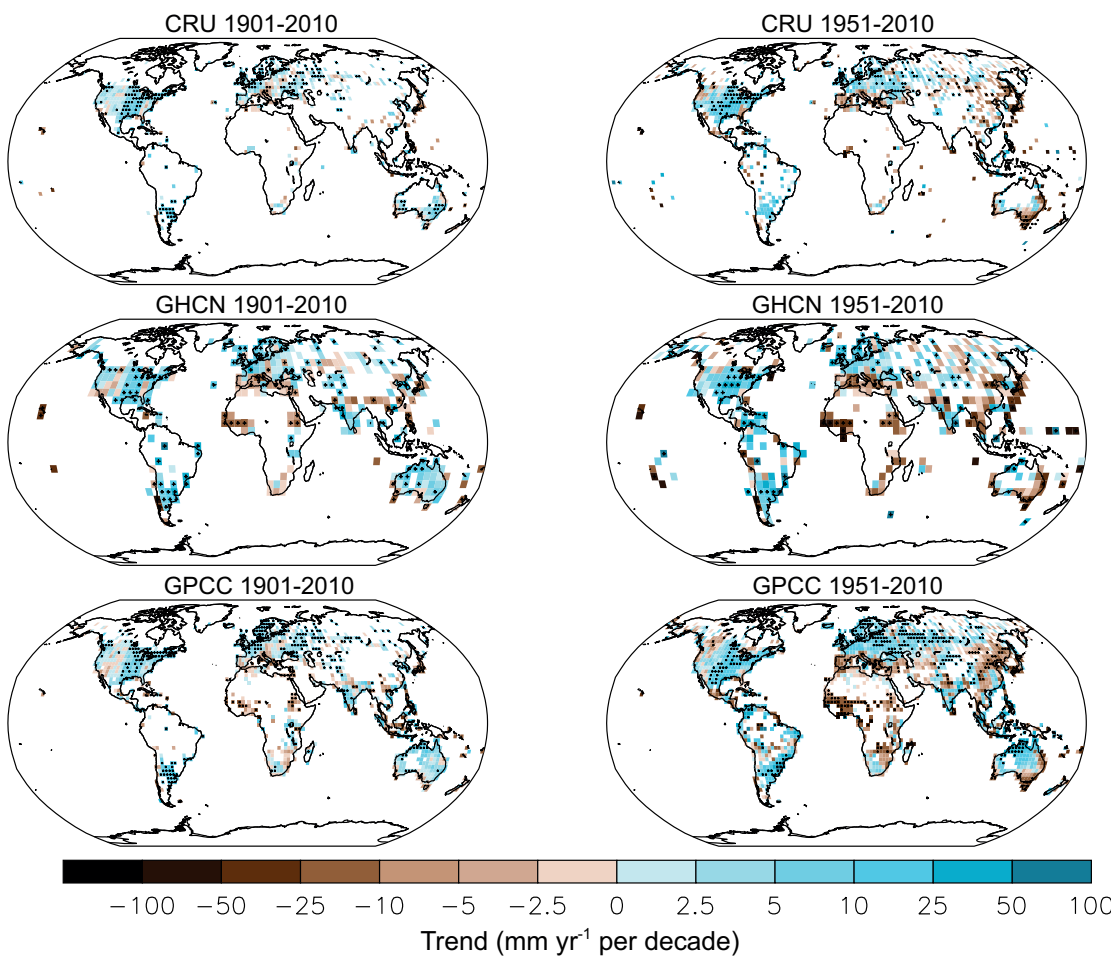


Figure 2.29 | Trends in annual precipitation over land from the CRU, GHCN and GPCC data sets for 1901–2010 (left-hand panels) and 1951–2010 (right-hand panels). Trends have been calculated only for those grid boxes with greater than 70% complete records and more than 20% data availability in first and last decile of the period. White areas indicate incomplete or missing data. Black plus signs (+) indicate grid boxes where trends are significant (i.e., a trend of zero lies outside the 90% confidence interval).

to local climatology (Supplementary Material 2.SM.6.1). Increases for the period 1901–2010 are seen in the mid- and higher-latitudes of both the NH and SH consistent with the reported changes for latitudinal bands. At the grid box scale, statistically significant trends occur in most of the same areas, in each data set but are far more limited than for temperature over a similar length period (cf. Figure 2.21). The GPCC map shows the most areas with significant trends. Comparing the maps in Figure 2.29, most areas for which trends can be calculated for both periods show similar trends between the 1901–2010 period and the 1951–2010 period with few exceptions (e.g., South Eastern Australia,). Trends over shorter periods can differ from those implied for the longest periods. For example, since the late 1980s trends in the Sahel region have been significantly positive (not shown).

In summary, when averaged over the land areas of the mid-latitudes of the NH, all datasets show a *likely* overall increase in precipitation (*medium confidence* since 1901, but *high confidence* after 1951). For all other zones one or more of data sparsity, quality, or a lack of quantitative agreement amongst available estimates yields *low confidence* in characterisation of such long-term trends in zonally averaged precipitation. Nevertheless, changes in some more regional or shorter-term recent changes can be quantified. It is *likely* there was an abrupt decline in SH mid-latitude precipitation in the early 2000s consistent with enhanced drying that has very recently recovered. Precipitation in the tropical land areas has increased (*medium confidence*) over the last decade, reversing the drying trend that occurred from the mid-1970s to mid-1990s reported in AR4.

2.5.1.3 Changes in Snowfall

AR4 draws no conclusion on global changes in snowfall. Changes in snowfall are discussed on a region-by-region basis, but focussed mainly on North America and Eurasia. Statistically significant increases were found in most of Canada, parts of northern Europe and Russia. A number of areas showed a decline in the number of snowfall events, especially those where climatological averaged temperatures were close to 0°C and where warming led to earlier onset of spring. Also, an increase in lake-effect snowfall was found for areas near the North American Great Lakes.

Since AR4, most published literature has considered again changes in snowfall in North America. These studies have confirmed that more winter-time precipitation is falling as rain rather than snow in the western USA (Knowles et al., 2006), the Pacific Northwest and Central USA (Feng and Hu, 2007). Kunkel et al. (2009) analyzed trends using a specially quality-controlled data set of snowfall observations over the contiguous USA and found that snowfall has been declining in the western USA, northeastern USA and southern margins of the seasonal snow region, but increasing in the western Great Plains and Great Lakes regions. Snowfall in Canada has increased mainly in the north while a significant decrease was observed in the southwestern part of the country for 1950–2009 (Mekis and Vincent, 2011).

Other regions that have been analyzed include Japan (Takeuchi et al., 2008), where warmer winters in the heavy snowfall areas on Honshu are associated with decreases in snowfall and precipitation in general. Shekar et al. (2010) found declines in total seasonal snowfall along

with increases in maximum and minimum temperatures in the western Himalaya. Serquet et al. (2011) analyzed snowfall and rainfall days since 1961 and found the proportion of snowfall days to rainfall days in Switzerland was declining in association with increasing temperatures. Scherrer and Appenzeller (2006) found a trend in a pattern of variability of snowfall in the Swiss Alps that indicated decreasing snow at low altitudes relative to high altitudes, but with large decadal variability in key snow indicators (Scherrer et al., 2013). Van Ommen and Morgan (2010) draw a link between increased snowfall in coastal East Antarctica and increased southwest Western Australia drought. However, Monaghan and Bromwich (2008) found an increase in snow accumulation over all Antarctica from the late 1950s to 1990, then a decline to 2004. Thus snowfall changes in Antarctica remain uncertain.

In summary, in most regions analyzed, it is *likely* that decreasing numbers of snowfall events are occurring where increased winter temperatures have been observed (North America, Europe, Southern and East Asia). *Confidence* is *low* for the changes in snowfall over Antarctica.

2.5.2 Streamflow and Runoff

AR4 concluded that runoff and river discharge generally increased at high latitudes, with some exceptions. No consistent long-term trend in discharge was reported for the world's major rivers on a global scale.

River discharge is unique among water cycle components in that it both spatially and temporally integrates surplus waters upstream within a catchment (Shiklomanov et al., 2010) which makes it well suited for *in situ* monitoring (Arndt et al., 2010). The most recent comprehensive analyses (Milliman et al., 2008; Dai et al., 2009) do not support earlier work (Labat et al., 2004) that reported an increasing trend in global river discharge associated with global warming during the 20th century. It must be noted that many if not most large rivers, especially those for which a long-term streamflow record exists, have been impacted by human influences such as dam construction or land use, so results must be interpreted with caution. Dai et al. (2009) assembled a data set of 925 most downstream stations on the largest rivers monitoring 80% of the global ocean draining land areas and capturing 73% of the continental runoff. They found that discharges in about one-third of the 200 largest rivers (including the Congo, Mississippi, Yenisey, Paraná, Ganges, Colombia, Uruguay and Niger) show statistically significant trends during 1948–2004, with the rivers having downward trends (45) outnumbering those with upward trends (19). Decreases in streamflow were found over many low and mid-latitude river basins such as the Yellow River in northern China since 1960s (Piao et al., 2010) where precipitation has decreased. Increases in streamflow during the latter half of the 20th century also have been reported over regions with increased precipitation, such as parts of the USA (Groisman et al., 2004), and in the Yangtze River in southern China (Piao et al., 2010). In the Amazon basin an increase of discharge extremes is observed over recent decades (Espinoza Villar et al., 2009). For France, Giuntoli et al. (2013) found that the sign of the temporal trends in natural streamflows varies with period studied. In that case study, significant correlations between median to low flows and the Atlantic Multidecadal Oscillation (AMO; Section 2.7.8) result in long quasi-periodic oscillations.

At high latitudes, increasing winter base flow and mean annual stream flow resulting from possible permafrost thawing were reported in northwest Canada (St. Jacques and Sauchyn, 2009). Rising minimum daily flows also have been observed in northern Eurasian rivers (Smith et al., 2007). For ocean basins other than the Arctic, and for the global ocean as a whole, the data for continental discharge show small or downward trends, which are statistically significant for the Pacific ($-9.4 \text{ km}^3 \text{ yr}^{-1}$). Precipitation is a major driver for the discharge trends and for the large interannual-to-decadal variations (Dai et al., 2009). However, for the Arctic drainage areas, Adam and Lettenmaier (2008) found that upward trends in streamflow are not accompanied by increasing precipitation, especially over Siberia, based on available observations. Zhang et al. (2012a) argued that precipitation measurements are sparse and exhibit large cold-season biases in the Arctic drainage areas and hence there would be large uncertainties using these data to investigate their influence on streamflow.

Recently, Stahl et al. (2010) and Stahl and Tallaksen (2012) investigated streamflow trends based on a data set of near-natural streamflow records from more than 400 small catchments in 15 countries across Europe for 1962–2004. A regional coherent pattern of annual streamflow trends was revealed with negative trends in southern and eastern regions, and generally positive trends elsewhere. Subtle regional differences in the subannual changes in various streamflow metrics also can be captured in regional studies such as by Monk et al. (2011) for Canadian rivers.

In summary, the most recent comprehensive analyses lead to the conclusion that *confidence is low* for an increasing trend in global river discharge during the 20th century.

2.5.3 Evapotranspiration Including Pan Evaporation

AR4 concluded that decreasing trends were found in records of pan evaporation over recent decades over the USA, India, Australia, New Zealand, China and Thailand and speculated on the causes including decreased surface solar radiation, sunshine duration, increased specific humidity and increased clouds. However, AR4 also reported that direct measurements of evapotranspiration over global land areas are scarce, and concluded that reanalysis evaporation fields are not reliable because they are not well constrained by precipitation and radiation.

Since AR4 gridded data sets have been developed that estimate actual evapotranspiration from either atmospheric forcing and thermal remote sensing, sometimes in combination with direct measurements (e.g., from FLUXNET, a global network of flux towers), or interpolation of FLUXNET data using regression techniques, providing an unprecedented look at global evapotranspiration (Mueller et al., 2011). On a global scale, evapotranspiration over land increased from the early 1980s up to the late 1990s (Wild et al., 2008; Jung et al., 2010; Wang et al., 2010) and Wang et al. (2010) found that global evapotranspiration increased at a rate of 0.6 W m^{-2} per decade for the period 1982–2002. After 1998, a lack of moisture availability in SH land areas, particularly decreasing soil moisture, has acted as a constraint to further increase of global evapotranspiration (Jung et al., 2010).

Zhang et al. (2007b) found decreasing pan evaporation at stations across the Tibetan Plateau, even with increasing air temperature. Similarly, decreases in pan evaporation were also found for northeastern India (Jhajharia et al., 2009) and the Canadian Prairies (Burn and Hesch, 2007). A continuous decrease in reference and pan evaporation for the period 1960–2000 was reported by Xu et al. (2006a) for a humid region in China, consistent with reported continuous increase in aerosol levels over China (Qian et al., 2006; Section 2.2.4). Roderick et al. (2007) examined the relationship between pan evaporation changes and many of the possible causes listed above using a physical model and conclude that many of the decreases (USA, China, Tibetan Plateau, Australia) cited previously are related to declining wind speeds and to a lesser extent decreasing solar radiation. Fu et al. (2009) provided an overview of pan evaporation trends and concluded the major possible causes, changes in wind speed, humidity and solar radiation, have been occurring, but that the importance of each is regionally dependent.

The recent increase in incoming shortwave radiation in regions with decreasing aerosol concentrations (Section 2.2.3) can explain positive evapotranspiration trends only in the humid part of Europe. In semiarid and arid regions, trends in evapotranspiration largely follow trends in precipitation (Jung et al., 2010). Trends in surface winds (Section 2.7.2) and CO_2 (Section 2.2.1.1.1) also alter the partitioning of available energy into evapotranspiration and sensible heat. While surface wind trends may explain pan evaporation trends over Australia (Rayner, 2007; Roderick et al., 2007), their impact on actual evapotranspiration is limited due to the compensating effect of boundary-layer feedbacks (van Heerwaarden et al., 2010). In vegetated regions, where a large part of evapotranspiration comes from transpiration through plants' stomata, rising CO_2 concentrations can lead to reduced stomatal opening and evapotranspiration (Idso and Brazel, 1984; Leakey et al., 2006). Additional regional effects that impact evapotranspiration trends are lengthening of the growing season and land use change.

In summary, there is *medium confidence* that pan evaporation continued to decline in most regions studied since AR4 related to changes in wind speed, solar radiation and humidity. On a global scale, evapotranspiration over land increased (*medium confidence*) from the early 1980s up to the late 1990s. After 1998, a lack of moisture availability in SH land areas, particularly decreasing soil moisture, has acted as a constraint to further increase of global evapotranspiration.

2.5.4 Surface Humidity

AR4 reported widespread increases in surface air moisture content since 1976, along with near-constant relative humidity over large scales though with some significant changes specific to region, time of day or season.

In good agreement with previous analysis from Dai (2006), Willett et al. (2008) show widespread increasing specific humidity across the globe from the homogenized gridded monthly mean anomaly product HadCRUH (1973–2003). Both Dai and HadCRUH products that are blended land and ocean data products end in 2003 but HadISDH (1973–2012) (Willett et al., 2013) and the NOCS product (Berry and Kent, 2009) are available over the land and ocean respectively through 2012. There

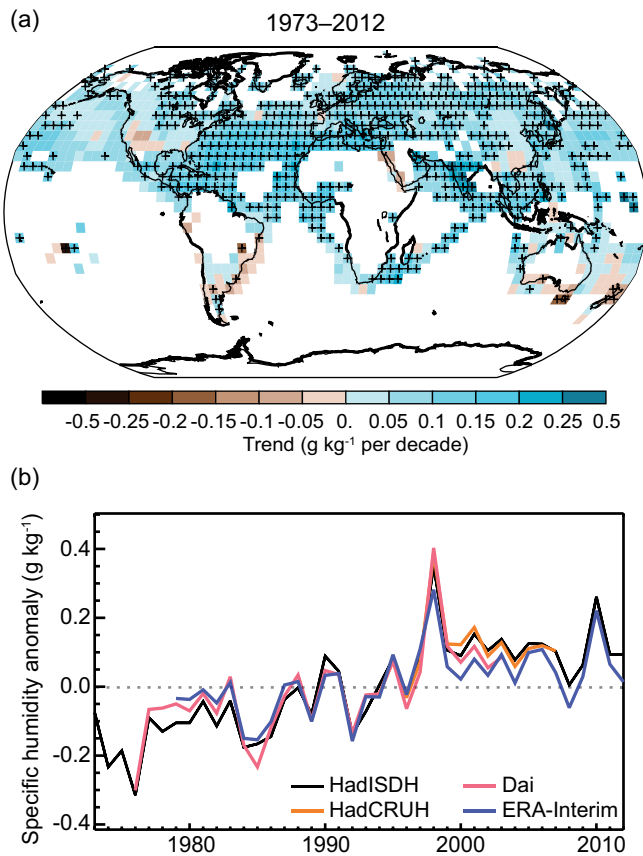


Figure 2.30 | (a) Trends in surface specific humidity from HadISDH and NOCS over 1973–2012. Trends have been calculated only for those grid boxes with greater than 70% complete records and more than 20% data availability in first and last decile of the period. White areas indicate incomplete or missing data. Black plus signs (+) indicate grid boxes where trends are significant (i.e., a trend of zero lies outside the 90% confidence interval). (b) Global annual average anomalies in land surface specific humidity from Dai (2006; red), HadCRUH (Willett et al., 2013; orange), HadISDH (Willett et al., 2013; black), and ERA-Interim (Simmons et al., 2010; blue). Anomalies are relative to the 1979–2003 climatology.

are some small isolated but coherent areas of drying over some of the more arid land regions (Figure 2.30a). Moistening is largest in the tropics and in the extratropics during summer over both land and ocean. Large uncertainty remains over the SH where data are sparse. Global specific humidity is sensitive to large-scale phenomena such as ENSO (Figure 2.30b; Box 2.5). It is strongly correlated with land surface temperature averages over the 23 Giorgi and Francisco (2000) regions for the period 1973–1999 and exhibits increases mostly at or above the

increase expected from the Clausius–Clapeyron relation (about 7% °C⁻¹; Annex III: Glossary) with *high confidence* (Willett et al., 2010). Land surface humidity trends are similar in ERA-Interim to observed estimates of homogeneity-adjusted data sets (Simmons et al., 2010; Figure 2.30b).

Since 2000 surface specific humidity over land has remained largely unchanged (Figure 2.30) whereas land areas have on average warmed slightly (Figure 2.14), implying a reduction in land region relative humidity. This may be linked to the greater warming of the land surface relative to the ocean surface (Joshi et al., 2008). The marine specific humidity (Berry and Kent, 2009), like that over land, shows widespread increases that correlate strongly with SST. However, there is a marked decline in marine relative humidity around 1982. This is reported in Willett et al. (2008) where its origin is concluded to be a non-climatic data issue owing to a change in reporting practice for dewpoint temperature.

In summary, it is *very likely* that global near surface air specific humidity has increased since the 1970s. However, during recent years the near surface moistening over land has abated (*medium confidence*). As a result, fairly widespread decreases in relative humidity near the surface are observed over the land in recent years.

2.5.5 Tropospheric Humidity

As reported in AR4, observations from radiosonde and GPS measurements over land, and satellite measurements over ocean indicate increases in tropospheric water vapour at near-global spatial scales which are consistent with the observed increase in atmospheric temperature over the last several decades. Tropospheric water vapour plays an important role in regulating the energy balance of the surface and TOA, provides a key feedback mechanism and is essential to the formation of clouds and precipitation.

2.5.5.1 Radiosonde

Radiosonde humidity data for the troposphere were used sparingly in AR4, noting a renewed appreciation for biases with the operational radiosonde data that had been highlighted by several major field campaigns and intercomparisons. Since AR4 there have been three distinct efforts to homogenize the tropospheric humidity records from operational radiosonde measurements (Durre et al., 2009; McCarthy et al., 2009; Dai et al., 2011) (Supplementary Material 2.SM.6.1, Table 2.SM.9). Over the common period of record from 1973 onwards, the resulting estimates are in substantive agreement regarding specific

Table 2.11 | Trend estimates and 90% confidence intervals (Box 2.2) for surface humidity over two periods.

	Data Set	Trends in % per decade	
		1976–2003	1973–2012
Land	HadISDH (Willett et al., 2008)	0.127 ± 0.037	0.091 ± 0.023
	HadCRUH_land (Willett et al., 2008)	0.128 ± 0.043	
	Dai_land (Dai, 2006)	0.099 ± 0.046	
Ocean	NOCS (Berry and Kent, 2009)	0.114 ± 0.064	0.090 ± 0.033
	HadCRUH_marine (Willett et al., 2008)	0.065 ± 0.049	
	Dai_marine (Dai, 2006)	0.058 ± 0.044	

humidity trends at the largest geographical scales. On average, the impact of the correction procedures is to remove an artificial temporal trend towards drying in the raw data and indicate a positive trend in free tropospheric specific humidity over the period of record. In each analysis, the rate of increase in the free troposphere is concluded to be largely consistent with that expected from the Clausius–Clapeyron relation (about 7% per degree Celsius). There is no evidence for a significant change in free tropospheric relative humidity, although a decrease in relative humidity at lower levels is observed (Section 2.5.5). Indeed, McCarthy et al. (2009) show close agreement between their radiosonde product at the lowest levels and HadCRUH (Willett et al., 2008).

2.5.5.2 Global Positioning System

Since the early 1990s, estimates of column integrated water vapour have been obtained from ground-based Global Positioning System (GPS) receivers. An international network started with about 100 stations in 1997 and has currently been expanded to more than 500 (primarily land-based) stations. Several studies have compiled GPS water vapour data sets for climate studies (Jin et al., 2007; Wang et al., 2007; Wang and Zhang, 2008, 2009). Using such data, Mears et al. (2010) demonstrated general agreement of the interannual anomalies between ocean-based satellite and land-based GPS column integrated water vapour data. The interannual water vapour anomalies are closely tied to the atmospheric temperature changes in a manner consistent with that expected from the Clausius–Clapeyron relation. Jin et al. (2007) found an average column integrated water vapour trend of about 2 kg m^{-2} per decade during 1994–2006 for 150 (primarily land-based) stations over the globe, with positive trends at most NH stations and negative trends in the SH. However, given the short length (about 10 years) of the GPS records, the estimated trends are very sensitive to the start and end years and the analyzed time period (Box 2.2).

2.5.5.3 Satellite

AR4 reported positive decadal trends in lower and upper tropospheric water vapour based on satellite observations for the period 1988–2004. Since AR4, there has been continued evidence for increases in lower tropospheric water vapour from microwave satellite measurements of column integrated water vapour over oceans (Santer et al., 2007; Wentz et al., 2007) and globally from satellite measurements of spectrally resolved reflected solar radiation (Mieruch et al., 2008). The interannual variability and longer-term trends in column-integrated water vapour over oceans are closely tied to changes in SST at the global scale and interannual anomalies show remarkable agreement with low-level specific humidity anomalies from HadCRUH (O’Gorman et al., 2012). The rate of moistening at large spatial scales over oceans is close to that expected from the Clausius–Clapeyron relation (about 7% per degree Celsius) with invariant relative humidity (Figure 2.31). Satellite measurements also indicate that the globally averaged upper tropospheric relative humidity has changed little over the period 1979–2010 while the troposphere has warmed, implying an increase in the mean water vapour mass in the upper troposphere (Shi and Bates, 2011).

Interannual variations in temperature and upper tropospheric water vapour from IR satellite data are consistent with a constant RH

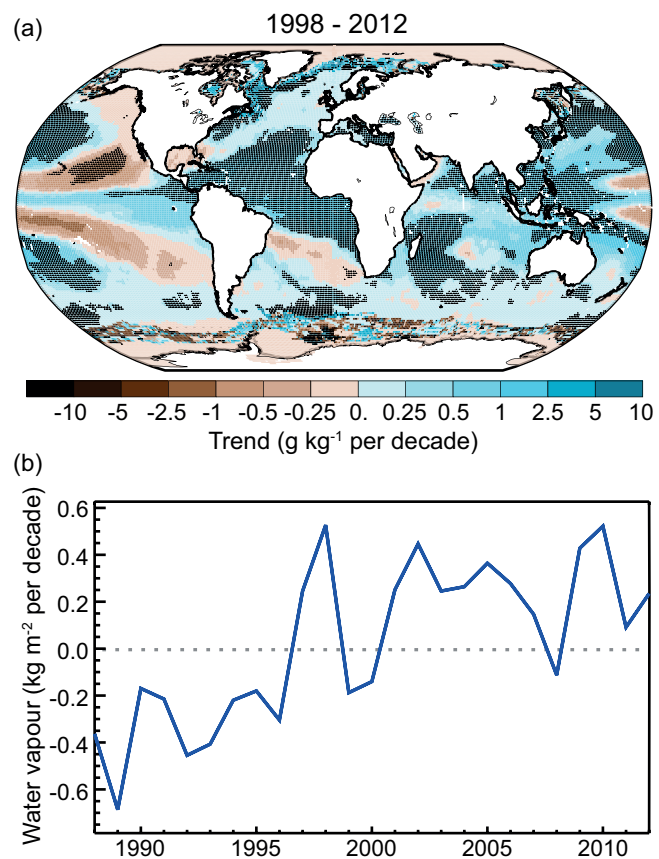


Figure 2.31 | (a) Trends in column integrated water vapour over ocean surfaces from Special Sensor Microwave Imager (Wentz et al., 2007) for the period 1988–2010. Trends have been calculated only for those grid boxes with greater than 70% complete records and more than 20% data availability in first and last decile of the period. Black plus signs (+) indicate grid boxes where trends are significant (i.e., a trend of zero lies outside the 90% confidence interval). (b) Global annual average anomalies in column integrated water vapour averaged over ocean surfaces. Anomalies are relative to the 1988–2007 average.

behavior at large spatial scales (Dessler et al., 2008; Gettelman and Fu, 2008; Chung et al., 2010). On decadal time-scales, increased GHG concentrations reduce clear-sky outgoing long-wave radiation (Allan, 2009; Chung and Soden, 2010), thereby influencing inferred relationships between moisture and temperature. Using Meteosat IR radiances, Brogniez et al. (2009) demonstrated that interannual variations in free tropospheric humidity over subtropical dry regions are heavily influenced by meridional mixing between the deep tropics and the extra tropics. Regionally, upper tropospheric humidity changes in the tropics were shown to relate strongly to the movement of the ITCZ based upon microwave satellite data (Xavier et al., 2010). Shi and Bates (2011) found an increase in upper tropospheric humidity over the equatorial tropics from 1979 to 2008. However there was no significant trend found in tropical-mean or global-mean averages, indicating that on these time and space scales the upper troposphere has seen little change in relative humidity over the past 30 years. While microwave satellite measurements have become increasingly relied upon for studies of upper tropospheric humidity, the absence of a homogenized data set across multiple satellite platforms presents some difficulty in documenting coherent trends from these records (John et al., 2011).

2.5.5.4 Reanalyses

Using NCEP reanalyses for the period 1973–2007, Paltridge et al. (2009) found negative trends in specific humidity above 850 hPa over both the tropics and southern mid-latitudes, and above 600 hPa in the NH mid-latitudes. However, as noted in AR4, reanalysis products suffer from time dependent biases and have been shown to simulate unrealistic trends and variability over the ocean (Mears et al., 2007; John et al., 2009) (Box 2.3). Some reanalysis products do reproduce observed variability in low level humidity over land (Simmons et al., 2010), more complete assessments of multiple reanalysis products yield substantially different and even opposing trends in free tropospheric specific humidity (Chen et al., 2008; Dessler and Davis, 2010). Consequently, reanalysis products are still considered to be unsuitable for the analysis of tropospheric water vapour trends (Sherwood et al., 2010).

In summary, radiosonde, GPS and satellite observations of tropospheric water vapour indicate *very likely* increases at near global scales since the 1970s occurring at a rate that is generally consistent with the Clausius-Clapeyron relation (about 7% per degree Celsius) and the observed increase in atmospheric temperature. Significant trends in tropospheric relative humidity at large spatial scales have not been observed, with the exception of near-surface air over land where relative humidity has decreased in recent years (Section 2.5.5).

2.5.6 Clouds

2.5.6.1 Surface Observations

AR4 reported that surface-observed total cloud cover may have increased over many land areas since the middle of the 20th century, including the USA, the former USSR, Western Europe, mid-latitude Canada and Australia. A few regions exhibited decreases, including China and central Europe. Trends were less globally consistent since the early 1970s, with regional reductions in cloud cover reported for western Asia and Europe but increases over the USA.

Analyses since AR4 have indicated decreases in cloud occurrence/cover in recent decades over Poland (Wibig, 2008), China and the Tibetan Plateau (Duan and Wu, 2006; Endo and Yasunari, 2006; Xia, 2010b), in particular for upper level clouds (Warren et al., 2007) and also over Africa, Eurasia and in particular South America (Warren et al., 2007). Increased frequency of overcast conditions has been reported for some regions, such as Canada, from 1953 to 2002 (Milewska, 2004), with no statistically significant trends evident over Australia (Jovanovic et al., 2011) and North America (Warren et al., 2007). A global analysis of surface observations spanning the period 1971–2009 (Eastman and Warren, 2012) indicates a small decline in total cloud cover of about 0.4% per decade which is largely attributed to declining mid- and high-level cloud cover and is most prominent in the middle latitudes.

Regional variability in surface-observed cloudiness over the ocean appeared more credible than zonal and global mean variations in AR4. Multidecadal changes in upper-level cloud cover and total cloud cover over particular areas of the tropical Indo-Pacific Ocean were consistent with island precipitation records and SST variability. This has been extended more recently by Deser et al. (2010a), who found that an

eastward shift in tropical convection and total cloud cover from the western to central equatorial Pacific occurred over the 20th century and attributed it to a long-term weakening of the Walker circulation (Section 2.7.5). Eastman et al. (2011) report that, after the removal of apparently spurious globally coherent variability, cloud cover decreased in all subtropical stratocumulus regions from 1954 to 2008.

2.5.6.2 Satellite Observations

Satellite cloud observations offer the advantage of much better spatial and temporal coverage compared to surface observations. However they require careful efforts to identify and correct for temporal discontinuities in the data sets associated with orbital drift, sensor degradation, and inter-satellite calibration differences. AR4 noted that there were substantial uncertainties in decadal trends of cloud cover in all satellite data sets available at the time and concluded that there was no clear consensus regarding the decadal changes in total cloud cover. Since AR4 there has been continued effort to assess the quality of and develop improvements to multi-decadal cloud products from operational satellite platforms (Evan et al., 2007; O'Dell et al., 2008; Heidinger and Pavolonis, 2009).

Several satellite data sets offer multi-decadal records of cloud cover (Stubenrauch et al., 2013). AR4 noted that there were discrepancies in global cloud cover trends between ISCCP and other satellite data products, notably a large downward trend of global cloudiness in ISCCP since the late 1980s which is inconsistent with PATMOS-x and surface observations (Baringer et al., 2010). Recent work has confirmed the conclusion of AR4, that much of the downward trend in ISCCP is spurious and an artefact of changes in satellite viewing geometry (Evan et al., 2007). An assessment of long-term variations in global-mean cloud amount from nine different satellite data sets by Stubenrauch et al. (2013) found differences between data sets were comparable in magnitude to the interannual variability (2.5 to 3.5%). Such inconsistencies result from differences in sampling as well as changes in instrument calibration and inhibit an accurate assessment of global-scale cloud cover trends.

Satellite observations of low-level marine clouds suggest no long-term trends in cloud liquid water path or optical properties (O'Dell et al., 2008; Rausch et al., 2010). On regional scales, trends in cloud properties over China have been linked to changes in aerosol concentrations (Qian et al., 2009; Bennartz et al., 2011) (Section 2.2.3).

In summary, surface-based observations show region- and height-specific variations and trends in cloudiness but there remains substantial ambiguity regarding global-scale cloud variations and trends, especially from satellite observations. Although trends of cloud cover are consistent between independent data sets in certain regions, substantial ambiguity and therefore *low confidence* remains in the observations of global-scale cloud variability and trends.

2.6 Changes in Extreme Events

AR4 highlighted the importance of understanding changes in extreme climate events (Annex III: Glossary) because of their disproportionate

impact on society and ecosystems compared to changes in mean climate (see also IPCC Working Group II). More recently a comprehensive assessment of observed changes in extreme events was undertaken by the IPCC Special Report on Managing the Risks of Extreme Events and Disasters to Advance Climate Change Adaptation (SREX) (Seneviratne et al., 2012; Section 1.3.3).

Data availability, quality and consistency especially affect the statistics of extremes and some variables are particularly sensitive to changing measurement practices over time. For example, historical tropical cyclone records are known to be heterogeneous owing to changing observing technology and reporting protocols (Section 14.6.1) and when records from multiple ocean basins are combined to explore global trends, because data quality and reporting protocols vary substantially between regions (Knapp and Kruk, 2010). Similar problems have been discovered when analysing wind extremes, because of the sensitivity of measurements to changing instrumentation and observing practice (e.g., Smits et al., 2005; Wan et al., 2010).

Numerous regional studies indicate that changes observed in the frequency of extremes can be explained or inferred by shifts in the overall probability distribution of the climate variable (Griffiths et al., 2005; Ballester et al., 2010; Simolo et al., 2011). However, it should be noted that these studies refer to counts of threshold exceedance—frequency, duration—which closely follow mean changes. Departures from high percentiles/return periods (intensity, severity, magnitude) are highly sensitive to changes in the shape and scale parameters of the distribution (Schär et al., 2004; Clark et al., 2006; Della-Marta et al., 2007a, 2007b; Fischer and Schär, 2010) and geographical location. Debate continues over whether variance as well as mean changes are affecting global temperature extremes (Hansen et al., 2012; Rhines and Huybers, 2013) as illustrated in Figure 1.8 and FAQ 2.2, Figure 1. In the following sections the conclusions from both AR4 and SREX are reviewed along with studies subsequent to those assessments.

2.6.1 Temperature Extremes

AR4 concluded that it was *very likely* that a large majority of global land areas had experienced decreases in indices of cold extremes and increases in indices of warm extremes, since the middle of the 20th century, consistent with warming of the climate. In addition, globally averaged multi-day heat events had *likely* exhibited increases over a similar period. SREX updated AR4 but came to similar conclusions while using the revised AR5 uncertainty guidance (Seneviratne et al., 2012). Further evidence since then indicates that the level of *confidence* that the majority of warm and cool extremes show warming remains *high*.

A large amount of evidence continues to support the conclusion that most global land areas analysed have experienced significant warming of both maximum and minimum temperature extremes since about 1950 (Donat et al., 2013c). Changes in the occurrence of cold and warm days (based on daily maximum temperatures) are generally less marked (Figure 2.32). ENSO (Box 2.5) influences both maximum and minimum temperature variability especially around the Pacific Rim (e.g., Kenyon and Hegerl, 2008; Alexander et al., 2009) but often affecting cold and warm extremes differently. Different data sets using different gridding methods and/or input data (Supplementary Material 2.SM.7) indicate large coherent trends in temperature extremes globally, associated with warming (Figure 2.32). The level of quality control varies between these data sets. For example, HadEX2 (Donat et al., 2013c) uses more rigorous quality control which leads to a reduced station sample compared to GHCNDEX (Donat et al., 2013a) or HadGHCND (Caesar et al., 2006). However, despite these issues data sets compare remarkably consistently even though the station networks vary through time (Figure 2.32; Table 2.12). Other data sets that have assessed these indices, but cover a shorter period, also agree very well over the period of overlapping data, e.g., HadEX (Alexander et al., 2006) and Duke (Morak et al., 2011, 2013).

The shift in the distribution of nighttime temperatures appears greater than daytime temperatures although whether distribution changes are simply linked to increases in the mean or other moments is an active area of research (Ballester et al., 2010; Simolo et al., 2011; Donat and Alexander, 2012; Hansen et al., 2012). Indeed, all data sets examined (Duke, GHCNDEX, HadEX, HadEX2 and HadGHCND), indicate a faster increase in minimum temperature extremes than maximum temperature extremes. While DTR declines have only been assessed with *medium confidence* (Section 2.4.1.2), *confidence* of accelerated increases in minimum temperature extremes compared to maximum temperature extremes is *high* due to the more consistent patterns of warming in minimum temperature extremes globally.

Regional changes in a range of climate indices are assessed in Table 2.13. These indicate *likely* increases across most continents in unusually warm days and nights and/or reductions in unusually cold days and nights including frosts. Some regions have experienced close to a doubling of the occurrence of warm and a halving of the occurrence of cold nights, for example, parts of the Asia-Pacific region (Choi et al., 2009) and parts of Eurasia (Klein Tank et al., 2006; Donat et al., 2013a, 2013c) since the mid-20th century. Changes in both local and global SST patterns (Section 2.4.2) and large scale circulation patterns (Section 2.7) have been shown to be associated with regional changes in temperature extremes (Barrucand et al., 2008; Scaife et al., 2008;

Table 2.12 | Trend estimates and 90% confidence intervals (Box 2.2) for global values of cold nights (TN10p), cold days (TX10p), warm nights (TN90p) and warm days (TX90p) over the periods 1951–2010 and 1979–2010 (see Box 2.4, Table 1 for more information on indices).

Data Set	Trends in % per decade							
	TN10p		TX10p		TN90p		TX90p	
	1951–2010	1979–2010	1951–2010	1979–2010	1951–2010	1979–2010	1951–2010	1979–2010
HadEX2 (Donat et al., 2013c)	-3.9 ± 0.6	-4.2 ± 1.2	-2.5 ± 0.7	-4.1 ± 1.4	4.5 ± 0.9	6.8 ± 1.8	2.9 ± 1.2	6.3 ± 2.2
HadGHCND (Caesar et al., 2006)	-4.5 ± 0.7	-4.0 ± 1.5	-3.3 ± 0.8	-5.0 ± 1.6	5.8 ± 1.3	8.6 ± 2.3	4.2 ± 1.8	9.4 ± 2.7
GHCNDEX (Donat et al., 2013a)	-3.9 ± 0.6	-3.9 ± 1.3	-2.6 ± 0.7	-3.9 ± 1.4	4.3 ± 0.9	6.3 ± 1.8	2.9 ± 1.2	6.1 ± 2.2

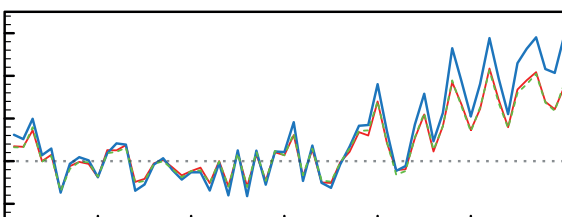
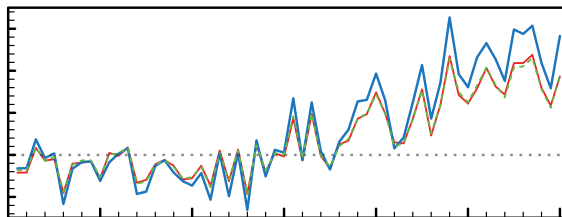
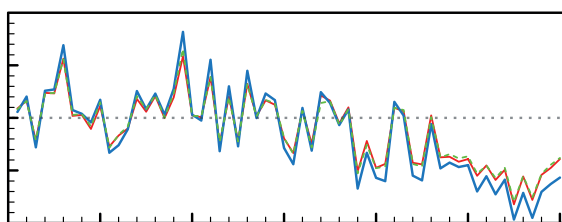
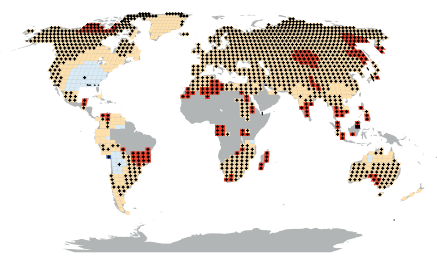
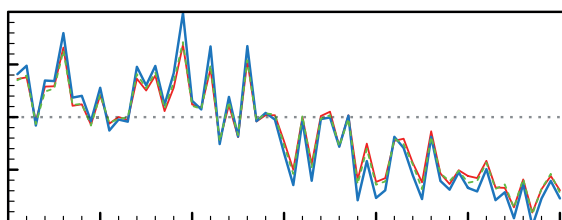
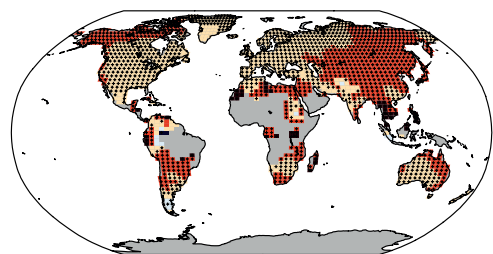


Figure 2.32 | Trends in annual frequency of extreme temperatures over the period 1951–2010, for (a) cold nights (TN10p), (b) cold days (TX10p), (c) warm nights (TN90p) and (d) warm days (TX90p) (Box 2.4, Table 1). Trends were calculated only for grid boxes that had at least 40 years of data during this period and where data ended no earlier than 2003. Grey areas indicate incomplete or missing data. Black plus signs (+) indicate grid boxes where trends are significant (i.e., a trend of zero lies outside the 90% confidence interval). The data source for trend maps is HadEX2 (Donat et al., 2013c) updated to include the latest version of the European Climate Assessment data set (Klok and Tank, 2009). Beside each map are the near-global time series of annual anomalies of these indices with respect to 1961–1990 for three global indices data sets: HadEX2 (red); HadGHCND (Caesar et al., 2006; blue) and updated to 2010 and GHCNDEX (Donat et al., 2013a; green). Global averages are only calculated using grid boxes where all three data sets have at least 90% of data over the time period. Trends are significant (i.e., a trend of zero lies outside the 90% confidence interval) for all the global indices shown.

Table 2.13 | Regional observed changes in a range of climate indices since the middle of the 20th century. Assessments are based on a range of ‘global’ studies and assessments (Groisman et al., 2005; Alexander et al., 2006; Caesar et al., 2006; Sheffield and Wood, 2008; Dai, 2011a, 2011b, 2013; Seneviratne et al., 2012; Sheffield et al., 2012; Donat et al., 2013a, 2013c; van der Schrier et al., 2013) and selected regional studies as indicated. Bold text indicates where the assessment is somewhat different to SREX Table 3-2. In each such case a footnote explains why the assessment is different. See also Figures 2.32 and 2.33.

Region	Warm Days (e.g., TX90p ^a)	Cold Days (e.g., TX10p ^a)	Warm Nights (e.g., TN90p ^a , TR ^a)	Cold Nights/Frosts (e.g., TN10p ^a , FD ^a)	Heat Waves / Warm Spells ^g	Extreme Precipitation (e.g., RX1day ^a , R95p ^a , R99p ^a)	Dryness (e.g., CDD ^a) / Drought ^h
North America and Central America	<i>High confidence:</i> Likely overall increase but spatially varying trends ^{1,2}	<i>High confidence:</i> Likely overall decrease but with spatially varying trends ^{1,2}	<i>High confidence:</i> Likely overall increase ^{1,2}	<i>High confidence:</i> Likely overall decrease ^{1,2}	<i>Medium confidence:</i> increases in more regions than decreases ^{1,3} but 1930s dominates longer term trends in the USA ⁴	<i>High confidence:</i> Likely overall increase ^{1,2,5} but some spatial variation <i>High confidence:</i> Very likely increase central North America ^{6,7}	<i>Medium confidence:</i> decrease ¹ but spatially varying trends <i>High confidence^b:</i> Likely decrease central North America ⁴
South America	<i>Medium confidence^b:</i> Overall increase ⁸	<i>Medium confidence^b:</i> Overall decrease ⁸	<i>Medium confidence^b:</i> Overall increase ⁸	<i>Medium confidence^b:</i> Overall decrease ⁸	<i>Low confidence:</i> insufficient evidence (lack of literature) and spatially varying trends but some evidence of increases in more areas than decreases ⁸	<i>Medium confidence^b:</i> Increases in more regions than decreases ^{8,9} but spatially varying trends	<i>Low confidence:</i> limited literature and spatially varying trends ⁸
Europe and Mediterranean	<i>High confidence:</i> Likely overall increase ^{10,11,12}	<i>High confidence:</i> Likely overall decrease ^{11,12}	<i>High confidence:</i> Likely overall increase ^{11,12}	<i>High confidence:</i> Likely overall decrease ^{10,11,12}	<i>High confidence^b:</i> Likely increases in most regions ^{3,13}	<i>High confidence^{b,c}:</i> Likely increases in more regions than decreases ^{5,15,16} but regional and seasonal variation	<i>Medium confidence:</i> spatially varying trends <i>High confidence^b:</i> Likely increase in Mediterranean ^{17,18}
Africa and Middle East	<i>Low to medium confidence^{b,d}:</i> limited data in many regions but increases in most regions assessed	<i>Low to medium confidence^{b,d}:</i> limited data in many regions but decreases in most regions assessed	<i>Medium confidence^{b,d}:</i> limited data in many regions but increases in most regions assessed	<i>Medium confidence^{b,d}:</i> limited data in many regions but decreases in most regions assessed	<i>Low confidence^d:</i> insufficient evidence (lack of literature) <i>Medium confidence:</i> increase in North Africa and Middle East and southern Africa ^{3,19,21,22}	<i>Low confidence^d:</i> insufficient evidence and spatially varying trends <i>Medium confidence^b:</i> increases in more regions than decreases in southern Africa but spatially varying trends depending on index ^{5,21,22}	<i>Medium confidence^d:</i> increase ^{19,22,24} <i>High confidence^b:</i> Likely increase in West Africa ^{25,26} although 1970s Sahel drought dominates the trend
Asia (excluding South-east Asia)	<i>High confidence^{b,e}:</i> Likely overall increase ^{27,28,29,30,31,32}	<i>High confidence^{b,e}:</i> Likely overall decrease ^{27,28,29,30,31,32}	<i>High confidence^{b,e}:</i> Likely overall increase ^{27,28,29,30,31,32}	<i>High confidence^{b,e}:</i> Likely overall increase ^{27,28,29,30,31,32}	<i>Medium confidence^{b,e}:</i> Spatially varying trends and insufficient data in some regions <i>High confidence^{b,c}:</i> Likely more areas of increases than decreases ^{3,28,33}	<i>Low to medium confidence^{b,e}:</i> <i>Low confidence</i> due to insufficient evidence or spatially varying trends. <i>Medium confidence:</i> increases in more regions than decreases ^{5,34,35,36}	<i>Low to medium confidence^{b,e}</i> <i>Medium confidence:</i> Increase in eastern Asia ^{36,37}
South-east Asia and Oceania	<i>High confidence^{b,f}:</i> Likely overall increase ^{27,38,39,40}	<i>High confidence^{b,f}:</i> Likely overall decrease ^{27,38,39}	<i>High confidence^{b,f}:</i> Likely overall increase ^{27,38,39,40}	<i>High confidence^{b,f}:</i> Likely overall decrease ^{27,38,39}	<i>Low confidence</i> (due lack of literature) to <i>high confidence^{b,f}</i> depending on region <i>High confidence²:</i> Likely overall increase in Australia ^{3,14,41}	<i>Low confidence</i> (lack of literature) to <i>high confidence^{b,f}</i> <i>High confidence:</i> Likely decrease in southern Australia ^{42,43} but index and season dependent	<i>Low to medium confidence^{b,f}:</i> inconsistent trends between studies in SE Asia. Overall increase in dryness in southern and eastern Australia <i>High confidence^b:</i> Likely decrease northwest Australia ^{25,26,44}

(continued on next page)

(Table 2.13 continued)

Notes:

- ^a See Table 1 in Box 2.4, for definitions.
- ^b More recent literature updates the assessment from SREX Table 3-2 (including 'global' studies).
- ^c This represents a measure of the area affected which is different from what was assessed in SREX Table 3-2.
- ^d This represents a slightly different region than that assessed in SREX Table 3-2 as it includes the Middle East.
- ^e This represents a slightly different region than that assessed in SREX Table 3-2 as it excludes Southeast Asia.
- ^f This represents a slightly different region than that assessed in SREX Table 3-2 as it combines SE Asia and Oceania.
- ^g Definitions for warm spells and heat waves vary (Perkins and Alexander, 2012) but here we are commonly assessing the Warm Spell Duration Index (WSDI; Zhang et al., 2011) or other heat wave indices (e.g., HWF, HWM; Fischer and Schär, 2010; Perkins et al., 2012) that have defined multi-day heat extremes relative to either daily maximum or minimum temperatures (or both) above a high (commonly 90th) percentile relative to a late-20th century reference period.
- ^h See Box 2.4 and Section 2.6.1 for definitions.
- ¹ Kunkel et al. (2008), ² Peterson et al. (2008), ³ Perkins et al. (2012), ⁴ Peterson et al. (2013), ⁵ Westra et al. (2013), ⁶ Groisman et al. (2012), ⁷ Villarini et al. (2013), ⁸ Skansi et al. (2013), ⁹ Haylock et al. (2006), ¹⁰ Andrade et al. (2012), ¹¹ Efthymiadis et al. (2011), ¹² Moberg et al. (2006), ¹³ Della-Marta et al. (2007a), ¹⁴ Perkins and Alexander (2012), ¹⁵ Van den Besselaar et al. (2012), ¹⁶ Zolina et al. (2009), ¹⁷ Sousa et al. (2011), ¹⁸ Hoerling et al. (2012), ¹⁹ Donat et al. (2013b), ²⁰ Zhang et al. (2005), ²¹ Kruger and Sekele (2013), ²² New et al. (2006), ²³ Vincent et al. (2011), ²⁴ Aguilar et al. (2009), ²⁵ Dai (2013), ²⁶ Sheffield et al. (2012), ²⁷ Choi et al. (2009), ²⁸ Rahimzadeh et al. (2009), ²⁹ Revadekar et al. (2012), ³⁰ Tank et al. (2006), ³¹ You et al. (2010), ³² Zhou and Ren (2011), ³³ Ding et al. (2010), ³⁴ Krishna Moorthy et al. (2009), ³⁵ Pattaika and Rajeevan (2010), ³⁶ Wang et al. (2012b), ³⁷ Fischer et al. (2011), ³⁸ Caesar et al. (2011), ³⁹ Chambers and Griffiths (2008), ⁴⁰ Wang et al. (2013), ⁴¹ Tryhorn and Risbey (2006), ⁴² Gallant et al. (2007), ⁴³ King et al. (2013), ⁴⁴ Jones et al. (2009).

2

Alexander et al., 2009; Li et al., 2012), particularly in regions around the Pacific Rim (Kenyon and Hegerl, 2008). Globally, there is evidence of large-scale warming trends in the extremes of temperature, especially minimum temperature, since the beginning of the 20th century (Donat et al., 2013c).

There are some exceptions to this large-scale warming of temperature extremes including central North America, eastern USA (Alexander et al., 2006; Kunkel et al., 2008; Peterson et al., 2008) and some parts of South America (Alexander et al., 2006; Rusticucci and Renom, 2008; Skansi et al., 2013) which indicate changes consistent with cooling in these locations. However, these exceptions appear to be mostly associated with changes in maximum temperatures (Donat et al., 2013c). The so-called 'warming hole' in central North America and eastern USA, where temperatures have cooled relative to the significant warming elsewhere in the region, is associated with observed changes in the hydrological cycle and land–atmosphere interaction (Pan et al., 2004; Portmann et al., 2009a; Portmann et al., 2009b; Misra et al., 2012) and decadal and multi-decadal variability linked with the Atlantic and Pacific Oceans (Meehl et al., 2012; Weaver, 2012).

Since AR4 many studies have analysed local to regional changes in multi-day temperature extremes in more detail, specifically addressing different heat wave aspects such as frequency, intensity, duration and spatial extent (Box 2.4, FAQ 2.2). Several high-profile heat waves have occurred in recent years (e.g., in Europe in 2003 (Beniston, 2004), Australia in 2009 (Pezza et al., 2012), Russia in 2010 (Barriopedro et al., 2011; Dole et al., 2011; Trenberth and Fasullo, 2012a) and USA in 2010/2011 (Hoerling et al., 2012) (Section 10.6.2) which have had severe impacts (see WGI). Heat waves are often associated with quasi-stationary anticyclonic circulation anomalies that produce prolonged hot conditions at the surface (Black and Sutton, 2007; Garcia-Herrera et al., 2010), but long-term changes in the persistence of these anomalies are still relatively poorly understood (Section 2.7). Heat waves can also be amplified by pre-existing dry soil conditions in transitional climate zones (Ferranti and Viterbo, 2006; Fischer et al., 2007; Seneviratne et al., 2010; Mueller and Seneviratne, 2012) and the persistence of those soil-moisture anomalies (Lorenz et al., 2010). Dry soil-moisture conditions are either induced by precipitation deficits (Della-Mar-

ta et al., 2007b; Vautard et al., 2007), or evapotranspiration excesses (Black and Sutton, 2007; Fischer et al., 2007), or a combination of both (Seneviratne et al., 2010). This amplification of soil moisture–temperature feedbacks is suggested to have partly enhanced the duration of extreme summer heat waves in southeastern Europe during the latter part of the 20th century (Hirschi et al., 2011), with evidence emerging of a signature in other moisture-limited regions (Mueller and Seneviratne, 2012).

Table 2.13 shows that there has been a *likely* increasing trend in the frequency of heatwaves since the middle of the 20th century in Europe and Australia and across much of Asia where there are sufficient data. However, *confidence* on a global scale is *medium* owing to lack of studies over Africa and South America but also in part owing to differences in trends depending on how heatwaves are defined (Perkins et al., 2012). Using monthly means as a proxy for heatwaves Coumou et al. (2013) and Hansen et al. (2012) indicate that record-breaking temperatures in recent decades substantially exceed what would be expected by chance but caution is required when making inferences between these studies and those that deal with multi-day events and/or use more complex definitions for heatwave events. There is also evidence in some regions that periods prior to the 1950s had more heatwaves (e.g., over the USA, the decade of the 1930s stands out and is also associated with extreme drought conditions (Peterson et al., 2013) whereas conversely in other regions heatwave trends may have been underestimated owing to poor quality and/or consistency of data (e.g., Della-Marta et al. (2007a) over Western Europe; Kuglitsch et al. (2009, 2010) over the Mediterranean). Recent available studies also suggest that the number of cold spells has reduced significantly since the 1950s (Donat et al., 2013a, 2013c).

In summary, new analyses continue to support the AR4 and SREX conclusions that since about 1950 it is *very likely* that the numbers of cold days and nights have decreased and the numbers of warm days and nights have increased overall on the global scale, that is, for land areas with sufficient data. It is *likely* that such changes have also occurred across most of North America, Europe, Asia and Australia. There is *low to medium confidence* in historical trends in daily temperature extremes in Africa and South America as there is either

insufficient data or trends vary across these regions. This, combined with issues with defining events, leads to the assessment that there is *medium confidence* that globally the length and frequency of warm spells, including heat waves, has increased since the middle of the 20th century although it is *likely* that heatwave frequency has increased during this period in large parts of Europe, Asia and Australia.

2.6.2 Extremes of the Hydrological Cycle

In Section 2.5 mean state changes in different aspects of the hydrological cycle are discussed. In this section we focus on the more extreme aspects of the cycle including extreme rainfall, severe local weather events like hail, flooding and droughts. Extreme events associated with tropical and extratropical storms are discussed in Sections 2.6.3 and 2.6.4 respectively.

2.6.2.1 Precipitation Extremes

AR4 concluded that substantial increases are found in heavy precipitation events. It was *likely* that annual heavy precipitation events had disproportionately increased compared to mean changes between 1951 and 2003 over many mid-latitude regions, even where there had been a reduction in annual total precipitation. Rare precipitation (such as the highest annual daily precipitation total) events were *likely* to have increased over regions with sufficient data since the late 19th century. SREX supported this view, as have subsequent analyses, but noted large spatial variability within and between regions (Table 3.2 of Seneviratne et al., 2012).

Given the diverse climates across the globe, it has been difficult to provide a universally valid definition of 'extreme precipitation'. However, Box 2.4 Table 1 indicates some of the common definitions that are used in the scientific literature. In general, statistical tests indicate changes in precipitation extremes are consistent with a wetter climate (Section 7.6.5), although with a less spatially coherent pattern of change than temperature, in that there are large areas that show increasing trends and large areas that show decreasing trends and a lower level of statistical significance than for temperature change (Alexander et al., 2006; Donat et al., 2013a, 2013c). Using R95p and SDII indices (Box 2.4), Figures 2.33a and 2.33b show these areas for heavy precipitation amounts and precipitation intensity where sufficient data are available in the HadEX2 data set (Donat et al., 2013c) although there are more areas showing significant increases than decreases. Although changes in large-scale circulation patterns have a substantial influence on precipitation extremes globally (Alexander et al., 2009; Kenyon and Hegerl, 2010), Westra et al. (2013) showed, using *in situ* data over land, that trends in the wettest day of the year indicate more increases than would be expected by chance. Over the tropical oceans satellite measurements show an increase in the frequency of the heaviest rainfall during warmer (El Niño) years (Allan and Soden, 2008).

Regional trends in precipitation extremes since the middle of the 20th century are varied (Table 2.13). In most continents *confidence* in trends is not higher than *medium* except in North America and Europe where there have been *likely* increases in either the frequency or intensity of heavy precipitation. This assessment increases to *very likely* for central North America. For North America it is also *likely* that increases

have occurred during the whole of the 20th century (Pryor et al., 2009; Donat et al., 2013c; Villarini et al., 2013). For South America the most recent integrative studies indicate heavy rain events are increasing in frequency and intensity over the continent as a whole (Donat et al., 2013c; Skansi et al., 2013). For Europe and the Mediterranean, the assessment masks some regional and seasonal variation. For example, much of the increase reported in Table 2.13 is found in winter although with decreasing trends in some other regions such as northern Italy, Poland and some Mediterranean coastal sites (Pavan et al., 2008; Lupi-Kasza, 2010; Toreti et al., 2010). There are mixed regional trends across Asia and Oceania but with some indication that increases are being observed in more regions than decreases while recent studies focused on Africa, in general, have not found significant trends in extreme precipitation (see Chapter 14 for more on regional variations and trends).

The above studies generally use indices which reflect 'moderate' extremes, for example, events occurring as often as 5% or 10% of the time (Box 2.4). Only a few regions have sufficient data to assess trends in rarer precipitation events reliably, for example, events occurring on average once in several decades. Using Extreme Value Theory, DeGaetano (2009) showed a 20% reduction in the return period for extreme precipitation events over large parts of the contiguous USA from 1950 to 2007. For Europe from 1951 to 2010, Van den Besselaar et al. (2012) reported a median reduction in 5- to 20-year return periods of 21%, with a range between 2% and 58% depending on the subregion and season. This decrease in return times for rare extremes is qualitatively similar to the increase in moderate extremes for these regions reported above, and also consistent with earlier local results for the extreme tail of the distribution reported in AR4.

The aforementioned studies refer to daily precipitation extremes, although rainfall will often be limited to part of the day only. The literature on sub-daily scales is too limited for a global assessment although it is clear that analysis and framing of questions regarding sub-daily precipitation extremes is becoming more critical (Trenberth, 2011). Available regional studies have shown results that are even more complex than for daily precipitation and with variations in the spatial patterns of trends depending on event formulation and duration. However, regional studies show indications of more increasing than decreasing trends (Sen Roy, 2009; for India) (Sen Roy and Rouault, 2013; for South Africa) (Westra and Sisson, 2011; for Australia). Some studies present evidence of scaling of sub-daily precipitation with temperature that is outside that expected from the Clausius–Clapeyron relation (about 7% per degree Celsius) (Lenderink and Van Meijgaard, 2008; Haerter et al., 2010; Jones et al., 2010; Lenderink et al., 2011; Utsumi et al., 2011), but scaling beyond that expected from thermodynamic theories is controversial (Section 7.6.5).

In summary, further analyses continue to support the AR4 and SREX conclusions that it is *likely* that since 1951 there have been statistically significant increases in the number of heavy precipitation events (e.g., above the 95th percentile) in more regions than there have been statistically significant decreases, but there are strong regional and sub-regional variations in the trends. In particular, many regions present statistically non-significant or negative trends, and, where seasonal changes have been assessed, there are also variations between seasons (e.g., more consistent trends in winter than in summer in Europe). The

overall most consistent trends towards heavier precipitation events are found in central North America (*very likely* increase) but assessment for Europe shows *likely* increases in more regions than decreases.

2.6.2.2 Floods

AR4 WGI Chapter 3 (Trenberth et al., 2007) did not assess changes in floods but AR4 WGII concluded that there was not a general global trend in the incidence of floods (Kundzewicz et al., 2007). SREX went further to suggest that there was low agreement and thus *low confidence* at the global scale regarding changes in the magnitude or frequency of floods or even the sign of changes.

AR5 WGII assesses floods in regional detail accounting for the fact that trends in floods are strongly influenced by changes in river management (see also Section 2.5.2). Although the most evident flood trends appear to be in northern high latitudes, where observed warming trends have been largest, in some regions no evidence of a trend in extreme flooding has been found, for example, over Russia based on daily river discharge (Shiklomanov et al., 2007). Other studies for Europe (Hannaford and Marsh, 2008; Renard et al., 2008; Petrow and Merz, 2009; Stahl et al., 2010) and Asia (Jiang et al., 2008; Delgado et al., 2010) show evidence for upward, downward or no trend in the magnitude and frequency of floods, so that there is currently no clear and widespread evidence for observed changes in flooding except for the earlier spring flow in snow-dominated regions (Seneviratne et al., 2012).

In summary, there continues to be a lack of evidence and thus *low confidence* regarding the sign of trend in the magnitude and/or frequency of floods on a global scale.

2.6.2.3 Droughts

AR4 concluded that droughts had become more common, especially in the tropics and sub-tropics since about 1970. SREX provided a comprehensive assessment of changes in observed droughts (Section 3.5.1 and Box 3.3 of SREX), updated the conclusions provided by AR4 and stated that the type of drought considered and the complexities in defining drought (Annex III: Glossary) can substantially affect the conclusions regarding trends on a global scale (Chapter 10). Based on evidence since AR4, SREX concluded that there were not enough direct observations of dryness to suggest *high confidence* in observed trends globally, although there was *medium confidence* that since the 1950s some regions of the world have experienced more intense and longer droughts. The differences between AR4 and SREX are due primarily to analyses post-AR4, differences in how both assessments considered drought and updated IPCC uncertainty guidance.

There are very few direct measurements of drought related variables, such as soil moisture (Robock et al., 2000), so drought proxies (e.g., PDSI, SPI, SPEI; Box 2.4) and hydrological drought proxies (e.g., Vidal et al., 2010; Dai, 2011b) are often used to assess drought. The chosen proxy (e.g., precipitation, evapotranspiration, soil moisture or streamflow) and time scale can strongly affect the ranking of drought events (Sheffield et al., 2009; Vidal et al., 2010). Analyses of these indirect indices come with substantial uncertainties. For example, PDSI may not

be comparable across climate zones. A self-calibrating (sc-) PDSI can replace the fixed empirical constants in PDSI with values representative of the local climate (Wells et al., 2004). Furthermore, for studies using simulated soil moisture, the type of potential evapotranspiration model used can lead to significant differences in the estimation of the regions affected and the areal extent of drought (Sheffield et al., 2012), but the overall effect of a more physically realistic parameterisation is debated (van der Schrier et al., 2013).

Because drought is a complex variable and can at best be incompletely represented by commonly used drought indices, discrepancies in the interpretation of changes can result. For example, Sheffield and Wood (2008) found decreasing trends in the duration, intensity and severity of drought globally. Conversely, Dai (2011a,b) found a general global increase in drought, although with substantial regional variation and individual events dominating trend signatures in some regions (e.g., the 1970s prolonged Sahel drought and the 1930s drought in the USA and Canadian Prairies). Studies subsequent to these continue to provide somewhat different conclusions on trends in global droughts and/or dryness since the middle of the 20th century (Sheffield et al., 2012; Dai, 2013; Donat et al., 2013c; van der Schrier et al., 2013).

Van der Schrier et al. (2013), using monthly sc-PDSI, found no strong case either for notable drying or moisture increase on a global scale over the periods 1901–2009 or 1950–2009, and this largely agrees with the results of Sheffield et al. (2012) over the latter period. A comparison between the sc-PDSI calculated by van der Schrier et al. (2013) and that of Dai (2011a) shows that the dominant mode of variability is very similar, with a temporal evolution suggesting a trend toward drying. However, the same analysis for the 1950–2009 period shows an initial increase in drying in the Van der Schrier et al. data set, followed by a decrease from the mid-1980s onwards, while the Dai data show a continuing increase until 2000. The difference in trends between the sc-PDSI data set of Van der Schrier et al. and Dai appears to be due to the different calibration periods used, the shorter 1950–1979 period in the latter study resulting in higher index values from 1980 onwards, although the associated spatial patterns are similar. In addition, the observed precipitation forcing data set differs between studies, with van der Schrier et al. (2013) and Sheffield et al. (2012) using CRU TS 3.10.01 (updated from Mitchell and Jones, 2005). This data set uses fewer stations and has been wetter than some other precipitation products in the last couple of decades (Figure 2.29, Table 2.9), although the best data set to use is still an open question. Despite this, a measure of sc-PDSI with potential evapotranspiration estimated using the Penman–Monteith equation shows an increase in the percentage of land area in drought since 1950 (Sheffield et al., 2012; Dai, 2013), while van der Schrier et al. (2013) also finds a slight increase in the percentage of land area in severe drought using the same measure. This is qualitatively consistent with the trends in surface soil moisture found for the shorter period 1988–2010 by Dorigo et al. (2012) using a new multi-satellite data set and changes in observed streamflow (Dai, 2011b). However all these studies draw somewhat different conclusions and the compelling arguments both for (Dai, 2011b, 2013) and against (Sheffield et al., 2012; van der Schrier et al., 2013) a significant increase in the land area experiencing drought has hampered global assessment.

Studies that support an increasing trend towards the land area affected by drought seem to be at odds with studies that look at trends in dryness (i.e., lack of rainfall). For example, Donat et al. (2013c) found that the annual maximum number of consecutive dry days has declined since the 1950s in more regions than it has increased (Figure 2.33c). However, only regions in Russia and the USA indicate significant changes and there is a lack of information for this index over large regions, especially Africa. Most other studies focussing on global dryness find similar results, with decadal variability dominating longer-term trends (Frich et al., 2002; Alexander et al., 2006; Donat et al., 2013a). However, Giorgi et al. (2011) indicate that 'hydroclimatic intensity' (Box 2.4, Chapter 7), a measure which combines both dry spell length and precipitation intensity, has increased over the latter part of the 20th century in response to a warming climate. They show that positive trends (reflecting an increase in the length of drought and/or extreme precipitation events) are most marked in Europe, India, parts of South America and East Asia although trends appear to have decreased (reflecting a decrease in the length of drought and/or extreme precipitation events) in Australia and northern South America (Figure 2.33c). Data availability, quality and length of record remain issues in drawing conclusions on a global scale, however.

Despite differences between the conclusions drawn by global studies, there are some areas in which they agree. Table 2.13 indicates that there is *medium confidence* of an increase in dryness or drought in East Asia with *high confidence* that this is the case in the Mediterranean and West Africa. There is also *high confidence* of decreases in dryness or drought in central North America and north-west Australia.

In summary, the current assessment concludes that there is not enough evidence at present to suggest more than *low confidence* in a global-scale observed trend in drought or dryness (lack of rainfall) since the middle of the 20th century, owing to lack of direct observations, geographical inconsistencies in the trends, and dependencies of inferred trends on the index choice. Based on updated studies, AR4 conclusions regarding global increasing trends in drought since the 1970s were probably overstated. However, it is *likely* that the frequency and intensity of drought has increased in the Mediterranean and West Africa and decreased in central North America and north-west Australia since 1950.

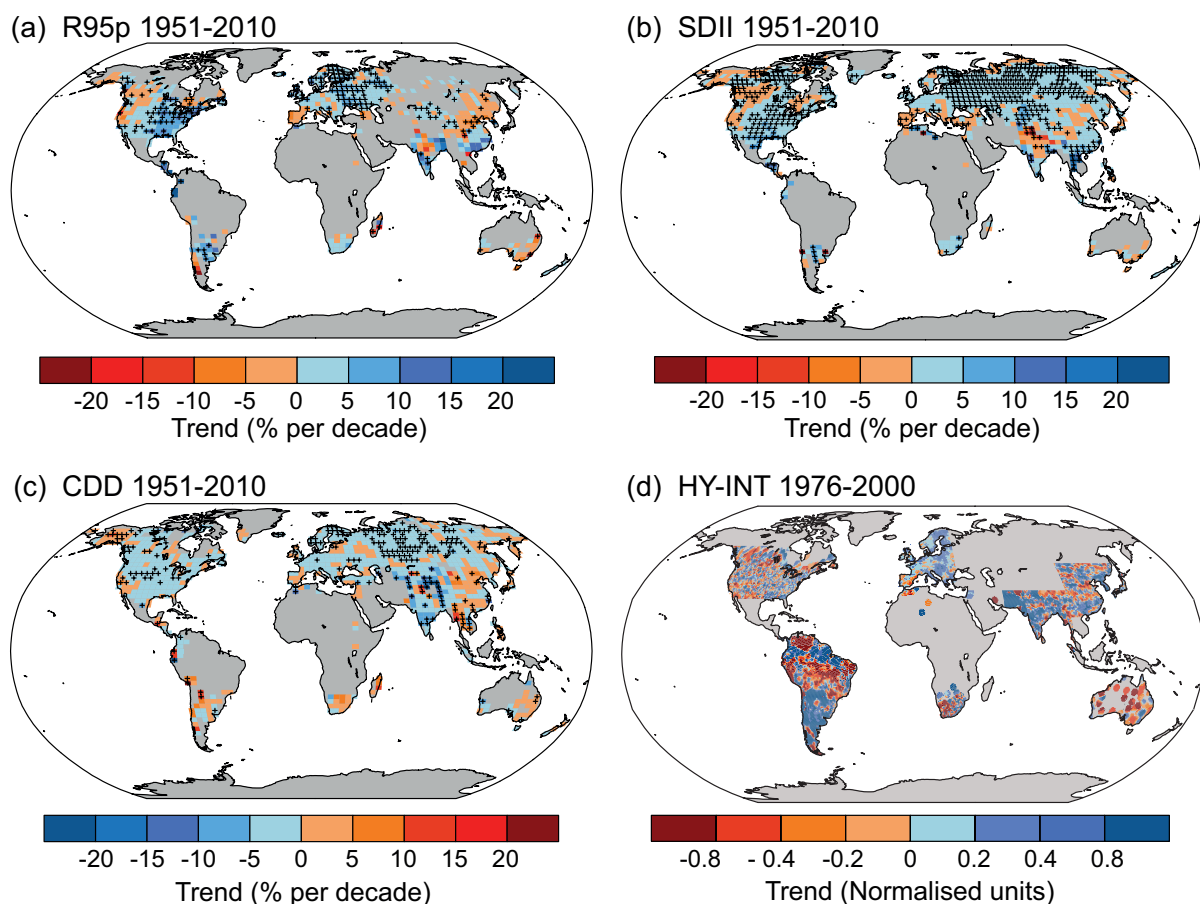


Figure 2.33 | Trends in (a) annual amount of precipitation from days >95th percentile (R95p), (b) daily precipitation intensity (SDII) and (c) frequency of the annual maximum number of consecutive dry days (CDD) (Box 2.4, Table 1). Trends are shown as relative values for better comparison across different climatic regions. Trends were calculated only for grid boxes that had at least 40 years of data during this period and where data ended no earlier than 2003. Grey areas indicate incomplete or missing data. Black plus signs (+) indicate grid boxes where trends are significant (i.e., a trend of zero lies outside the 90% confidence interval). The data source for trend maps is HadEX2 (Donat et al., 2013a) updated to include the latest version of the European Climate Assessment data set (Klok and Tank, 2009). (d) Trends (normalized units) in hydroclimatic intensity (HY-INT: a multiplicative measure of length of dry spell and precipitation intensity) over the period 1976–2000 (adapted from Giorgi et al., 2011). An increase (decrease) in HY-INT reflects an increase (decrease) in the length of drought and /or extreme precipitation events.

2.6.2.4 Severe Local Weather Events

Another extreme aspect of the hydrological cycle is severe local weather phenomena such as hail or thunder storms. These are not well observed in many parts of the world because the density of surface meteorological observing stations is too coarse to measure all such events. Moreover, homogeneity of existing reporting is questionable (Verbout et al., 2006; Doswell et al., 2009). Alternatively, measures of severe thunderstorms or hailstorms can be derived by assessing the environmental conditions that are favourable for their formation but this method is very uncertain (Seneviratne et al., 2012). SREX highlighted studies such as those of Brooks and Dotzek (2008), who found significant variability but no clear trend in the past 50 years in severe thunderstorms in a region east of the Rocky Mountains in the USA, Cao (2008), who found an increasing frequency of severe hail events in Ontario, Canada during the period 1979–2002 and Kunz et al. (2009), who found that hail days significantly increased during the period 1974–2003 in southwest Germany. Hailpad studies from Italy (Eccel et al., 2012) and France (Berthet et al., 2011) suggest slight increases in larger hail sizes and a correlation between the fraction of precipitation falling as hail with average summer temperature while in Argentina between 1960 and 2008 the annual number of hail events was found to be increasing in some regions and decreasing in others (Mezher et al., 2012). In China between 1961 and 2005, the number of hail days has been found to generally decrease, with the highest occurrence between 1960 and 1980 but with a sharp drop since the mid-1980s (CMA, 2007; Xie et al., 2008). However, there is little consistency in hail size changes in different regions of China since 1980 (Xie et al., 2010). Remote sensing offers a potential alternative to surface-based meteorological networks for detecting changes in small scale severe weather phenomenon such as proxy measurements of lightning from satellites (Zipser et al., 2006) but there remains little convincing evidence that changes in severe thunderstorms or hail have occurred since the middle of the 20th century (Brooks, 2012).

In summary, there is *low confidence* in observed trends in small-scale severe weather phenomena such as hail and thunderstorms because of historical data inhomogeneities and inadequacies in monitoring systems.

2.6.3 Tropical Storms

AR4 concluded that it was *likely* that an increasing trend had occurred in intense tropical cyclone activity since 1970 in some regions but that there was no clear trend in the annual numbers of tropical cyclones. Subsequent assessments, including SREX and more recent literature indicate that it is difficult to draw firm conclusions with respect to the confidence levels associated with observed trends prior to the satellite era and in ocean basins outside of the North Atlantic.

Section 14.6.1 discusses changes in tropical storms in detail. Current data sets indicate no significant observed trends in global tropical cyclone frequency over the past century and it remains uncertain whether any reported long-term increases in tropical cyclone frequency are robust, after accounting for past changes in observing capabilities (Knutson et al., 2010). Regional trends in tropical cyclone frequency and the frequency of very intense tropical cyclones have been identified in the

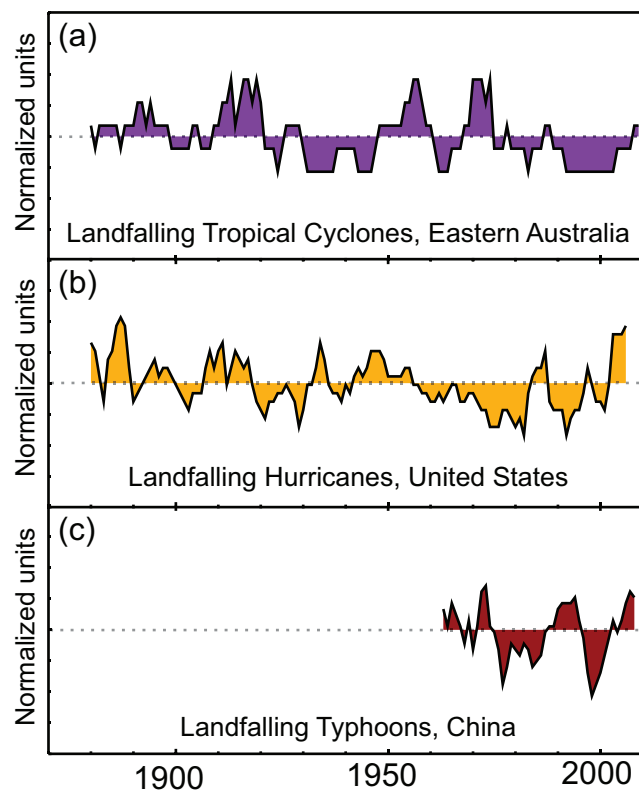


Figure 2.34 | Normalized 5-year running means of the number of (a) adjusted land falling eastern Australian tropical cyclones (adapted from Callaghan and Power (2011) and updated to include 2010/2011 season) and (b) unadjusted land falling U.S. hurricanes (adapted from Vecchi and Knutson (2011)) and (c) land-falling typhoons in China (adapted from CMA, 2011). Vertical axis ticks represent one standard deviation, with all series normalized to unit standard deviation after a 5-year running mean was applied.

North Atlantic and these appear robust since the 1970s (Kossin et al. 2007) (*very high confidence*). However, argument reigns over the cause of the increase and on longer time scales the fidelity of these trends is debated (Landsea et al., 2006; Holland and Webster, 2007; Landsea, 2007; Mann et al., 2007b) with different methods for estimating undercounts in the earlier part of the record providing mixed conclusions (Chang and Guo, 2007; Mann et al., 2007a; Kunkel et al., 2008; Vecchi and Knutson, 2008, 2011). No robust trends in annual numbers of tropical storms, hurricanes and major hurricanes counts have been identified over the past 100 years in the North Atlantic basin. Measures of land-falling tropical cyclone frequency (Figure 2.34) are generally considered to be more reliable than counts of all storms which tend to be strongly influenced by those that are weak and/or short lived. Callaghan and Power (2011) find a statistically significant decrease in Eastern Australia land-falling tropical cyclones since the late 19th century although including 2010/2011 season data this trend becomes non-significant (i.e., a trend of zero lies just inside the 90% confidence interval). Significant trends are not found in other oceans on shorter time scales (Chan and Xu, 2009; Kubota and Chan, 2009; Mohapatra et al., 2011; Weinkle et al., 2012), although Grinsted et al. (2012) find a significant positive trend in eastern USA using tide-gauge data from 1923–2008 as a proxy for storm surges associated with land-falling hurricanes. Differences between tropical cyclone studies highlight the challenges that still lie ahead in assessing long-term trends.

Arguably, storm frequency is of limited usefulness if not considered in tandem with intensity and duration measures. Intensity measures in historical records are especially sensitive to changing technology and improving methodology. However, over the satellite era, increases in the intensity of the strongest storms in the Atlantic appear robust (Kossin et al., 2007; Elsner et al., 2008) but there is limited evidence for other regions and the globe. Time series of cyclone indices such as power dissipation, an aggregate compound of tropical cyclone frequency, duration and intensity that measures total wind energy by tropical cyclones, show upward trends in the North Atlantic and weaker upward trends in the western North Pacific since the late 1970s (Emanuel, 2007), but interpretation of longer-term trends is again constrained by data quality concerns (Landsea et al., 2011).

In summary, this assessment does not revise the SREX conclusion of *low confidence* that any reported long-term (centennial) increases in tropical cyclone activity are robust, after accounting for past changes in observing capabilities. More recent assessments indicate that it is *unlikely* that annual numbers of tropical storms, hurricanes and major hurricanes counts have increased over the past 100 years in the North Atlantic basin. Evidence, however, is for a *virtually certain* increase in the frequency and intensity of the strongest tropical cyclones since the 1970s in that region.

2.6.4 Extratropical Storms

AR4 noted a *likely* net increase in frequency/intensity of NH extreme extratropical cyclones and a poleward shift in storm tracks since the 1950s. SREX further consolidated the AR4 assessment of poleward shifting storm tracks, but revised the assessment of the confidence levels associated with regional trends in the intensity of extreme extratropical cyclones.

Studies using reanalyses continue to support a northward and eastward shift in the Atlantic cyclone activity during the last 60 years with both more frequent and more intense wintertime cyclones in the high-latitude Atlantic (Schneidereit et al., 2007; Raible et al., 2008; Vilicic and Sepic, 2010) and fewer in the mid-latitude Atlantic (Wang et al., 2006b; Raible et al., 2008). Some studies show an increase in intensity and number of extreme Atlantic cyclones (Paciorek et al., 2002; Lehmann et al., 2011) while others show opposite trends in eastern Pacific and North America (Gulev et al., 2001). Comparisons between studies are hampered because of the sensitivities in identification schemes and/or different definitions for extreme cyclones (Ulbrich et al., 2009; Neu et al., 2012). The fidelity of research findings also rests largely with the underlying reanalyses products that are used (Box 2.3). See also Section 14.6.2.

Over longer periods studies of severe storms or storminess have been performed for Europe where long running *in situ* pressure and wind observations exist. Direct wind speed measurements, however, either have short records or are hampered by inconsistencies due to changing instrumentation and observing practice over time (Smits et al., 2005; Wan et al., 2010). In most cases, therefore wind speed or storminess proxies are derived from *in situ* pressure measurements or reanalyses data, the quality and consistency of which vary. *In situ* observations indicate no clear trends over the past century or longer (Hanna et al., 2008; Matulla et al., 2008; Allan et al., 2009; Barring and Fortuniak,

2009), with substantial decadal and longer fluctuations but with some regional and seasonal trends (Wang et al., 2009c, 2011). Figure 2.35 shows some of these changes for boreal winter using geostrophic wind speeds indicating that decreasing trends outnumber increasing trends (Wang et al., 2011), although with few that are statistically significant. Although Donat et al. (2011) and Wang et al. (2012h) find significant increases in both the strength and frequency of wintertime storms for large parts of Europe using the 20CR (Compo et al., 2011), there is debate over whether this is an artefact of the changing number of assimilated observations over time (Cornes and Jones, 2011; Krueger et al., 2013) even though Wang et al. (2012h) find good agreement between the 20CR trends and those derived from geostrophic wind extremes in the North Sea region.

SREX noted that available studies using reanalyses indicate a decrease in extratropical cyclone activity (Zhang et al., 2004) and intensity (Zhang et al., 2004; Wang et al., 2009d) over the last 50 years has been reported for northern Eurasia (60°N to 40°N) linked to a possible northward shift with increased cyclone frequency in the higher latitudes and decrease in the lower latitudes. The decrease at lower latitudes was also found in East Asia (Wang et al., 2012h) and is also supported by a study of severe storms by Zou et al. (2006b) who used sub-daily *in situ* pressure data from a number of stations across China.

SREX also notes that, based on reanalyses, North American cyclone numbers have increased over the last 50 years, with no statistically significant change in cyclone intensity (Zhang et al., 2004). Hourly SLP data from Canadian stations showed that winter cyclones have become significantly more frequent, longer lasting, and stronger in the lower Canadian Arctic over the last 50 years (1953–2002), but less frequent and weaker in the south, especially along the southeast and southwest Canadian coasts (Wang et al., 2006a). Further south, a tendency toward weaker low-pressure systems over the past few decades was found for U.S. east coast winter cyclones using reanalyses, but no statistically significant trends in the frequency of occurrence of systems (Hirsch et al., 2001).

Using the 20CR (Compo et al., 2011), Wang et al. (2012h) found substantial increases in extratropical cyclone activity in the SH (20°S to 90°S). However, for southeast Australia, a decrease in activity is found and this agrees well with geostrophic wind extremes derived from *in situ* surface pressure observations (Alexander et al., 2011). This strengthens the evidence of a southward shift in storm tracks previously noted using older reanalyses products (Fyfe, 2003; Hope et al., 2006). Frederiksen and Frederiksen (2007) linked the reduction in cyclogenesis at 30°S and southward shift to a decrease in the vertical mean meridional temperature gradient. There is some inconsistency among reanalysis products for the SH regarding trends in the frequency of intense extratropical cyclones (Lim and Simmonds, 2007; Pezza et al., 2007; Lim and Simmonds, 2009) although studies tend to agree on a trend towards more intense systems, even when inhomogeneities associated with changing numbers of observations have been taken into account (Wang et al., 2012h). However, further undetected contamination of these trends owing to issues with the reanalyses products cannot be ruled out (Box 2.3) and this lowers our confidence in long-term trends. Links between extratropical cyclone activity and large-scale variability are discussed in Sections 2.7 and 14.6.2.

Frequently Asked Questions

FAQ 2.2 | Have There Been Any Changes in Climate Extremes?

There is strong evidence that warming has lead to changes in temperature extremes—including heat waves—since the mid-20th century. Increases in heavy precipitation have probably also occurred over this time, but vary by region. However, for other extremes, such as tropical cyclone frequency, we are less certain, except in some limited regions, that there have been discernable changes over the observed record.

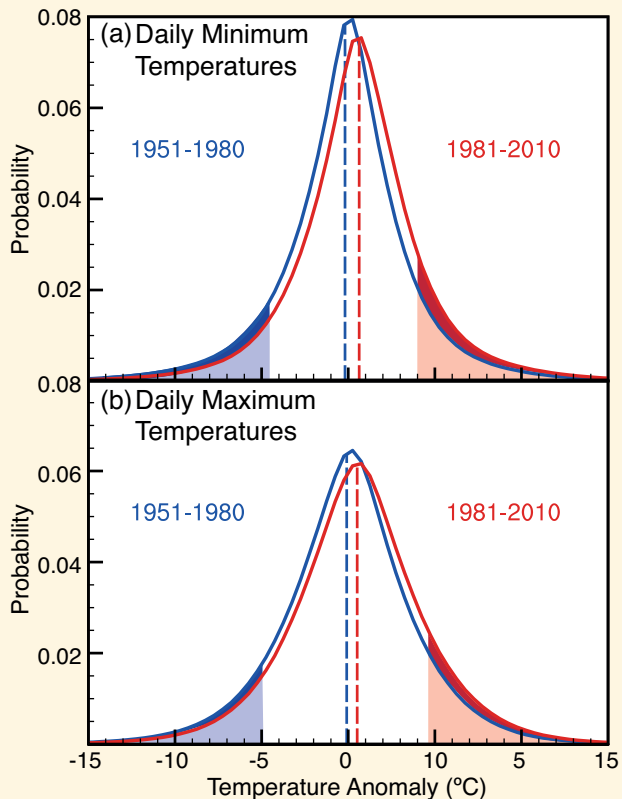
From heat waves to cold snaps or droughts to flooding rains, recording and analysing climate extremes poses unique challenges, not just because these events are rare, but also because they invariably happen in conjunction with disruptive conditions. Furthermore, there is no consistent definition in the scientific literature of what constitutes an extreme climatic event, and this complicates comparative global assessments.

Although, in an absolute sense, an extreme climate event will vary from place to place—a hot day in the tropics, for instance, may be a different temperature to a hot day in the mid-latitudes—international efforts to monitor extremes have highlighted some significant global changes.

For example, using consistent definitions for cold (<10th percentile) and warm (>90th percentile) days and nights it is found that warm days and nights have increased and cold days and nights have decreased for most regions of the globe; a few exceptions being central and eastern North America, and southern South America but mostly only related to daytime temperatures. Those changes are generally most apparent in minimum temperature extremes, for example, warm nights. Data limitations make it difficult to establish a causal link to increases in average temperatures, but FAQ 2.2, Figure 1 indicates that daily global temperature extremes have indeed changed. Whether these changes are simply associated with the average of daily temperatures increasing (the dashed lines in FAQ 2.2, Figure 1) or whether other changes in the distribution of daytime and nighttime temperatures have occurred is still under debate.

Warm spells or heat waves, that is, periods containing consecutive extremely hot days or nights, have also been assessed, but there are fewer studies of heat wave characteristics than those that compare changes in merely warm days or nights. Most global land areas with available data have experienced more heat waves since the middle of the 20th century. One exception is the south-eastern USA, where heat wave frequency and duration measures generally show decreases. This has been associated with a so-called ‘warming hole’ in this region, where precipitation has also increased and may be related to interactions between the land and the atmosphere and long-term variations in the Atlantic and Pacific Oceans. However, for large regions, particularly in Africa and South America, information on changes in heatwaves is limited.

For regions such as Europe, where historical temperature reconstructions exist going back several hundreds of years, indications are that some areas have experienced a disproportionate number of extreme heat waves in recent decades. (continued on next page)



FAQ 2.2, Figure 1 | Distribution of (a) daily minimum and (b) daily maximum temperature anomalies relative to a 1961–1990 climatology for two periods: 1951–1980 (blue) and 1981–2010 (red) using the HadGHCND data set. The shaded blue and red areas represent the coldest 10% and warmest 10% respectively of (a) nights and (b) days during the 1951–1980 period. The darker shading indicates by how much the number of the coldest days and nights has reduced (dark blue) and by how much the number of the warmest days and nights has increased (dark red) during the 1981–2010 period compared to the 1951–1980 period.

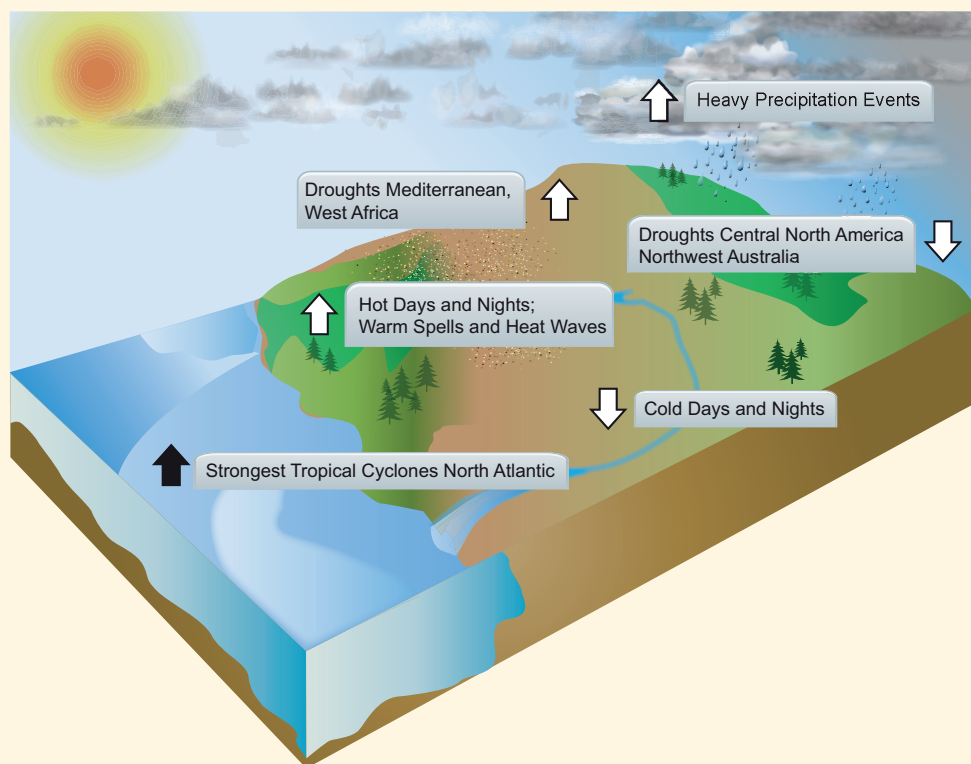
FAQ 2.2 (continued)

Changes in extremes for other climate variables are generally less coherent than those observed for temperature, owing to data limitations and inconsistencies between studies, regions and/or seasons. However, increases in precipitation extremes, for example, are consistent with a warmer climate. Analyses of land areas with sufficient data indicate increases in the frequency and intensity of extreme precipitation events in recent decades, but results vary strongly between regions and seasons. For instance, evidence is most compelling for increases in heavy precipitation in North America, Central America and Europe, but in some other regions—such as southern Australia and western Asia—there is evidence of decreases. Likewise, drought studies do not agree on the sign of the global trend, with regional inconsistencies in trends also dependent on how droughts are defined. However, indications exist that droughts have increased in some regions (e.g., the Mediterranean) and decreased in others (e.g., central North America) since the middle of the 20th century.

Considering other extremes, such as tropical cyclones, the latest assessments show that due to problems with past observing capabilities, it is difficult to make conclusive statements about long-term trends. There is very strong evidence, however, that storm activity has increased in the North Atlantic since the 1970s.

Over periods of a century or more, evidence suggests slight decreases in the frequency of tropical cyclones making landfall in the North Atlantic and the South Pacific, once uncertainties in observing methods have been considered. Little evidence exists of any longer-term trend in other ocean basins. For extratropical cyclones, a poleward shift is evident in both hemispheres over the past 50 years, with further but limited evidence of a decrease in wind storm frequency at mid-latitudes. Several studies suggest an increase in intensity, but data sampling issues hamper these assessments.

FAQ 2.2, Figure 2 summarizes some of the observed changes in climate extremes. Overall, the most robust global changes in climate extremes are seen in measures of daily temperature, including to some extent, heat waves. Precipitation extremes also appear to be increasing, but there is large spatial variability, and observed trends in droughts are still uncertain except in a few regions. While robust increases have been seen in tropical cyclone frequency and activity in the North Atlantic since the 1970s, the reasons for this are still being debated. There is limited evidence of changes in extremes associated with other climate variables since the mid-20th century.



FAQ 2.2, Figure 2 | Trends in the frequency (or intensity) of various climate extremes (arrow direction denotes the sign of the change) since the middle of the 20th century (except for North Atlantic storms where the period covered is from the 1970s).

Studies that have examined trends in wind extremes from observations or regional reanalysis products tend to point to declining trends in extremes in mid-latitudes (Pirazzoli and Tomasin, 2003; Smits et al., 2005; Pryor et al., 2007; Zhang et al., 2007b) and increasing trends in high latitudes (Lynch et al., 2004; Turner et al., 2005; Hundecha et al., 2008; Stegall and Zhang, 2012). Other studies have compared the trends from observations with reanalysis data and reported differing or even opposite trends in the reanalysis products (Smits et al., 2005; McVicar et al., 2008). On the other hand, declining trends reported by Xu et al. (2006b) over China between 1969 and 2000 were generally consistent with trends in NCEP reanalysis. Trends extracted from

reanalysis products must be treated with caution however, although usually with later generation products providing improvements over older products (Box 2.3).

In summary, *confidence* in large scale changes in the intensity of extreme extratropical cyclones since 1900 is *low*. There is also *low confidence* for a clear trend in storminess proxies over the last century due to inconsistencies between studies or lack of long-term data in some parts of the world (particularly in the SH). Likewise, *confidence* in trends in extreme winds is *low*, owing to quality and consistency issues with analysed data.

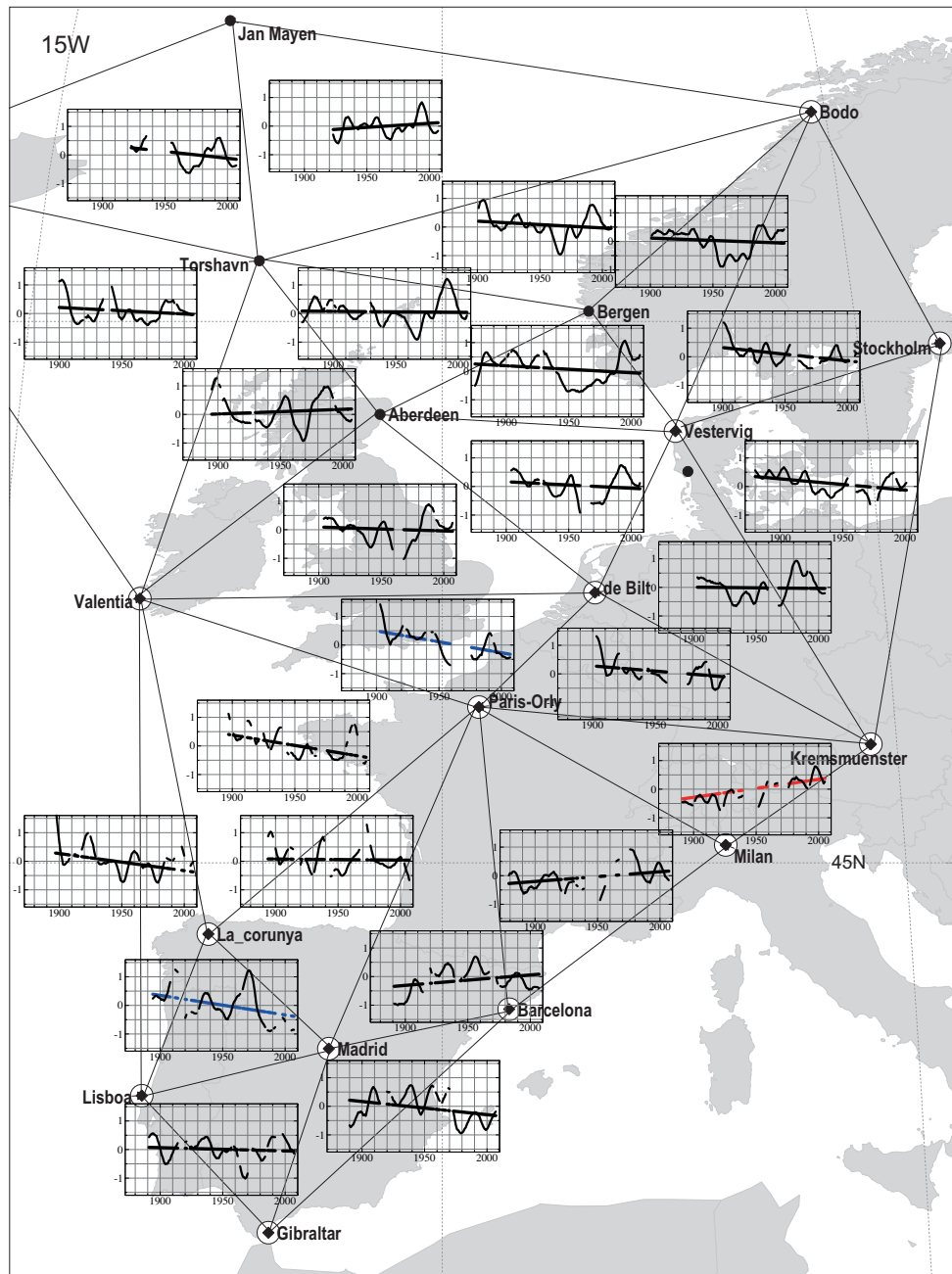


Figure 2.35 | 99th percentiles of geostrophic wind speeds for winter (DJF). Triangles show regions where geostrophic wind speeds have been calculated from *in situ* surface pressure observations. Within each pressure triangle, Gaussian low-pass filtered curves and estimated linear trends of the 99th percentile of these geostrophic wind speeds for winter are shown. The ticks of the time (horizontal) axis range from 1875 to 2005, with an interval of 10 years. Disconnections in lines show periods of missing data. Red (blue) trend lines indicate upward (downward) significant trends (i.e., a trend of zero lies outside the 95% confidence interval). (From Wang et al., 2011.)

Box 2.4 | Extremes Indices

As SREX highlighted, there is no unique definition of what constitutes a climate extreme in the scientific literature given variations in regions and sectors affected (Stephenson et al., 2008). Much of the available research is based on the use of so-called 'extremes indices' (Zhang et al., 2011). These indices can either be based on the probability of occurrence of given quantities or on absolute or percentage threshold exceedances (relative to a fixed climatological period) but also include more complex definitions related to duration, intensity and persistence of extreme events. For example, the term 'heat wave' can mean very different things depending on the index formulation for the application for which it is required (Perkins and Alexander, 2012).

Box 2.4, Table 1 lists a number of specific indices that appear widely in the literature and have been chosen to provide some consistency across multiple chapters in AR5 (along with the location of associated figures and text). These indices have been generally chosen for their robust statistical properties and their applicability across a wide range of climates. Another important criterion is that data for these indices are broadly available over both space and time. The existing near-global land-based data sets cover at least the post-1950 period but for regions such as Europe, North America, parts of Asia and Australia much longer analyses are available. The same indices used in observational studies (this chapter) are also used to diagnose climate model output (Chapters 9, 10, 11 and 12).

The types of indices discussed here do not include indices such as NIÑO3 representing positive and negative phases of ENSO (Box 2.5), nor do they include extremes such as 1 in 100 year events. Typically extreme indices assessed here reflect more 'moderate' extremes, for example, events occurring as often as 5% or 10% of the time (Box 2.4, Table 1). Predefined extreme indices are usually easier to obtain than the underlying daily climate data, which are not always freely exchanged by meteorological services. However, some of these indices do represent rarer events, for example, annual maxima or minima. Analyses of these and rarer extremes (e.g., with longer

(continued on next page)

Box 2.4, Table 1 | Definitions of extreme temperature and precipitation indices used in IPCC (after Zhang et al., 2011). The most common units are shown but these may be shown as normalized or relative depending on application in different chapters.

Index	Descriptive name	Definition	Units	Figures/Tables	Section
TXx	Warmest daily Tmax	Seasonal/annual maximum value of daily maximum temperature	°C	Box 2.4, Figure 1, Figures 9.37, 10.17, 12.13	Box 2.4, 9.5.4.1, 10.6.1.1, 12.4.3.3
TNx	Warmest daily Tmin	Seasonal/annual maximum value of daily minimum temperature	°C	Figures 9.37, 10.17	9.5.4.1, 10.6.1.1
TXn	Coldest daily Tmax	Seasonal/annual minimum value of daily maximum temperature	°C	Figures 9.37, 10.17, 12.13	9.5.4.1, 10.6.1.1, 12.4.3.3
TNn	Coldest daily Tmin	Seasonal/annual minimum value of daily minimum temperature	°C	Figures 9.37, 10.17, 12.13	9.5.4.1, 10.6.1.1
TN10p	Cold nights	Days (or fraction of time) when daily minimum temperature <10th percentile	Days (%)	Figures 2.32, 9.37, 10.17 Tables 2.11, 2.12	2.6.1, 9.5.4.1, 10.6.1.1, 11.3.2.5.1
TX10p	Cold days	Days (or fraction of time) when daily maximum temperature <10th percentile	Days (%)	Figures 2.32, 9.37, 10.17, 11.17	2.6.1, 9.5.4.1, 10.6.1.1, 11.3.2.5.1,
TN90p	Warm nights	Days (or fraction of time) when daily minimum temperature >90th percentile	Days (%)	Figures 2.32, 9.37, 10.17 Tables 2.11, 2.12	2.6.1, 9.5.4.1, 10.6.1.1, 11.3.2.5.1
TX90p	Warm days	Days (or fraction of time) when daily maximum temperature >90th percentile	Days (%)	Figures 2.32, 9.37, 10.17, 11.17 Tables 2.11, 2.12	2.6.1, 9.5.4.1, 10.6.1.1, 11.3.2.5.1,
FD	Frost days	Frequency of daily minimum temperature <0°C	Days	Figures 9.37, 12.13 Table 2.12	2.6.1, 9.5.4.1, 10.6.1.1, 12.4.3.3
TR	Tropical nights	Frequency of daily minimum temperature >20°C	Days	Figures 9.37, 12.13	9.5.4.1, 12.4.3.3
RX1day	Wettest day	Maximum 1-day precipitation	mm	Figures 9.37, 10.10 Table 2.12, 12.27	2.6.2.1, 9.5.4.1, 10.6.1.2, 12.4.5.5
RX5day	Wettest consecutive five days	Maximum of consecutive 5-day precipitation	mm	Figures 9.37, 12.26, 14.1	9.5.4.1, 10.6.1.2, 12.4.5.5, 14.2.1
SDII	Simple daily intensity index	Ratio of annual total precipitation to the number of wet days (≥ 1 mm)	mm day ⁻¹	Figures 2.33, 9.37, 14.1	2.6.2.1, 9.5.4.1, 14.2.1
R95p	Precipitation from very wet days	Amount of precipitation from days >95th percentile	mm	Figures 2.33, 9.37, 11.17 Table 2.12	2.6.2.1, 9.5.4.1, 11.3.2.5.1
CDD	Consecutive dry days	Maximum number of consecutive days when precipitation <1 mm	Days	Figures 2.33, 9.37, 12.26, 14.1	2.6.2.3, 9.5.4.1, 12.4.5.5, 14.2.1

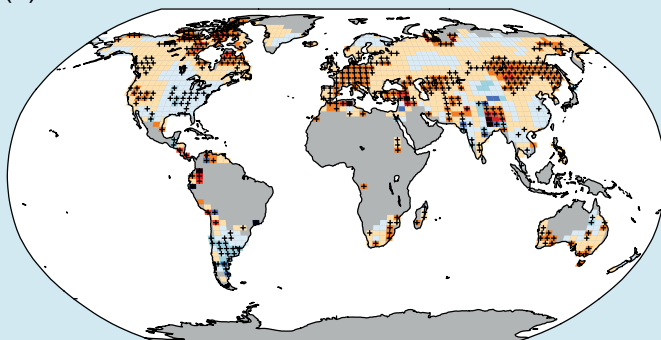
Box 2.4 (continued)

return period thresholds) are making their way into a growing body of literature which, for example, are using Extreme Value Theory (Coles, 2001) to study climate extremes (Zwiers and Kharin, 1998; Brown et al., 2008; Sillmann et al., 2011; Zhang et al., 2011; Kharin et al., 2013).

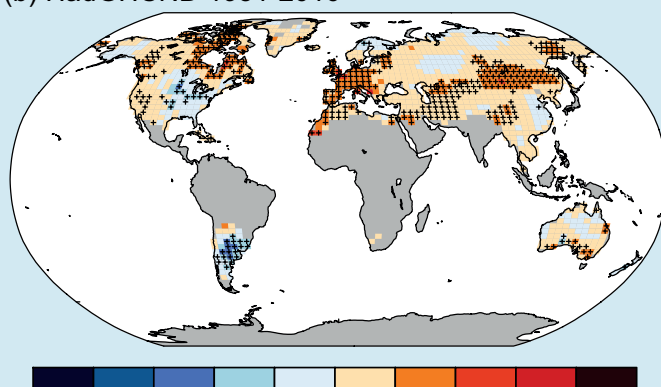
Extreme indices are more generally defined for daily temperature and precipitation characteristics (Zhang et al., 2011) although research is developing on the analysis of sub-daily events but mostly only on regional scales (Sen Roy, 2009; Shiu et al., 2009; Jones et al., 2010; Jakob et al., 2011; Lenderink et al., 2011; Shaw et al., 2011). Temperature and precipitation indices are sometimes combined to investigate ‘extremeness’ (e.g., hydroclimatic intensity, HY-INT; Giorgi et al., 2011) and/or the areal extent of extremes (e.g., the Climate Extremes Index (CEI) and its variants (Gleason et al., 2008; Gallant and Karoly, 2010; Ren et al., 2011)). Indices rarely include other weather and climate variables, such as wind speed, humidity or physical impacts (e.g., streamflow) and phenomena. Some examples are available in the literature for wind-based (Della-Marta et al., 2009) and pressure-based (Beniston, 2009) indices, for health-relevant indices combining temperature and relative humidity characteristics (Diffenbaugh et al., 2007; Fischer and Schär, 2010) and for a range of dryness or drought indices (e.g., Palmer Drought Severity Index (PDSI) Palmer, 1965; Standardised Precipitation Index (SPI), Standardised Precipitation Evapotranspiration Index (SPEI) Vicente-Serrano et al., 2010) and wetness indices (e.g., Standardized Soil Wetness Index (SSWI); Vidal et al., 2010). (continued on next page)

In addition to the complication of defining an index, the results depend also on the way in which indices are calculated (to create global averages, for example). This is due to the fact that different algorithms may be employed to create grid box averages from station data, or that extremes indices may be calculated from gridded daily data or at station locations and then gridded. All of these factors add uncertainty to the calculation of an extreme. For example, the spatial patterns of trends in the warmest day of the year differ slightly between data sets, although when globally averaged, trends are similar over the second half of the 20th century (Box 2.4, Figure 1). Further discussion of the parametric and structural uncertainties in data sets is given in Box 2.1.

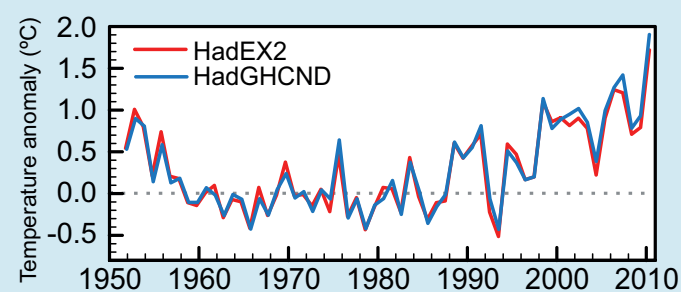
(a) HadEX2 1951–2010



(b) HadGHCND 1951–2010



(c) Global land average



Box 2.4, Figure 1 | Trends in the warmest day of the year using different data sets for the period 1951–2010. The data sets are (a) HadEX2 (Donat et al., 2013c) updated to include the latest version of the European Climate Assessment data set (Klok and Tank, 2009), (b) HadGHCND (Caesar et al., 2006) using data updated to 2010 (Donat et al., 2013a) and (c) Globally averaged annual warmest day anomalies for each data set. Trends were calculated only for grid boxes that had at least 40 years of data during this period and where data ended no earlier than 2003. Grey areas indicate incomplete or missing data. Black plus signs (+) indicate grid boxes where trends are significant (i.e., a trend of zero lies outside the 90% confidence interval). Anomalies are calculated using grid boxes only where both data sets have data and where 90% of data are available.

2.7 Changes in Atmospheric Circulation and Patterns of Variability

Changes in atmospheric circulation and indices of climate variability, as expressed in sea level pressure (SLP), wind, geopotential height (GPH), and other variables were assessed in AR4. Substantial multi-decadal variability was reported in the large-scale atmospheric circulation over the Atlantic and the Pacific. With respect to trends, a decrease was found in tropospheric GPH over high latitudes of both hemispheres and an increase over the mid-latitudes in boreal winter for the period 1979–2001. These changes were found to be associated with an intensification and poleward displacement of Atlantic and southern mid-latitude jet streams and enhanced storm track activity in the NH from the 1960s to at least the 1990s. Changes in the North Atlantic Oscillation (NAO) and the Southern Annular Mode (SAM) towards their positive phases were observed, but it was noted that the NAO returned to its long-term mean state from the mid-1990s to the early 2000s.

Since AR4, more and improved observational data sets and reanalysis data sets (Box 2.3) have been published. Uncertainties and inaccuracies in all data sets are better understood (Box 2.1). The studies since AR4 assessed in this section support the poleward movement of circulation features since the 1970s and the change in the SAM. At the same time, large decadal-to-multidecadal variability in atmospheric circulation is found that partially offsets previous trends in other circulation features such as the NAO or the Pacific Walker circulation.

This section assesses observational evidence for changes in atmospheric circulation in fields of SLP, GPH, and wind, in circulation features (such as the Hadley and Walker circulation, monsoons, or jet streams; Annex III: Glossary), as well as in circulation variability modes. Regional climate effects of the circulation changes are discussed in Chapter 14.

2.7.1 Sea Level Pressure

AR4 concluded that SLP in December to February decreased between 1948 and 2005 in the Arctic, Antarctic and North Pacific. More recent studies using updated data for the period 1949–2009 (Gillett and Stott, 2009) also find decreases in SLP in the high latitudes of both hemispheres in all seasons and increasing SLP in the tropics and subtropics most of the year. However, due to decadal variability SLP trends are sensitive to the choice of the time period (Box 2.2), and they depend on the data set.

The spatial distribution of SLP represents the distribution of atmospheric mass, which is the surface imprint of the atmospheric circulation. Barometric measurements are made in weather stations or on board ships. Fields are produced from the observations by interpolation or using data assimilation into weather models. One of the most widely used observational data sets is HadSLP2 (Allan and Ansell, 2006), which integrates 2228 historical global terrestrial stations with marine observations from the ICOADS on a $5^\circ \times 5^\circ$ grid. Other observation products (e.g., Trenberth and Paolino, 1980; for the extratropical NH) or reanalyses are also widely used to address changes in SLP. Although the quality of SLP data is considered good, there are discrepancies between gridded SLP data sets in regions with sparse observations, e.g., over Antarctica (Jones and Lister, 2007).

Van Haren et al. (2012) found a strong SLP decrease over the Mediterranean in January to March from 1961 to 2000. For the more recent period (1979–2012) trends in SLP, consistent across different data sets (shown in Figure 2.36 for ERA-Interim), are negative in the tropical and northern subtropical Atlantic during most of the year as well as, in May to October, in northern Siberia. Positive trends are found year-round over the North and South Pacific and South Atlantic. Trends in

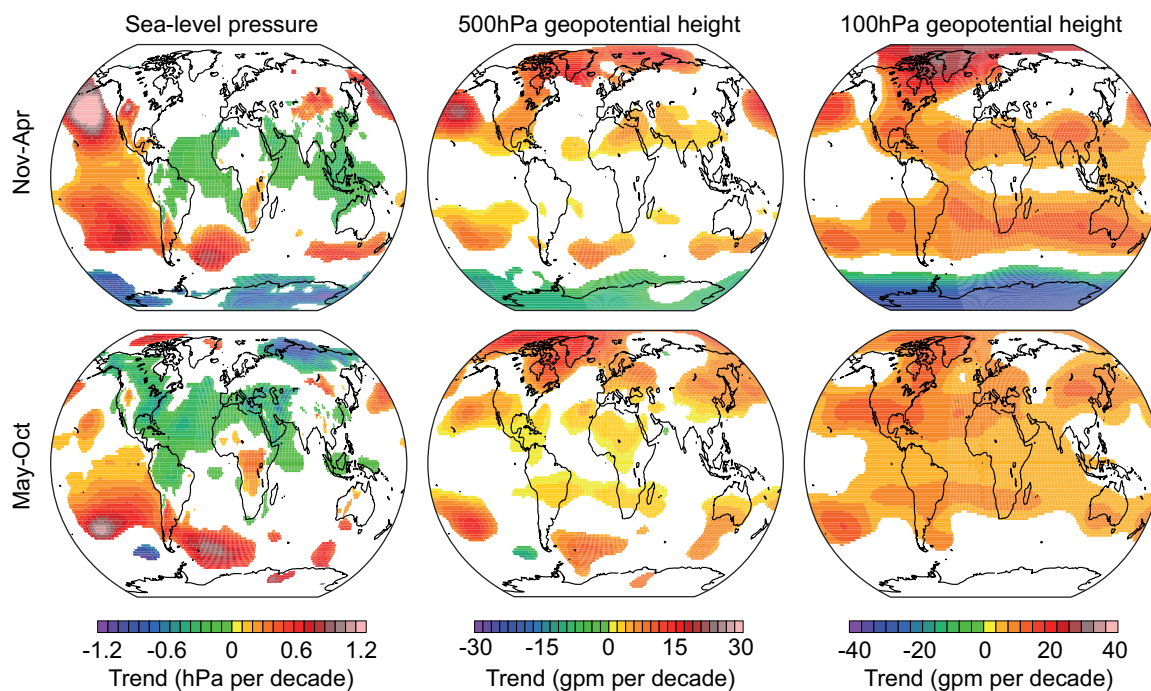


Figure 2.36 | Trends in (left) sea level pressure (SLP), (middle) 500 hPa geopotential height (GPH) and (right) 100 hPa GPH in (top) November to April 1979/1980 to 2011/2012 and (bottom) May to October 1979 to 2011 from ERA-Interim data. Trends are shown only if significant (i.e., a trend of zero lies outside the 90% confidence interval).

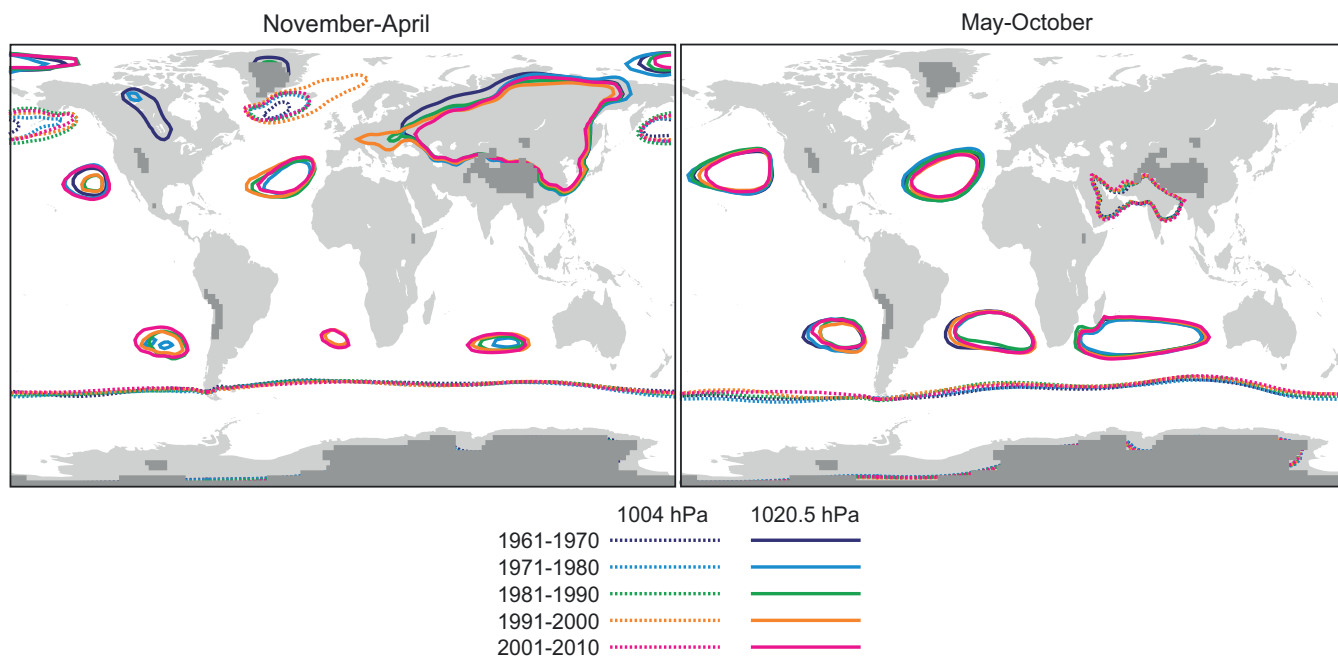


Figure 2.37 | Decadal averages of sea level pressure (SLP) from the 20th Century Reanalysis (20CR) for (left) November of previous year to April and (right) May to October shown by two selected contours: 1004 hPa (dashed lines) and 1020.5 hPa (solid lines). Topography above 2 km above mean sea level in 20CR is shaded in dark grey.

the equatorial Pacific zonal SLP gradient during the 20th century (e.g., Vecchi et al., 2006; Power and Kociuba, 2011a, 2011b) are discussed in Section 2.7.5.

The position and strength of semi-permanent pressure centres show no clear evidence for trends since 1951. However, prominent variability is found on decadal time scales (Figure 2.37). Consistent across different data sets, the Azores high and the Icelandic low in boreal winter, as captured by the high and low SLP contours, were both small in the 1960s and 1970s, large in the 1980s and 1990s, and again smaller in the 2000s. Favre and Gershunov (2006) find an eastward shift of the Aleutian low from the mid-1970s to 2001, which persisted during the 2000s (Figure 2.37). The Siberian High exhibits pronounced decadal-to-multidecadal variability (Panagiotopoulos et al., 2005; Huang et al., 2010), with a recent (1998 to 2012) strengthening and northwestward expansion (Zhang et al., 2012b). In boreal summer, the Atlantic and Pacific high-pressure systems extended more westward in the 1960s and 1970s than later. On interannual time scales, variations in pressure centres are related to modes of climate variability. Trends in the indices that capture the strength of these modes are reported in Section 2.7.8, their characteristics and impacts are discussed in Chapter 14.

In summary, sea level pressure has *likely* decreased from 1979 to 2012 over the tropical Atlantic and increased over large regions of the Pacific and South Atlantic, but trends are sensitive to the time period analysed owing to large decadal variability.

2.7.2 Surface Wind Speed

AR4 concluded that mid-latitude westerly winds have generally increased in both hemispheres. Because of shortcomings in the observations, SREX stated that *confidence* in surface wind trends is *low*. Further studies assessed here confirm this assessment.

Surface wind measurements over land and ocean are based on largely separate observing systems. Early marine observations were based on ship speed through the water or sails carried or on visual estimates of sea state converted to the wind speed using the Beaufort scale. Anemometer measurements were introduced starting in the 1950s. The transition from Beaufort to measured winds introduced a spurious trend, compounded by an increase in mean anemometer height over time (Kent et al., 2007; Thomas et al., 2008). ICOADS release 2.5 (Woodruff et al., 2011) contains information on measurement methods and wind measurement heights, permitting adjustment for these effects. The ICOADS-based data set WASWind (1950–2010; Tokinaga and Xie, 2011a) and the interpolated product NOCS v.2.0 (1973–present; Berry and Kent, 2011) include such corrections, among other improvements.

Marine surface winds are also measured from space using various microwave range instruments: scatterometers and synthetic aperture radars retrieve wind vectors, while altimeters and passive radiometers measure wind speed only (Bourassa et al., 2010). The latter type provides the longest continuous record, starting in July 1987. Satellite-based interpolated marine surface wind data sets use objective analysis methods to blend together data from different satellites and atmospheric reanalyses. The latter provide wind directions as in Blended Sea Winds (BSW; Zhang et al., 2006), or background fields as in Cross-Calibrated Multi-Platform winds (CCMP; Atlas et al., 2011) and OAFlux (Yu and Weller, 2007). CCMP uses additional dynamical constraints, *in situ* data and a recently homogenized data set of SSM/I observations (Wentz et al., 2007), among other satellite sources.

Figure 2.38 compares 1988–2010 linear trends in surface wind speeds from interpolated data sets based on satellite data, from interpolated and non-interpolated data sets based on *in situ* data, and from atmospheric reanalyses. Note that these trends over a 23-year-long period primarily reflect decadal variability in winds, rather than long-

term climate change (Box 2.2). Kent et al. (2012) recently intercompared several of these data sets and found large differences. The differences in trend patterns in Figure 2.38 are large as well. Nevertheless, some statistically significant features are present in most data sets, including a pattern of positive and negative trend bands across the North Atlantic Ocean (Section 2.7.6.2.) and positive trends along the west coast of North America. Strengthening of the Southern Ocean winds, consistent with the increasing trend in the SAM (Section 2.7.8) and with the observed changes in wind stress fields described in Section 3.4.4, can be seen in satellite-based analyses and atmospheric reanalyses in Figure 2.38. Alternating Southern Ocean trend signs in the NOCS v.2.0 panel are due to interpolation of very sparse *in situ* data (cf. the panel for the uninterpolated WASWind product).

Surface winds over land have been measured with anemometers on a global scale for decades, but until recently the data have been rarely

used for trend analysis. Global data sets lack important meta information on instrumentation and siting (McVicar et al., 2012). Long, homogenized instrumental records are rare (e.g., Usbeck et al., 2010; Wan et al., 2010). Moreover, wind speed trends are sensitive to the anemometer height (Troppoli et al., 2012). Winds near the surface can be derived from reanalysis products (Box 2.3), but discrepancies are found when comparing trends therein with trends for land stations (Smits et al., 2005; McVicar et al., 2008).

Over land, a weakening of seasonal and annual mean as well as maximum winds is reported for many regions from around the 1960s or 1970s to the early 2000s (a detailed review is given in McVicar et al. (2012)), including China and the Tibetan Plateau (Xu et al., 2006b; Guo et al., 2010) (but levelling off since 2000; Lin et al., 2012), Western and southern Europe (e.g., Earl et al., 2013), much of the USA (Pryor et al., 2007), Australia (McVicar et al., 2008) and southern and western

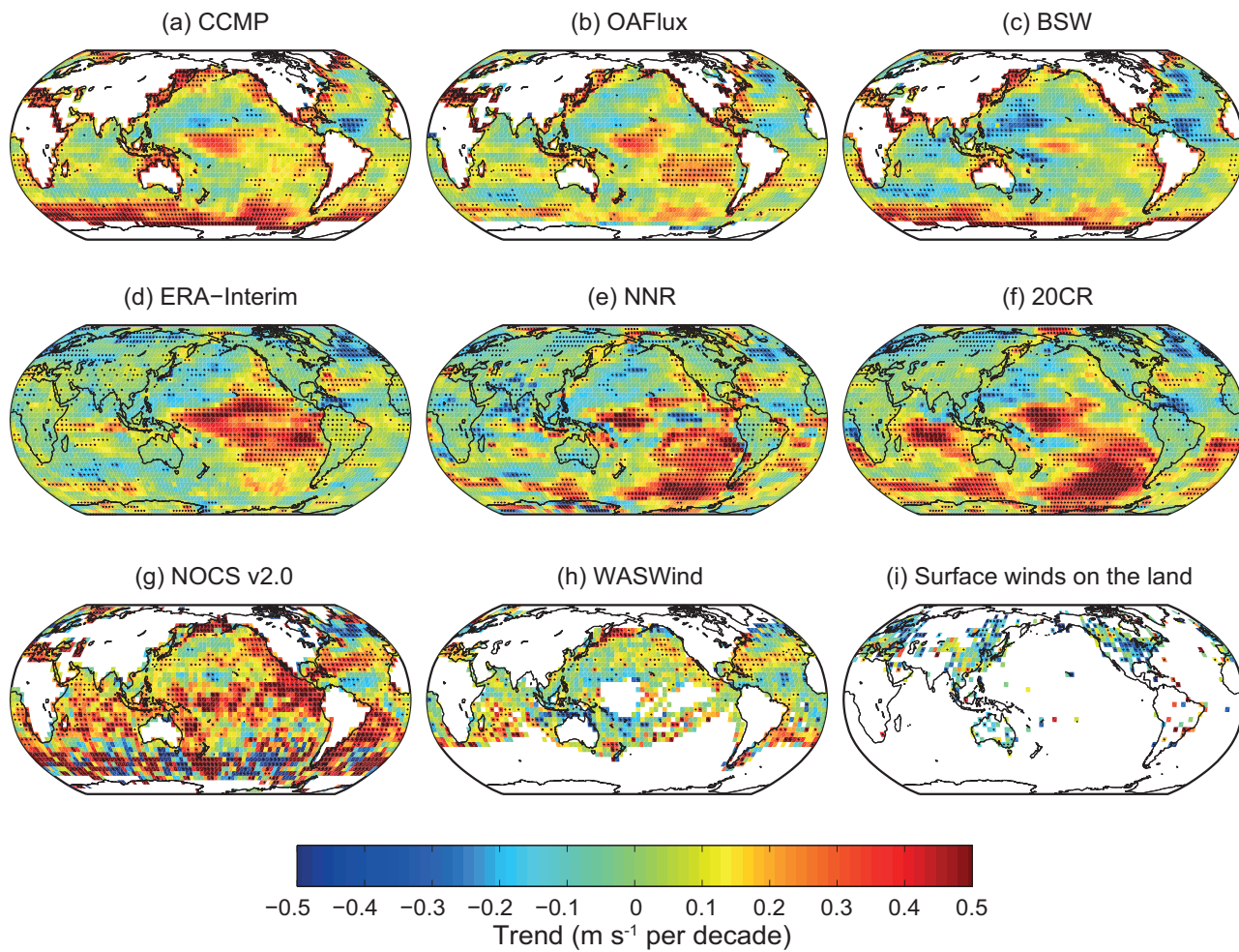


Figure 2.38 | Trends in surface wind speed for 1988–2010. Shown in the top row are data sets based on the satellite wind observations: (a) Cross-Calibrated Multi-Platform wind product (CCMP; Atlas et al., 2011); (b) wind speed from the Objectively Analyzed Air-Sea Heat Fluxes data set, release 3 (OAFlux); (c) Blended Sea Winds (BSW; Zhang et al., 2006); in the middle row are data sets based on surface observations: (d) ERA-Interim; (e) NCEP-NCAR, v.1 (NNR); (f) 20th Century Reanalysis (20CR, Compo et al., 2011), and in the bottom row are surface wind speeds from atmospheric reanalyses: (g) wind speed from the Surface Flux Data set, v.2, from NOC, Southampton, UK (Berry and Kent, 2009); (h) Wave- and Anemometer-based Sea Surface Wind (WASWind; Tokinaga and Xie, 2011a)); and (i) Surface Winds on the Land (Vautard et al., 2010). Wind speeds correspond to 10 m heights in all products. Land station winds (panel f) are also for 10 m (but anemometer height is not always reported) except for the Australian data where they correspond to 2 m height. To improve readability of plots, all data sets (including land station data) were averaged to the $4^\circ \times 4^\circ$ uniform longitude-latitude grid. Trends were computed for the annually averaged timeseries of $4^\circ \times 4^\circ$ cells. For all data sets except land station data, an annual mean was considered available only if monthly means for no less than eight months were available in that calendar year. Trend values were computed only if no less than 17 years had values and at least 1 year was available among the first and last 3 years of the period. White areas indicate incomplete or missing data. Black plus signs (+) indicate grid boxes where trends are significant (i.e., a trend of zero lies outside the 90% confidence interval).

Canada (Wan et al., 2010). Increasing wind speeds were found at high latitudes in both hemispheres, namely in Alaska from 1921 to 2001 (Lynch et al., 2004), in the central Canadian Arctic and Yukon from the 1950 to the 2000s (Wan et al., 2010) and in coastal Antarctica over the second half of the 20th century (Turner et al., 2005). A global review of 148 studies showed that near-surface terrestrial wind speeds are declining in the Tropics and the mid-latitudes of both hemispheres at a rate of -0.14 m s^{-1} per decade (McVicar et al., 2012). Vautard et al. (2010), analysing a global land surface wind data set from 1979 to 2008, found negative trends on the order of -0.1 m s^{-1} per decade over large portions of NH land areas. The wind speed trend pattern over land inferred from their data (1988–2010, Figure 2.38) has many points with magnitudes much larger than those in the reanalysis products, which appear to underestimate systematically the wind speed over land, as well as in coastal regions (Kent et al., 2012).

2

In summary, *confidence* is *low* in changes in surface wind speed over the land and over the oceans owing to remaining uncertainties in data sets and measures used.

2.7.3 Upper-Air Winds

In contrast to surface winds, winds above the planetary boundary layer have received little attention in AR4. Radiosondes and pilot balloon observations are available from around the 1930s (Stickler et al., 2010). Temporal inhomogeneities in radiosonde wind records are less common, but also less studied, than those in radiosonde temperature records (Gruber and Haimberger, 2008; Section 2.4.4.3). Upper air winds can also be derived from tracking clouds or water vapour in satellite imagery (Menzel, 2001) or from measurements using wind profilers, aircraft or thermal observations, all of which serve as an input to reanalyses (Box 2.3).

In the past few years, interest in an accurate depiction of upper air winds has grown, as they are essential for estimating the state and changes of the general atmospheric circulation and for explaining changes in the surface winds (Vautard et al., 2010). Allen and Sherwood (2008), analysing wind shear from radiosonde data, found significant positive zonal mean zonal wind trends in the northern extratropics in the upper troposphere and stratosphere and negative trends in the tropical upper troposphere for the period 1979–2005. Vautard et al. (2010) find increasing wind speed in radiosonde observations in the lower and middle troposphere from 1979 to 2008 over Europe and North America and decreasing wind speeds over Central and East Asia. However, systematic global trend analyses of radiosonde winds are rare, prohibiting an assessment of upper-air wind trends (specific features such as monsoons, jet streams and storms are discussed in Sections 2.7.5, 2.7.6 and 2.6, respectively).

In summary, upper-air winds are less studied than other aspects of the circulation, and less is known about the quality of data products, hence *confidence* in upper-air wind trends is *low*.

2.7.4 Tropospheric Geopotential Height and Tropopause

AR4 concluded that over the NH between 1960 and 2000, boreal winter and annual means of tropospheric GPH decreased over high latitudes and increased over the mid-latitudes. AR4 also reported an increase in tropical tropopause height and a slight cooling of the tropical cold-point tropopause.

Changes in GPH, which can be addressed using radiosonde data or reanalysis data (Box 2.3), reflect SLP and temperature changes in the atmospheric levels below. The spatial gradients of the trend indicate changes in the upper-level circulation. As for SLP, tropospheric GPH trends strongly depend on the period analysed due to pronounced decadal variability. For the 1979–2012 period, trends for 500 hPa GPH from the ERA-Interim reanalysis (Figure 2.36) as well as for other reanalyses show a significant decrease only at southern high latitudes in November to April, but significant positive GPH trends in the subtropics and northern high latitudes. Hence the change in the time period leads to a different trend pattern as compared to AR4. The seasonality and spatial dependence of 500 hPa GPH trends over Antarctica was highlighted by Neff et al. (2008), based upon radiosonde data over the period 1957–2007.

Minimum temperatures near the tropical tropopause (and therefore tropical tropopause height) are important as they affect the water vapour input into the stratosphere (Section 2.2.2.1). Studies since AR4 confirm the increase in tropopause height (Wang et al., 2012c). For tropical tropopause temperatures, studies based on radiosonde data and reanalyses partly support a cooling between the 1990s and the early 2000s (Randel et al., 2006; Randel and Jensen, 2013), but uncertainties in long-term trends of the tropical cold-point tropopause temperature from radiosondes (Wang et al., 2012c; Randel and Jensen, 2013) and reanalyses (Gettelman et al., 2010) are large and *confidence* is therefore *low*.

In summary, tropospheric geopotential height *likely* decreased from 1979 to 2012 at SH high latitudes in austral summer and increased in the subtropics and NH high latitudes. *Confidence* in trends of the tropical cold-point tropopause is *low* owing to remaining uncertainties in the data.

2.7.5 Tropical Circulation

In AR4, large interannual variability of the Hadley and Walker circulation was highlighted, as well as the difficulty in addressing changes in these features in the light of discrepancies between data sets. AR4 also found that rainfall in many monsoon systems exhibits decadal changes, but that data uncertainties restrict confidence in trends. SREX also attributed *low confidence* to observed trends in monsoons.

Observational evidence for trends and variability in the strength of the Hadley and Walker circulations (Annex III: Glossary), the monsoons, and the width of the tropical belt is based on radiosonde and reanalyses data (Box 2.3). In addition, changes in the tropical circulation imprint on other fields that are observed from space (e.g., total ozone, outgoing longwave radiation). Changes in the average state of the tropical circulation are constrained to some extent by changes in the water

cycle (Held and Soden, 2006; Schneider et al., 2010). Changes in the monsoon systems are expressed through altered circulation, moisture transport and convergence, and precipitation. Only a few monsoon studies address circulation changes, while most work focuses on precipitation.

Several studies report a weakening of the global monsoon circulations as well as a decrease of global land monsoon rainfall or of the number of precipitation days over the past 40 to 50 years (Zhou et al., 2008, see also SREX; Liu et al., 2011). Concerning the East Asian Monsoon, a year-round decrease is reported for wind speeds over China at the surface and in the lower troposphere based on surface observations and radiosonde data (Guo et al., 2010; Jiang et al., 2010; Vautard et al., 2010; Xu et al., 2010). The changes in wind speed are concomitant with changes in pressure centres such as a westward extension of the Western Pacific Subtropical High (Gong and Ho, 2002; Zhou et al., 2009b). A weakening of the East Asian summer monsoon since the

1920s is also found in SLP gradients (Zhou et al., 2009a). However, trends derived from wind observations and circulation trends from reanalysis data carry large uncertainties (Figure 2.38), and monsoon rainfall trends depend, for example, on the definition of the monsoon area (Hsu et al., 2011). For instance, using a new definition of monsoon area, an increase in northern hemispheric and global summer monsoon (land and ocean) precipitation is reported from 1979 to 2008 (Hsu et al., 2011; Wang et al., 2012a).

The additional data sets that became available since AR4 confirm the large interannual variability of the Hadley and Walker circulation. The strength of the northern Hadley circulation (Figure 2.39) in boreal winter and of the Pacific Walker circulation in boreal fall and winter is largely related to the ENSO (Box 2.5). This association dominates interannual variability and affects trends. Data sets do not agree well with respect to trends in the Hadley circulation (Figure 2.39). Two widely used reanalysis data sets, NNR and ERA-40, both have demonstrated

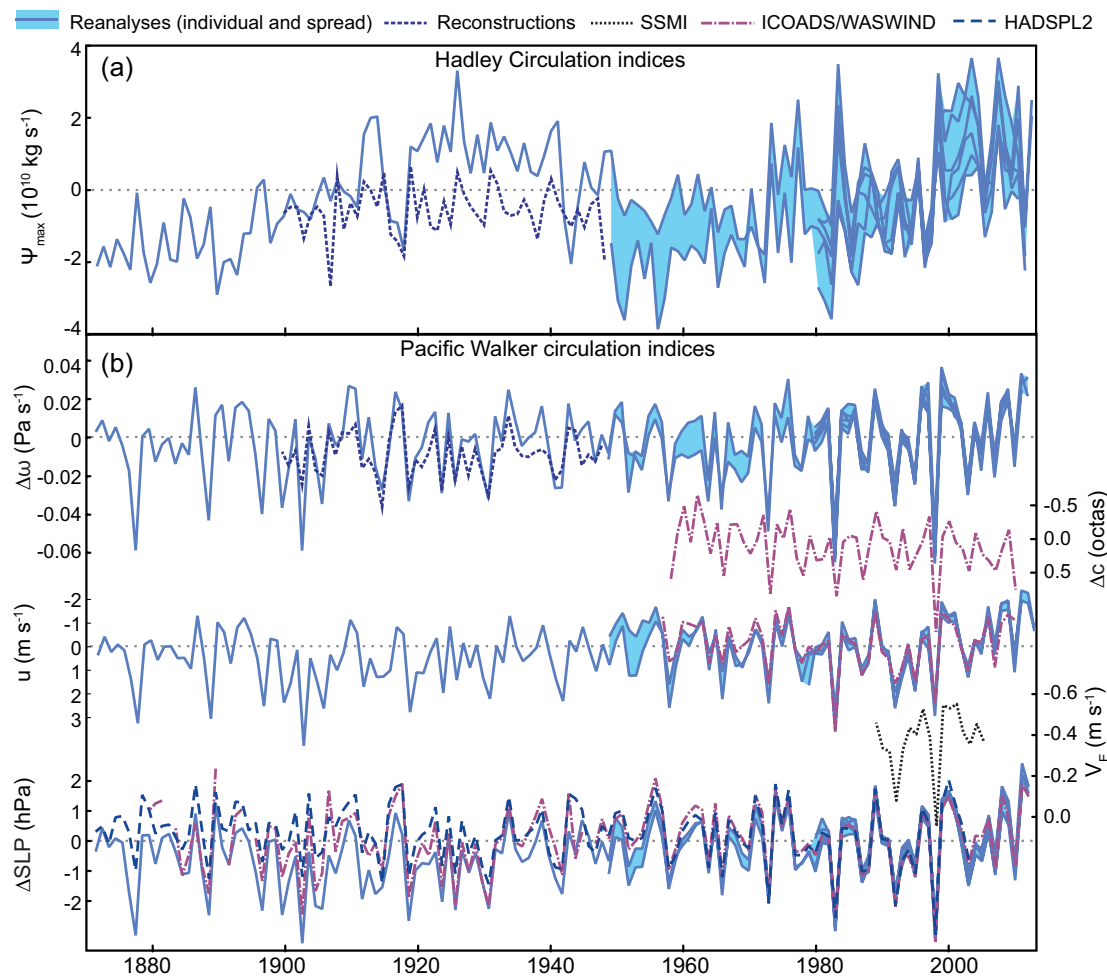


Figure 2.39 | (a) Indices of the strength of the northern Hadley circulation in December to March (Ψ_{\max} is the maximum of the meridional mass stream function at 500 hPa between the equator and 40°N). (b) Indices of the strength of the Pacific Walker circulation in September to January ($\Delta\omega$ is the difference in the vertical velocity between $[10^{\circ}\text{S}$ to 10°N , 180°W to 100°W] and $[10^{\circ}\text{S}$ to 10°N , 100°E to 150°E] as in Oort and Yienger (1996), Δc is the difference in cloud cover between $[6^{\circ}\text{N}$ to 12°S , 165°E to 149°W] and $[18^{\circ}\text{N}$ to 6°N , 165°E to 149°W] as in Deser et al. (2010a), v_E is the effective wind index from SSMI satellite data, updated from Sohn and Park (2010), u is the zonal wind at 10 m averaged in the region $[10^{\circ}\text{S}$ to 10°N , 160°E to 160°W], ΔSLP is the SLP difference between $[5^{\circ}\text{S}$ to 5°N , 160°W to 80°W] and $[5^{\circ}\text{S}$ to 5°N , 80°E to 160°E] as in Vecchi et al. (2006)). Reanalysis data sets include 20CR, NCEP/NCAR, ERA-Interim, JRA-25, MERRA, and CFSR, except for the zonal wind at 10 m (20CR, NCEP/NCAR, ERA-Interim), where available until January 2013. ERA-40 and NCEP2 are not shown as they are outliers with respect to the strength trend of the northern Hadley circulation (Mitas and Clement, 2005; Song and Zhang, 2007; Hu et al., 2011; Stachnik and Schumacher, 2011). Observation data sets include HadSLP2 (Section 2.7.1), ICOADS (Section 2.7.2; only 1957–2009 data are shown) and WASWIND (Section 2.7.2), reconstructions are from Brönnimann et al. (2009). Where more than one time series was available, anomalies from the 1980/1981 to 2009/2010 mean values of each series are shown.

shortcomings with respect to tropical circulation; hence their increases in the Hadley circulation strength since the 1970s might be artificial (Mitas and Clement, 2005; Song and Zhang, 2007; Hu et al., 2011; Stachnik and Schumacher, 2011). Later generation reanalysis data sets including ERA-Interim (Brönnimann et al., 2009; Nguyen et al., 2013) as well as satellite humidity data (Sohn and Park, 2010) also suggest a strengthening from the mid 1970s to present, but the magnitude is strongly data set dependent.

Consistent changes in different observed variables suggest a weakening of the Pacific Walker circulation during much of the 20th century that has been largely offset by a recent strengthening. A weakening is indicated by trends in the zonal SLP gradient across the equatorial Pacific (Section 2.7.1, Table 2.14) from 1861 to 1992 (Vecchi et al., 2006), or from 1901 to 2004 (Power and Kociuba, 2011b). Boreal spring and summer contribute most strongly to the centennial trend (Nicholls, 2008; Karnauskas et al., 2009), as well as to the trend in the second half of the 20th century (Tokinaga et al., 2012). For boreal fall and winter, when the circulation is strongest, no trend is found in the Pacific Walker circulation based on the vertical velocity at 500 hPa from reanalyses (Compo et al., 2011), equatorial Pacific 10 m zonal winds, or SLP in Darwin (Nicholls, 2008; Figure 2.39). However, there are inconsistencies between ERA-40 and NNR (Chen et al., 2008). Deser et al. (2010a) find changes in marine air temperature and cloud cover over the Pacific that are consistent with a weakening of the Walker circulation during most of the 20th century (Section 2.5.7.1 and Yu and Zwiers, 2010). Tokinaga et al. (2012) find robust evidence for a weakening of the Walker circulation (most notably over the Indian Ocean) from 1950 to 2008 based on observations of cloud cover, surface wind, and SLP. Since the 1980s or 1990s, however, trends in the Pacific Walker

circulation have reversed (Figure 2.39; Luo et al., 2012). This is evident from changes in SLP (see equatorial Southern Oscillation Index (SOI) trends in Table 2.14 and Box 2.5, Figure 1), vertical velocity (Compo et al., 2011), water vapour flux from satellite and reanalysis data (Sohn and Park, 2010), or sea level height (Merrifield, 2011). It is also consistent with the SST trend pattern since 1979 (Meng et al., 2012; see also Figure 2.22).

Observed changes in several atmospheric parameters suggest that the width of the tropical belt has increased at least since 1979 (Seidel et al., 2008; Forster et al., 2011; Hu et al., 2011). Since AR4, wind, temperature, radiation, and ozone information from radiosondes, satellites, and reanalyses had been used to diagnose the tropical belt width and estimate their trends. Annual mean time series of the tropical belt width from various sources are shown in Figure 2.40.

Since 1979 the region of low column ozone values typical of the tropics has expanded in the NH (Hudson et al., 2006; Hudson, 2012). Based on radiosonde observations and reanalyses, the region of the high tropical tropopause has expanded since 1979, and possibly since 1960 (Seidel and Randel, 2007; Birner, 2010; Lucas et al., 2012), although widening estimates from different reanalyses and using different methodologies show a range of magnitudes (Seidel and Randel, 2007; Birner, 2010).

Several lines of evidence indicate that climate features at the edges of the Hadley cell have also moved poleward since 1979. Subtropical jet metrics from reanalysis zonal winds (Strong and Davis, 2007, 2008; Archer and Caldeira, 2008b, 2008a) and layer-average satellite temperatures (Fu et al., 2006; Fu and Lin, 2011) also indicate widening, although 1979–2009 wind-based trends (Davis and Rosenlof, 2011)

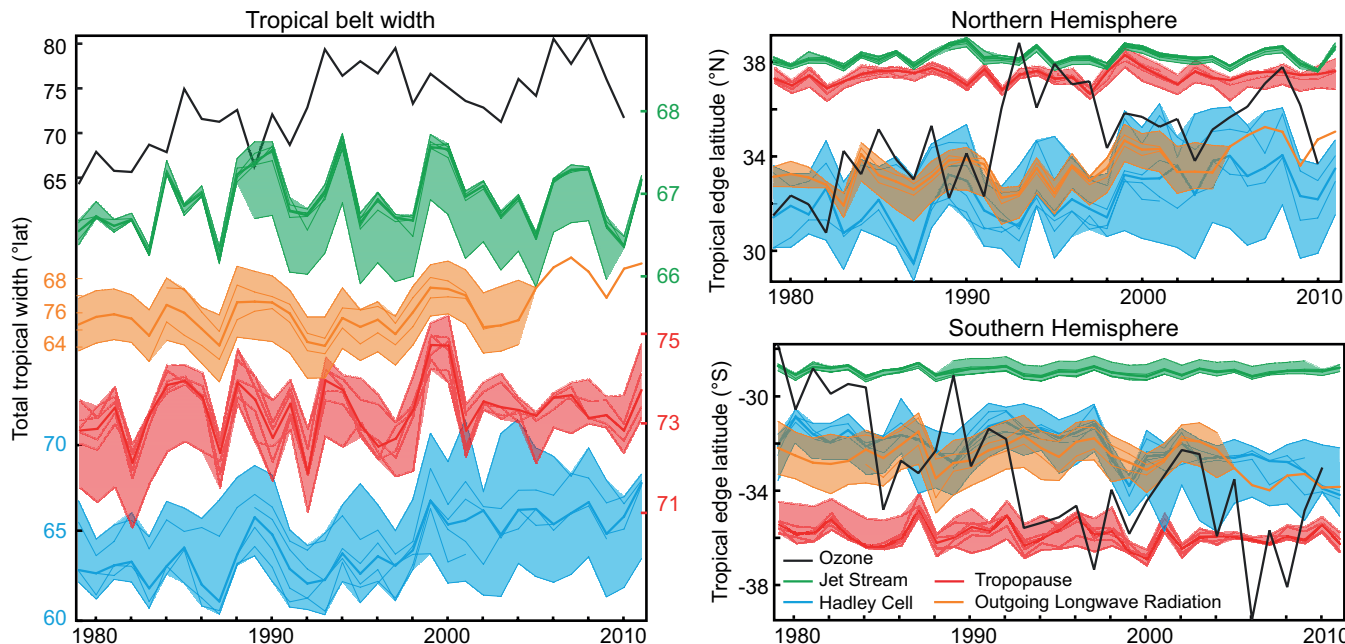


Figure 2.40 | Annual average tropical belt width (left) and tropical edge latitudes in each hemisphere (right). The tropopause (red), Hadley cell (blue), and jet stream (green) metrics are based on reanalyses (NCEP/NCAR, ERA-40, JRA25, ERA-Interim, CFSR, and MERRA, see Box 2.3); outgoing longwave radiation (orange) and ozone (black) metrics are based on satellite measurements. The ozone metric refers to equivalent latitude (Hudson et al., 2006; Hudson, 2012). Adapted and updated from Seidel et al. (2008) using data presented in Davis and Rosenlof (2011) and Hudson (2012). Where multiple data sets are available for a particular metric, all are shown as light solid lines, with shading showing their range and a heavy solid line showing their median.

are not statistically significant. Changes in subtropical outgoing long-wave radiation, a surrogate for high cloud, also suggest widening (Hu and Fu, 2007), but the methodology and results are disputed (Davis and Rosenlof, 2011). Widening of the tropical belt is also found in precipitation patterns (Hu and Fu, 2007; Davis and Rosenlof, 2011; Hu et al., 2011; Kang et al., 2011; Zhou et al., 2011), including in SH regions (Cai et al., 2012).

The qualitative consistency of these observed changes in independent data sets suggests a widening of the tropical belt between at least 1979 and 2005 (Seidel et al., 2008), and possibly longer. Widening estimates range between around 0° and 3° latitude per decade, but their uncertainties have been only partially explored (Birner, 2010; Davis and Rosenlof, 2011).

In summary, large interannual-to-decadal variability is found in the strength of the Hadley and Walker circulation. The *confidence* in trends in the strength of the Hadley circulation is *low* due to uncertainties in reanalysis data sets. Recent strengthening of the Pacific Walker circulation has largely offset the weakening trend from the 19th century to the 1990s (*high confidence*). Several lines of independent evidence indicate a widening of the tropical belt since the 1970s. The suggested weakening of the East Asian monsoon has *low confidence*, given the nature and quality of the evidence.

2.7.6 Jets, Storm Tracks and Weather Types

2.7.6.1 Mid-latitude and Subtropical Jets and Storm Track Position

AR4 reported a poleward displacement of Atlantic and southern polar front jet streams from the 1960s to at least the mid-1990s and a poleward shift of the northern hemispheric storm tracks. However, it was also noted that uncertainties are large and that NNR and ERA-40 disagree in important aspects. SREX also reported a poleward shift of NH and SH storm tracks. Studies since AR4 confirm that in the NH, the jet core has been migrating towards the pole since the 1970s, but trends in the jet speed are uncertain. Additional studies assessed here further support the poleward shift of the North Atlantic storm track from the 1950s to the early 2000s.

Subtropical and mid-latitude jet streams are three-dimensional entities that vary meridionally, zonally, and vertically. The position of the mid-latitude jet streams is related to the position of the mid-latitude storm tracks; regions of enhanced synoptic activity due to the passage of cyclones (Section 2.6). Jet stream winds can be determined from radiosonde measurements of GPH using quasi-geostrophic flow assumptions. Using reanalysis data sets (Box 2.3), it is possible to track three-dimensional jet variations by identifying a surface of maximum wind (SMW), although a high vertical resolution is required for identification of jets.

Various new analyses based on NCEP/NCAR and ERA-40 reanalyses as well as MSU/AMSU lower stratospheric temperatures (Section 2.4.4) confirm that the jet streams (mid-latitude and subtropical) have been moving poleward in most regions in the NH over the last three decades (Fu et al., 2006; Hu and Fu, 2007; Strong and Davis, 2007; Archer and

Caldeira, 2008a; Fu and Lin, 2011) but no clear trend is found in the SH (Swart and Fyfe, 2012). There is inconsistency with respect to jet speed trends based upon whether one uses an SMW-based or isobaric-based approach (Strong and Davis, 2007, 2008; Archer and Caldeira, 2008b, 2008a) and the choice of analysis periods due to inhomogeneities in reanalyses (Archer and Caldeira, 2008a). In general, jets have become more common (and jet speeds have increased) over the western and central Pacific, eastern Canada, the North Atlantic and Europe (Strong and Davis, 2007; Barton and Ellis, 2009), trends that are concomitant with regional increases in GPH gradients and circumpolar vortex contraction (Frauenfeld and Davis, 2003; Angell, 2006). From a climate dynamics perspective, these trends are driven by regional patterns of tropospheric and lower stratospheric warming or cooling and thus are coupled to large-scale circulation variability.

The North Atlantic storm track is closely associated with the NAO (Schneidereit et al., 2007). Studies based on ERA-40 reanalysis (Schneidereit et al., 2007), SLP measurements from ships (Chang, 2007), sea level time series (Vilibic and Sepic, 2010), and cloud analyses (Bender et al., 2012) support a poleward shift and intensification of the North Atlantic cyclone tracks from the 1950s to the early 2000s (Sorteberg and Walsh, 2008; Cornes and Jones, 2011).

2.7.6.2 Weather Types and Blocking

In AR4, weather types were not assessed as such, but an increase in blocking frequency in the Western Pacific and a decrease in North Atlantic were noted.

Changes in the frequency of weather types are of interest since weather extremes are often associated with specific weather types. For instance, persistent blocking of the westerly flow was essential in the development of the 2010 heat wave in Russia (Dole et al., 2011) (Section 9.5.2.2 and Box 14.2). Synoptic classifications or statistical clustering (Philipp et al., 2007) are commonly used to classify the weather on a given day. Feature-based methods are also used (Croci-Maspoli et al., 2007a). All these methods require daily SLP or upper-level fields.

Trends in synoptic weather types have been best analysed for central Europe since the mid-20th century, where several studies describe an increase in westerly or cyclonic weather types in winter but an increase of anticyclonic, dry weather types in summer (Philipp et al., 2007; Werner et al., 2008; Trnka et al., 2009). An eastward shift of blocking events over the North Atlantic (fewer cases of blocking over Greenland and more frequent blocking over the eastern North Atlantic) and the North Pacific was found by Davini et al. (2012) using NCEP/NCAR reanalysis since 1951 and by Croci-Maspoli et al. (2007a) in ERA-40 reanalysis during the period 1957–2001. Mokhov et al. (2013) find an increase in blocking duration over the NH year-round since about 1990 in a study based on NCEP/NCAR reanalysis data from 1969–2011. For the SH, Dong et al. (2008) found a decrease in number of blocking days but increase in intensity of blocking over the period 1948–1999. Differences in blocking index definitions, the sensitivity of some indices to changes in the mean field, and strong interannual variability in all seasons (Kreienkamp et al., 2010), partly related to circulation variability modes (Croci-Maspoli et al., 2007b), complicate a global assessment of blocking trends.

In summary, there is evidence for a poleward shift of storm tracks and jet streams since the 1970s. Based on the consistency of these trends with the widening of the tropical belt (Section 2.7.5), trends that are based on many different data sets, variables, and approaches, it is *likely* that circulation features have moved poleward since the 1970s. Methodological differences between studies mean there is *low confidence* in characterizing the global nature of any change in blocking.

2.7.7 Stratospheric Circulation

Changes in the polar vortices were assessed in AR4. A significant decrease in lower-stratospheric GPH in summer over Antarctica since 1969 was found, whereas trends in the Northern Polar Vortex were considered uncertain owing to its large variability.

The most important characteristics of the stratospheric circulation for climate and for trace gas distribution are the winter and spring polar vortices and Sudden Stratospheric Warmings (rapid warmings of the middle stratosphere that may lead to a collapse of the Polar Vortex), the Quasi-Biennial Oscillation (an oscillation of equatorial zonal winds with a downward phase propagation) and the Brewer-Dobson circulation (BDC, the meridional overturning circulation transporting air upward in the tropics, poleward to the winter hemisphere, and downward at polar and subpolar latitudes; Annex III: Glossary). Radiosonde observations, reanalysis data sets and space-borne temperature or trace gas observations are used to address changes in the stratospheric circulation, but all of these sources of information carry large trend uncertainties.

The AR4 assessment was corroborated further in Forster et al. (2011) and in updated 100 hPa GPH trends from ERA-Interim reanalysis (Box 2.3, Figure 2.36). There is *high confidence* that lower stratospheric GPH over Antarctica has decreased in spring and summer at least since 1979. Cohen et al. (2009) reported an increase in the number of Arctic sudden stratospheric warmings during the last two decades. However, interannual variability in the Arctic Polar Vortex is large, uncertainties in reanalysis products are high (Tegtmeier et al., 2008), and trends depend strongly on the time period analysed (Langematz and Kunze, 2008).

The BDC is only indirectly observable via wave activity diagnostics (which represent the main driving mechanism of the BDC), via temperatures or via the distribution of trace gases which may allow the determination of the ‘age of air’ (i.e., the time an air parcel has resided in the stratosphere after its entry from the troposphere). Randel et al. (2006), found a sudden decrease in global lower stratospheric water vapour and ozone around 2001 that is consistent with an increase in the mean tropical upwelling, that is, the tropical branch of the BDC (Rosenlof and Reid, 2008; Section 2.2.2.1; Lanzante, 2009; Randel and Jensen, 2013). On the other hand, Engel et al. (2009) found no statistically significant change in the age of air in the 24–35 km layer over the NH mid-latitudes from measurements of chemically inert trace gases from 1975 to 2005. However, this does not rule out trends in the lower stratospheric branch of the BDC or trends in mid to low latitude mixing (Bonisch et al., 2009; Ray et al., 2010). All of these methods are subject to considerable uncertainties, and they might shed light only on some aspects of the BDC. *Confidence* in trends in the BDC is therefore *low*.

In summary, it is *likely* that lower-stratospheric geopotential height over Antarctica has decreased in spring and summer at least since 1979. Owing to uncertainties in the data and approaches used, *confidence* in trends in the Brewer–Dobson circulation is *low*.

2.7.8 Changes in Indices of Climate Variability

AR4 assessed changes in indices of climate variability. The NAO and SAM were found to exhibit positive trends (strengthened mid-latitude westerlies) from the 1960s to 1990s, but the NAO has returned to its long-term mean state since then.

Indices of climate variability describe the state of the climate system with regards to individual modes of climate variability. Together with corresponding spatial patterns, they summarize large fractions of spatio-temporal climate variability. Inferences about significant trends in indices are generally hampered by relative shortness of climate records, their uncertainties and the presence of large variability on decadal and multidecadal time scales.

Table 2.14 summarizes observed changes in well-known indices of climate variability (see Box 2.5, Table 1 for precise definitions). Even the indices that explicitly include detrending of the entire record (e.g., Deser et al., 2010b), can exhibit statistically significant trends over shorter sub-periods. Confidence intervals in Table 2.14 that do not contain zero indicate trend significance at 10% level; however, the trends significant at 5% and 1% levels are emphasized in the discussion that follows. Chapter 14 discusses the main features and physical meaning of individual climate modes.

The NAO index reached very low values in the winter of 2010 (Osborn, 2011). As a result, with the exception of the principal component (PC) -based NAO index, which still shows a 5% significant positive trend from 1951 to present, other NAO or North Annular Mode (NAM) indices do not show significant trends of either sign for the periods presented in Table 2.14. In contrast, the SAM maintained the upward trend (Table 2.14). Fogt et al. (2009) found a positive trend in the SAM index from 1957 to 2005. Visbeck (2009), in a station-based index, found an increase in recent decades (1970s to 2000s).

The observed detrended multidecadal SST anomaly averaged over the North Atlantic Ocean area is often called Atlantic Multi-decadal Oscillation Index (AMO; see Box 2.5, Table 1, Figure 1). The warming trend in the “revised” AMO index since 1979 is significant at 1% level (Table 2.14) but cannot be readily interpreted because of the difficulty with reliable removal of the SST warming trend from it (Deser et al., 2010b).

On decadal and inter-decadal time scales the Pacific climate shows an irregular oscillation with long periods of persistence in individual stages and prominent shifts between them. Pacific Decadal Oscillation (PDO), Inter-decadal Pacific Oscillation (IPO) and North Pacific Index (NPI) indices characterize this variability for both hemispheres and agree well with each other (Box 2.5, Figure 1). While AR4 noted climate impacts of the 1976–1977 PDO phase transition, the shift in the opposite direction, both in PDO and IPO, may have occurred at the end of 1990s (Cai and van Renssch, 2012; Dai, 2012). Significance of 1979–2012 trends in PDO and NPI then would be an artefact of this

Table 2.14 | Trends for selected indices listed in Box 2.5, Table 1. Each index was standardized for its longest available period contained within the 1870–2012 interval. Standardization was done on the December-to-March (DJFM) means for the NAO, NAM and Pacific-North American pattern (PNA), on seasonal anomalies for Pacific-South American patterns (PSA1, PSA2) and on monthly anomalies for all other indices. Standardized monthly and seasonal anomalies were further averaged to annual means. Trend values computed for annual or DJFM means are given in standard deviation per decade with their 90% confidence intervals. Index records where the source is not explicitly indicated were computed from either HadISST1 (for SST-based indices), or HadSLP2r (for SLP-based indices) or NNR fields of 500 hPa or 850 hPa geopotential height. CoA stands for ‘Centers of Action’ index definitions. Linear trends for 1870–2012 were removed from ATL3, BMI and DMI.

Index Name	Trends in standard deviation units per decade		
	1901–2012	1951–2012	1979–2012
(–1)*SOI from CPC		0.004 ± 0.103	–0.243 ± 0.233
(–1)*SOI Troup from BOM records	0.012 ± 0.039	0.018 ± 0.104	–0.247 ± 0.236
SOI Darwin from BOM records	0.028 ± 0.036	0.082 ± 0.085	–0.116 ± 0.195
(–1)*EQSOI	0.001 ± 0.051	–0.076 ± 0.143	–0.558 ^b ± 0.297
NIÑO3.4	–0.003 ± 0.042	0.012 ± 0.105	–0.156 ± 0.274
NIÑO3.4 (ERSST v.3b)	0.067 ^a ± 0.045	0.054 ± 0.103	–0.085 ± 0.259
NIÑO3.4 (COBE SST)	0.024 ± 0.041	0.008 ± 0.107	–0.154 ± 0.289
NIÑO3	0.007 ± 0.039	0.043 ± 0.095	–0.143 ± 0.256
NIÑO3 (ERSST v.3b)	0.069 ± 0.039	0.098 ± 0.092	–0.073 ± 0.236
NIÑO3 (COBE SST)	0.034 ± 0.036	0.054 ± 0.096	–0.113 ± 0.258
NIÑO4	0.026 ± 0.054	0.068 ± 0.145	–0.102 ± 0.380
EMI	–0.059 ± 0.061	–0.119 ± 0.189	–0.131 ± 0.580
(–1)*TNI	0.019 ± 0.052	0.066 ± 0.167	0.030 ± 0.550
PDO from Mantua et al. (1997)	–0.017 ± 0.071	0.112 ± 0.189	–0.460 ^a ± 0.284
(–1)*NPI	–0.026 ^a ± 0.022	0.010 ± 0.046	–0.169 ^a ± 0.105
AMO revised	–0.001 ± 0.111	–0.012 ± 0.341	0.779 ^b ± 0.291
NAO stations from Jones et al. (1997)	–0.044 ± 0.056	0.095 ± 0.149	–0.136 ± 0.394
NAO stations from Hurrell (1995)	–0.001 ± 0.066	0.171 ± 0.179	–0.214 ± 0.400
NAO PC from Hurrell (1995)	0.012 ± 0.059	0.198 ^a ± 0.148	–0.037 ± 0.401
NAM PC	0.003 ± 0.048	0.141 ± 0.123	0.029 ± 0.360
SAM Z850 PC		0.268 ^b ± 0.063	0.100 ± 0.109
SAM SLP grid 40°S to 70°S	0.139 ^b ± 0.026	0.198 ^b ± 0.052	0.294 ^b ± 0.131
SAM SLP stations from Marshall (2003)			0.128 ^a ± 0.097
PNA CoA		0.113 ± 0.114	–0.103 ± 0.298
PNA RPC from CPC		0.202 ^b ± 0.111	0.019 ± 0.271
PSA Karoly (1989) CoA definition		–0.267 ^b ± 0.079	–0.233 ^a ± 0.174
(–1)*PSA Yuan and Li (2008) CoA definition		–0.211 ^b ± 0.069	–0.208 ± 0.189
PSA1 PC		–0.163 ^a ± 0.103	–0.368 ^a ± 0.245
PSA2 PC		0.200 ^b ± 0.066	0.036 ± 0.156
ATL3	0.035 ± 0.043	0.125 ^a ± 0.088	0.186 ± 0.193
AONM PC	0.064 ^a ± 0.051	0.138 ^a ± 0.109	0.327 ^a ± 0.230
AMM PC	0.019 ± 0.058	–0.015 ± 0.155	0.309 ± 0.324
IOBM PC	0.075 ^a ± 0.051	0.314 ^b ± 0.082	0.201 ± 0.206
BMI	0.072 ^a ± 0.050	0.294 ^b ± 0.083	0.189 ± 0.206
IODM PC	–0.016 ± 0.034	–0.031 ± 0.093	–0.052 ± 0.203
DMI	0.030 ± 0.033	0.080 ± 0.090	0.211 ± 0.210

Notes:

^a Trend values significant at the 5% level.

^b Trend values significant at the 1% level.

change; incidentally, no significant trends in these indices were seen for longer periods (Table 2.14). Nevertheless, Pacific changes since the 1980s (positive for NPI and negative for PDO and IPO) are consistent with the observed SLP changes (Section 2.7.1) and with reversing trends in the Walker Circulation (Section 2.7.5), which was reported to be slowing down during much of the 20th century but sped up again since the 1990s. Equatorial SOI shows an increasing trend since 1979 at 1% significance; more traditionally defined SOI indices do not show significant trends (Table 2.14).

NIÑO3.4 and NIÑO3 show a century-scale warming trend significant at 5% level, if computed from the ERSTv3b data set (Section 2.4.2) but not if calculated from other data sets (Table 2.14). Furthermore, the sign (and significance) of the trend in east–west SST gradient across the Pacific remains ambiguous (Vecchi and Soden, 2007; Bunge and Clarke, 2009; Karnauskas et al., 2009; Deser et al., 2010a) (Section 14.4.1).

In addition to changes in the mean values of climate indices, changes in the associated spatial patterns are also possible. In particular, the diversity of detail of different ENSO events and possible distinction between their “flavors” have received significant attention (Section 14.4.2). These efforts also intensified the discussion of useful ENSO indices in the literature. Starting from the work of Trenberth and Stepaniak (2001), who proposed to characterize the evolution of ENSO events with the Trans-Niño Index (TNI), which is virtually uncorrelated with the standard ENSO index NIÑO3.4, other alternative ENSO indices have been introduced and proposals were made for classifying ENSO events according to the indices they primarily maximize. While a traditional, ‘canonical’ El Niño event type (Rasmusson and Carpenter, 1982) is viewed as the ‘eastern Pacific’ type, some of the alternative indices purport to identify events that have central Pacific maxima and are called dateline El Niño (Larkin and Harrison, 2005), Modoki (Ashok et al., 2007), or Central Pacific El Niño (Kao and Yu, 2009). However, no consensus has been reached regarding the appropriate classification

of ENSO events. Takahashi et al. (2011) and Ren and Jin (2011) have presented many of the popular ENSO indices as elements in a two-dimensional linear space spanned by a pair of such indices. ENSO indices that involve central and western Pacific SST (NIÑO4, EMI, TNI) show no significant trends.

Significant positive PNA trends and negative and positive trends in the first and second PSA modes respectively are observed over the last 60 years (Table 2.14). However, the level of significance of these trends depends on the index definition and on the data set used. The positive trend in the Atlantic Ocean ‘Niño’ mode (AONM) index and in ATL3 are due to the intensified warming in the eastern Tropical Atlantic that causes the the weakening of the Atlantic equatorial cold tongue: these changes were noticed by Tokinaga and Xie (2011b) with regards to the last 60-year period. The Indian Ocean Basin Mode (IOBM) has a strong warming trend (significant at 1% since the middle of the 20th century). This phenomenon is well-known (Du and Xie, 2008) and its consequences for the regional climate is a subject of active research (Du et al., 2009; Xie et al., 2009).

In summary, large variability on interannual to decadal time scales and remaining differences between data sets precludes robust conclusions on long-term changes in indices of climate variability. *Confidence* is *high* that the increase in the NAO index from the 1950s to the 1990s has been largely offset by recent changes. It is *likely* that the SAM index has become more positive since the 1950s.

Box 2.5 | Patterns and Indices of Climate Variability

Much of the spatial structure of climate variability can be described as a combination of ‘preferred’ patterns. The most prominent of these are known as modes of climate variability and they impact weather and climate on many spatial and temporal scales (Chapter 14). Individual climate modes historically have been identified through spatial teleconnections: correlations between regional climate variations at widely separated, geographically fixed spatial locations. An index describing temporal variations of the climate mode in question can be formed, for example, by adding climate anomalies calculated from meteorological records at stations exhibiting the strongest correlation with the mode and subtracting anomalies at stations exhibiting anticorrelation. By regressing climate records from other places on this index, one derives a spatial climate pattern characterizing this mode. Patterns of climate variability have also been derived using a variety of mathematical techniques such as principal component analysis (PCA). These patterns and their indices are useful both because they efficiently describe climate variability in terms of a few preferred modes and also because they can provide clues about how the variability is sustained (Box 14.1 provides formal definitions of these terms).

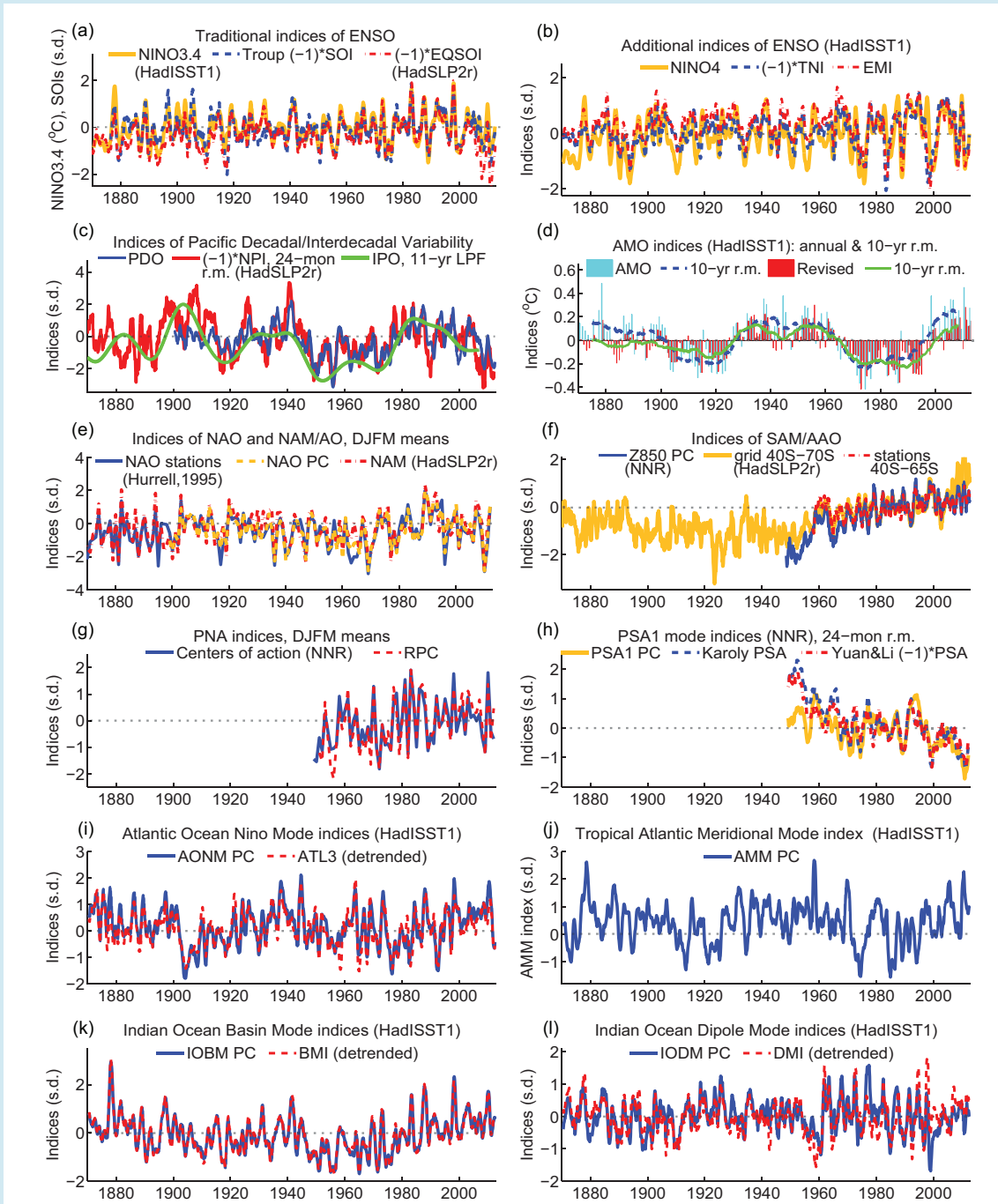
Box 2.5, Table 1 lists some prominent modes of large-scale climate variability and indices used for defining them. Changes in these indices are associated with large-scale climate variations on interannual and longer time scales. With some exceptions, indices shown have been used by a variety of authors. They are defined relatively simply from raw or statistically analyzed observations of a single climate variable, which has a history of surface observations. For most of these indices at least a century-long record is available for climate research. (*continued on next page*)

Box 2.5, Table 1 | Established indices of climate variability with global or regional influence. Z500, Z700 and Z850 denote geopotential height at the 500, 700 and 850 hPa levels, respectively. The subscripts s and a denote “standardized” and “anomalies”, respectively. Further information is given in Supplementary Material 2.SM.8. Climate impacts of these modes are listed in Box 14.1. (*continued on next page*)

Climate Phenomenon	Index Name	Index Definition	Primary Reference(s)
El Niño – Southern Oscillation (ENSO)	NIÑO1+2	SST _a averaged over [10°S–0°, 90°W–80°W]	Rasmusson and Wallace (1983), Cane (1986)
	NIÑO3	Same as above but for [5°S–5°N, 150°W–90°W]	
	NIÑO4	Same as above but for [5°S–5°N, 160°E–150°W]	
	NIÑO3.4	Same as above but for [5°S–5°N, 170°W–120°W]	Trenberth (1997)
	Troup Southern Oscillation Index (SOI)	Standardized for each calendar month SLP _a difference: Tahiti minus Darwin, ×10	Troup (1965)
	SOI	Standardized difference of SLP _{sa} : Tahiti minus Darwin	Trenberth (1984); Ropelewski and Jones (1987)
	Darwin SOI	Darwin SLP _{sa}	Trenberth and Hoar (1996)
	Equatorial SOI (EQSOI)	Standardized difference of standardized averages of SLP _a over equatorial [5°S–5°N] Pacific Ocean areas: [130°W–80°W] minus [90°E–140°E]	Bell and Halpert (1998)
Indices of ENSO events evolution and type	Trans-Niño Index (TNI)	NIÑO1+2 _s minus NIÑO4 _s	Trenberth and Stepaniak (2001)
	El Niño Modoki Index (EMI)	SST _a [165°E–140°W, 10°S–10°N] minus ½*[110°W–70°W, 15°S–5°N] minus ½*[125°E–145°E, 10°S–20°N]	Ashok et al. (2007)
Pacific Decadal and Interdecadal Variability	Pacific Decadal Oscillation (PDO)	1st PC of monthly N. Pacific SST _a field [20°N–70°N] with subtracted global mean	Mantua et al. (1997); Zhang et al. (1997)
	Inter-decadal Pacific Oscillation (IPO)	Projection of a global SST _a onto the IPO pattern, which is found as one of the leading Empirical Orthogonal Functions of a low-pass filtered global SST _a field	Folland et al. (1999); Power et al. (1999); Parker et al. (2007)
	North Pacific Index (NPI)	SLP _a averaged over [30°N–65°N; 160°E–140°W]	Trenberth and Hurrell (1994)
North Atlantic Oscillation (NAO)	Azores-Iceland NAO Index	SLP _{sa} difference: Lisbon/Ponta Delgada minus Stykkisholmur/ Reykjavik	Hurrell (1995)
	PC-based NAO Index	Leading PC of SLP _a over the Atlantic sector	Hurrell (1995)
	Gibraltar – South-west Iceland NAO Index	Standardized for each calendar month SLP _a difference: Gibraltar minus SW Iceland / Reykjavik	Jones et al. (1997)
Annular modes	Northern Annular Mode (NAM)	PC-based NAM or Arctic Oscillation (AO) index	Thompson and Wallace (1998, 2000)
	Southern Annular Mode (SAM)	PC-based SAM or Antarctic Oscillation (AAO) index	Thompson and Wallace (2000)
		Grid-based SAM index: 40°S–70°S difference	Nan and Li (2003)
		Station-based SAM index: 40°S–65°S	Marshall (2003)
Pacific/North America (PNA) atmospheric teleconnection	PNA index based on centers of action	¼[(20°N, 160°W) – (45°N, 165°W) + (55°N, 115°W) – (30°N, 85°W)] in the Z500 _{sa} field	Wallace and Gutzler (1981)
	PNA from rotated PCA	Rotated PC (RPC) from the analysis of the NH Z500 _a field	Barnston and Livezey (1987)
Pacific/South America (PSA) atmospheric teleconnection	PSA1 and PSA2 mode indices (PC-based)	2nd and 3rd PCs respectively of SH seasonal Z500 _a	Mo and Paegle (2001)
	PSA index (centers of action)	[–(35°S, 150°W) + (60°S, 120°W) – (45°S, 60°W)] in the Z500 _a field	Karoly (1989)
		[(45°S, 170°W) – (67.5°S, 120°W) + (50°S, 45°W)]/3 in the Z500 _a field	Yuan and Li (2008)
Atlantic Ocean Multidecadal Variability	Atlantic Multi-decadal Oscillation (AMO) index	10-year running mean of linearly detrended Atlantic mean SST _a [0°–70°N]	Enfield et al. (2001)
	Revised AMO index	As above, but detrended by subtracting SST _a [60°S–60°N] mean	Trenberth and Shea (2006)
Tropical Atlantic Ocean Variability	Atlantic Ocean Niño Mode (AONM)	ATL3	Zebiak (1993)
	Tropical Atlantic Meridional Mode (AMM)	PC-based AONM	Deser et al. (2010b)
		PC-based AMM Index	
Tropical Indian Ocean Variability	Indian Ocean Basin Mode (IOBM)	Basin mean index (BMI)	Yang et al. (2007)
	IOBM, PC-based Index	The first PC of the IO detrended SST _a (40°E–110°E, 20°S–20°N)	Deser et al. (2010b)
		PC-based IODM index	
	Indian Ocean Dipole Mode (IODM)	Dipole Mode Index (DMI)	Saji et al. (1999)

Box 2.5 (continued)

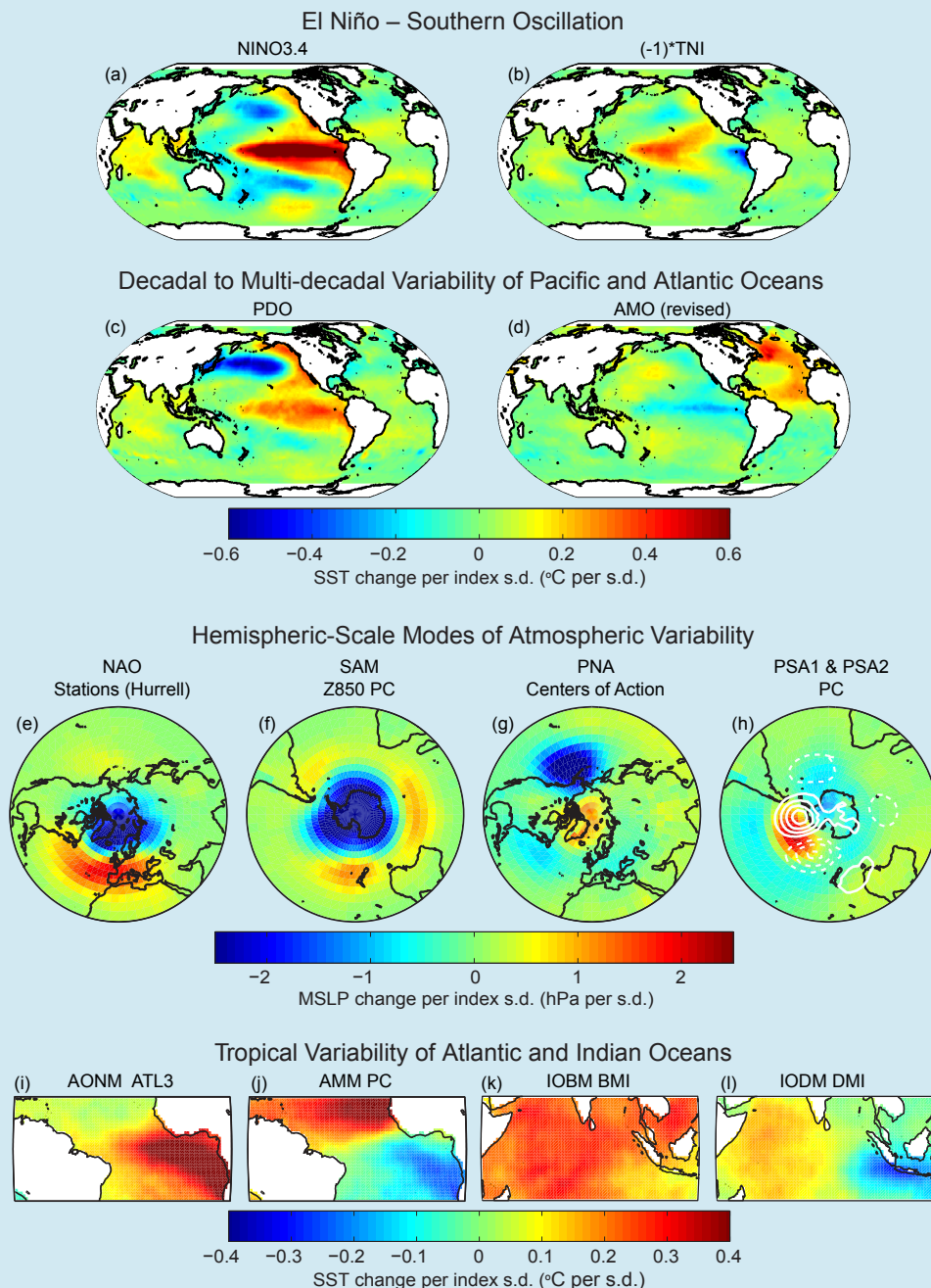
Most climate modes are illustrated by several indices (Box 2.5, Figure 1), which often behave similarly to each other. Spatial patterns of SST or SLP associated with these climate modes are illustrated in Box 2.5, Figure 2. They can be interpreted as a change in the SST or SLP field associated with one standard deviation change in the index. (*continued on next page*)



Box 2.5, Figure 1 | Some indices of climate variability, as defined in Box 2.5, Table 1, plotted in the 1870–2012 interval. Where ‘HadISST1’, ‘HadSLP2r’, or ‘NNR’ are indicated, the indices were computed from the sea surface temperature (SST) or sea level pressure (SLP) values of the former two data sets or from 500 or 850 hPa geopotential height fields from the NNR. Data set references given in the panel titles apply to all indices shown in that panel. Where no data set is specified, a publicly available version of an index from the authors of a primary reference given in Box 2.5, Table 1 was used. All indices were standardized with regard to 1971–2000 period except for NIÑO3.4 (centralized for 1971–2000) and AMO indices (centralized for 1901–1970). Indices marked as “detrended” had their linear trend for 1870–2012 removed. All indices are shown as 12-month running means except when the temporal resolution is explicitly indicated (e.g., ‘DJFM’ for December-to-March averages) or smoothing level (e.g., 11-year LPF for a low-pass filter with half-power at 11 years).

Box 2.5 (continued)

The difficulty of identifying a universally ‘best’ index for any particular climate mode is due to the fact that no simply defined indicator can achieve a perfect separation of the target phenomenon from all other effects occurring in the climate system. As a result, each index is affected by many climate phenomena whose relative contributions may change with the time period and the data set used. Limited length and quality of the observational record further compound this problem. Thus the choice of index is always application specific.



Box 2.5, Figure 2 | Spatial patterns of climate modes listed in Box 2.5, Table 1. All patterns shown here are obtained by regression of either sea surface temperature (SST) or sea level pressure (SLP) fields on the standardized index of the climate mode. For each climate mode one of the specific indices shown in Box 2.5, Figure 1 was used, as identified in the panel subtitles. SST and SLP fields are from HadISST1 and HadSLP2r data sets (interpolated gridded products based on data sets of historical observations). Regressions were done on monthly means for all patterns except for NAO and PNA, which were done with the DJFM means, and for PSA1 and PSA2, where seasonal means were used. Each regression was done for the longest period within the 1870–2012 interval when the index was available. For each pattern the time series was linearly de-trended over the entire regression interval. All patterns are shown by color plots, except for PSA2, which is shown by white contours over the PSA1 color plot (contour steps are 0.5 hPa, zero contour is skipped, negative values are indicated by dash).

Acknowledgements

The authors of Chapter 2 wish to thank Wenche Aas (NILU, Kjeller), Erika Coppola (ICTP, Trieste), Ritesh Gautam (NASA GSFC, Greenbelt), Jenny Hand (CIRA, Fort Collins), Andreas Hilboll (U. Bremen, Bremen), Glenn Hyatt (NOAA NCDC, Asheville), David Parrish (NOAA ESRL-CSD, Boulder), Deborah Misch (LMI, Inc, Asheville), Jared Rennie (CICS-NC, Asheville), Deborah Riddle (NOAA NCDC, Asheville), Sara Veasey (NOAA NCDC, Asheville), Mark Weber (U. Bremen, Bremen), Yin Xun-gang (STG Inc., Asheville), Teresa Young (STG, Asheville) and Jianglong Zhang (U. North Dakota, Grand Forks) for their critical contributions to the production of figures in this work.

References

- Abakumova, G. M., E. V. Gorbarenko, E. I. Nezval, and O. A. Shilovtseva, 2008: Fifty years of actinometrical measurements in Moscow. *Int. J. Remote Sens.*, **29**, 2629–2665.
- Adam, J. C., and D. P. Lettenmaier, 2008: Application of new precipitation and reconstructed streamflow products to streamflow trend attribution in northern Eurasia. *J. Clim.*, **21**, 1807–1828.
- Adler, R. F., G. J. Gu, and G. J. Huffman, 2012: Estimating climatological bias errors for the Global Precipitation Climatology Project (GPCP). *J. Appl. Meteor. Climatol.*, **51**, 84–99.
- Adler, R. F., et al., 2003: The version-2 global precipitation climatology project (GPCP) monthly precipitation analysis (1979–present). *J. Hydrometeor.*, **4**, 1147–1167.
- Aguilar, E., et al., 2009: Changes in temperature and precipitation extremes in western central Africa, Guinea Conakry, and Zimbabwe, 1955–2006. *J. Geophys. Res. Atmos.*, **114**, D02115.
- Alexander, L. V., P. Uotila, and N. Nicholls, 2009: Influence of sea surface temperature variability on global temperature and precipitation extremes. *J. Geophys. Res. Atmos.*, **114**, D18116.
- Alexander, L. V., X. L. L. Wang, H. Wan, and B. Trewin, 2011: Significant decline in storminess over southeast Australia since the late 19th century. *Aust. Meteor. Ocean. J.*, **61**, 23–30.
- Alexander, L. V., et al., 2006: Global observed changes in daily climate extremes of temperature and precipitation. *J. Geophys. Res. Atmos.*, **111**, D05109.
- Allan, R., and T. Ansell, 2006: A new globally complete monthly historical gridded mean sea level pressure dataset (HadSLP2): 1850–2004. *J. Clim.*, **19**, 5816–5842.
- Allan, R., S. Tett, and L. Alexander, 2009: Fluctuations in autumn-winter severe storms over the British Isles: 1920 to present. *Int. J. Climatol.*, **29**, 357–371.
- Allan, R. P., 2009: Examination of relationships between clear-sky longwave radiation and aspects of the atmospheric hydrological cycle in climate models, reanalyses, and observations. *J. Clim.*, **22**, 3127–3145.
- Allan, R. P., and A. Slingo, 2002: Can current climate model forcings explain the spatial and temporal signatures of decadal OLR variations? *Geophys. Res. Lett.*, **29**, 1141.
- Allan, R. P., and B. J. Soden, 2008: Atmospheric warming and the amplification of precipitation extremes. *Science*, **321**, 1481–1484.
- Allan, R. P., B. J. Soden, V. O. John, W. Ingram, and P. Good, 2010: Current changes in tropical precipitation. *Environ. Res. Lett.*, **5**, 025205.
- Allen, R. J., and S. C. Sherwood, 2007: Utility of radiosonde wind data in representing climatological variations of tropospheric temperature and baroclinicity in the western tropical Pacific. *J. Clim.*, **20**, 5229–5243.
- Allen, R. J., and S. C. Sherwood, 2008: Warming maximum in the tropical upper troposphere deduced from thermal winds. *Nature Geosci.*, **1**, 399–403.
- Alpert, P., and P. Kishcha, 2008: Quantification of the effect of urbanization on solar dimming. *Geophys. Res. Lett.*, **35**, L08801.
- Alpert, P., P. Kishcha, Y. J. Kaufman, and R. Schwarzbard, 2005: Global dimming or local dimming? Effect of urbanization on sunlight availability. *Geophys. Res. Lett.*, **32**, L17802.
- Andrade, C., S. Leite, and J. Santos, 2012: Temperature extremes in Europe: Overview of their driving atmospheric patterns. *Nat. Hazards Earth Syst. Sci.*, **12**, 1671–1691.
- Andronova, N., J. E. Penner, and T. Wong, 2009: Observed and modeled evolution of the tropical mean radiation budget at the top of the atmosphere since 1985. *J. Geophys. Res. Atmos.*, **114**, D14106.
- Angell, J. K., 2006: Changes in the 300-mb North Circumpolar Vortex, 1963–2001. *J. Clim.*, **19**, 2984–2994.
- Anthes, R. A., 2011: Exploring Earth's atmosphere with radio occultation: contributions to weather, climate and space weather. *Atmos. Meas. Tech.*, **4**, 1077–1103.
- Anthes, R. A., et al., 2008: The COSMO/Formosat-3 Mission—Early results. *Bull. Am. Meteor. Soc.*, **89**, 313.
- Archer, C. L., and K. Caldeira, 2008a: Reply to comment by Courtenay Strong and Robert E. Davis on "Historical trends in the jet streams". *Geophys. Res. Lett.*, **35**, L24807.
- Archer, C. L., and K. Caldeira, 2008b: Historical trends in the jet streams. *Geophys. Res. Lett.*, **35**, L08803.
- Arndt, D. S., M. O. Baringer, and M. R. Johnson, 2010: State of the Climate in 2009. *Bull. Am. Meteor. Soc.*, **91**, S1–.
- Arnold, T., et al., 2013: Nitrogen trifluoride global emissions estimated from updated atmospheric measurements. *Proc. Natl. Acad. Sci. U.S.A.*, **110**, 2029–2034.
- Ashok, K., S. K. Behera, S. A. Rao, H. Y. Weng, and T. Yamagata, 2007: El Niño Modoki and its possible teleconnection. *J. Geophys. Res. Oceans*, **112**, C11007.
- Asmi, A., et al., 2013: Aerosol decadal trends – Part 2: In-situ aerosol particle number concentrations at GAW and ACTRIS stations. *Atmos. Chem. Phys.*, **13**, 895–916.
- Atlas, R., R. Hoffman, J. Ardizzone, S. Leidner, J. Jusem, D. Smith, and D. Gombos, 2011: A cross-calibrated multiplatform ocean wind velocity product for meteorological and oceanographic applications. *Bull. Am. Meteor. Soc.*, **92**, 157–.
- Augustine, J. A., and E. G. Dutton, 2013: Variability of the surface radiation budget over United States from 1996 through 2011 from high-quality measurements. *J. Geophys. Res.*, **118**, 43–53,
- Aydin, M., et al., 2011: Recent decreases in fossil-fuel emissions of ethane and methane derived from firn air. *Nature*, **476**, 198–201.
- Ballester, J., F. Giorgi, and X. Rodo, 2010: Changes in European temperature extremes can be predicted from changes in PDF central statistics. *Clim. Change*, **98**, 277–284.
- Baringer, M. O., D. S. Arndt, and M. R. Johnson, 2010: State of the Climate in 2009. *Bull. Am. Meteor. Soc.*, **91**, S1–.
- Barmpadimos, I., J. Keller, D. Oderbolz, C. Hueglin, and A. S. H. Prévôt, 2012: One decade of parallel fine (PM2.5) and coarse (PM10–PM2.5) particulate matter measurements in Europe: trends and variability. *Atmos. Chem. Phys.*, **12**, 3189–3203.
- Barnston, A. G., and R. E. Livezey, 1987: Classification, seasonality and persistence of low-frequency atmospheric circulation patterns. *Mon. Weather Rev.*, **115**, 1083–1126.
- Barring, L., and K. Fortuniak, 2009: Multi-indices analysis of southern Scandinavian storminess 1780–2005 and links to interdecadal variations in the NW Europe–North Sea region. *Int. J. Climatol.*, **29**, 373–384.
- Barriopedro, D., E. M. Fischer, J. Luterbacher, R. Trigo, and R. García-Herrera, 2011: The hot summer of 2010: Redrawing the temperature record map of Europe. *Science*, **332**, 220–224.
- Barrucand, M., M. Rusticucci, and W. Vargas, 2008: Temperature extremes in the south of South America in relation to Atlantic Ocean surface temperature and Southern Hemisphere circulation. *J. Geophys. Res. Atmos.*, **113**, D20111.
- Barton, N. P., and A. W. Ellis, 2009: Variability in wintertime position and strength of the North Pacific jet stream as represented by re-analysis data. *Int. J. Climatol.*, **29**, 851–862.
- Becker, A., et al., 2013: A description of the global land-surface precipitation data products of the Global Precipitation Climatology Centre with sample applications including centennial (trend) analysis from 1901–present. *Earth Syst. Sci. Data*, **5**, 71–99.
- Beig, G., and V. Singh, 2007: Trends in tropical tropospheric column ozone from satellite data and MOZART model. *Geophys. Res. Lett.*, **34**, L17801.
- Bell, G. D., and M. S. Halpert, 1998: Climate assessment for 1997. *Bull. Am. Meteor. Soc.*, **79**, S1–S50.
- Bender, F. A. M., V. Ramanathan, and G. Tselioudis, 2012: Changes in extratropical storm track cloudiness 1983–2008: Observational support for a poleward shift. *Clim. Dyn.*, **38**, 2037–2053.
- Bengtsson, L., and K. I. Hodges, 2011: On the evaluation of temperature trends in the tropical troposphere. *Clim. Dyn.*, **36**, 419–430.
- Beniston, M., 2004: The 2003 heat wave in Europe: A shape of things to come? An analysis based on Swiss climatological data and model simulations. *Geophys. Res. Lett.*, **31**, L02202.
- Beniston, M., 2009: Decadal-scale changes in the tails of probability distribution functions of climate variables in Switzerland. *Int. J. Climatol.*, **29**, 1362–1368.
- Bennartz, R., J. Fan, J. Rausch, L. Leung, and A. Heidinger, 2011: Pollution from China increases cloud droplet number, suppresses rain over the East China Sea. *Geophys. Res. Lett.*, **38**, L09704.
- Berrisford, P., et al., 2011: Atmospheric conservation properties in ERA-Interim. *Q. J. R. Meteor. Soc.*, **137**, 1381–1399.
- Berry, D., and E. Kent, 2011: Air-Sea fluxes from ICOADS: The construction of a new gridded dataset with uncertainty estimates. *Int. J. Climatol.*, **31**, 987–1001.
- Berry, D. I., and E. C. Kent, 2009: A new air-sea interaction gridded dataset from ICOADS with uncertainty estimates. *Bull. Am. Meteor. Soc.*, **90**, 645–656.

- Berthet, C., J. Dessens, and J. Sanchez, 2011: Regional and yearly variations of hail frequency and intensity in France. *Atmos. Res.*, **100**, 391–400.
- Birner, T., 2010: Recent widening of the tropical belt from global tropopause statistics: Sensitivities. *J. Geophys. Res. Atmos.*, **115**, D23109.
- Bitz, C. M., and Q. Fu, 2008: Arctic warming aloft is data set dependent. *Nature*, **455**, E3–E4.
- Black, E., and R. Sutton, 2007: The influence of oceanic conditions on the hot European summer of 2003. *Clim. Dyn.*, **28**, 53–66.
- Blunden, J., D. S. Arndt, and M. O. Baringer, 2011: State of the Climate in 2010. *Bull. Am. Meteorol. Soc.*, **92**, S17–.
- Bohm, R., P. D. Jones, J. Hiebl, D. Frank, M. Brunetti, and M. Maugeri, 2010: The early instrumental warm-bias: A solution for long central European temperature series 1760–2007. *Clim. Change*, **101**, 41–67.
- Bonfills, C., P. B. Duffy, B. D. Santer, T. M. L. Wigley, D. B. Lobell, T. J. Phillips, and C. Doutriaux, 2008: Identification of external influences on temperatures in California. *Clim. Change*, **87**, S43–S55.
- Bonisch, H., A. Engel, J. Curtiss, T. Birner, and P. Hoor, 2009: Quantifying transport into the lowermost stratosphere using simultaneous in-situ measurements of SF₆ and CO₂. *Atmos. Chem. Phys.*, **9**, 5905–5919.
- Bosilovich, M. G., F. R. Robertson, and J. Chen, 2011: Global energy and water budgets in MERRA. *J. Clim.*, **24**, 5721–5739..
- Bourassa, M. A., S. T. Gille, D. L. Jackson, J. B. Roberts, and G. A. Wick, 2010: Ocean winds and turbulent air-sea fluxes inferred from remote sensing. *Oceanography*, **23**, 36–51.
- Bousquet, P., 2011: Source attribution of the changes in atmospheric methane for 2006–2008. *Atmos. Chem. Phys. Discuss.*, **10**, 27603–27630.
- Brøgniez, H., R. Roca, and L. Picon, 2009: Study of the free tropospheric humidity interannual variability using meteosat data and an advection-condensation transport model. *J. Clim.*, **22**, 6773–6787.
- Brönnimann, S., 2009: Early twentieth-century warming. *Nature Geosci.*, **2**, 735–736.
- Brönnimann, S., et al., 2009: Variability of large-scale atmospheric circulation indices for the Northern Hemisphere during the past 100 years. *Meteorol. Z.*, **18**, 379–396.
- Brooks, C. F., 1926: Observing water-surface temperatures at sea. *Mon. Wea. Rev.*, **54**, 241–253.
- Brooks, H., 2012: Severe thunderstorms and climate change. *Atmos. Res.*, **123**, SI, 129–138.
- Brooks, H. E., and N. Dotzek, 2008: The spatial distribution of severe convective storms and an analysis of their secular changes. In: *Climate Extremes and Society* [H. F. Diaz and R. J. Murnane (eds.)] Cambridge University Press, pp. 35–53.
- Brown, S. J., J. Caesar, and C. A. T. Ferro, 2008: Global changes in extreme daily temperature since 1950. *J. Geophys. Res. Atmos.*, **113**, D05115.
- Brunet, M., et al., 2011: The minimization of the screen bias from ancient Western Mediterranean air temperature records: an exploratory statistical analysis. *Int. J. Climatol.*, **31**, 1879–1895.
- Bunge, L., and A. J. Clarke, 2009: A verified estimation of the El Niño Index Niño-3.4 since 1877. *J. Clim.*, **22**, 3979–3992.
- Burn, D. H., and N. M. Hesch, 2007: Trends in evaporation for the Canadian prairies. *J. Hydrol.*, **336**, 61–73.
- Caesar, J., L. Alexander, and R. Vose, 2006: Large-scale changes in observed daily maximum and minimum temperatures: Creation and analysis of a new gridded data set. *J. Geophys. Res. Atmos.*, **111**, D05101.
- Caesar, J., et al., 2011: Changes in temperature and precipitation extremes over the Indo-Pacific region from 1971 to 2005. *Int. J. Climatol.*, **31**, 791–801.
- Cai, W., and P. van Renssch, 2012: The 2011 southeast Queensland extreme summer rainfall: A confirmation of a negative Pacific Decadal Oscillation phase? *Geophys. Res. Lett.*, **39**, L08702.
- Cai, W., T. Cowan, and M. Thatcher, 2012: Rainfall reductions over Southern Hemisphere semi-arid regions: The role of subtropical dry zone expansion. *Sci. Rep.*, **2**, 702.
- Callaghan, J., and S. B. Power, 2011: Variability and decline in the number of severe tropical cyclones making land-fall over eastern Australia since the late nineteenth century. *Clim. Dyn.*, **37**, 647–662.
- Canada, 2012: Canadian Smog Science Assessment – Highlights and Key Messages. Environment Canada and Health Canada, 64 pp.
- Cane, M. A., 1986: El-Niño. *Annu. Rev. Earth Planet. Sci.*, **14**, 43–70.
- Cao, Z. H., 2008: Severe hail frequency over Ontario, Canada: Recent trend and variability. *Geophys. Res. Lett.*, **35**, L14803.
- Carslaw, K. S., O. Boucher, D. Spracklen, G. Mann, J. G. Rae, S. Woodward, and M. Kumala, 2010: A review of natural aerosol interactions and feedbacks within the Earth system. *Atmos. Chem. Phys.*, **10**, 1701–1737.
- Casey, K. S., T. B. Brandon, P. Cornillon, and R. Evans, 2010: The past, present and future of the AVHRR Pathfinder SST Program. In: *Oceanography from Space: Revisited* [V. Barale, J. F. R. Gower, and L. Alberotanza (eds.)]. Springer Science+Business Media, New York, 323–341.
- Castellanos, P., and K. F. Boersma, 2012: Reductions in nitrogen oxides over Europe driven by environmental policy and economic recession. *Sci. Rep.*, **2**, 265.
- Cermak, J., M. Wild, R. Knutti, M. I. Mishchenko, and A. K. Heidinger, 2010: Consistency of global satellite-derived aerosol and cloud data sets with recent brightening observations. *Geophys. Res. Lett.*, **37**, L21704.
- Chambers, L., and G. Griffiths, 2008: The changing nature of temperature extremes in Australia and New Zealand. *Aust. Meteorol. Mag.*, **57**, 13–35.
- Chan, J. C. L., and M. Xu, 2009: Inter-annual and inter-decadal variations of landfalling tropical cyclones in East Asia. Part I: time series analysis. *Int. J. Climatol.*, **29**, 1285–1293.
- Chandler, R. E., and E. M. Scott, 2011: *Statistical Methods for Trend Detection and Analysis in the Environmental Sciences*. John Wiley & Sons, Hoboken, NJ.
- Chang, E. K. M., 2007: Assessing the increasing trend in Northern Hemisphere winter storm track activity using surface ship observations and a statistical storm track model. *J. Clim.*, **20**, 5607–5628.
- Chang, E. K. M., and Y. J. Guo, 2007: Is the number of North Atlantic tropical cyclones significantly underestimated prior to the availability of satellite observations? *Geophys. Res. Lett.*, **34**, L14801.
- Chapman, W. L., and J. E. Walsh, 2007: A synthesis of Antarctic temperatures. *J. Clim.*, **20**, 4096–4117.
- Che, H. Z., et al., 2005: Analysis of 40 years of solar radiation data from China, 1961–2000. *Geophys. Res. Lett.*, **32**, L06803.
- Chen, J. Y., B. E. Carlson, and A. D. Del Genio, 2002: Evidence for strengthening of the tropical general circulation in the 1990s. *Science*, **295**, 838–841.
- Chen, J. Y., A. D. Del Genio, B. E. Carlson, and M. G. Bosilovich, 2008: The spatio-temporal structure of twentieth-century climate variations in observations and reanalyses. Part I: Long-term trend. *J. Clim.*, **21**, 2611–2633.
- Chiachio, M., and M. Wild, 2010: Influence of NAO and clouds on long-term seasonal variations of surface solar radiation in Europe. *J. Geophys. Res. Atmos.*, **115**, D00d22.
- Choi, G., et al., 2009: Changes in means and extreme events of temperature and precipitation in the Asia Pacific Network region, 1955–2007. *Int. J. Climatol.*, **29**, 1906–1925.
- Christy, J. R., and W. B. Norris, 2006: Satellite and VIZ-radiosonde intercomparisons for diagnosis of nonclimatic influences. *J. Atmos. Ocean. Technol.*, **23**, 1181–1194.
- Christy, J. R., and W. B. Norris, 2009: Discontinuity issues with radiosonde and satellite temperatures in the Australian Region 1979–2006. *J. Atmos. Ocean. Technol.*, **26**, 508–522.
- Christy, J. R., W. B. Norris, and R. T. McNider, 2009: Surface temperature variations in East Africa and possible causes. *J. Clim.*, **22**, 3342–3356.
- Christy, J. R., R. W. Spencer, and W. B. Norris, 2011: The role of remote sensing in monitoring global bulk tropospheric temperatures. *Int. J. Remote Sens.*, **32**, 671–685.
- Christy, J. R., W. B. Norris, K. Redmond, and K. P. Gallo, 2006: Methodology and results of calculating central California surface temperature trends: Evidence of human-induced climate change? *J. Clim.*, **19**, 548–563.
- Christy, J. R., W. B. Norris, R. W. Spencer, and J. J. Hnilo, 2007: Tropospheric temperature change since 1979 from tropical radiosonde and satellite measurements. *J. Geophys. Res. Atmos.*, **112**, D06102.
- Christy, J. R., R. W. Spencer, W. B. Norris, W. D. Braswell, and D. E. Parker, 2003: Error estimates of version 5.0 of MSU-AMSU bulk atmospheric temperatures. *J. Atmos. Ocean. Technol.*, **20**, 613–629.
- Christy, J. R., et al., 2010: What do observational datasets say about modeled tropospheric temperature trends since 1979? , 2148–2169.
- Chu, W. P., M. P. McCormick, J. Lenoble, C. Brøgniez, and P. Pruvost, 1989: SAGE II inversion algorithm. *J. Geophys. Res. Atmos.*, **94**, 8339–8351.
- Chung, E. S., and B. J. Soden, 2010: Investigating the influence of carbon dioxide and the stratosphere on the long-term tropospheric temperature monitoring from HIRS. *J. Appl. Meteor. Climatol.*, **49**, 1927–1937.

- Chung, E. S., D. Yeomans, and B. J. Soden, 2010: An assessment of climate feedback processes using satellite observations of clear-sky OLR. *Geophys. Res. Lett.*, **37**, L02702.
- Clark, R. T., S. J. Brown, and J. M. Murphy, 2006: Modeling Northern Hemisphere summer heat extreme changes and their uncertainties using a physics ensemble of climate sensitivity experiments. *J. Clim.*, **19**, 4418–4435.
- Clement, A. C., and B. Soden, 2005: The sensitivity of the tropical-mean radiation budget. *J. Clim.*, **18**, 3189–3203.
- CMA, 2007: *Atlas of China Disastrous Weather and Climate*. Chinese Meteorological Administration. Beijing, China.
- CMA, 2011: China Climate Change Bulletin. Chinese Meteorological Administration. Beijing, China.
- Cohen, J., M. Barlow, and K. Saito, 2009: Decadal fluctuations in planetary wave forcing modulate global warming in late boreal winter. *J. Clim.*, **22**, 4418–4426.
- Cohen, J. L., J. C. Furtado, M. Barlow, V. A. Alexeev, and J. E. Cherry, 2012: Asymmetric seasonal temperature trends. *Geophys. Res. Lett.*, **39**, L04705.
- Cohn, T. A., and H. F. Lins, 2005: Nature's style: Naturally trendy. *Geophys. Res. Lett.*, **32**, L23402.
- Coles, S., 2001: *An Introduction to Statistical Modeling of Extreme Values*. Springer Science+Business Media, New York, 208 pp.
- Collaud Coen, M., et al., 2013: Aerosol decadal trends – Part 1: In-situ optical measurements at GAW and IMPROVE stations. *Atmos. Chem. Phys.*, **13**, 869–894.
- Compo, G. P., et al., 2011: The twentieth century reanalysis project. *Q. J. Roy. Meteorol. Soc.*, **137**, 1–28.
- Cooper, O. R., R. S. Gao, D. Tarasick, T. Leblanc, and C. Sweeney, 2012: Long-term ozone trends at rural ozone monitoring sites across the United States, 1990–2010. *J. Geophys. Res.*, **117**, D22307.
- Cornes, R. C., and P. D. Jones, 2011: An examination of storm activity in the northeast Atlantic region over the 1851–2003 period using the EMULATE gridded MSLP data series. *J. Geophys. Res. Atmos.*, **116**, D16110.
- Coumou, D., A. Robinson, and S. Rahmstorf, 2013: Global increase in record-breaking monthly-mean temperatures. *Clim. Change*, **118**, 771–782.
- Craigmile, P. F., and P. Guttorp, 2011: Space-time modelling of trends in temperature series. *J. Time Ser. Anal.*, **32**, 378–395.
- Croci-Maspoli, M., C. Schwierz, and H. C. Davies, 2007a: A multifaceted climatology of atmospheric blocking and its recent linear trend. *J. Clim.*, **20**, 633–649.
- Croci-Maspoli, M., C. Schwierz, and H. C. Davies, 2007b: Atmospheric blocking: Space-time links to the NAO and PNA. *Clim. Dyn.*, **29**, 713–725.
- Cutforth, H. W., and D. Judiesch, 2007: Long-term changes to incoming solar energy on the Canadian Prairie. *Agr. Forest Meteor.*, **145**, 167–175.
- Dai, A., 2006: Recent climatology, variability, and trends in global surface humidity. *J. Clim.*, **19**, 3589–3606.
- Dai, A., 2011a: Characteristics and trends in various forms of the Palmer Drought Severity Index during 1900–2008. *J. Geophys. Res. Atmos.*, **116**, D12115.
- Dai, A., 2012: The influence of the inter-decadal Pacific oscillation on US precipitation during 1923–2010. *Clim. Dyn.*, **41**, 633–646.
- Dai, A., 2013: Increasing drought under global warming in observations and models. *Nature Clim. Change*, **3**, 52–58.
- Dai, A., T. Qian, K. E. Trenberth, and J. D. Milliman, 2009: Changes in continental freshwater diSchärge from 1948 to 2004. *J. Clim.*, **22**, 2773–2792.
- Dai, A. G., 2011b: Drought under global warming: A review. *Clim. Change*, **2**, 45–65.
- Dai, A. G., J. H. Wang, P. W. Thorne, D. E. Parker, L. Haimberger, and X. L. L. Wang, 2011: A new approach to homogenize daily radiosonde humidity data. *J. Clim.*, **24**, 965–991.
- Das, L., J. D. Annan, J. C. Hargreaves, and S. Emori, 2011: Centennial scale warming over Japan: Are the rural stations really rural? *Atmos. Sci. Lett.*, **12**, 362–367.
- Davidson, E., 2009: The contribution of manure and fertilizer nitrogen to atmospheric nitrous oxide since 1860. *Nature Geosci.*, **2**, 659–662.
- Davini, P., C. Cagnazzo, S. Gualdi, and A. Navarra, 2012: Bidimensional diagnostics, variability, and trends of Northern Hemisphere blocking. *J. Clim.*, **25**, 6496–6509.
- Davis, S. M., and K. H. Rosenlof, 2011: A multidagnostic intercomparison of tropical width time series using reanalyses and satellite observations. *J. Clim.*, **25**, 1061–1078.
- De Laat, A. T. J., and A. N. Maurellis, 2006: Evidence for influence of anthropogenic surface processes on lower tropospheric and surface temperature trends. *Int. J. Climatol.*, **26**, 897–913.
- de Meij, A., A. Pozzer, and J. Lelieveld, 2012: Trend analysis in aerosol optical depths and pollutant emission estimates between 2000 and 2009. *Atmos. Environ.*, **51**, 75–85.
- De Smedt, I., T. Stavrakou, J. F. Müller, R. J. van der A, and M. Van Roozendael, 2010: Trend detection in satellite observations of formaldehyde tropospheric columns. *Geophys. Res. Lett.*, **37**, L18808.
- Dee, D. P., E. Kallen, A. J. Simmons, and L. Haimberger, 2011a: Comments on "Reanalyses suitable for characterizing long-term trends". *Bull. Am. Meteor. Soc.*, **92**, 65–70.
- Dee, D. P., et al., 2011b: The ERA-Interim reanalysis: Configuration and performance of the data assimilation system. *Q. J. R. Meteor. Soc.*, **137**, 553–597.
- Deeds, D., et al., 2008: Evidence for crustal degassing of CF4 and SF6 in Mojave Desert groundwaters. *Geochim. Cosmochim. Acta*, **72**, 999–1013.
- DeGaetano, A. T., 2009: Time-dependent changes in extreme-precipitation return-period amounts in the continental United States. *J. Appl. Meteor. Climatol.*, **48**, 2086–2099.
- Delgado, J. M., H. Apel, and B. Merz, 2010: Flood trends and variability in the Mekong River. *Hydrol. Earth Syst. Sci.*, **14**, 407–418.
- Della-Marta, P. M., M. R. Haylock, J. Luterbacher, and H. Wanner, 2007a: Doubled length of western European summer heat waves since 1880. *J. Geophys. Res. Atmos.*, **112**, D15103.
- Della-Marta, P. M., J. Luterbacher, H. von Weissenfluh, E. Xoplaki, M. Brunet, and H. Wanner, 2007b: Summer heat waves over western Europe 1880–2003, their relationship to large-scale forcings and predictability. *Clim. Dyn.*, **29**, 251–275.
- Della-Marta, P. M., H. Mathis, C. Frei, M. A. Liniger, J. Kleinn, and C. Appenzeller, 2009: The return period of wind storms over Europe. *Int. J. Climatol.*, **29**, 437–459.
- Deser, C., A. S. Phillips, and M. A. Alexander, 2010a: Twentieth century tropical sea surface temperature trends revisited. *Geophys. Res. Lett.*, **37**, L10701.
- Deser, C., M. A. Alexander, S. P. Xie, and A. S. Phillips, 2010b: Sea surface temperature variability: Patterns and mechanisms. *Annu. Rev. Mar. Sci.*, **2**, 115–143.
- Dessler, A. E., and S. M. Davis, 2010: Trends in tropospheric humidity from reanalysis systems. *J. Geophys. Res. Atmos.*, **115**, D19127.
- Dessler, A. E., Z. Zhang, and P. Yang, 2008: Water-vapor climate feedback inferred from climate fluctuations, 2003–2008. *Geophys. Res. Lett.*, **35**, L20704.
- Diffenbaugh, N. S., J. S. Pal, F. Giorgi, and X. J. Gao, 2007: Heat stress intensification in the Mediterranean climate change hotspot. *Geophys. Res. Lett.*, **34**, L11706.
- Ding, T., W. H. Qian, and Z. W. Yan, 2010: Changes in hot days and heat waves in China during 1961–2007. *Int. J. Climatol.*, **30**, 1452–1462.
- Ding, Y. H., G. Y. Ren, Z. C. Zhao, Y. Xu, Y. Luo, Q. P. Li, and J. Zhang, 2007: Detection, causes and projection of climate change over China: An overview of recent progress. *Adv. Atmos. Sci.*, **24**, 954–971.
- Dlugokencky, E., E. Nisbet, R. Fisher, and D. Lowry, 2011: Global atmospheric methane: Budget, changes and dangers. *Philos. Trans. R. Soc. London Ser. A*, **369**, 2058–2072.
- Dlugokencky, E., et al., 2005: Conversion of NOAA atmospheric dry air CH4 mole fractions to a gravimetrically prepared standard scale. *J. Geophys. Res. Atmos.*, **110**, D18306.
- Dlugokencky, E., et al., 2009: Observational constraints on recent increases in the atmospheric CH4 burden. *Geophys. Res. Lett.*, **L18803**.
- Dlugokencky, E., J. K. A. Masaire, P. M. Lang, P. P. Steele, and E. G. Nisbet, 1994: A dramatic decrease in the growth rate of atmospheric methane in the Northern Hemisphere during 1992. *Geophys. Res. Lett.*, **21**, 45–48.
- Dole, R., et al., 2011: Was there a basis for anticipating the 2010 Russian heat wave? *Geophys. Res. Lett.*, **38**, L06702.
- Donat, M. G., and L. V. Alexander, 2012: The shifting probability distribution of global daytime and night-time temperatures. *Geophys. Res. Lett.*, **39**, L14707.
- Donat, M. G., D. Rennigli, S. Wild, L. V. Alexander, G. C. Leckebusch, and U. Ulbrich, 2011: Reanalysis suggests long-term upward trends in European storminess since 1871. *Geophys. Res. Lett.*, **38**, L14703.
- Donat, M. G., L. V. Alexander, H. Yang, I. Durre, R. Vose, and J. Caesar, 2013a: Global land-based datasets for monitoring climatic extremes. *Bull. Am. Meteor. Soc.*, **94**, 997–1006.
- Donat, M. G., et al., 2013b: Changes in extreme temperature and precipitation in the Arab region: Long-term trends and variability related to ENSO and NAO. *Int. J. Climatol.*, doi:10.1002/joc.3707.
- Donat, M. G., et al., 2013c: Updated analyses of temperature and precipitation extreme indices since the beginning of the twentieth century: The HadEX2 dataset. *J. Geophys. Res. Atmos.*, **118**, 2098–2118.
- Dong, L., T. J. Vogelsang, and S. J. Colucci, 2008: Interdecadal trend and ENSO-related interannual variability in Southern Hemisphere blocking. *J. Clim.*, **21**, 3068–3077.

- Dorigo, W., R. de Jeu, D. Chung, R. Parinussa, Y. Liu, W. Wagner, and D. Fernández-Prieto, 2012: Evaluating global trends (1988–2010) in harmonized multi-satellite surface soil moisture. *Geophys. Res. Lett.*, **39**, L18405.
- Doswell, C., H. Brooks, and N. Dotzek, 2009: On the implementation of the enhanced Fujita scale in the USA. *Atmos. Res.*, **93**, 554–563.
- Douglass, A., et al., 2008: Relationship of loss, mean age of air and the distribution of CFCs to stratospheric circulation and implications for atmospheric lifetimes. *J. Geophys. Res. Atmos.*, **113**, D14309.
- Douglass, A., et al., 2011: WMO/UNEP scientific assessment of ozone depletion: 2010. In: *Stratospheric Ozone and Surface Ultraviolet Radiation*. World Meteorological Organisation, Geneva, Switzerland.
- Du, Y., and S. Xie, 2008: Role of atmospheric adjustments in the tropical Indian Ocean warming during the 20th century in climate models. *Geophys. Res. Lett.*, **35**, L08712.
- Du, Y., S. Xie, G. Huang, and K. Hu, 2009: Role of air-sea interaction in the long persistence of El Niño-induced North Indian Ocean warming. *J. Clim.*, **22**, 2023–2038.
- Duan, A. M., and G. X. Wu, 2006: Change of cloud amount and the climate warming on the Tibetan Plateau. *Geophys. Res. Lett.*, **33**, L22704.
- Durre, I., C. N. Williams, X. G. Yin, and R. S. Vose, 2009: Radiosonde-based trends in precipitable water over the Northern Hemisphere: An update. *J. Geophys. Res. Atmos.*, **114**, D05112.
- Dutton, E. G., and B. A. Bodhaine, 2001: Solar irradiance anomalies caused by clear-sky transmission variations above Mauna Loa: 1958–99. *J. Clim.*, **14**, 3255–3262.
- Dutton, E. G., D. W. Nelson, R. S. Stone, D. Longenecker, G. Carbaugh, J. M. Harris, and J. Wendell, 2006: Decadal variations in surface solar irradiance as observed in a globally remote network. *J. Geophys. Res. Atmos.*, **111**, D19101.
- Earl, N., S. Dorling, R. Hewston, and R. von Glasow, 2013: 1980–2010 Variability in U.K. surface wind climate. *J. Climate*, **26**, 1172–1191.
- Easterling, D., and M. Wehner, 2009: Is the climate warming or cooling? *Geophys. Res. Lett.*, **36**, L08706.
- Eastman, R., and S. G. Warren, 2012: A 39-yr survey of cloud changes from land stations worldwide 1971–2009: Long-term trends, relation to aerosols, and expansion of the Tropical Belt. *J. Clim.*, **26**, 1286–1303.
- Eastman, R., S. G. Warren, and C. J. Hahn, 2011: Variations in cloud cover and cloud types over the ocean from surface observations, 1954–2008. *J. Clim.*, **24**, 5914–5934.
- Ebita, A., et al., 2011: The Japanese 55-year reanalysis "JRA-55": An interim report. *Sola*, **7**, 149–152.
- Eccel, E., P. Cau, K. Riemann-Campe, and F. Biasioli, 2012: Quantitative hail monitoring in an alpine area: 35-year climatology and links with atmospheric variables. *Int. J. Climatol.*, **32**, 503–517.
- Efthymiadis, D., C. M. Goodess, and P. D. Jones, 2011: Trends in Mediterranean gridded temperature extremes and large-scale circulation influences. *Nat. Hazards Earth Syst. Sci.*, **11**, 2199–2214.
- Efthymiadis, D. A., and P. D. Jones, 2010: Assessment of maximum possible urbanization influences on land temperature data by comparison of land and marine data around coasts. *Atmosphere*, **1**, 51–61.
- Elkins, J. W., and G. S. Dutton, 2011: Nitrous oxide and sulfur hexafluoride. *Bull. Am. Meteor. Soc.*, **92**, 2.
- Elsner, J. B., J. P. Kossin, and T. H. Jagger, 2008: The increasing intensity of the strongest tropical cyclones. *Nature*, **455**, 92–95.
- Emanuel, K., 2007: Environmental factors affecting tropical cyclone power dissipation. *J. Clim.*, **20**, 5497–5509.
- Embry, O., and C. J. Merchant, 2011: Reprocessing for climate of sea surface temperature from the along-track scanning radiometers: A new retrieval scheme. *Remote Sens. Environ.*, **116**, 47–61.
- Embry, O., C. J. Merchant, and G. K. Corlett, 2011: A reprocessing for climate of sea surface temperature from the along-track scanning radiometers: Preliminary validation, accounting for skin and diurnal variability. *Remote Sens. Environ.*, **116**, 62–78.
- Endo, N., and T. Yasunari, 2006: Changes in low cloudiness over China between 1971 and 1996. *J. Clim.*, **19**, 1204–1213.
- Enfield, D. B., A. M. Mestas-Nunez, and P. J. Trimble, 2001: The Atlantic multidecadal oscillation and its relation to rainfall and river flows in the continental US. *Geophys. Res. Lett.*, **28**, 2077–2080.
- Engel, A., et al., 2009: Age of stratospheric air unchanged within uncertainties over the past 30 years. *Nature Geosci.*, **2**, 28–31.
- Espinosa Villar, J. C., et al., 2009: Contrasting regional diSchärge evolutions in the Amazon basin (1974–2004). *J. Hydrol.*, **375**, 297–311.
- Etheridge, D., L. Steele, R. Francey, and R. Langenfelds, 1998: Atmospheric methane between 1000 AD and present: Evidence of anthropogenic emissions and climatic variability. *J. Geophys. Res. Atmos.*, **103**, 15979–15993.
- Etheridge, D. M., L. P. Steele, R. L. Langenfelds, R. J. Francey, J. M. Barnola, and V. I. Morgan, 1996: Natural and anthropogenic changes in atmospheric CO₂ over the last 1000 years from air in Antarctic ice and firn. *J. Geophys. Res. Atmos.*, **101**, 4115–4128.
- Evan, A. T., A. K. Heidinger, and D. J. Vimont, 2007: Arguments against a physical long-term trend in global ISCCP cloud amounts. *Geophys. Res. Lett.*, **34**, L04701.
- Fall, S., D. Niyogi, A. Gluhovsky, R. A. Pielke, E. Kalnay, and G. Rochon, 2010: Impacts of land use/land cover on temperature trends over the continental United States: Assessment using the North American regional reanalysis. *Int. J. Climatol.*, **30**, 1980–1993.
- Fall, S., A. Watts, J. Nielsen-Gammon, E. Jones, D. Niyogi, J. R. Christy, and R. A. Pielke, 2011: Analysis of the impacts of station exposure on the US Historical Climatology Network temperatures and temperature trends. *J. Geophys. Res. Atmos.*, **116**, D14120.
- Falvey, M., and R. D. Garreaud, 2009: Regional cooling in a warming world: Recent temperature trends in the southeast Pacific and along the west coast of subtropical South America (1979–2006). *J. Geophys. Res. Atmos.*, **114**, D04102.
- Favre, A., and A. Gershunov, 2006: Extra-tropical cyclonic/anticyclonic activity in north-eastern Pacific and air temperature extremes in western North America. *Clim. Dyn.*, **26**, 617–629.
- Feng, S., and Q. Hu, 2007: Changes in winter snowfall/precipitation ratio in the contiguous United States. *J. Geophys. Res. Atmos.*, **112**, D15109.
- Ferguson, C. R., and G. Villarini, 2012: Detecting inhomogeneities in the twentieth century reanalysis over the central United States. *J. Geophys. Res. Atmos.*, **117**, D05123.
- Ferranti, L., and P. Viterbo, 2006: The European summer of 2003: Sensitivity to soil water initial conditions. *J. Clim.*, **19**, 3659–3680.
- FERRETTI, D., et al., 2005: Unexpected changes to the global methane budget over the past 2000 years. *Science*, **309**, 1714–1717.
- Fischer, E. M., and C. Schär, 2010: Consistent geographical patterns of changes in high-impact European heatwaves. *Nature Geosci.*, **3**, 398–403.
- Fischer, E. M., S. I. Seneviratne, P. L. Vidale, D. Luthi, and C. Schär, 2007: Soil moisture–atmosphere interactions during the 2003 European summer heat wave. *J. Clim.*, **20**, 5081–5099.
- Fischer, T., M. Gemmer, L. Liu, and B. Su, 2011: Temperature and precipitation trends and dryness/wetness pattern in the Zhujiang River Basin, South China, 1961–2007. *Quatern. Int.*, **244**, 138–148.
- Fogt, R. L., J. Perlitz, A. J. Monaghan, D. H. Bromwich, J. M. Jones, and G. J. Marshall, 2009: Historical SAM variability. Part II: Twentieth-century variability and trends from reconstructions, observations, and the IPCC AR4 models. *J. Clim.*, **22**, 5346–5365.
- Folland, C. K., and D. E. Parker, 1995: Correction of instrumental biases in historical sea-surface temperature data. *Q. J. R. Meteor. Soc.*, **121**, 319–367.
- Folland, C. K., D. E. Parker, A. Colman, and W. R., 1999: Large scale modes of ocean surface temperature since the late nineteenth century. In: *Beyond El Niño: Decadal and Interdecadal Climate Variability* [A. Navarra (ed.)] Springer-Verlag, New York, pp. 73–102.
- Forster, P., et al., 2007: Changes in atmospheric constituents and in radiative forcing. In: *Climate Change 2007: The Physical Science Basis. Contribution of Working Group I to the Fourth Assessment Report of the Intergovernmental Panel on Climate Change* [Solomon, S., D. Qin, M. Manning, Z. Chen, M. Marquis, K. B. Averyt, M. Tignor and H. L. Miller (eds.)] Cambridge University Press, Cambridge, United Kingdom and New York, NY, USA, 129–234.
- Forster, P. M., et al., 2011: Stratospheric changes and climate. Scientific Assessment of Ozone Depletion: 2010. Global Ozone Research and Monitoring Project—Report No. 52. World Meteorological Organization, Geneva, Switzerland, 1–60.
- Fortems-Cheiney, A., F. Chevallier, I. Pison, P. Bousquet, S. Szopa, M. N. Deeter, and C. Clerbaux, 2011: Ten years of CO emissions as seen from Measurements of Pollution in the Troposphere (MOPITT). *J. Geophys. Res.*, **116**, D05304.
- Foster, G., and S. Rahmstorf, 2011: Global temperature evolution 1979–2010. *Environ. Res. Lett.*, **6**, 044022.
- Frauenfeld, O. W., and R. E. Davis, 2003: Northern Hemisphere circumpolar vortex trends and climate change implications. *J. Geophys. Res. Atmos.*, **108**, 4423.
- Frederiksen, J. S., and C. S. Frederiksen, 2007: Interdecadal changes in Southern Hemisphere winter storm track modes. *Tellus A*, **59**, 599–617.

- Free, M., and D. J. Seidel, 2007: Comments on "biases in stratospheric and tropospheric temperature trends derived from historical radiosonde data". *J. Clim.*, **20**, 3704–3709.
- Free, M., D. J. Seidel, J. K. Angell, J. Lanzante, I. Durre, and T. C. Peterson, 2005: Radiosonde Atmospheric Temperature Products for Assessing Climate (RATPAC): A new data set of large-area anomaly time series. *J. Geophys. Res. Atmos.*, **110**, D22101.
- Frich, P., L. V. Alexander, P. Della-Marta, B. Gleason, M. Haylock, A. Tank, and T. Peterson, 2002: Observed coherent changes in climatic extremes during the second half of the twentieth century. *Clim. Res.*, **19**, 193–212.
- Fu, G. B., S. P. Charles, and J. J. Yu, 2009: A critical overview of pan evaporation trends over the last 50 years. *Clim. Change*, **97**, 193–214.
- Fu, Q., and P. Lin, 2011: Poleward shift of subtropical jets inferred from satellite-observed lower stratospheric temperatures. *J. Clim.*, **24**, 5597–5603.
- Fu, Q., C. M. Johanson, S. G. Warren, and D. J. Seidel, 2004: Contribution of stratospheric cooling to satellite-inferred tropospheric temperature trends. *Nature*, **429**, 55–58.
- Fu, Q., C. M. Johanson, J. M. Wallace, and T. Reichler, 2006: Enhanced mid-latitude tropospheric warming in satellite measurements. *Science*, **312**, 1179–1179.
- Fueglistaler, S., and P. H. Haynes, 2005: Control of interannual and longer-term variability of stratospheric water vapor. *J. Geophys. Res. Atmos.*, **110**, D24108.
- Fujibe, F., 2009: Detection of urban warming in recent temperature trends in Japan. *Int. J. Climatol.*, **29**, 1811–1822.
- Fujiwara, M., et al., 2010: Seasonal to decadal variations of water vapor in the tropical lower stratosphere observed with balloon-borne cryogenic frost point hygrometers. *J. Geophys. Res. Atmos.*, **115**, D18304.
- Fyfe, J. C., 2003: Extratropical southern hemisphere cyclones: Harbingers of climate change? *J. Clim.*, **16**, 2802–2805.
- Gallant, A., K. Hennessy, and J. Risbey, 2007: Trends in rainfall indices for six Australian regions: 1910–2005. *Aust. Meteor. Mag.*, **56**, 223–239.
- Gallant, A. J. E., and D. J. Karoly, 2010: A Combined Climate Extremes Index for the Australian Region. *J. Clim.*, **23**, 6153–6165.
- Garcia-Herrera, R., J. Diaz, R. M. Trigo, J. Luterbacher, and E. M. Fischer, 2010: A review of the European summer heat wave of 2003. *Crit. Rev. Environ. Sci. Technol.*, **40**, 267–306.
- Gentemann, C., F. Wentz, C. Mears, and D. Smith, 2004: In situ validation of Tropical Rainfall Measuring Mission microwave sea surface temperatures. *J. Geophys. Res. Oceans*, **109**, C04021.
- Gettelman, A., and Q. Fu, 2008: Observed and simulated upper-tropospheric water vapor feedback. *J. Clim.*, **21**, 3282–3289.
- Gettelman, A., et al., 2010: Multimodel assessment of the upper troposphere and lower stratosphere: Tropics and global trends. *J. Geophys. Res. Atmos.*, **115**, D00M08.
- Gilgen, H., A. Roesch, M. Wild, and A. Ohmura, 2009: Decadal changes in shortwave irradiance at the surface in the period from 1960 to 2000 estimated from Global Energy Balance Archive Data. *J. Geophys. Res. Atmos.*, **114**, D00d08.
- Gillett, N. P., and P. A. Stott, 2009: Attribution of anthropogenic influence on seasonal sea level pressure. *Geophys. Res. Lett.*, **36**, L23709.
- Giorgi, F., and R. Francisco, 2000: Evaluating uncertainties in the prediction of regional climate change. *Geophys. Res. Lett.*, **27**, 1295–1298.
- Giorgi, F., E. S. Im, E. Coppola, N. S. Diffenbaugh, X. J. Gao, L. Mariotti, and Y. Shi, 2011: Higher hydroclimatic intensity with global warming. *J. Clim.*, **24**, 5309–5324.
- Giuntoli, I., B. Renard, J. P. Vidal, and A. Bard, 2013: Low flows in France and their relationship to large-scale climate indices. *J. Hydrol.*, **482**, 105–118.
- Gleason, K. L., J. H. Lawrimore, D. H. Levinson, T. R. Karl, and D. J. Karoly, 2008: A revised US Climate Extremes Index. *J. Clim.*, **21**, 2124–2137.
- Gong, D. Y., and C. H. Ho, 2002: The Siberian High and climate change over middle to high latitude Asia. *Theor. Appl. Climatol.*, **72**, 1–9.
- Gouretski, V., J. Kennedy, T. Boyer, and A. Kohl, 2012: Consistent near-surface ocean warming since 1900 in two largely independent observing networks. *Geophys. Res. Lett.*, **39**, L19606.
- Granier, C., et al., 2011: Evolution of anthropogenic and biomass burning emissions of air pollutants at global and regional scales during the 1980–2010 period. *Clim. Change*, **109**, 163–190.
- Grant, A. N., S. Brönnimann, and L. Haimberger, 2008: Recent Arctic warming vertical structure contested. *Nature*, **455**, E2–E3.
- Graversen, R. G., T. Mauritsen, M. Tjernstrom, E. Kallen, and G. Svensson, 2008: Vertical structure of recent Arctic warming. *Nature*, **451**, 53–U54.
- Greally, B., et al., 2007: Observations of 1,1-difluoroethane (HFC-152a) at AGAGE and SOGE monitoring stations in 1994–2004 and derived global and regional emission estimates. *J. Geophys. Res. Atmos.*, **112**, D06308.
- Griffiths, G. M., et al., 2005: Change in mean temperature as a predictor of extreme temperature change in the Asia-Pacific region. *Int. J. Climatol.*, **25**, 1301–1330.
- Grinsted, A., J. C. Moore, and S. Jevrejeva, 2012: Homogeneous record of Atlantic hurricane surge threat since 1923. *Proc. Natl. Acad. Sci. U.S.A.*, **109**, 19601–19605.
- Groisman, P., R. Knight, and T. Karl, 2012: Changes in intense precipitation over the central United States. *J. Hydrometeor.*, **13**, 47–66.
- Groisman, P., R. Knight, T. R. Karl, D. Easterling, B. M. Sun, and J. Lawrimore, 2004: Contemporary changes of the hydrological cycle over the contiguous United States: Trends derived from in situ observations. *J. Hydrometeor.*, **5**, 64–85.
- Groisman, P. Y., R. W. Knight, D. R. Easterling, T. R. Karl, G. C. Hegerl, and V. A. N. Razuvayev, 2005: Trends in intense precipitation in the climate record. *J. Clim.*, **18**, 1326–1350.
- Gruber, C., and L. Haimberger, 2008: On the homogeneity of radiosonde wind time series. *Meteorol. Z.*, **17**, 631–643.
- Gulev, S. K., O. Zolina, and S. Grigoriev, 2001: Extratropical cyclone variability in the Northern Hemisphere winter from the NCEP/NCAR reanalysis data. *Clim. Dyn.*, **17**, 795–809.
- Guo, H., M. Xu, and Q. Hub, 2010: Changes in near-surface wind speed in China: 1969–2005. *Int. J. Climatol.*, **31**, 349–358.
- Haerter, J., P. Berg, and S. Hagemann, 2010: Heavy rain intensity distributions on varying time scales and at different temperatures. *J. Geophys. Res. Atmos.*, **115**, D17102.
- Haimberger, L., 2007: Homogenization of radiosonde temperature time series using innovation statistics. *J. Clim.*, **20**, 1377–1403.
- Haimberger, L., C. Tavolato, and S. Sperka, 2008: Toward elimination of the warm bias in historic radiosonde temperature records—Some new results from a comprehensive intercomparison of upper-air data. *J. Clim.*, **21**, 4587–4606.
- Haimberger, L., C. Tavolato, and S. Sperka, 2012: Homogenization of the global radiosonde temperature dataset through combined comparison with reanalysis background series and neighboring stations. *J. Clim.*, **25**, 8108–8131.
- Hand, J. L., et al., 2011: IMPROVE, spatial and seasonal patterns and temporal variability of haze and its constituents in the United States. Cooperative Institute for Research in the Atmosphere and Colorado University.
- Hanna, E., J. Cappelen, R. Allan, T. Jonsson, F. Le Blancq, T. Lillington, and K. Hickey, 2008: New insights into North European and North Atlantic surface pressure variability, storminess, and related climatic change since 1830. *J. Clim.*, **21**, 6739–6766.
- Hannaford, J., and T. Marsh, 2008: High-flow and flood trends in a network of undisturbed catchments in the UK. *Int. J. Climatol.*, **28**, 1325–1338.
- Hansen, J., M. Sato, and R. Ruedy, 2012: Perception of climate change. *Proc. Natl. Acad. Sci. U.S.A.*, **109**, E2415–E2423.
- Hansen, J., R. Ruedy, M. Sato, and K. Lo, 2010: Global surface temperature change. *Rev. Geophys.*, **48**, RG4004.
- Hansen, J., M. Sato, P. Kharecha, and K. von Schuckmann, 2011: Earth's energy imbalance and implications. *Atmos. Chem. Phys.*, **11**, 13421–13449.
- Harries, J. E., and C. Belotti, 2010: On the variability of the global net radiative energy balance of the nonequilibrium Earth. *J. Clim.*, **23**, 1277–1290.
- Hatzianastassiou, N., C. Matsoukas, A. Fotiadis, K. G. Pavlakis, E. Drakakis, D. Hatzidimitriou, and I. Vardavas, 2005: Global distribution of Earth's surface shortwave radiation budget. *Atmos. Chem. Phys.*, **5**, 2847–2867.
- Hatzianastassiou, N., C. D. Papadimas, C. Matsoukas, K. Pavlakis, A. Fotiadis, M. Wild, and I. Vardavas, 2012: Recent regional surface solar radiation dimming and brightening patterns: inter-hemispherical asymmetry and a dimming in the Southern Hemisphere. *Atmos. Sci. Lett.*, **13**, 43–48.
- Hausfather, Z., M. J. Menne, C. N. Williams, T. Masters, R. Broberg, and D. Jones, 2013: Quantifying the effect of urbanization on U.S. Historical Climatology Network temperature records. *J. Geophys. Res. Atmos.*, **118**, 481–494.
- Haylock, M. R., et al., 2006: Trends in total and extreme South American rainfall in 1960–2000 and links with sea surface temperature. *J. Clim.*, **19**, 1490–1512.
- He, W. Y., S. P. Ho, H. B. Chen, X. J. Zhou, D. Hunt, and Y. H. Kuo, 2009: Assessment of radiosonde temperature measurements in the upper troposphere and lower stratosphere using COSMIC radio occultation data. *Geophys. Res. Lett.*, **36**, L17807.
- Heidinger, A. K., and M. J. Pavolonis, 2009: Gazing at cirrus clouds for 25 years through a split window. Part I: Methodology. *J. Appl. Meteor. Climatol.*, **48**, 1100–1116.

- Held, I. M., and B. J. Soden, 2006: Robust responses of the hydrological cycle to global warming. *J. Clim.*, **19**, 5686–5699.
- Helmig, D., et al., 2007: A review of surface ozone in the polar regions. *Atmos. Environ.*, **41**, 5138–5161.
- Hidy, G. M., and G. T. Pennell, 2010: Multipollutant air quality management: 2010 critical review. *J. Air Waste Manage. Assoc.*, **60**, 645–674.
- Hilboll, A., A. Richter, and J. P. Burrows, 2013: Long-term changes of tropospheric NO₂ over megacities derived from multiple satellite instruments. *Atmos. Chem. Phys.*, **13**, 4145–4169.
- Hinkelmann, L. M., P. W. Stackhouse, B. A. Wielicki, T. P. Zhang, and S. R. Wilson, 2009: Surface insolation trends from satellite and ground measurements: Comparisons and challenges. *J. Geophys. Res. Atmos.*, **114**, D00d20.
- Hirdman, D., et al., 2010: Long-term trends of black carbon and sulphate aerosol in the Arctic: Changes in atmospheric transport and source region emissions. *Atmos. Chem. Phys.*, **10**, 9351–9368.
- Hirsch, M. E., A. T. DeGaetano, and S. J. Colucci, 2001: An East Coast winter storm climatology. *J. Clim.*, **14**, 882–899.
- Hirschi, M., et al., 2011: Observational evidence for soil-moisture impact on hot extremes in southeastern Europe. *Nature Geosci.*, **4**, 17–21.
- Ho, S. P., W. He, and Y. H. Kuo, 2009a: Construction of consistent temperature records in the lower stratosphere using Global Positioning System Radio Occultation Data and Microwave Sounding measurements. *New Horizons in Occultation Research*, Springer-Verlag Berlin, 207–217.
- Ho, S. P., Y. H. Kuo, Z. Zeng, and T. C. Peterson, 2007: A comparison of lower stratosphere temperature from microwave measurements with CHAMP GPS RO data. *Geophys. Res. Lett.*, **34**, L15701.
- Ho, S. P., M. Goldberg, Y. H. Kuo, C. Z. Zou, and W. Schreiner, 2009b: Calibration of temperature in the lower stratosphere from microwave measurements using COSMIC radio occultation data: Preliminary results. *Terr. Atmos. Ocean. Sci.*, **20**, 87–100.
- Ho, S. P., et al., 2012: Reproducibility of GPS radio occultation data for climate monitoring: Profile-to-profile inter-comparison of CHAMP climate records 2002 to 2008 from six data centers. *J. Geophys. Res. Atmos.*, **117**, D18111.
- Hoerling, M., et al., 2012: Anatomy of an extreme event. *J. Clim.*, **26**, 2811–2832.
- Holben, B. N., et al., 1998: AERONET—A federated instrument network and data archive for aerosol characterization. *Remote Sens. Environ.*, **66**, 1–16.
- Holland, G. J., and P. J. Webster, 2007: Heightened tropical cyclone activity in the North Atlantic: Natural variability or climate trend? *Philos. Trans. R. Soc. London Ser. A*, **365**, 2695–2716.
- Hope, P. K., W. Drosdowsky, and N. Nicholls, 2006: Shifts in the synoptic systems influencing southwest Western Australia. *Clim. Dyn.*, **26**, 751–764.
- Hsu, N. C., et al., 2012: Global and regional trends of aerosol optical depth over land and ocean using SeaWiFS measurements from 1997 to 2010. *Atmos. Chem. Phys. Discuss.*, **12**, 8465–8501.
- Hsu, P. C., T. Li, and B. Wang, 2011: Trends in global monsoon area and precipitation over the past 30 years. *Geophys. Res. Lett.*, **38**, L08701.
- Hu, Y., and Q. Fu, 2007: Observed poleward expansion of the Hadley circulation since 1979. *Atmos. Chem. Phys.*, **7**, 5229–5236.
- Hu, Y. C., W. J. Dong, and Y. He, 2010: Impact of land surface forcings on mean and extreme temperature in eastern China. *J. Geophys. Res. Atmos.*, **115**, 11.
- Hu, Y. Y., C. Zhou, and J. P. Liu, 2011: Observational evidence for the poleward expansion of the Hadley circulation. *Adv. Atmos. Sci.*, **28**, 33–44.
- Huang, J., et al., 2008: Estimation of regional emissions of nitrous oxide from 1997 to 2005 using multinetwerk measurements, a chemical transport model, and an inverse method. *J. Geophys. Res. Atmos.*, **113**, D17313.
- Huang, W.-R., S.-Y. Wang, and J. C. L. Chan, 2010: Discrepancies between global reanalyses and observations in the interdecadal variations of Southeast Asian cold surge. *Int. J. Climatol.*, **31**, 2272–2280..
- Hudson, R. D., 2012: Measurements of the movement of the jet streams at mid-latitudes, in the Northern and Southern Hemispheres, 1979 to 2010. *Atmos. Chem. Phys.*, **12**, 7797–7808.
- Hudson, R. D., M. F. Andrade, M. B. Follette, and A. D. Frolov, 2006: The total ozone field separated into meteorological regimes—Part II: Northern Hemisphere mid-latitude total ozone trends. *Atmos. Chem. Phys.*, **6**, 5183–5191.
- Hundecka, Y., A. St-Hilaire, T. Ouarda, S. El Adlouni, and P. Gachon, 2008: A nonstationary extreme value analysis for the assessment of changes in extreme annual wind speed over the Gulf of St. Lawrence, Canada. *J. Appl. Meteor. Climatol.*, **47**, 2745–2759.
- Hurrell, J. W., 1995: Decadal trends in the North Atlantic Oscillation: Regional temperatures and precipitation. *Science*, **269**, 676–679.
- Hurst, D., 2011: Stratospheric water vapor trends over Boulder, Colorado: Analysis of the 30 year Boulder record. *J. Geophys. Res.*, **116**, D02306.
- Idso, S. B., and A. J. Brazel, 1984: Rising atmospheric carbon-dioxide concentrations may increase streamflow. *Nature*, **312**, 51–53.
- IPCC, 2007: *Clim. Change 2007: The Physical Science Basis. Contribution of Working Group I to the Fourth Assessment Report of the Intergovernmental Panel on Climate Change (IPCC)* [Solomon, S., D. Qin, M. Manning, Z. Chen, M. Marquis, K. B. Averyt, M. Tignor and H. L. Miller (eds.)]. Cambridge University Press, Cambridge, United Kingdom and New York, NY, USA, 996 pp.
- Ishii, M., A. Shouji, S. Sugimoto, and T. Matsumoto, 2005: Objective analyses of sea-surface temperature and marine meteorological variables for the 20th century using ICOADS and the Kobe collection. *Int. J. Climatol.*, **25**, 865–879.
- Ishijima, K., et al., 2007: Temporal variations of the atmospheric nitrous oxide concentration and its delta N-15 and delta O-18 for the latter half of the 20th century reconstructed from firn air analyses. *J. Geophys. Res. Atmos.*, **112**, D03305 .
- Jain, S. K., and V. Kumar, 2012: Trend analysis of rainfall and temperature data for India. *Curr. Sci.*, **102**, 37–49.
- Jakob, D., D. Karoly, and A. Seed, 2011: Non-stationarity in daily and sub-daily intense rainfall—Part 2: Regional assessment for sites in south-east Australia. *Nat. Hazards Earth Syst. Sci.*, **11**, 2273–2284.
- Jhajharia, D., S. Srivastava, D. Sarkar, and S. Sarkar, 2009: Temporal characteristics of pan evaporation trends under humid conditions of northeast India. *Agr. Forest Meteorol.*, **336**, 61–73.
- Jiang, T., Z. W. Kundzewicz, and B. Su, 2008: Changes in monthly precipitation and flood hazard in the Yangtze River Basin, China. *Int. J. Climatol.*, **28**, 1471–1481.
- Jiang, X., W. Ku, R. Shia, Q. Li, J. Elkins, R. Prinn, and Y. Yung, 2007: Seasonal cycle of N₂O: Analysis of data. *Global Biogeochem. Cycles*, **21**, GB1006.
- Jiang, Y., Y. Luo, Z. C. Zhao, and S. W. Tao, 2010: Changes in wind speed over China during 1956–2004. *Theor. Appl. Climatol.*, **99**, 421–430.
- Jin, S. G., J. U. Park, J. H. Cho, and P. H. Park, 2007: Seasonal variability of GPS-derived zenith tropospheric delay (1994–2006) and climate implications. *J. Geophys. Res. Atmos.*, **112**, D09110.
- John, V. O., R. P. Allan, and B. J. Soden, 2009: How robust are observed and simulated precipitation responses to tropical ocean warming? *Geophys. Res. Lett.*, **36**, L14702.
- John, V. O., G. Holl, R. P. Allan, S. A. Buehler, D. E. Parker, and B. J. Soden, 2011: Clear-sky biases in satellite infrared estimates of upper tropospheric humidity and its trends. *J. Geophys. Res. Atmos.*, **116**, D14108.
- Jones, D. A., W. Wang, and R. Fawcett, 2009: High-quality spatial climate data-sets for Australia. *Australian Meteor. Ocean. J.*, **58**, 233–248.
- Jones, P. D., and D. H. Lister, 2007: Intercomparison of four different Southern Hemisphere sea level pressure datasets. *Geophys. Res. Lett.*, **34**, L10704.
- Jones, P. D., and D. H. Lister, 2009: The urban heat island in Central London and urban-related warming trends in Central London since 1900. *Weather*, **64**, 323–327.
- Jones, P. D., T. Jonsson, and D. Wheeler, 1997: Extension to the North Atlantic Oscillation using early instrumental pressure observations from Gibraltar and southwest Iceland. *Int. J. Climatol.*, **17**, 1433–1450.
- Jones, P. D., D. H. Lister, and Q. Li, 2008: Urbanization effects in large-scale temperature records, with an emphasis on China. *J. Geophys. Res. Atmos.*, **113**, D16122.
- Jones, P. D., D. H. Lister, T. J. Osborn, C. Harpham, M. Salmon, and C. P. Morice, 2012: Hemispheric and large-scale land-surface air temperature variations: An extensive revision and an update to 2010. *J. Geophys. Res. Atmos.*, **117**, D05127.
- Jones, R., S. Westra, and A. Sharma, 2010: Observed relationships between extreme sub-daily precipitation, surface temperature, and relative humidity. *Geophys. Res. Lett.*, **37**, L22805.
- Joshi, M. M., J. M. Gregory, M. J. Webb, D. M. H. Sexton, and T. C. Johns, 2008: Mechanisms for the land/sea warming contrast exhibited by simulations of climate change. *Clim. Dyn.*, **30**, 455–465.
- Jovanovic, B., D. Collins, K. Braganza, D. Jakob, and D. A. Jones, 2011: A high-quality monthly total cloud amount dataset for Australia. *Clim. Change*, **108**, 485–517.
- Jung, M., et al., 2010: Recent decline in the global land evapotranspiration trend due to limited moisture supply. *Nature*, **467**, 951–954.
- Kahn, R. A., et al., 2007: Satellite-derived aerosol optical depth over dark water from MISR and MODIS: Comparisons with AERONET and implications for climatological studies. *J. Geophys. Res. Atmos.*, **112**, D18205.

- Kanamitsu, M., W. Ebisuzaki, J. Woollen, S. K. Yang, J. J. Hnilo, M. Fiorino, and G. L. Potter, 2002: NCEP-DOE AMIP-II reanalysis (R-2). *Bull. Am. Meteor. Soc.*, **83**, 1631–1643.
- Kang, S. M., L. M. Polvani, J. C. Fyfe, and M. Sigmond, 2011: Impact of polar ozone depletion on subtropical Precipitation. *Science*, **332**, 951–954.
- Kao, H. Y., and J. Y. Yu, 2009: Contrasting Eastern-Pacific and Central-Pacific types of ENSO. *J. Clim.*, **22**, 615–632.
- Karnauskas, K. B., R. Seager, A. Kaplan, Y. Kushnir, and M. A. Cane, 2009: Observed strengthening of the zonal sea surface temperature gradient across the equatorial Pacific Ocean. *J. Clim.*, **22**, 4316–4321.
- Karnieli, A., et al., 2009: Temporal trend in anthropogenic sulfur aerosol transport from central and eastern Europe to Israel. *J. Geophys. Res. Atmos.*, **114**, D00d19.
- Karoly, D., 1989: Southern-Hemisphere circulation features associated with El Niño-Southern Oscillation. *J. Clim.*, **2**, 1239–1252.
- Kato, S., et al.: Surface irradiances consistent with CERES-derived top-of-atmosphere shortwave and longwave irradiances. *J. Clim.*, **26**, 2719–2740
- Keeling, C., R. Bacastow, A. Bainbridge, C. Ekdahl, P. Guenther, L. Waterman, and J. Chin, 1976a: Atmospheric Carbon-Dioxide Variations at Mauna-Loa Observatory, Hawaii. *Tellus*, **28**, 538–551.
- Keeling, C. D., J. A. Adams, and C. A. Ekdahl, 1976b: Atmospheric carbo-dioxide variations at South Pole. *Tellus*, **28**, 553–564.
- Keller, C., D. Brunner, S. Henne, M. Vollmer, S. O'Doherty, and S. Reimann, 2011: Evidence for under-reported western European emissions of the potent greenhouse gas HFC-23. *Geophys. Res. Lett.*, **38**, L15808.
- Kennedy, J. J., N. A. Rayner, and R. O. Smith, 2012: Using AATSR data to assess the quality of in situ sea surface temperature observations for climate studies. *Remote Sens. Environ.*, **116**, 79–92.
- Kennedy, J. J., N. A. Rayner, R. O. Smith, D. E. Parker, and M. Saunby, 2011a: Reassessing biases and other uncertainties in sea surface temperature observations measured in situ since 1850: 2. Biases and homogenization. *J. Geophys. Res. Atmos.*, **116**, D14104.
- Kennedy, J. J., N. A. Rayner, R. O. Smith, M. Saunby, and D. E. Parker, 2011b: Reassessing biases and other uncertainties in sea surface temperature observations since 1850, part 1: Measurement and sampling uncertainties. *J. Geophys. Res.*, **116**, D14103.
- Kent, E. C., and D. I. Berry, 2008: Assessment of the Marine Observing System (ASMOS): Final report. *National Oceanography Centre Southampton Research and Consultancy Report*, 55 pp.
- Kent, E. C., S. D. Woodruff, and D. I. Berry, 2007: Metadata from WMO publication no. 47 and an assessment of voluntary observing ship observation heights in ICOADS. *J. Atmos. Ocean Technol.*, **24**, 214–234.
- Kent, E. C., S. Fangohr, and D. I. Berry, 2012: A comparative assessment of monthly mean wind speed products over the global ocean. *Int. J. Climatol.*, **33**, 2530–2541.
- Kent, E. C., J. J. Kennedy, D. I. Berry, and R. O. Smith, 2010: Effects of instrumentation changes on sea surface temperature measured in situ. *Clim. Change*, **1**, 718–728.
- Kent, E. C., N. A. Rayner, D. I. Berry, M. Saunby, B. I. Moat, J. J. Kennedy, and D. E. Parker, 2013: Global analysis of night marine air temperature and its uncertainty since 1880, the HadINMAT2 Dataset. *J. Geophys. Res.*, **118**, 1281–1298.
- Kenyon, J., and G. C. Hegerl, 2008: Influence of modes of climate variability on global temperature extremes. *J. Clim.*, **21**, 3872–3889.
- Kenyon, J., and G. C. Hegerl, 2010: Influence of modes of climate variability on global precipitation extremes. *J. Clim.*, **23**, 6248–6262.
- Kharin, V., F. Zwiers, X. Zhang, and M. Wehner, 2013: Changes in temperature and precipitation extremes in the CMIP5 ensemble. *Climatic Change*, **119**, 345–357.
- Kiehl, J. T., and K. E. Trenberth, 1997: Earth's annual global mean energy budget. *Bull. Am. Meteor. Soc.*, **78**, 197–208.
- Kim, D., and V. Ramanathan, 2012: Improved estimates and understanding of global albedo and atmospheric solar absorption. *Geophys. Res. Lett.*, **39**, L24704.
- Kim, D. Y., and V. Ramanathan, 2008: Solar radiation budget and radiative forcing due to aerosols and clouds. *J. Geophys. Res. Atmos.*, **113**, D02203.
- Kim, J., et al., 2010: Regional atmospheric emissions determined from measurements at Jeju Island, Korea: Halogenated compounds from China. *Geophys. Res. Lett.*, **37**, L12801.
- King, A., L. Alexander, and M. Donat, 2013: The efficacy of using gridded data to examine extreme rainfall characteristics: A case study for Australia. *Int. J. Climatol.*, **33**, 2376–2387.
- Kistler, R., et al., 2001: The NCEP-NCAR 50-year reanalysis: Monthly means CD-ROM and documentation. *Bull. Am. Meteor. Soc.*, **82**, 247–267.
- Klein Tank, A. M. G., et al., 2006: Changes in daily temperature and precipitation extremes in central and south Asia. *J. Geophys. Res. Atmos.*, **111**, D16105.
- Klok, E. J., and A. Tank, 2009: Updated and extended European dataset of daily climate observations. *Int. J. Climatol.*, **29**, 1182–1191.
- Knapp, K. R., and M. C. Kruk, 2010: Quantifying interagency differences in tropical cyclone best-track wind speed estimates. *Mon. Weather Rev.*, **138**, 1459–1473.
- Knowles, N., M. D. Dettinger, and D. R. Cayan, 2006: Trends in snowfall versus rainfall in the western United States. *J. Clim.*, **19**, 4545–4559.
- Knutson, T. R., et al., 2010: Tropical cyclones and climate change. *Nature Geosci.*, **3**, 157–163.
- Kobayashi, S., M. Matricardi, D. Dee, and S. Uppala, 2009: Toward a consistent reanalysis of the upper stratosphere based on radiance measurements from SSU and AMSU-A. *Q. J. R. Meteorol. Soc.*, **135**, 2086–2099.
- Kopp, G., and G. Lawrence, 2005: The Total Irradiance Monitor (TIM): Instrument design. *Solar Phys.*, **230**, 91–109.
- Kopp, G., and J. L. Lean, 2011: A new, lower value of total solar irradiance: Evidence and climate significance. *Geophys. Res. Lett.*, **38**, L01706.
- Kopp, G., G. Lawrence, and G. Rottman, 2005: The Total Irradiance Monitor (TIM): Science results. *Solar Phys.*, **230**, 129–139.
- Kossin, J. P., K. R. Knapp, D. J. Vimont, R. J. Murnane, and B. A. Harper, 2007: A globally consistent reanalysis of hurricane variability and trends. *Geophys. Res. Lett.*, **34**, L04815.
- Koutsoyiannis, D., and A. Montanari, 2007: Statistical analysis of hydroclimatic time series: Uncertainty and insights. *Water Resour. Res.*, **43**, W05429.
- Kreienkamp, F., A. Spekat, and W. Enke, 2010: Stationarity of atmospheric waves and blocking over Europe-based on a reanalysis dataset and two climate scenarios. *Theor. Appl. Climatol.*, **102**, 205–212.
- Krishna Moorthy, K., S. Suresh Babu, and S. K. Satheesh, 2007: Temporal heterogeneity in aerosol characteristics and the resulting radiative impact at a tropical coastal station—Part 1: Microphysical and optical properties. *Ann. Geophys.*, **25**, 2293–2308.
- Krishna Moorthy, K., S. Suresh Babu, M. R. Manoj, and S. K. Satheesh, 2013: Buildup of Aerosols over the Indian Region. *Geophys. Res. Lett.*, **40**, 1011–1014.
- Krishna Moorthy, K., S. S. Babu, S. K. Satheesh, S. Lal, M. M. Sarin, and S. Ramachandran, 2009: Climate implications of atmospheric aerosols and trace gases: Indian Scenario, Climate Sense. World Meteorological Organisation, Geneva, Switzerland, pp. 157–160.
- Krueger, O., F. Schenk, F. Feser, and R. Weisse, 2013: Inconsistencies between long-term trends in storminess derived from the 20CR reanalysis and observations. *J. Clim.*, **26**, 868–874.
- Kruger, A., and S. Sekele, 2013: Trends in extreme temperature indices in South Africa: 1962–2009. *Int. J. Climatol.*, **33**, 661–676.
- Kubota, H., and J. C. L. Chan, 2009: Interdecadal variability of tropical cyclone landfall in the Philippines from 1902 to 2005. *Geophys. Res. Lett.*, **36**, L12802.
- Kudo, R., A. Uchiyama, A. Yamazaki, T. Sakami, and O. Iijima, 2011: Decadal changes in aerosol optical thickness and single scattering albedo estimated from ground-based broadband radiometers: A case study in Japan. *J. Geophys. Res.*, **116**, D03207.
- Kudo, R., A. Uchiyama, O. Iijima, N. Ohkawara, and S. Ohta, 2012: Aerosol impact on the brightening in Japan. *J. Geophys. Res. Atmos.*, **117**, 11.
- Kueppers, L. M., M. A. Snyder, and L. C. Sloan, 2007: Irrigation cooling effect: Regional climate forcing by land-use change. *Geophys. Res. Lett.*, **34**, L03703.
- Kuglitsch, F. G., A. Toreti, E. Xoplaki, P. M. Della-Marta, J. Luterbacher, and H. Wanner, 2009: Homogenization of daily maximum temperature series in the Mediterranean. *J. Geophys. Res. Atmos.*, **114**, D15108.
- Kuglitsch, F. G., A. Toreti, E. Xoplaki, P. M. Della-Marta, C. S. Zerefos, M. Turkes, and J. Luterbacher, 2010: Heat wave changes in the eastern Mediterranean since 1960. *Geophys. Res. Lett.*, **37**, L04802.
- Kumari, B. P., and B. N. Goswami, 2010: Seminal role of clouds on solar dimming over the Indian monsoon region. *Geophys. Res. Lett.*, **37**, L06703.
- Kumari, B. P., A. L. Londhe, S. Daniel, and D. B. Jadhav, 2007: Observational evidence of solar dimming: Offsetting surface warming over India. *Geophys. Res. Lett.*, **34**, L21810.

- Kundzewicz, Z. W., et al., 2007: Freshwater resources and their management. *Climate Change 2007: Impacts, Adaptation and Vulnerability. Contribution of Working Group II to the Fourth Assessment Report of the Intergovernmental Panel on Climate Change* [Solomon, S., D. Qin, M. Manning, Z. Chen, M. Marquis, K. B. Averyt, M. Tignor and H. L. Miller (eds.)]. Cambridge University Press, Cambridge, United Kingdom and New York, NY, USA, 172–210.
- Kunkel, K. E., M. A. Palecki, L. Ensor, D. Easterling, K. G. Hubbard, D. Robinson, and K. Redmond, 2009: Trends in twentieth-century US extreme snowfall seasons. *J. Clim.*, **22**, 6204–6216.
- Kunkel, K. E., et al., 2008: Observed changes in weather and climate extremes. In: *Weather and Climate Extremes in a Changing Climate. Regions of Focus: North America, Hawaii, Caribbean, and U.S. Pacific Islands* [T. R. Karl, G. A. Meehl, D. M. Christopher, S. J. Hassol, A. M. Waple, and W. L. Murray (eds.)]. A Report by the U.S. Climate Change Science Program and the Subcommittee on Global Change Research.
- Kunz, M., J. Sander, and C. Kottmeier, 2009: Recent trends of thunderstorm and hail-storm frequency and their relation to atmospheric characteristics in southwest Germany. *Int. J. Climatol.*, **29**, 2283–2297.
- Kuo, Y. H., W. S. Schreiner, J. Wang, D. L. Rossiter, and Y. Zhang, 2005: Comparison of GPS radio occultation soundings with radiosondes. *Geophys. Res. Lett.*, **32**, L05817.
- Kvalevag, M. M., and G. Myhre, 2007: Human impact on direct and diffuse solar radiation during the industrial era. *J. Clim.*, **20**, 4874–4883.
- L'Ecuyer, T. S., N. B. Wood, T. Haladay, G. L. Stephens, and P. W. Stackhouse, 2008: Impact of clouds on atmospheric heating based on the R04 CloudSat fluxes and heating rates data set. *J. Geophys. Res. Atmos.*, **113**, 15.
- Labat, D., Y. Godderis, J. L. Probst, and J. L. Guyot, 2004: Evidence for global runoff increase related to climate warming. *Adv. Water Resour.*, **27**, 631–642.
- Ladstädter, F., A. K. Steiner, U. Foelsche, L. Haimberger, C. Tavolato, and G. Kirchnebngast, 2011: An assessment of differences in lower stratospheric temperature records from (A)MSU, radiosondes and GPS radio occultation. *Atmos. Meas. Tech.*, **4**, 1965–1977.
- Landsea, C. W., 2007: Counting Atlantic tropical cyclones back to 1900. *EOS Trans. (AGU)*, **88**, 197–202.
- Landsea, C. W., B. A. Harper, K. Hoarau, and J. A. Knaff, 2006: Can we detect trends in extreme tropical cyclones? *Science*, **313**, 452–454.
- Landsea, C. W., et al., 2011: A reanalysis of the 1921–30 Atlantic Hurricane Database. *J. Clim.*, **25**, 865–885.
- Langematz, U., and M. Kunze, 2008: Dynamical changes in the Arctic and Antarctic stratosphere during spring. In: *Climate Variability and Extremes during the Past 100 Years. Advances in Global Change Research* [S. Brönnimann, J. Luterbacher, T. Ewen, H. F. Diaz, R. S. Stolarski, and U. Neu (eds.)], Springer, pp. 293–301.
- Lanzante, J. R., 2009: Comment on "Trends in the temperature and water vapor content of the tropical lower stratosphere: Sea surface connection" by Karen H. Rosenlof and George C. Reid. *J. Geophys. Res. Atmos.*, **114**, D12104.
- Laprise, R., 1992: The resolution of global spectral models. *Bull. Am. Meteor. Soc.*, **73**, 1453–1454.
- Larkin, N. K., and D. E. Harrison, 2005: On the definition of El Niño and associated seasonal average US weather anomalies. *Geophys. Res. Lett.*, **32**, L13705.
- Lawrimore, J. H., M. J. Menne, B. E. Gleason, C. N. Williams, D. B. Wuertz, R. S. Vose, and J. Rennie, 2011: An overview of the Global Historical Climatology Network monthly mean temperature data set, version 3. *J. Geophys. Res. Atmos.*, **116**, D19121.
- Leakey, A. D. B., M. Uribe Larrea, E. A. Ainsworth, S. L. Naidu, A. Rogers, D. R. Ort, and S. P. Long, 2006: Photosynthesis, productivity, and yield of maize are not affected by open-air elevation of CO₂ concentration in the absence of drought. *Plant Physiol.*, **140**, 779–790.
- Lee, H. T., A. Gruber, R. G. Ellingson, and I. Laszlo, 2007: Development of the HIRS outgoing longwave radiation climate dataset. *J. Atmos. Ocean Technol.*, **24**, 2029–2047.
- Lefohn, A. S., D. Shadwick, and S. J. Oltmans, 2010: Characterizing changes in surface ozone levels in metropolitan and rural areas in the United States for 1980–2008 and 1994–2008. *Atmos. Environ.*, **44**, 5199–5210.
- Lehmann, A., K. Getzlaff, and J. Harlass, 2011: Detailed assessment of climate variability in the Baltic Sea area for the period 1958 to 2009. *Clim. Res.*, **46**, 185–196.
- Lelieveld, J., J. van Aardenne, H. Fischer, M. de Reus, J. Williams, and P. Winkler, 2004: Increasing ozone over the Atlantic Ocean. *Science*, **304**, 1483–1487.
- Lenderink, G., and E. Van Meijgaard, 2008: Increase in hourly precipitation extremes beyond expectations from temperature changes. *Nature Geosci.*, **1**, 511–514.
- Lenderink, G., H. Y. Mok, T. C. Lee, and G. J. van Oldenborgh, 2011: Scaling and trends of hourly precipitation extremes in two different climate zones – Hong Kong and the Netherlands. *Hydrol. Earth Syst. Sci. Discuss.*, **8**, 4701–4719.
- Lennartz, S., and A. Bunde, 2009: Trend evaluation in records with long-term memory: Application to global warming. *Geophys. Res. Lett.*, **36**, L16706.
- Levin, I., et al., 2010: The global SF6 source inferred from long-term high precision atmospheric measurements and its comparison with emission inventories. *Atmos. Chem. Phys.*, **10**, 2655–2662.
- Levitus, S., J. I. Antonov, T. P. Boyer, R. A. Locarnini, H. E. Garcia, and A. V. Mishonov, 2009: Global ocean heat content 1955–2008 in light of recently revealed instrumentation problems. *Geophys. Res. Lett.*, **36**, 5.
- Levy, R. C., L. A. Remer, R. G. Kleidman, S. Mattoo, C. Ichoku, R. Kahn, and T. F. Eck, 2010: Global evaluation of the Collection 5 MODIS dark-target aerosol products over land. *Atmos. Chem. Phys.*, **10**, 10399–10420.
- Li, Q., H. Zhang, X. Liu, J. Chen, W. Li, and P. Jones, 2009: A mainland China homogenized historical temperature dataset of 1951–2004. *Bull. Am. Meteor. Soc.*, **90**, 1062–1065.
- Li, Q., W. Dong, W. Li, X. Gao, P. Jones, J. Kennedy, and D. Parker, 2010a: Assessment of the uncertainties in temperature change in China during the last century. *Chin. Sci. Bull.*, **55**, 1974–1982.
- Li, Q. X., et al., 2010b: Assessment of surface air warming in northeast China, with emphasis on the impacts of urbanization. *Theor. Appl. Climatol.*, **99**, 469–478.
- Li, Z., et al., 2012: Changes of daily climate extremes in southwestern China during 1961–2008. *Global Planet. Change*, **80–81**, 255–272.
- Liang, F., and X. A. Xia, 2005: Long-term trends in solar radiation and the associated climatic factors over China for 1961–2000. *Ann. Geophys.*, **23**, 2425–2432.
- Liebmann, B., R. M. Dole, C. Jones, I. Blade, and D. Allured, 2010: Influence of choice of time period on global surface temperature trend estimates. *Bull. Am. Meteor. Soc.*, **91**, 1485–U1471.
- Liepert, B. G., 2002: Observed reductions of surface solar radiation at sites in the United States and worldwide from 1961 to 1990. *Geophys. Res. Lett.*, **29**, 1421.
- Liley, J. B., 2009: New Zealand dimming and brightening. *J. Geophys. Res. Atmos.*, **114**, D00d10.
- Lim, E. P., and I. Simmonds, 2007: Southern Hemisphere winter extratropical cyclone characteristics and vertical organization observed with the ERA-40 data in 1979–2001. *J. Clim.*, **20**, 2675–2690.
- Lim, E. P., and I. Simmonds, 2009: Effect of tropospheric temperature change on the zonal mean circulation and SH winter extratropical cyclones. *Clim. Dyn.*, **33**, 19–32.
- Lim, Y. K., M. Cai, E. Kalnay, and L. Zhou, 2008: Impact of vegetation types on surface temperature change. *J. Appl. Meteor. Climatol.*, **47**, 411–424.
- Lin, C., K. Yang, J. Qin, and R. Fu, 2012: Observed coherent trends of surface and upper-air wind speed over China since 1960. *J. Clim.*, **26**, 2891–2903..
- Liu, B., M. Xu, and M. Henderson, 2011: Where have all the showers gone? Regional declines in light precipitation events in China, 1960–2000. *Int. J. Climatol.*, **31**, 1177–1191.
- Liu, B. H., M. Xu, M. Henderson, and W. G. Gong, 2004a: A spatial analysis of pan evaporation trends in China, 1955–2000. *J. Geophys. Res. Atmos.*, **109**, D15102.
- Liu, B. H., M. Xu, M. Henderson, Y. Qi, and Y. Q. Li, 2004b: Taking China's temperature: Daily range, warming trends, and regional variations, 1955–2000. *J. Clim.*, **17**, 4453–4462.
- Liu, Q. H., and F. Z. Weng, 2009: Recent stratospheric temperature observed from satellite measurements. *Sola*, **5**, 53–56.
- Lo, M.-H., and J. S. Famiglietti, 2013: Irrigation in California's Central Valley strengthens the southwestern U.S. water cycle. *Geophys. Res. Lett.*, **40**, 301–306.
- Loeb, N. G., et al., 2009: Toward optimal closure of the Earth's top-of-atmosphere radiation budget. *J. Clim.*, **22**, 748–766.
- Loeb, N. G., et al., 2012a: Advances in understanding top-of-atmosphere radiation variability from satellite observations. *Surv. Geophys.*, **33**, 359–385.
- Loeb, N. G., et al., 2012b: Observed changes in top-of-the-atmosphere radiation and upper-ocean heating consistent within uncertainty. *Nature Geosci.*, **5**, 110–113.
- Logan, J. A., et al., 2012: Changes in ozone over Europe since 1990: Analysis of ozone measurements from sondes, regular aircraft (MOZAIC), and alpine surface sites. *J. Geophys. Res.*, **117**, D09301.
- Long, C. N., E. G. Dutton, J. A. Augustine, W. Wiscombe, M. Wild, S. A. McFarlane, and C. J. Flynn, 2009: Significant decadal brightening of downwelling shortwave in the continental United States. *J. Geophys. Res. Atmos.*, **114**, D00d06.

- Lorenz, R., E. B. Jaeger, and S. I. Seneviratne, 2010: Persistence of heat waves and its link to soil moisture memory. *Geophys. Res. Lett.*, **37**, L09703.
- Lucas, C., H. Nguyen, and B. Timbal, 2012: An observational analysis of Southern Hemisphere tropical expansion. *J. Geophys. Res.*, **117**, D17112.
- Luo, J. J., W. Sasaki, and Y. Masumoto, 2012: Indian Ocean warming modulates Pacific climate change. *Proc. Natl. Acad. Sci. U.S.A.*, **109**, 18701–18706.
- Lupikasza, E., 2010: Spatial and temporal variability of extreme precipitation in Poland in the period 1951–2006. *Int. J. Climatol.*, **30**, 991–1007.
- Lyman, J. M., et al., 2010: Robust warming of the global upper ocean. *Nature*, **465**, 334–337.
- Lynch, A. H., J. A. Curry, R. D. Brunner, and J. A. Maslanik, 2004: Toward an integrated assessment of the impacts of extreme wind events on Barrow, Alaska. *Bull. Am. Meteor. Soc.*, **85**, 209–.
- Mahowald, N., et al., 2010: Observed 20th century desert dust variability: Impact on climate and biogeochemistry. *Atmos. Chem. Phys.*, **10**, 10875–10893.
- Makowski, K., M. Wild, and A. Ohmura, 2008: Diurnal temperature range over Europe between 1950 and 2005. *Atmos. Chem. Phys.*, **8**, 6483–6498.
- Makowski, K., E. B. Jaeger, M. Chiacchio, M. Wild, T. Ewen, and A. Ohmura, 2009: On the relationship between diurnal temperature range and surface solar radiation in Europe. *J. Geophys. Res. Atmos.*, **114**, D00d07.
- Manabe, S., and R. F. Strickler, 1964: Thermal equilibrium of the atmosphere with a convective adjustment. *Journal of the Atmospheric Sciences*, **21**, 361–385.
- Mann, M. E., 2011: On long range dependence in global surface temperature series. *Clim. Change*, **107**, 267–276.
- Mann, M. E., T. A. Sabbatelli, and U. Neu, 2007a: Evidence for a modest undercount bias in early historical Atlantic tropical cyclone counts. *Geophys. Res. Lett.*, **34**, L22707.
- Mann, M. E., K. A. Emanuel, G. J. Holland, and P. J. Webster, 2007b: Atlantic tropical cyclones revisited. *EOS Transactions (AGU)*, **88**, 349–350.
- Manney, G. L., et al., 2011: Unprecedented Arctic ozone loss in 2011. *Nature*, **478**, 469–475.
- Mantua, N. J., S. R. Hare, Y. Zhang, J. M. Wallace, and R. C. Francis, 1997: A Pacific interdecadal climate oscillation with impacts on salmon production. *Bull. Am. Meteor. Soc.*, **78**, 1069–1079.
- Marenci, A., H. Gouget, P. Nédélec, and J. P. Pagés, 1994: Evidence of a long-term increase in tropospheric ozone from Pic du Midi series: Consequences: positive radiative forcing. *J. Geophys. Res.*, **99**, 16,617–16,616, 632.
- Marshall, G. J., 2003: Trends in the southern annular mode from observations and reanalyses. *J. Clim.*, **16**, 4134–4143.
- Martinerie, P., et al., 2009: Long-lived halocarbon trends and budgets from atmospheric chemistry modelling constrained with measurements in polar firn. *Atmos. Chem. Phys.*, **3911–3934**.
- Mastrandrea, M., et al., 2011: The IPCC AR5 guidance note on consistent treatment of uncertainties: A common approach across the working groups. *Clim. Change*, **108**, 675–691.
- Matulla, C., W. Schoner, H. Alexandersson, H. von Storch, and X. L. Wang, 2008: European storminess: Late nineteenth century to present. *Clim. Dyn.*, **31**, 125–130.
- McCarthy, M. P., P. W. Thorne, and H. A. Titchner, 2009: An analysis of tropospheric humidity trends from radiosondes. *J. Clim.*, **22**, 5820–5838.
- McCarthy, M. P., H. A. Titchner, P. W. Thorne, S. F. B. Tett, L. Haimberger, and D. E. Parker, 2008: Assessing bias and uncertainty in the HadAT-adjusted radiosonde climate record. *J. Clim.*, **21**, 817–832.
- McKittrick, R., 2010: Atmospheric circulations do not explain the temperature-industrialization correlation. *Stat. Politics Policy*, **1**, issue 1 .
- McKittrick, R., and P. J. Michaels, 2004: A test of corrections for extraneous signals in gridded surface temperature data. *Clim. Res.*, **26**, 159–173.
- McKittrick, R., and N. Nierenberg, 2010: Socioeconomic patterns in climate data. *J. Econ. Soc. Meas.*, **35**, 149–175.
- McKittrick, R. R., and P. J. Michaels, 2007: Quantifying the influence of anthropogenic surface processes and inhomogeneities on gridded global climate data. *J. Geophys. Res. Atmos.*, **112**, D24S09.
- McNider, R. T., et al., 2012: Response and sensitivity of the nocturnal boundary layer over land to added longwave radiative forcing. *J. Geophys. Res.*, **117**, D14106.
- McVicar, T. R., T. G. Van Niel, L. T. Li, M. L. Roderick, D. P. Rayner, L. Ricciardulli, and R. J. Donohue, 2008: Wind speed climatology and trends for Australia, 1975–2006: Capturing the stilling phenomenon and comparison with near-surface reanalysis output. *Geophys. Res. Lett.*, **35**, L20403.
- McVicar, T. R., et al., 2012: Global review and synthesis of trends in observed terrestrial near-surface wind speeds: Implications for evaporation. *J. Hydrol.*, **416**, 182–205.
- Mears, C., J. Wang, S. Ho, L. Zhang, and X. Zhou, 2010: Total column water vapor, in State of the Climate in 2009. *Bull. Am. Meteor. Soc.* [D. S. Arndt, M. O. Baringer, and M. R. Johnson (eds.)].
- Mears, C. A., and F. J. Wentz, 2009a: Construction of the remote sensing systems V3.2 atmospheric temperature records from the MSU and AMSU microwave sounders. *J. Atmos. Ocean Technol.*, **26**, 1040–1056.
- Mears, C. A., and F. J. Wentz, 2009b: Construction of the RSS V3.2 lower-tropospheric temperature dataset from the MSU and AMSU microwave sounders. *J. Atmos. Ocean Technol.*, **26**, 1493–1509.
- Mears, C. A., F. J. Wentz, and P. W. Thorne, 2012: Assessing the value of Microwave Sounding Unit-radiosonde comparisons in ascertaining errors in climate data records of tropospheric temperatures. *J. Geophys. Res. Atmos.*, **117**, D19103.
- Mears, C. A., F. J. Wentz, P. Thorne, and D. Bernie, 2011: Assessing uncertainty in estimates of atmospheric temperature changes from MSU and AMSU using a Monte-Carlo estimation technique. *J. Geophys. Res. Atmos.*, **116**.
- Mears, C. A., C. E. Forest, R. W. Spencer, R. S. Vose, and R. W. Reynolds, 2006: What is our understanding of the contribution made by observational or methodological uncertainties to the previously reported vertical differences in temperature trends? In: *Temperature Trends in the Lower Troposphere: Steps for Understanding and Reconciling Differences* [T. R. Karl, S. J. Hassol, C. D. Miller, and W. L. Murray (eds.)], 71–88.
- Mears, C. A., B. D. Santer, F. J. Wentz, K. E. Taylor, and M. F. Wehner, 2007: Relationship between temperature and precipitable water changes over tropical oceans. *Geophys. Res. Lett.*, **34**, L24709.
- Meehl, G. A., J. M. Arblaster, and G. Branstator, 2012: Mechanisms contributing to the warming hole and the consequent U.S. East–West differential of heat extremes. *J. Clim.*, **25**, 6394–6408.
- Mekis, É., and L. A. Vincent, 2011: An overview of the second generation adjusted daily precipitation dataset for trend analysis in Canada. *Atmosphere-Ocean*, **49**, 163–177.
- Meng, Q. J., M. Latif, W. Park, N. S. Keenlyside, V. A. Semenov, and T. Martin, 2012: Twentieth century Walker Circulation change: Data analysis and model experiments. *Clim. Dyn.*, **38**, 1757–1773.
- Menne, M. J., and C. N. Williams, 2009: Homogenization of temperature series via pairwise comparisons. *J. Clim.*, **22**, 1700–1717.
- Menne, M. J., C. N. Williams, and M. A. Palecki, 2010: On the reliability of the US surface temperature record. *J. Geophys. Res. Atmos.*, **115**, D11108.
- Menzel, W. P., 2001: Cloud tracking with satellite imagery: From the pioneering work of Ted Fujita to the present. *Bull. Am. Meteor. Soc.*, **82**, 33–47.
- Merchant, C. J., et al., 2012: A 20 year independent record of sea surface temperature for climate from Along Track Scanning Radiometer. *J. Geophys. Res.*, **117**, C12013.
- Merrifield, M. A., 2011: A shift in western tropical Pacific sea level trends during the 1990s. *J. Clim.*, **24**, 4126–4138.
- Mezher, R. N., M. Doyle, and V. Barros, 2012: Climatology of hail in Argentina. *Atmos. Res.*, **114–115**, 70–82.
- Mieruch, S., S. Noel, H. Bovensmann, and J. P. Burrows, 2008: Analysis of global water vapour trends from satellite measurements in the visible spectral range. *Atmos. Chem. Phys.*, **8**, 491–504.
- Milewska, E. J., 2004: Baseline cloudiness trends in Canada 1953–2002. *Atmos. Ocean*, **42**, 267–280.
- Miller, B., et al., 2010: HFC-23 (CHF3) emission trend response to HCFC-22 (CHClF2) production and recent HFC-23 emission abatement measures. *Atmos. Chem. Phys.*, **10**, 7875–7890.
- Milliman, J. D., K. L. Farnsworth, P. D. Jones, K. H. Xu, and L. C. Smith, 2008: Climatic and anthropogenic factors affecting river diSchärge to the global ocean, 1951–2000. *Global Planet. Change*, **62**, 187–194.
- Mills, T. C., 2010: ‘Skinning a cat’: Alternative models of representing temperature trends. *Clim. Change*, **101**, 415–426.
- Milz, M., et al., 2005: Water vapor distributions measured with the Michelson Interferometer for passive atmospheric sounding on board Envisat (MIPAS/Envisat). *J. Geophys. Res.*, **110**, D24307.
- Mishchenko, M. I., et al., 2007: Long-term satellite record reveals likely recent aerosol trend. *Science*, **315**, 1543–1543.

- Mishchenko, M. I., et al., 2012: Aerosol retrievals from channel-1 and -2 AVHRR radiances: Long-term trends updated and revisited. *J. Quant. Spectr. Radiat. Trans.*, **113**, 1974–1980.
- Misra, V., J. P. Michael, R. Boyles, E. P. Chassignet, M. Griffin, and J. J. O'Brien, 2012: Reconciling the spatial distribution of the surface temperature trends in the southeastern United States. *J. Clim.*, **25**, 3610–3618.
- Mitas, C. M., and A. Clement, 2005: Has the Hadley cell been strengthening in recent decades? *Geophys. Res. Lett.*, **32**, L030809.
- Mitchell, T. D., and P. D. Jones, 2005: An improved method of constructing a database of monthly climate observations and associated high-resolution grids. *Int. J. Climatol.*, **25**, 693–712.
- Mo, K., and J. Paegle, 2001: The Pacific-South American modes and their downstream effects. *Int. J. Climatol.*, **21**, 1211–1229.
- Moberg, A., et al., 2006: Indices for daily temperature and precipitation extremes in Europe analyzed for the period 1901–2000. *J. Geophys. Res. Atmos.*, **111**, D22106.
- Mohapatra, M., B. K. Mandiyopadhyay, and A. Tyagi, 2011: Best track parameters of tropical cyclones over the North Indian Ocean: A review. *Natural Hazards*, **63**, 1285–1317.
- Mokhov, I. I., M. G. Akperov, M. A. Prokofyeva, A. V. Timazhev, A. R. Lupo, and H. Le Treut, 2013: Blockings in the Northern Hemisphere and Euro-Atlantic region: Estimates of changes from reanalyses data and model simulations. *Doklady, Earth Sci.*, **449**, 430–433.
- Monaghan, A. J., and D. H. Bromwich, 2008: Advances describing recent Antarctic climate variability. *Bull. Am. Meteorol. Soc.*, **89**, 1295–1306.
- Monaghan, A. J., D. H. Bromwich, W. Chapman, and J. C. Comiso, 2008: Recent variability and trends of Antarctic near-surface temperature. *J. Geophys. Res. Atmos.*, **113**, D04105.
- Monk, W., D. L. Peters, D. J. Baird, and R. A. Curry, 2011: Trends in indicator hydrological variables for Canadian rivers. *Hydrolog. Proc.*, **25**, 3086–3100.
- Monks, P. S., et al., 2009: Atmospheric composition change – global and regional air quality. *Atmos. Environ.*, **43**, 5268–5350.
- Montzka, S., B. Hall, and J. Elkins, 2009: Accelerated increases observed for hydrochlorofluorocarbons since 2004 in the global atmosphere. *Geophys. Res. Lett.*, **36**, L03804.
- Montzka, S., M. Krol, E. Dlugokencky, B. Hall, P. Jockel, and J. Lelieveld, 2011: Small interannual variability of global atmospheric hydroxyl. *Science*, **331**, 67–69.
- Montzka, S., L. Kuijpers, M. Battle, M. Aydin, K. Verhulst, E. Saltzman, and D. Fahey, 2010: Recent increases in global HFC-23 emissions. *Geophys. Res. Lett.*, **37**, L02808.
- Montzka, S. A., et al., 2011b: Ozone-depleting substances (ODSs) and related chemicals. In Scientific Assessment of Ozone Depletion: 2010, Global Ozone Research and Monitoring Project—Report No. 52. World Meteorological Organization, Geneva, Switzerland, 516 pp.
- Morak, S., G. C. Hegerl, and J. Kenyon, 2011: Detectable regional changes in the number of warm nights. *Geophys. Res. Lett.*, **38**, 5.
- Morak, S., G. C. Hegerl, and N. Christidis, 2013: Detectable changes in the frequency of temperature extremes. *J. Clim.*, **26**, 1561–1574.
- Morice, C. P., J. J. Kennedy, N. A. Rayner, and P. D. Jones, 2012: Quantifying uncertainties in global and regional temperature change using an ensemble of observational estimates: The HadCRUT4 data set. *J. Geophys. Res. Atmos.*, **117**, 22.
- Mueller, B., and S. Seneviratne, 2012: Hot days induced by precipitation deficits at the global scale. *Proc. Natl. Acad. Sci. U.S.A.*, **109**, 12398–12403.
- Mueller, B., et al., 2011: Evaluation of global observations-based evapotranspiration datasets and IPCC AR4 simulations. *Geophys. Res. Lett.*, **38**, L06402.
- Muhle, J., et al., 2010: Perfluorocarbons in the global atmosphere: tetrafluoromethane, hexafluoroethane, and octafluoropropane. *Atmos. Chem. Phys.*, **10**, 5145–5164.
- Murphy, D. M., et al., 2011: Decreases in elemental carbon and fine particle mass in the United States. *Atmos. Chem. Phys.*, **11**, 4679–4686.
- Nan, S., and J. P. Li, 2003: The relationship between the summer precipitation in the Yangtze River Valley and the boreal spring Southern Hemisphere annular mode. *Geophys. Res. Lett.*, **30**, 2266.
- Nash, J., and P. R. Edge, 1989: Temperature changes in the stratosphere and lower mesosphere 197–1988 inferred from TOVS radiance observations. *Adv. Space Res.*, **9**, 333–341.
- Neff, W., J. Perlitz, and M. Hoerling, 2008: Observational evidence for asymmetric changes in tropospheric heights over Antarctica on decadal time scales. *Geophys. Res. Lett.*, **35**, L18703.
- Neu, U., et al., 2012: IMILAST: A community effort to intercompare extratropical cyclone detection and tracking algorithms. *Bull. Am. Meteorol. Soc.*, **94**, 529–547.
- Neivison, C., et al., 2011: Exploring causes of interannual variability in the seasonal cycles of tropospheric nitrous oxide. *Atmos. Chem. Phys.*, **11**, 3713–3730.
- New, M., et al., 2006: Evidence of trends in daily climate extremes over southern and west Africa. *J. Geophys. Res. Atmos.*, **111**, D14102.
- Nguyen, H., B. Timbal, I. Smith, A. Evans, and C. Lucas, 2013: The Hadley circulation in reanalyses: Climatology, variability and change. *J. Clim.*, **26**, 3357–3376.
- Nicholls, N., 2008: Recent trends in the seasonal and temporal behaviour of the El Niño–Southern Oscillation. *Geophys. Res. Lett.*, **35**, L19703.
- Nisbet, E., and R. Weiss, 2010: Top-down versus bottom-up. *Science*, **328**, 1241–1243.
- Norris, J. R., and M. Wild, 2007: Trends in aerosol radiative effects over Europe inferred from observed cloud cover, solar “dimming” and solar “brightening”. *J. Geophys. Res. Atmos.*, **112**, D08214.
- Norris, J. R., and M. Wild, 2009: Trends in aerosol radiative effects over China and Japan inferred from observed cloud cover, solar dimming, and solar brightening. *J. Geophys. Res. Atmos.*, **114**, D00d15.
- O’Dell, C. W., F. J. Wentz, and R. Bennartz, 2008: Cloud liquid water path from satellite-based passive microwave observations: A new climatology over the global oceans. *J. Clim.*, **21**, 1721–1739.
- O’Doherty, S., et al., 2009: Global and regional emissions of HFC-125 (CHF2CF3) from in situ and air archive atmospheric observations at AGAGE and SOGE observatories. *J. Geophys. Res. Atmos.*, **109**, D06310.
- O’Donnell, R., N. Lewis, S. McIntyre, and J. Condon, 2011: Improved methods for PCA-based reconstructions: Case study using the Steig et al. (2009) Antarctic Temperature Reconstruction. *J. Clim.*, **24**, 2099–2115.
- O’Gorman, P., R. P. Allan, M. P. Byrne, and M. Previdi, 2012: Energetic constraints on precipitation under climate change. *Surv. Geophys.*, **33**, 585–608.
- Ohmura, A., 2009: Observed decadal variations in surface solar radiation and their causes. *J. Geophys. Res. Atmos.*, **114**, D00d05.
- Ohmura, A., et al., 1998: Baseline Surface Radiation Network (BSRN/WCRP): New precision radiometry for climate research. *Bull. Am. Meteorol. Soc.*, **79**, 2115–2136.
- Ohvri, H., et al., 2009: Global dimming and brightening versus atmospheric column transparency, Europe, 1906–2007. *J. Geophys. Res. Atmos.*, **114**, D00d12.
- Oltmans, S. J., et al., 2013: Recent tropospheric ozone changes – A pattern dominated by slow or no growth. *Atmos. Environ.*, **67**, 331–351.
- Onogi, K., et al., 2007: The JRA-25 reanalysis. *J. Meteorol. Soc. Jpn.*, **85**, 369–432.
- Oort, A. H., and J. J. Yienger, 1996: Observed interannual variability in the Hadley circulation and its connection to ENSO. *J. Clim.*, **9**, 2751–2767.
- Osborn, T. J., 2011: Winter 2009/2010 temperatures and a record breaking North Atlantic Oscillation index. *Weather*, **66**, 19–21.
- Paciorek, C. J., J. S. Risbey, V. Ventura, and R. D. Rosen, 2002: Multiple indices of Northern Hemisphere cyclone activity, winters 1949–99. *J. Clim.*, **15**, 1573–1590.
- Palmer, M. D., K. Haines, S. F. B. Tett, and T. J. Ansell, 2007: Isolating the signal of ocean global warming. *Geophys. Res. Lett.*, **34**, 6.
- Palmer, W. C., 1965: Meteorological drought. *US Weather Bureau Research Paper*, 45, 58 pages.
- Paltridge, G., A. Arking, and M. Pook, 2009: Trends in middle- and upper-level tropospheric humidity from NCEP reanalysis data. *Theor. Appl. Climatol.*, **98**, 351–359.
- Pan, Z. T., R. W. Arritt, E. S. Takle, W. J. Gutowski, C. J. Anderson, and M. Segal, 2004: Altered hydrologic feedback in a warming climate introduces a “warming hole”. *Geophys. Res. Lett.*, **31**, L17109.
- Panagiotopoulos, F., M. Shahgedanova, A. Hannachi, and D. B. Stephenson, 2005: Observed trends and teleconnections of the Siberian high: A recently declining center of action. *J. Clim.*, **18**, 1411–1422.
- Parker, D., C. Folland, A. Scaife, J. Knight, A. Colman, P. Baines, and B. Dong, 2007: Decadal to multidecadal variability and the climate change background. *J. Geophys. Res. Atmos.*, **112**, D18115.
- Parker, D. E., 2006: A demonstration that large-scale warming is not urban. *J. Clim.*, **19**, 2882–2895.
- Parker, D. E., 2011: Recent land surface air temperature trends assessed using the 20th century reanalysis. *J. Geophys. Res. Atmos.*, **116**, D20125.
- Parker, D. E., P. Jones, T. C. Peterson, and J. Kennedy, 2009: Comment on “Unresolved issues with the assessment of multidecadal global land surface temperature trends” by Roger A. Pielke Sr. et al. *J. Geophys. Res. Atmos.*, **114**, D05104.
- Parrish, D. D., et al., 2012: Long-term changes in lower tropospheric baseline ozone concentrations at northern mid-latitudes. *Atmos. Chem. Phys.*, **12**, 11485–11504.

- Pattanaik, D. R., and M. Rajeevan, 2010: Variability of extreme rainfall events over India during southwest monsoon season. *Meteorol. Appl.*, **17**, 88–104.
- Pavan, V., R. Tomozeiu, C. Cacciamani, and M. Di Lorenzo, 2008: Daily precipitation observations over Emilia-Romagna: Mean values and extremes. *Int. J. Climatol.*, **28**, 2065–2079.
- Pavelin, E. G., C. E. Johnson, S. Rughooputh, and R. Toumi, 1999: Evaluation of pre-industrial surface ozone measurements made using Schlonbein's method. *Atmos. Environ.*, **33**, 919–929.
- Perkins, S. E., and L. V. Alexander, 2012: On the measurement of heat waves. *J. Clim.*, **26**, 4500–4517.
- Perkins, S. E., L. V. Alexander, and J. R. Nairn, 2012: Increasing frequency, intensity and duration of observed global heatwaves and warm spells. *Geophys. Res. Lett.*, **39**, L20714.
- Peterson, T. C., K. M. Willett, and P. W. Thorne, 2011: Observed changes in surface atmospheric energy over land. *Geophys. Res. Lett.*, **38**, L16707.
- Peterson, T. C., X. B. Zhang, M. Brunet-India, and J. L. Vazquez-Aguirre, 2008: Changes in North American extremes derived from daily weather data. *J. Geophys. Res. Atmos.*, **113**, D07113.
- Peterson, T. C., et al., 2009: State of the Climate in 2008. *Bull. Am. Meteor. Soc.*, **90**, S13–.
- Peterson, T. C., et al., 2013: Monitoring and understanding changes in heat waves, cold waves, floods and droughts in the United States: State of knowledge. *Bull. Am. Meteor. Soc.*, **94**, 821–834.
- Petrow, T., and B. Merz, 2009: Trends in flood magnitude, frequency and seasonality in Germany in the period 1951–2002. *J. Hydrol.*, **371**, 129–141.
- Pezza, A., P. van Rensch, and W. Cai, 2012: Severe heat waves in Southern Australia: Synoptic climatology and large scale connections. *Clim. Dyn.*, **38**, 209–224.
- Pezza, A. B., I. Simmonds, and J. A. Renwick, 2007: Southern Hemisphere cyclones and anticyclones: Recent trends and links with decadal variability in the Pacific Ocean. *Int. J. Climatol.*, **27**, 1403–1419.
- Philipona, R., 2012: Greenhouse warming and solar brightening in and around the Alps. *Int. J. Climatol.*, **33**, 1530–1537.
- Philipona, R., K. Behrens, and C. Ruckstuhl, 2009: How declining aerosols and rising greenhouse gases forced rapid warming in Europe since the 1980s. *Geophys. Res. Lett.*, **36**, L02806.
- Philipona, R., B. Dürr, A. Ohmura, and C. Ruckstuhl, 2005: Anthropogenic greenhouse forcing and strong water vapor feedback increase temperature in Europe. *Geophys. Res. Lett.*, **32**, L19809.
- Philipona, R., B. Dürr, C. Marty, A. Ohmura, and M. Wild, 2004: Radiative forcing measured at Earth's surface—corroborate the increasing greenhouse effect. *Geophys. Res. Lett.*, **31**, L03202.
- Philipp, A., P. M. Della-Marta, J. Jacobbeit, D. R. Fereday, P. D. Jones, A. Moberg, and H. Wanner, 2007: Long-term variability of daily North Atlantic-European pressure patterns since 1850 classified by simulated annealing clustering. *J. Clim.*, **20**, 4065–4095.
- Piao, S., et al., 2010: The impacts of climate change on water resources and agriculture in China. *Nature*, **467**, 43–51.
- Pielke, R. A., and T. Matsui, 2005: Should light wind and windy nights have the same temperature trends at individual levels even if the boundary layer averaged heat content change is the same? *Geophys. Res. Lett.*, **32**, L21813.
- Pielke, R. A., Sr., et al., 2007: Unresolved issues with the assessment of multidecadal global land surface temperature trends. *J. Geophys. Res. Atmos.*, **112**, D24S08.
- Pinker, R. T., B. Zhang, and E. G. Dutton, 2005: Do satellites detect trends in surface solar radiation? *Science*, **308**, 850–854.
- Pirazzoli, P. A., and A. Tomasini, 2003: Recent near-surface wind changes in the central Mediterranean and Adriatic areas. *Int. J. Climatol.*, **23**, 963–973.
- Po-Chedley, S., and Q. Fu, 2012: A bias in the Midtropospheric Channel Warm Target Factor on the NOAA-9 Microwave Sounding Unit. *J. Atmos. Ocean Technol.*, **29**, 646–652.
- Portmann, R., S. Solomon, and G. Hegerl, 2009a: Spatial and seasonal patterns in climate change, temperatures, and precipitation across the United States. *Proc. Natl. Acad. Sci. U.S.A.*, **106**, 7324–7329.
- Portmann, R. W., S. Solomon, and G. C. Hegerl, 2009b: Linkages between climate change, extreme temperature and precipitation across the United States. *Proc. Natl. Acad. Sci. U.S.A.*, **106**, 7324–7329.
- Power, S., T. Casey, C. Folland, A. Colman, and V. Mehta, 1999: Inter-decadal modulation of the impact of ENSO on Australia. *Clim. Dyn.*, **15**, 319–324.
- Power, S. B., and G. Kociuba, 2011a: The impact of global warming on the Southern Oscillation Index. *Clim. Dynamics*, **37**, 1745–1754.
- Power, S. B., and G. Kociuba, 2011b: What caused the observed twentieth-century weakening of the Walker Circulation? *J. Clim.*, **24**, 6501–6514.
- Pozzoli, L., et al., 2011: Reanalysis of tropospheric sulfate aerosol and ozone for the period 1980–2005 using the aerosol-chemistry-climate model ECHAM5–HAMMOZ. *Atmos. Chem. Phys.*, **11**, 9563–9594.
- Prata, F., 2008: The climatological record of clear-sky longwave radiation at the Earth's surface: Evidence for water vapour feedback? *Int. J. Remote Sens.*, **29**, 5247–5263.
- Prather, M., C. Holmes, and J. Hsu, 2012: Reactive greenhouse gas scenarios: Systematic exploration of uncertainties and the role of atmospheric chemistry. *Geophys. Res. Lett.*, **39**, L09803.
- Prinn, R., et al., 2005: Evidence for variability of atmospheric hydroxyl radicals over the past quarter century. *Geophys. Res. Lett.*, **L07809**.
- Pryor, S. C., R. J. Barthelmie, and E. S. Riley, 2007: Historical evolution of wind climates in the USA – art. no. 012065. In: *Science of Making Torque from Wind* [M. O. L. Hansen and K. S. Hansen (eds.)], **75**, 12065–12065.
- Pryor, S. C., J. A. Howe, and K. E. Kunkel, 2009: How spatially coherent and statistically robust are temporal changes in extreme precipitation in the contiguous USA? *Int. J. Climatol.*, **29**, 31–45.
- Qian, Y., D. P. Kaiser, L. R. Leung, and M. Xu, 2006: More frequent cloud-free sky and less surface solar radiation in China from 1955 to 2000. *Geophys. Res. Lett.*, **33**, L01812.
- Qian, Y., W. G. Wang, L. R. Leung, and D. P. Kaiser, 2007: Variability of solar radiation under cloud-free skies in China: The role of aerosols. *Geophys. Res. Lett.*, **34**, L12804.
- Qian, Y., D. Gong, J. Fan, L. Leung, R. Bennartz, D. Chen, and W. Wang, 2009: Heavy pollution suppresses light rain in China: Observations and modeling. *J. Geophys. Res. Atmos.*, **114**, D00K02.
- Rahimzadeh, F., A. Asgari, and E. Fattahi, 2009: Variability of extreme temperature and precipitation in Iran during recent decades. *Int. J. Climatol.*, **29**, 329–343.
- Raible, C. C., P. M. Della-Marta, C. Schwierz, H. Wernli, and R. Blender, 2008: Northern hemisphere extratropical cyclones: A comparison of detection and tracking methods and different reanalyses. *Mon. Weather Rev.*, **136**, 880–897.
- Rauchjik, C., 2011: Observed trends in sunshine duration over South America. *Int. J. Climatol.*, **32**, 669–680.
- Randall, R. M., and B. M. Herman, 2008: Using limited time period trends as a means to determine attribution of discrepancies in microwave sounding unit-derived tropospheric temperature time series. *J. Geophys. Res. Atmos.*, **113**, D05105.
- Randel, W. J., 2010: Variability and trends in stratospheric temperature and water vapor. *The Stratosphere: Dynamics, Transport and Chemistry*, S. Polvani, and Waugh, Ed., American Geophysical Union, 123–135.
- Randel, W. J., and E. J. Jensen, 2013: Physical processes in the tropical tropopause layer and their roles in a changing climate. *Nature Geosci.*, **169**–176.
- Randel, W. J., F. Wu, H. Vömel, G. E. Nedoluha, and P. Forster, 2006: Decreases in stratospheric water vapor after 2001: Links to changes in the tropical tropopause and the Brewer-Dobson circulation. *J. Geophys. Res. Atmos.*, **111**, D12312.
- Randel, W. J., et al., 2009: An update of observed stratospheric temperature trends. *J. Geophys. Res. Atmos.*, **114**, D02107.
- Rasmusson, E. M., and T. H. Carpenter, 1982: Variations in tropical sea surface temperature and surface wind fields associated with the Southern Oscillation/El Niño. *Mon. Weather Rev.*, **110**, 354–384.
- Rasmusson, E. M., and J. M. Wallace, 1983: Meteorological aspects of the El Niño–Southern Oscillation. *Science*, **222**, 1195–1202.
- Rausch, J., A. Heidinger, and R. Bennartz, 2010: Regional assessment of microphysical properties of marine boundary layer cloud using the PATMOS-x dataset. *J. Geophys. Res. Atmos.*, **115**, D23212.
- Ray, E. A., et al., 2010: Evidence for changes in stratospheric transport and mixing over the past three decades based on multiple data sets and tropical leaky pipe analysis. *J. Geophys. Res. Atmos.*, **115**, D21304.
- Rayner, D. P., 2007: Wind run changes: The dominant factor affecting pan evaporation trends in Australia. *J. Clim.*, **20**, 3379–3394.
- Rayner, N. A., et al., 2003: Global analyses of sea surface temperature, sea ice, and night marine air temperature since the late nineteenth century. *J. Geophys. Res. Atmos.*, **108**, 37.
- Rayner, N. A., et al., 2006: Improved analyses of changes and uncertainties in sea surface temperature measured in situ since the mid-nineteenth century: The HadSST2 dataset. *J. Clim.*, **19**, 446–469.

- Read, W. G., et al., 2007: Aura Microwave Limb Sounder upper tropospheric and lower stratospheric H₂O and relative humidity with respect to ice validation. *J. Geophys. Res. Atmos.*, **112**, D24S35.
- Ren, G., et al., 2011: Change in climatic extremes over mainland China based on an integrated extreme climate index. *Clim. Res.*, **50**, 113–124.
- Ren, G. Y., Z. Y. Chu, Z. H. Chen, and Y. Y. Ren, 2007: Implications of temporal change in urban heat island intensity observed at Beijing and Wuhan stations. *Geophys. Res. Lett.*, **34**, L05711.
- Ren, G. Y., Y. Q. Zhou, Z. Y. Chu, J. X. Zhou, A. Y. Zhang, J. Guo, and X. F. Liu, 2008: Urbanization effects on observed surface air temperature trends in north China. *J. Clim.*, **21**, 1333–1348.
- Ren, H.-L., and F.-F. Jin, 2011: Niño indices for two types of ENSO. *Geophys. Res. Lett.*, **38**, L04704.
- Ren, Y. Y., and G. Y. Ren, 2011: A remote-sensing method of selecting reference stations for evaluating urbanization effect on surface air temperature trends. *J. Clim.*, **24**, 3179–3189.
- Renard, B., et al., 2008: Regional methods for trend detection: Assessing field significance and regional consistency. *Water Resour. Res.*, **44**, W08419.
- Revadekar, J., D. Kothawale, S. Patwardhan, G. Pant, and K. Kumar, 2012: About the observed and future changes in temperature extremes over India. *Nat. Hazards*, **60**, 1133–1155.
- Reynolds, R., N. Rayner, T. Smith, D. Stokes, and W. Wang, 2002: An improved in situ and satellite SST analysis for climate. *J. Clim.*, **15**, 1609–1625.
- Reynolds, R. W., C. L. Gentemann, and G. K. Corlett, 2010: Evaluation of AATSR and TMI Satellite SST Data. *J. Clim.*, **23**, 152–165.
- Rhines, A., and P. Huybers, 2013: Frequent summer temperature extremes reflect changes in the mean, not the variance. *Proc. Natl. Acad. Sci. U.S.A.*, **110**, E546–E546.
- Rienecker, M. M., Suarez, M.J., Gelaro, R., Todling, R., Bacmeister, J., Liu, E., Bosilovich, M. G., Schubert, S. D., Takacs, L., Kim, G.-K., Bloom, S., Chen, J., Collins, D., Conaty, A., da Silva, A., Gu, W., Joiner, J., Koster, R. D., Lucchesi, R., Molod, A., Owens, T., Pawson, S., Pegion, P., Redder, C. R., Reichle, R., Robertson, F. R., Ruddick, A. G., Sienkiewicz, M., and Woollen, J., 2011: MERRA: NASA's modern-era retrospective analysis for research and applications. *J. Clim.*, **24**, 3624–3648.
- Rigby, M., et al., 2008: Renewed growth of atmospheric methane. *Geophys. Res. Lett.*, **35**, L22805.
- Rigby, M., et al., 2010: History of atmospheric SF₆ from 1973 to 2008. *Atmos. Chem. Phys.*, **10**, 10305–10320.
- Riihimaki, L. D., F. E. Vignola, and C. N. Long, 2009: Analyzing the contribution of aerosols to an observed increase in direct normal irradiance in Oregon. *J. Geophys. Res. Atmos.*, **114**, D00d02.
- Robock, A., et al., 2000: The Global Soil Moisture Data Bank. *Bull. Am. Meteor. Soc.*, **81**, 1281–1299.
- Rockmann, T., and I. Levin, 2005: High-precision determination of the changing isotopic composition of atmospheric N₂O from 1990 to 2002. *J. Geophys. Res. Atmos.*, **110**, D21304.
- Roderick, M. L., and G. D. Farquhar, 2002: The cause of decreased pan evaporation over the past 50 years. *Science*, **298**, 1410–1411.
- Roderick, M. L., L. D. Rotstayn, G. D. Farquhar, and M. T. Hobbins, 2007: On the attribution of changing pan evaporation. *Geophys. Res. Lett.*, **34**, L17403.
- Rohde, R., et al., 2013a: A new estimate of the average Earth surface land temperature spanning 1753 to 2011. *Geoinfor. Geostat.: An Overview*, **1**, doi:10.4172/gigs.1000101.
- Rohde, R., et al., 2013b: Berkeley Earth temperature averaging process. *Geoinfor. Geostat.: An Overview*, **1**, doi:10.4172/gigs.1000103.
- Rohs, S., et al., 2006: Long-term changes of methane and hydrogen in the stratosphere in the period 1978–2003 and their impact on the abundance of stratospheric water vapor. *J. Geophys. Res. Atmos.*, **111**, D14315.
- Ropelewski, C. F., and P. D. Jones, 1987: An extension of the Tahiti–Darwin Southern Oscillation Index. *Mon. Weather Rev.*, **115**, 2161–2165.
- Rosenlof, K. H., and G. C. Reid, 2008: Trends in the temperature and water vapor content of the tropical lower stratosphere: Sea surface connection. *J. Geophys. Res. Atmos.*, **113**, D06107.
- Ruckstuhl, C., et al., 2008: Aerosol and cloud effects on solar brightening and the recent rapid warming. *Geophys. Res. Lett.*, **35**, L12708.
- Ruddiman, W., 2003: The anthropogenic greenhouse era began thousands of years ago. *Clim. Change*, **261**–293.
- Ruddiman, W., 2007: The early anthropogenic hypothesis: Challenges and responses. *Rev. Geophys.*, **45**, RG4001.
- Russak, V., 2009: Changes in solar radiation and their influence on temperature trend in Estonia (1955–2007). *J. Geophys. Res. Atmos.*, **114**, D00d01.
- Russell, A. R., L. C. Valin, E. J. Bucsela, M. O. Wenig, and R. C. Cohen, 2010: Space-based constraints on spatial and temporal patterns of NO_x emissions in California, 2005–2008. *Environ. Sci. Technol.*, **44**, 3608–3615.
- Russell, J., et al., 1993: The halogen occultation experiment. *J. Geophys. Res. Atmos.*, **98**, 10777–10797.
- Rusticucci, M., and M. Renom, 2008: Variability and trends in indices of quality-controlled daily temperature extremes in Uruguay. *Int. J. Climatol.*, **28**, 1083–1095.
- Saha, S., et al., 2010: The NCEP climate forecast system reanalysis. *Bull. Am. Meteor. Soc.*, **91**, 1015–1057.
- Saikawa, E., et al., 2012: Global and regional emissions estimates for HCFC-22. *Atmos. Chem. Phys. Discuss.*, **12**, 18423–18285.
- Saji, N. H., B. N. Goswami, P. N. Vinayachandran, and T. Yamagata, 1999: A dipole mode in the tropical Indian Ocean. *Nature*, **401**, 360–363.
- Sakamoto, M., and J. R. Christy, 2009: The influences of TOVS radiance assimilation on temperature and moisture tendencies in JRA-25 and ERA-40. *J. Atmos. Ocean Technol.*, **26**, 1435–1455.
- Sanchez-Lorenzo, A., and M. Wild, 2012: Decadal variations in estimated surface solar radiation over Switzerland since the late 19th century. *Atmos. Chem. Phys. Discussion*, **12**, 10815–10843.
- Sanchez-Lorenzo, A., J. Calbo, and J. Martin-Vide, 2008: Spatial and temporal trends in sunshine duration over Western Europe (1938–2004). *J. Clim.*, **21**, 6089–6098.
- Sanchez-Lorenzo, A., J. Calbo, and M. Wild, 2013: Global and diffuse solar radiation in Spain: Building a homogeneous dataset and assessing their trends. *Global Planet. Change*, **100**, 343–352.
- Sanchez-Lorenzo, A., J. Calbo, M. Brunetti, and C. Deser, 2009: Dimming/brightening over the Iberian Peninsula: Trends in sunshine duration and cloud cover and their relations with atmospheric circulation. *J. Geophys. Res. Atmos.*, **114**, D00d09.
- Santer, B., et al., 2008: Consistency of modelled and observed temperature trends in the tropical troposphere. *Int. J. Climatol.*, **28**, 1703–1722.
- Santer, B. D., et al., 2007: Identification of human-induced changes in atmospheric moisture content. *Proc. Natl. Acad. Sci. U.S.A.*, **104**, 15248–15253.
- Santer, B. D., et al., 2011: Separating signal and noise in atmospheric temperature changes: The importance of timescale. *J. Geophys. Res. Atmos.*, **116**, D22105.
- Scaife, A., C. Folland, L. Alexander, A. Moberg, and J. Knight, 2008: European climate extremes and the North Atlantic Oscillation. *J. Clim.*, **21**, 72–83.
- Schär, C., P. L. Vidale, D. Luthi, C. Frei, C. Haberli, M. A. Liniger, and C. Appenzeller, 2004: The role of increasing temperature variability in European summer heat-waves. *Nature*, **427**, 332–336.
- Scherer, M., H. Vömel, S. Fueglistaler, S. J. Oltmans, and J. Staehelin, 2008: Trends and variability of midlatitude stratospheric water vapour deduced from the re-evaluated Boulder balloon series and HALOE. *Atmos. Chem. Phys.*, **8**, 1391–1402.
- Scherrer, S. C., and C. Appenzeller, 2006: Swiss Alpine snow pack variability: Major patterns and links to local climate and large-scale flow. *Clim. Res.*, **32**, 187–199.
- Scherrer, S. C., C. Wüthrich, M. Croci-Maspoli, R. Weingartner, and C. Appenzeller, 2013: Snow variability in the Swiss Alps 1864–2009. *Int. J. Climatol.*, doi: 10.1002/joc.3653.
- Schiller, C., J. U. Gross, P. Konopka, F. Plager, F. H. Silva dos Santos, and N. Spelten, 2009: Hydration and dehydration at the tropical tropopause. *Atmos. Chem. Phys.*, **9**, 9647–9660.
- Schmidt, G. A., 2009: Spurious correlations between recent warming and indices of local economic activity. *Int. J. Climatol.*, **29**, 2041–2048.
- Schnadt Poberaj, C., J. Staehelin, D. Brunner, V. Thouret, H. De Backer, and R. Stübi, 2009: Long-term changes in UT/LS ozone between the late 1970s and the 1990s deduced from the GASP and MOZAIC aircraft programs and from ozonesondes. *Atmos. Chem. Phys.*, **9**, 5343–5369.
- Schneider, T., P. A. O’Gorman, and X. J. Levine, 2010: Water vapour and the dynamics of climate changes. *Rev. Geophys.*, RG3001.
- Schneidereit, A., R. Blender, K. Fraedrich, and F. Lunkeit, 2007: Icelandic climate and north Atlantic cyclones in ERA-40 reanalyses. *Meteorol. Z.*, **16**, 17–23.
- Schwartz, R. D., 2005: Global dimming: Clear-sky atmospheric transmission from astronomical extinction measurements. *J. Geophys. Res. Atmos.*, **110**.
- Scinocca, J. F., D. B. Stephenson, T. C. Bailey, and J. Austin, 2010: Estimates of past and future ozone trends from multimodel simulations using a flexible smoothing spline methodology. *J. Geophys. Res. Atmos.*, **115**.
- Screen, J. A., and I. Simmonds, 2011: Erroneous Arctic temperature trends in the ERA-40 reanalysis: A closer look. *J. Clim.*, **24**, 2620–2627.

- Seidel, D. J., and J. R. Lanzante, 2004: An assessment of three alternatives to linear trends for characterizing global atmospheric temperature changes. *J. Geophys. Res. Atmos.*, **109**, D14108.
- Seidel, D. J., and W. J. Randel, 2007: Recent widening of the tropical belt: Evidence from tropopause observations. *J. Geophys. Res. Atmos.*, **112**, D20113.
- Seidel, D. J., Q. Fu, W. J. Randel, and T. J. Reichler, 2008: Widening of the tropical belt in a changing climate. *Nature Geosci.*, **1**, 21–24.
- Seidel, D. J., N. P. Gillett, J. R. Lanzante, K. P. Shine, and P. W. Thorne, 2011: Stratospheric temperature trends: Our evolving understanding. *Clim. Change*, **2**, 592–616.
- Sen Roy, S., 2009: A spatial analysis of extreme hourly precipitation patterns in India. *Int. J. Climatol.*, **29**, 345–355.
- Sen Roy, S., and R. C. Balling, 2005: Analysis of trends in maximum and minimum temperature, diurnal temperature range, and cloud cover over India. *Geophys. Res. Lett.*, **32**, L12702.
- Sen Roy, S., and M. Rouault, 2013: Spatial patterns of seasonal scale trends in extreme hourly precipitation in South Africa. *Appl. Geogr.*, **39**, 151–157.
- Seneviratne, S. I., et al., 2010: Investigating soil moisture-climate interactions in a changing climate: A review. *Earth Sci. Rev.*, **99**, 125–161.
- Seneviratne, S. I., et al., 2012: Changes in climate extremes and their impacts on the natural physical environment. In: *IPCC Special Report on Extremes*, 109–230.
- Serquet, G., C. Marty, J. P. Duxley, and M. Rebetez, 2011: Seasonal trends and temperature dependence of the snowfall/precipitation-day ratio in Switzerland. *Geophys. Res. Lett.*, **38**, L07703.
- Shaw, S. B., A. A. Royem, and S. J. Riha, 2011: The relationship between extreme hourly precipitation and surface temperature in different hydroclimatic regions of the United States. *J. Hydrometeor.*, **12**, 319–325.
- Sheffield, J., and E. F. Wood, 2008: Global trends and variability in soil moisture and drought characteristics, 1950–2000, from observation-driven simulations of the terrestrial hydrologic cycle. *J. Clim.*, **21**, 432–458.
- Sheffield, J., E. Wood, and M. Roderick, 2012: Little change in global drought over the past 60 years. *Nature*, **491**, 435–.
- Sheffield, J., K. Andreidis, E. Wood, and D. Lettenmaier, 2009: Global and continental drought in the second half of the twentieth century: Severity-area-duration analysis and temporal variability of large-scale events. *J. Clim.*, **22**, 1962–1981.
- Shekar, M., H. Chand, S. Kumar, K. Srinivasan, and A. Ganju, 2010: Climate change studies in the western Himalaya. *Ann. Glaciol.*, **51**, 105–112.
- Sherwood, S. C., R. Roca, and T. M. Weckwerth, 2010: Tropospheric water vapor, convection, and climate. *Rev. Geophys.*, **48**, RG2001.
- Sherwood, S. C., C. L. Meyer, R. J. Allen, and H. A. Titchner, 2008: Robust tropospheric warming revealed by iteratively homogenized radiosonde data. *J. Clim.*, **21**, 5336–5350.
- Shi, G. Y., et al., 2008: Data quality assessment and the long-term trend of ground solar radiation in China. *J. Appl. Meteor. Climatol.*, **47**, 1006–1016.
- Shi, L., and J. J. Bates, 2011: Three decades of intersatellite-calibrated High-Resolution Infrared Radiation Sounder upper tropospheric water vapor. *J. Geophys. Res. Atmos.*, **116**, D04108.
- Shiklomanov, A. I., R. B. Lammers, M. A. Rawlins, L. C. Smith, and T. M. Pavelsky, 2007: Temporal and spatial variations in maximum river discharge from a new Russian data set. *J. Geophys. Res. Biogeosci.*, **112**.
- Shiklomanov, I. A., V. Y. Georgievskii, V. I. Babkin, and Z. A. Balonishnikova, 2010: Research problems of formation and estimation of water resources and water availability changes of the Russian Federation. *Russ. Meteorol. Hydrol.*, **35**, 13–19.
- Shiu, C. J., S. C. Liu, and J. P. Chen, 2009: Diurnally asymmetric trends of temperature, humidity, and precipitation in Taiwan. *J. Clim.*, **22**, 5635–5649.
- Sillmann, J., M. Croci-Maspoli, M. Kallache, and R. W. Katz, 2011: Extreme cold winter temperatures in Europe under the influence of North Atlantic atmospheric blocking. *J. Clim.*, **24**, 5899–5913.
- Simmons, A. J., K. M. Willett, P. D. Jones, P. W. Thorne, and D. P. Dee, 2010: Low-frequency variations in surface atmospheric humidity, temperature, and precipitation: Inferences from reanalyses and monthly gridded observational data sets. *J. Geophys. Res. Atmos.*, **115**, D01110.
- Simolo, C., M. Brunetti, M. Maugeri, and T. Nanni, 2011: Evolution of extreme temperatures in a warming climate. *Geophys. Res. Lett.*, **38**, 6.
- Simpson, I. J., et al., 2012: Long-term decline of global atmospheric ethane concentrations and implications for methane. *Nature*, **488**, 490–494.
- Skansi, M., et al., 2013: Warming and wetting signals emerging from analysis of changes in climate extreme indices over South America. *Global Planet. Change*, **100**, 295–307.
- Skeie, R. B., T. K. Berntsen, G. Myhre, K. Tanaka, M. M. Kvæleåg, and C. R. Hoyle, 2011: Anthropogenic radiative forcing time series from pre-industrial times until 2010. *Atmos. Chem. Phys.*, **11**, 11827–11857.
- Smith, L. C., T. Pavelsky, G. MacDonald, I. A. Shiklomanov, and R. Lammers, 2007: Rising minimum daily flows in northern Eurasian rivers suggest a growing influence of groundwater in the high-latitude water cycle. *J. Geophys. Res.*, **112**, G04S47.
- Smith, T. M., and R. W. Reynolds, 2002: Bias corrections for historical sea surface temperatures based on marine air temperatures. *J. Clim.*, **15**, 73–87.
- Smith, T. M., T. C. Peterson, J. H. Lawrimore, and R. W. Reynolds, 2005: New surface temperature analyses for climate monitoring. *Geophys. Res. Lett.*, **32**, L14712.
- Smith, T. M., R. W. Reynolds, T. C. Peterson, and J. Lawrimore, 2008: Improvements to NOAA's historical merged land-ocean surface temperature analysis (1880–2006). *J. Clim.*, **21**, 2283–2296.
- Smith, T. M., P. A. Arkin, L. Ren, and S. S. P. Shen, 2012: Improved reconstruction of global precipitation since 1900. *J. Atmos. Ocean. Technol.*, **29**, 1505–1517.
- Smits, A., A. Tank, and G. P. Konnen, 2005: Trends in storminess over the Netherlands, 1962–2002. *Int. J. Climatol.*, **25**, 1331–1344.
- Sohn, B. J., and S. C. Park, 2010: Strengthened tropical circulations in past three decades inferred from water vapor transport. *J. Geophys. Res. Atmos.*, **115**, D15112.
- Solomon, S., K. Rosenlof, R. Portmann, J. Daniel, S. Davis, T. Sanford, and G. Plattner, 2010: Contributions of stratospheric water vapor to decadal changes in the rate of global warming. *Science*, **327**, 1219–1223.
- Song, H., and M. H. Zhang, 2007: Changes of the boreal winter Hadley circulation in the NCEP-NCAR and ECMWF reanalyses: A comparative study. *J. Clim.*, **20**, 5191–5200.
- Soni, V. K., G. Pandithurai, and D. S. Pai, 2012: Evaluation of long-term changes of solar radiation in India. *Int. J. Climatol.*, **32**, 540–551.
- Sorteberg, A., and J. E. Walsh, 2008: Seasonal cyclone variability at 70 degrees N and its impact on moisture transport into the Arctic. *Tellus A*, **60**, 570–586.
- Sousa, P., R. Trigo, P. Aizpurua, R. Nieto, L. Gimeno, and R. Garcia-Herrera, 2011: Trends and extremes of drought indices throughout the 20th century in the Mediterranean. *Nat. Hazards Earth Syst. Sci.*, **11**, 33–51.
- Spencer, R. W., and J. R. Christy, 1992: Precision and radiosonde validation of satellite gridpoint temperature anomalies. 2. A tropospheric retrieval and trends during 1979–90. *J. Clim.*, **5**, 858–866.
- St. Jacques, J.-M., and D. Sauchyn, 2009: Increasing winter baseflow and mean annual streamflow from possible permafrost thawing in the Northwest Territories, Canada. *Geophys. Res. Lett.*, **36**, L01401.
- Stachnik, J. P., and C. Schumacher, 2011: A comparison of the Hadley circulation in modern reanalyses. *J. Geophys. Res. Atmos.*, **116**, D22102.
- Stahl, K., and L. M. Tallaksen, 2012: Filling the white space on maps of European runoff trends: Estimates from a multi-model ensemble. *Hydrol. Earth Syst. Sci. Discuss.*, **9**, 2005–2032.
- Stahl, K., et al., 2010: Streamflow trends in Europe: Evidence from a dataset of near-natural catchments. *Hydrol. Earth Syst. Sci.*, **14**, 2367–2382.
- Stanhill, G., and S. Cohen, 2001: Global dimming: A review of the evidence for a widespread and significant reduction in global radiation with discussion of its probable causes and possible agricultural consequences. *Agr. Forest Meteorol.*, **107**, 255–278.
- Steeneveld, G. J., A. A. M. Holtslag, R. T. McNider, and R. A. Pielke, 2011: Screen level temperature increase due to higher atmospheric carbon dioxide in calm and windy nights revisited. *J. Geophys. Res. Atmos.*, **116**.
- Stegall, S., and J. Zhang, 2012: Wind field climatology, changes, and extremes in the Chukchi-Beaufort Seas and Alaska North Slope during 1979–2009. *J. Clim.*, **25**, 8075–8089.
- Steig, E. J., D. P. Schneider, S. D. Rutherford, M. E. Mann, J. C. Comiso, and D. T. Shindell, 2009: Warming of the Antarctic ice-sheet surface since the 1957 International Geophysical Year. *Nature*, **460**, 766–766.
- Stenke, A., and V. Grewe, 2005: Simulation of stratospheric water vapor trends: Impact on stratospheric ozone chemistry. *Atmos. Chem. Phys.*, **5**, 1257–1272.
- Stephens, G. L., M. Wild, P. W. Stackhouse, T. L'Ecuyer, S. Kato, and D. S. Henderson, 2012a: The global character of the flux of downward longwave radiation. *J. Clim.*, **25**, 2329–2340.

- Stephens, G. L., et al., 2012b: An update on Earth's energy balance in light of the latest global observations. *Nature Geosci.*, **5**, 691–696.
- Stephenson, D. B., H. F. Diaz, and R. J. Murnane, 2008: Definition, diagnosis and origin of extreme weather and climate events. In: *Climate Extremes and Society* [R. J. Murnane, and H. F. Diaz (eds.)] Cambridge University Press, Cambridge, United Kingdom and New York, NY, USA, pp. 11–23.
- Stern, D. I., 2006: Reversal of the trend in global anthropogenic sulfur emissions. *Global Environ. Change Hum. Policy Dimens.*, **16**, 207–220.
- Stickler, A., et al., 2010: The Comprehensive Historical Upper-Air Network. *Bull. Am. Meteor. Soc.*, **91**, 741–751.
- Stjern, C. W., J. E. Kristjansson, and A. W. Hansen, 2009: Global dimming and global brightening - an analysis of surface radiation and cloud cover data in northern Europe. *Int. J. Climatol.*, **29**, 643–653.
- Stohl, A., et al., 2009: An analytical inversion method for determining regional and global emissions of greenhouse gases: Sensitivity studies and application to halocarbons. *Atmos. Chem. Phys.*, **15**, 1597–1620.
- Stohl, A., et al., 2010: Hydrochlorofluorocarbon and hydrofluorocarbon emissions in East Asia determined by inverse modeling. *Atmos. Chem. Phys.*, **10**, 3545–3560.
- Streets, D. G., Y. Wu, and M. Chin, 2006: Two-decadal aerosol trends as a likely explanation of the global dimming/brightening transition. *Geophys. Res. Lett.*, **33**, L15806.
- Streets, D. G., et al., 2009: Anthropogenic and natural contributions to regional trends in aerosol optical depth, 1980–2006. *J. Geophys. Res. Atmos.*, **114**, D00D18.
- Strong, C., and R. E. Davis, 2007: Winter jet stream trends over the Northern Hemisphere. *Q. J. R. Meteorol. Soc.*, **133**, 2109–2115.
- Strong, C., and R. E. Davis, 2008: Comment on "Historical trends in the jet streams" by Cristina L. Archer and Ken Caldeira. *Geophys. Res. Lett.*, **L24806**.
- Stubenrauch, C. J., et al., 2013: Assessment of global cloud datasets from satellite: Project and database initiated by the GEWEX radiation panel. *Bull. Am. Meteorol. Soc.*, **94**, 1031–1049.
- Sun, B. M., A. Reale, D. J. Seidel, and D. C. Hunt, 2010: Comparing radiosonde and COSMIC atmospheric profile data to quantify differences among radiosonde types and the effects of imperfect collocation on comparison statistics. *J. Geophys. Res. Atmos.*, **115**, D23104.
- Swart, N. C., and J. C. Fyfe, 2012: Observed and simulated changes in the Southern Hemisphere surface westerly wind-stress. *Geophys. Res. Lett.*, **39**, L16711.
- Syakila, A., and C. Kroeze, 2011: The global nitrous oxide budget revisited. *Greenhouse Gas Meas. Management*, **1**, 17–26.
- Takahashi, K., A. Montecinos, K. Goubanova, and B. Dewitte, 2011: ENSO regimes: Reinterpreting the canonical and Modoki El Niño. *Geophys. Res. Lett.*, **38**, L10704.
- Takeuchi, Y., Y. Endo, and S. Murakami, 2008: High correlation between winter precipitation and air temperature in heavy-snowfall areas in Japan. *Ann. Glaciol.*, **49**, 7–10.
- Tang, G., Y. Ding, S. Wang, G. Ren, H. Liu, and L. Zhang, 2010: Comparative analysis of China surface air temperature series for the past 100 years. *Adv. Climate Change Res.*, **1**, 11–19.
- Tang, W. J., K. Yang, J. Qin, C. C. K. Cheng, and J. He, 2011: Solar radiation trend across China in recent decades: a revisit with quality-controlled data. *Atmos. Chem. Phys.*, **11**, 393–406.
- Tank, A., et al., 2006: Changes in daily temperature and precipitation extremes in central and south Asia. *J. Geophys. Res. Atmos.*, **111**, D16105.
- Tans, P., 2009: An accounting of the observed increase in oceanic and atmospheric CO₂ and an outlook for the future. *Oceanography*, **26**, 35–35.
- Tarasova, O. A., I. A. Senik, M. G. Sosonkin, J. Cui, J. Staehelin, and A. S. H. PrÃ©vÃ©t, 2009: Surface ozone at the Caucasian site Kislovodsk High Mountain Station and the Swiss Alpine site Jungfraujoch: Data analysis and trends (1990–2006). *Atmos. Chem. Phys.*, **9**, 4157–4175.
- Tegtmeier, S., K. Kruger, I. Wohltmann, K. Schoellhammer, and M. Rex, 2008: Variations of the residual circulation in the Northern Hemispheric winter. *J. Geophys. Res. Atmos.*, **113**, D16109.
- Teuling, A. J., et al., 2009: A regional perspective on trends in continental evaporation. *Geophys. Res. Lett.*, **36**, L02404.
- Thomas, B., E. Kent, V. Swail, and D. Berry, 2008: Trends in ship wind speeds adjusted for observation method and height. *Int. J. Climatol.*, **28**, 747–763.
- Thomas, G. E., et al., 2010: Validation of the GRAPE single view aerosol retrieval for ATSR-2 and insights into the long term global AOD trend over the ocean. *Atmos. Chem. Phys.*, **10**, 4849–4866.
- Thompson, D. W. J., and J. M. Wallace, 1998: The Arctic Oscillation signature in the wintertime geopotential height and temperature fields. *Geophys. Res. Lett.*, **25**, 1297–1300.
- Thompson, D. W. J., and J. M. Wallace, 2000: Annular modes in the extratropical circulation. Part I: Month-to-month variability. *J. Clim.*, **13**, 1000–1016.
- Thompson, D. W. J., J. J. Kennedy, J. M. Wallace, and P. D. Jones, 2008: A large discontinuity in the mid-twentieth century in observed global-mean surface temperature. *Nature*, **453**, 646–649.
- Thompson, D. W. J., et al., 2012: The mystery of recent stratospheric temperature trends. *Nature*, **491**, 692–697.
- Thorne, P. W., 2008: Arctic tropospheric warming amplification? *Nature*, **455**, E1–E2.
- Thorne, P. W., and R. S. Vose, 2010: Reanalyses suitable for characterizing long-term trends: Are They Really Achievable? *Bull. Am. Meteor. Soc.*, **91**, 353–.
- Thorne, P. W., D. E. Parker, S. F. B. Tett, P. D. Jones, M. McCarthy, H. Coleman, and P. Brohan, 2005: Revisiting radiosonde upper air temperatures from 1958 to 2002. *J. Geophys. Res. Atmos.*, **110**.
- Thorne, P. W., et al., 2011: A quantification of uncertainties in historical tropical tropospheric temperature trends from radiosondes. *J. Geophys. Res. Atmos.*, **116**, D12116.
- Tietavainen, H., H. Tuomenvirta, and A. Venalainen, 2010: Annual and seasonal mean temperatures in Finland during the last 160 years based on gridded temperature data. *Int. J. Climatol.*, **30**, 2247–2256.
- Titchner, H. A., P. W. Thorne, M. P. McCarthy, S. F. B. Tett, L. Haimberger, and D. E. Parker, 2009: Critically reassessing tropospheric temperature trends from radiosondes using realistic validation experiments. *J. Clim.*, **22**, 465–485.
- Tokinaga, H., and S.-P. Xie, 2011a: Wave and anemometer-based sea surface wind (WASWind) for climate change analysis. *J. Clim.*, **24**, 267–285.
- Tokinaga, H., and S. P. Xie, 2011b: Weakening of the equatorial Atlantic cold tongue over the past six decades. *Nature Geosci.*, **4**, 222–226.
- Tokinaga, H., S. P. Xie, A. Timmermann, S. McGregor, T. Ogata, H. Kubota, and Y. M. Okumura, 2012: Regional patterns of tropical Indo-Pacific climate change: Evidence of the Walker circulation weakening. *J. Clim.*, **25**, 1689–1710.
- Toreti, A., E. Xoplaki, D. Maraun, F. G. Kuglitsch, H. Wanner, and J. Luterbacher, 2010: Characterisation of extreme winter precipitation in Mediterranean coastal sites and associated anomalous atmospheric circulation patterns. *Nat. Hazards Earth Syst. Sci.*, **10**, 1037–1050.
- Tørseth, K., et al., 2012: Introduction to the European Monitoring and Evaluation Programme (EMEP) and observed atmospheric composition change during 1972–2009. *Atmos. Chem. Phys. Discuss.*, **12**, 1733–1820.
- Trenberth, K., 2011: Changes in precipitation with climate change. *Clim. Res.*, **47**, 123–138.
- Trenberth, K., and J. Fasullo, 2012a: Climate extremes and climate change: The Russian heat wave and other climate extremes of 2010. *J. Geophys. Res. Atmos.*, **117**, D17103.
- Trenberth, K. E., 1984: Signal versus noise in the Southern Oscillation. *Mon. Weather Rev.*, **112**, 326–332.
- Trenberth, K. E., 1997: The definition of El Niño. *Bull. Am. Meteor. Soc.*, **78**, 2771–2777.
- Trenberth, K. E., and D. A. Paolino, 1980: The Northern Hemisphere Sea-Level Pressure Data Set – Trends, errors, and discontinuities. *Mon. Weather Rev.*, **108**, 855–872.
- Trenberth, K. E., and J. W. Hurrell, 1994: Decadal atmosphere-ocean variations in the Pacific. *Clim. Dyn.*, **9**, 303–319.
- Trenberth, K. E., and T. J. Hoar, 1996: The 1990–1995 El Niño Southern Oscillation event: Longest on record. *Geophys. Res. Lett.*, **23**, 57–60.
- Trenberth, K. E., and D. P. Stepaniak, 2001: Indices of El Niño evolution. *J. Clim.*, **14**, 1697–1701.
- Trenberth, K. E., and D. J. Shea, 2006: Atlantic hurricanes and natural variability in 2005. *Geophys. Res. Lett.*, **33**, L12704.
- Trenberth, K. E., and J. T. Fasullo, 2010: Climate change tracking Earth's energy. *Science*, **328**, 316–317.
- Trenberth, K. E., and J. T. Fasullo, 2012b: Tracking Earth's energy: From El Niño to global warming. *Surv. Geophys.*, **33**, 413–426.
- Trenberth, K. E., J. T. Fasullo, and J. Kiehl, 2009: Earth's Global energy budget. *Bull. Am. Meteor. Soc.*, **90**, 311.
- Trenberth, K. E., J. T. Fasullo, and J. Mackaro, 2011: Atmospheric moisture transports from ocean to land and global energy flows in reanalyses. *J. Clim.*, **24**, 4907–4924.

- Trenberth, K. E., et al., 2007: Observations: Surface and atmospheric climate change. In: *Climate Change 2007: The Physical Science Basis. Contribution of Working Group I to the Fourth Assessment Report of the Intergovernmental Panel on Climate Change* [Solomon, S., D. Qin, M. Manning, Z. Chen, M. Marquis, K. B. Averyt, M. Tignor and H. L. Miller (eds.)]. Cambridge University Press, Cambridge, United Kingdom and New York, NY, USA.
- Trewin, B., 2012: A daily homogenized temperature data set for Australia. *Int. J. Climatol.*, **33**, 1510–1529.
- Trnka, M., J. Kysely, M. Mozny, and M. Dubrovsky, 2009: Changes in Central-European soil-moisture availability and circulation patterns in 1881–2005. *Int. J. Climatol.*, **29**, 655–672.
- Troccoli, A., K. Muller, P. Coppin, R. Davy, C. Russell, and A. L. Hirsch, 2012: Long-term wind speed trends over Australia. *J. Climate*, **25**, 170–183.
- Troup, A. J., 1965: Southern Oscillation. *Q. J. R. Meteorol. Soc.*, **91**, 490–.
- Tryhorn, L., and J. Risbey, 2006: On the distribution of heat waves over the Australian region. *Aust. Meteorol. Mag.*, **55**, 169–182.
- Tung, K.-K., and J. Zhou, 2013: Using data to attribute episodes of warming and cooling in instrumental records. *Proc. Natl. Acad. Sci. U.S.A.*, **110**, 2058–2063.
- Turner, J., et al., 2005: Antarctic climate change during the last 50 years. *Int. J. Climatol.*, **25**, 279–294.
- Ulbrich, U., G. C. Leckebusch, and J. G. Pinto, 2009: Extra-tropical cyclones in the present and future climate: A review. *Theor. Appl. Climatol.*, **96**, 117–131.
- Uppala, S. M., et al., 2005: The ERA-40 re-analysis. *Q. J. R. Meteorol. Soc.*, **131**, 2961–3012.
- Usbeck, T., T. Wohlgemuth, C. Pfister, R. Volz, M. Beniston, and M. Dobbertin, 2010: Wind speed measurements and forest damage in Canton Zurich (Central Europe) from 1891 to winter 2007. *Int. J. Climatol.*, **30**, 347–358.
- Utsumi, N., S. Seto, S. Kanae, E. Maeda, and T. Oki, 2011: Does higher surface temperature intensify extreme precipitation? *Geophys. Res. Lett.*, **38**, L16708.
- van den Besselaar, E. J. M., A. M. G. Klein Tank, and T. A. Buishand, 2012: Trends in European precipitation extremes over 1951–2010. *Int. J. Climatol.*, **33**, 2682–2689.
- van der Schrier, G., A. van Oldenborgh, and G. J. van Oldenborgh, 2011: The construction of a Central Netherlands temperature. *Clim. Past*, **7**, 527–542.
- van der Schrier, G., J. Barichivich, K. R. Briffa, and P. D. Jones, 2013: A scPDSI-based global dataset of dry and wet spells for 1901–2009. *J. Geophys. Res. Atmos.*, **118**, 4025–4048.
- van Haren, R., G. J. van Oldenborgh, G. Lenderink, M. Collins, and W. Hazleger, 2012: SST and circulation trend biases cause an underestimation of European precipitation trends. *Clim. Dyn.*, **40**, 1–20.
- van Heerwaarden, C. C., J. V. G. de Arellano, and A. J. Teuling, 2010: Land-atmosphere coupling explains the link between pan evaporation and actual evapotranspiration trends in a changing climate. *Geophys. Res. Lett.*, **37**, L21401.
- van Ommen, T. D., and V. Morgan, 2010: Snowfall increase in coastal East Antarctica linked with southwest Western Australian drought. *Nature Geosci.*, **3**, 267–272.
- Vautard, R., P. Yiou, and G. J. van Oldenborgh, 2009: Decline of fog, mist and haze in Europe over the past 30 years. *Nature Geosci.*, **2**, 115–119.
- Vautard, R., J. Cattiaux, P. Yiou, J. N. The paut, and P. Ciais, 2010: Northern Hemisphere atmospheric stilling partly attributed to an increase in surface roughness. *Nature Geosci.*, **3**, 756–761.
- Vautard, R., et al., 2007: Summertime European heat and drought waves induced by wintertime Mediterranean rainfall deficit. *Geophys. Res. Lett.*, **34**, L07711.
- Vecchi, G. A., and B. J. Soden, 2007: Global warming and the weakening of the tropical circulation. *J. Clim.*, **20**, 4316–4340.
- Vecchi, G. A., and T. R. Knutson, 2008: On estimates of historical north Atlantic tropical cyclone activity. *J. Clim.*, **21**, 3580–3600.
- Vecchi, G. A., and T. R. Knutson, 2011: Estimating annual numbers of Atlantic hurricanes missing from the HURDAT database (1878–1965) using ship track density. *J. Clim.*, **24**, 1736–1746.
- Vecchi, G. A., B. J. Soden, A. T. Wittenberg, I. M. Held, A. Leetmaa, and M. J. Harrison, 2006: Weakening of tropical Pacific atmospheric circulation due to anthropogenic forcing. *Nature*, **441**, 73–76.
- Velders, G., S. Andersen, J. Daniel, D. Fahey, and M. McFarland, 2007: The importance of the Montreal Protocol in protecting climate. *Proc. Natl. Acad. Sci. U.S.A.*, **104**, 4814–4819.
- Velders, G., D. Fahey, J. Daniel, M. McFarland, and S. Andersen, 2009: The large contribution of projected HFC emissions to future climate forcing. *Proc. Natl. Acad. Sci. U.S.A.*, **106**, 10949–10954.
- Venema, V. K. C., et al., 2012: Benchmarking homogenization algorithms for monthly data. *Clim. Past*, **8**, 89–115.
- Verbout, S., H. Brooks, L. Leslie, and D. Schultz, 2006: Evolution of the US tornado database: 1954–2003. *Weather Forecast.*, **21**, 86–93.
- Vicente-Serrano, S. M., S. Begueria, and J. I. Lopez-Moreno, 2010: A multiscalar drought index sensitive to global warming: The Standardized Precipitation Evapotranspiration Index. *J. Clim.*, **23**, 1696–1718.
- Vidal, J., E. Martin, L. Franchisteguy, F. Habets, J. Soubeyroux, M. Blanchard, and M. Baillon, 2010: Multilevel and multiscale drought reanalysis over France with the Safran-Isba-Modcou hydrometeorological suite. *Hydroclim. Earth Syst. Sci.*, **14**, 459–478.
- Vilibic, I., and J. Sepic, 2010: Long-term variability and trends of sea level storminess and extremes in European Seas. *Global Planet. Change*, **71**, 1–12.
- Villarini, G., J. Smith, and G. Vecchi, 2013: Changing frequency of heavy rainfall over the central United States. *J. Clim.*, **26**, 351–357.
- Vincent, L., et al., 2011: Observed trends in indices of daily and extreme temperature and precipitation for the countries of the western Indian Ocean, 1961–2008. *J. Geophys. Res. Atmos.*, **116**, D10108.
- Vincent, L. A., X. L. L. Wang, E. J. Milewska, H. Wan, F. Yang, and V. Swail, 2012: A second generation of homogenized Canadian monthly surface air temperature for climate trend analysis. *J. Geophys. Res. Atmos.*, **117**, D18110.
- Visbeck, M., 2009: A station-based Southern Annular Mode Index from 1884 to 2005. *J. Clim.*, **22**, 940–950.
- Volz, A., and D. Kley, 1988: Evaluation of the Montsouris series of ozone measurements made in the 19th century. *Nature*, **332**, 240–242.
- Vömel, H., D. E. David, and K. Smith, 2007a: Accuracy of tropospheric and stratospheric water vapor measurements by the cryogenic frost point hygrometer: Instrumental details and observations. *J. Geophys. Res. Atmos.*, **112**, D08305.
- Vömel, H., et al., 2007b: Validation of Aura Microwave Limb Sounder water vapor by balloon-borne cryogenic frost point hygrometer measurements. *J. Geophys. Res. Atmos.*, **112**, D24S37.
- von Clarmann, T., et al., 2009: Retrieval of temperature, H_2O , O_3 , HNO_3 , CH_4 , N_2O , $ClONO_2$, and ClO from MIPAS reduced resolution nominal mode limb emission measurements. *Atmos. Meas. Tech.*, **2**, 159–175.
- von Schuckmann, K., and P.-Y. Le Traon, 2011: How well can we derive global ocean indicators from Argo data? *Ocean Sci.*, **7**, 783–791.
- Von Storch, H., 1999: Misuses of statistical analysis in climate research. *Analysis of Climate Variability: Applications of Statistical Techniques*, 2nd edition [H. Von Storch and A. Navarra (eds.)]. Springer-Verlag, New York, and Heidelberg, Germany, pp. 11–26.
- Von Storch, H., and F. W. Zwiers, 1999: *Statistical Analysis in Climate Research*. Cambridge University Press, Cambridge, United Kingdom and New York, NY, USA, 484 pp.
- Vose, R. S., D. R. Easterling, and B. Gleason, 2005a: Maximum and minimum temperature trends for the globe: An update through 2004. *Geophys. Res. Lett.*, **32**, L23822.
- Vose, R. S., D. Wuertz, T. C. Peterson, and P. D. Jones, 2005b: An intercomparison of trends in surface air temperature analyses at the global, hemispheric, and grid-box scale. *Geophys. Res. Lett.*, **32**, L18718.
- Vose, R. S., S. Applequist, M. J. Menne, C. N. Williams, Jr., and P. Thorne, 2012a: An intercomparison of temperature trends in the US Historical Climatology Network and recent atmospheric reanalyses. *Geophys. Res. Lett.*, **39**, L10703.
- Vose, R. S., Oak Ridge National Laboratory. Environmental Sciences Division., U.S. Global Change Research Program, United States. Dept. of Energy. Office of Health and Environmental Research., Carbon Dioxide Information Analysis Center (U.S.), and Martin Marietta Energy Systems Inc., 1992: *The Global Historical Climatology Network: Long-Term Monthly Temperature, Precipitation, Sea Level Pressure, and Station Pressure Data*. Carbon Dioxide Information Analysis Center. Available to the public from N.T.I.S., 1 v. (various pagings)
- Vose, R. S., et al., 2012b: NOAA's Merged Land-Ocean Surface Temperature Analysis. *Bull. Am. Meteorol. Soc.*, **93**, 1677–1685.
- Wacker, S., J. Grobner, K. Hocke, N. Kampfer, and L. Vuilleumier, 2011: Trend analysis of surface cloud-free downwelling long-wave radiation from four Swiss sites. *J. Geophys. Res. Atmos.*, **116**, 13.
- Wallace, J. M., and D. S. Gutzler, 1981: Teleconnections in the geopotential height field during the Northern Hemisphere winter. *Mon. Weather Rev.*, **109**, 784–812.
- Wan, H., X. L. Wang, and V. R. Swail, 2010: Homogenization and trend analysis of Canadian near-surface wind speeds. *J. Clim.*, **23**, 1209–1225.

- Wan, H., X. Zhang, F. Zwiers, S. Emori, and H. Shiogama, 2013: Effect of data coverage on the estimation of mean and variability of precipitation at global and regional scales. *J. Geophys. Res.*, **118**, 534–546.
- Wang, B., J. Liu, H. J. Kim, P. J. Webster, and S. Y. Yim, 2012a: Recent change of the global monsoon precipitation (1979–2008). *Clim. Dyn.*, **39**, 1123–1135.
- Wang, H., et al., 2012b: Extreme climate in China: Facts, simulation and projection. *Meteorol. Z.*, **21**, 279–304.
- Wang, J. H., and L. Y. Zhang, 2008: Systematic errors in global radiosonde precipitable water data from comparisons with ground-based GPS measurements. *J. Clim.*, **21**, 2218–2238.
- Wang, J. H., and L. Y. Zhang, 2009: Climate applications of a global, 2-hourly atmospheric precipitable water dataset derived from IGS tropospheric products. *J. Geodes.*, **83**, 209–217.
- Wang, J. H., L. Y. Zhang, A. Dai, T. Van Hove, and J. Van Baelen, 2007: A near-global, 2-hourly data set of atmospheric precipitable water from ground-based GPS measurements. *J. Geophys. Res. Atmos.*, **112**, D11107.
- Wang, J. S., D. J. Seidel, and M. Free, 2012c: How well do we know recent climate trends at the tropical tropopause? *J. Geophys. Res. Atmos.*, **117**, D09118.
- Wang, K., R. E. Dickinson, and S. Liang, 2009a: Clear sky visibility has decreased over land globally from 1973 to 2007. *Science*, **323**, 1468–1470.
- Wang, K., H. Ye, F. Chen, Y. Z. Xiong, and C. P. Wang, 2012d: Urbanization effect on the diurnal temperature range: Different roles under solar dimming and brightening. *J. Clim.*, **25**, 1022–1027.
- Wang, K. C., and S. L. Liang, 2009: Global atmospheric downward longwave radiation over land surface under all-sky conditions from 1973 to 2008. *J. Geophys. Res. Atmos.*, **114**, D19101.
- Wang, K. C., R. E. Dickinson, and S. L. Liang, 2009b: Clear sky visibility has decreased over land globally from 1973 to 2007. *Science*, **323**, 1468–1470.
- Wang, K. C., R. E. Dickinson, M. Wild, and S. L. Liang, 2010: Evidence for decadal variation in global terrestrial evapotranspiration between 1982 and 2002: 2. Results. *J. Geophys. Res. Atmos.*, **115**, D20113.
- Wang, K. C., R. E. Dickinson, M. Wild, and S. Liang, 2012e: Atmospheric impacts on climatic variability of surface incident solar radiation. *Atmos. Chem. Phys.*, **12**, 9581–9592.
- Wang, K. C., R. E. Dickinson, L. Su, and K. E. Trenberth, 2012f: Contrasting trends of mass and optical properties of aerosols over the Northern Hemisphere from 1992 to 2011. *Atmos. Chem. Phys.*, **12**, 9387–9398.
- Wang, L. K., C. Z. Zou, and H. F. Qian, 2012g: Construction of stratospheric temperature data records from Stratospheric Sounding Units. *J. Clim.*, **25**, 2931–2946.
- Wang, X., H. Wan, and V. Swail, 2006a: Observed changes in cyclone activity in Canada and their relationships to major circulation regimes. *J. Clim.*, **19**, 896–915.
- Wang, X., B. Trewin, Y. Feng, and D. Jones, 2013: Historical changes in Australian temperature extremes as inferred from extreme value distribution analysis. *Geophys. Res. Lett.*, **40**, 573–578.
- Wang, X., Y. Feng, G. P. Compo, V. R. Swail, F. W. Zwiers, R. J. Allan, and P. D. Sardeshmukh, 2012: Trends and low frequency variability of extra-tropical cyclone activity in the ensemble of twentieth century reanalysis. *Clim. Dyn.*, **40**, 2775–2800.
- Wang, X., et al., 2011: Trends and low-frequency variability of storminess over western Europe, 1878–2007. *Clim. Dyn.*, **37**, 2355–2371.
- Wang, X., L. L. V. R. Swail, and F. W. Zwiers, 2006b: Climatology and changes of extra-tropical cyclone activity: Comparison of ERA-40 with NCEP-NCAR reanalysis for 1958–2001. *J. Clim.*, **19**, 3145–3166.
- Wang, X. L. L., F. W. Zwiers, V. R. Swail, and Y. Feng, 2009c: Trends and variability of storminess in the Northeast Atlantic region, 1874–2007. *Clim. Dyn.*, **33**, 1179–1195.
- Wang, X. M., P. M. Zhai, and C. C. Wang, 2009d: Variations in extratropical cyclone activity in northern East Asia. *Adv. Atmos. Sci.*, **26**, 471–479.
- Warren, S. G., R. M. Eastman, and C. J. Hahn, 2007: A survey of changes in cloud cover and cloud types over land from surface observations, 1971–96. *J. Clim.*, **20**, 717–738.
- Weaver, S. J., 2012: Factors associated with decadal variability in Great Plains summertime surface temperatures. *J. Clim.*, **26**, 343–350.
- Weber, M., W. Steinbrecht, C. Long, V. E. Fioletov, S. H. Frith, R. Stolarski, and P. A. Newman, 2012: Stratospheric ozone [in "State of the Climate in 2011"]. *Bull. Am. Met. Soc.*, **93**, S46–S44.
- Weinkle, J., R. Maue, and R. Pielke, 2012: Historical global tropical cyclone landfalls. *J. Clim.*, **25**, 4729–4735.
- Weinstock, E. M., et al., 2009: Validation of the Harvard Lyman-alpha in situ water vapor instrument: Implications for the mechanisms that control stratospheric water vapor. *J. Geophys. Res. Atmos.*, **114**.
- Weiss, R., J. Muhle, P. Salameh, and C. Harth, 2008: Nitrogen trifluoride in the global atmosphere. *Geophys. Res. Lett.*, **35**, L20821.
- Wells, N., S. Goddard, and M. J. Hayes, 2004: A self-calibrating Palmer Drought Severity Index. *J. Clim.*, **17**, 2335–2351.
- Wentz, F., C. Gentemann, D. Smith, and D. Chelton, 2000: Satellite measurements of sea surface temperature through clouds. *Science*, **288**, 847–850.
- Wentz, F. J., L. Ricciardulli, K. Hilburn, and C. Mears, 2007: How much more rain will global warming bring? *Science*, **317**, 233–235.
- Werner, P. C., F. W. Gerstengarbe, and F. Wechsung, 2008: Grosswetterlagen and precipitation trends in the Elbe River catchment. *Meteorol. Z.*, **17**, 61–66.
- Westra, S., and S. Sisson, 2011: Detection of non-stationarity in precipitation extremes using a max-stable process model. *J. Hydrol.*, **406**, 119–128.
- Westra, S., L. Alexander, and F. Zwiers, 2013: Global increasing trends in annual maximum daily precipitation. *J. Clim.*, **26**, 3904–3918.
- Wibig, J., 2008: Cloudiness variations in Lodz in the second half of the 20th century. *Int. J. Climatol.*, **28**, 479–491.
- Wickham, C., et al., 2013: Influence of urban heating on the global temperature land average using rural sites identified from MODIS classifications. *Geoinfor Geostat: An Overview*, **1**, 1:2. doi:10.4172/gigs.1000104.
- Wielicki, B. A., B. R. Barkstrom, E. F. Harrison, R. B. Lee, G. L. Smith, and J. E. Cooper, 1996: Clouds and the Earth's radiant energy system (CERES): An Earth observing system experiment. *Bull. Am. Meteor. Soc.*, **77**, 853–868.
- Wielicki, B. A., et al., 2002: Evidence for large decadal variability in the tropical mean radiative energy budget. *Science*, **295**, 841–844.
- Wilby, R. L., P. D. Jones, and D. H. Lister, 2011: Decadal variations in the nocturnal heat island of London. *Weather*, **66**, 59–64.
- Wild, M., 2009: Global dimming and brightening: A review. *J. Geophys. Res. Atmos.*, **114**, D00D16.
- Wild, M., 2012: Enlightening global dimming and brightening. *Bull. Am. Meteor. Soc.*, **93**, 27–37.
- Wild, M., A. Ohmura, and K. Makowski, 2007: Impact of global dimming and brightening on global warming. *Geophys. Res. Lett.*, **34**, L04702.
- Wild, M., J. Grieser, and C. Schaer, 2008: Combined surface solar brightening and increasing greenhouse effect support recent intensification of the global land-based hydrological cycle. *Geophys. Res. Lett.*, **35**, L17706.
- Wild, M., A. Ohmura, H. Gilgen, and D. Rosenfeld, 2004: On the consistency of trends in radiation and temperature records and implications for the global hydrological cycle. *Geophys. Res. Lett.*, **31**, L11201.
- Wild, M., A. Ohmura, H. Gilgen, E. Roeckner, M. Giorgetta, and J. J. Morcrette, 1998: The disposition of radiative energy in the global climate system: GCM-calculated versus observational estimates. *Clim. Dyn.*, **14**, 853–869.
- Wild, M., D. Folini, C. Schär, N. Loeb, E. G. Dutton, and G. König-Langlo, 2013: The global energy balance from a surface perspective. *Clim. Dyn.*, **40**, 3107–3134.
- Wild, M., B. Truesell, A. Ohmura, C. N. Long, G. König-Langlo, E. G. Dutton, and A. Tsvetkov, 2009: Global dimming and brightening: An update beyond 2000. *J. Geophys. Res. Atmos.*, **114**, D00d13.
- Wild, M., et al., 2005: From dimming to brightening: Decadal changes in solar radiation at Earth's surface. *Science*, **308**, 847–850.
- Wilks, D. S., 2006: *Statistical Methods in the Atmospheric Sciences*, 2nd edition. Elsevier, Philadelphia, 627 pp.
- Willett, K. M., P. D. Jones, N. P. Gillett, and P. W. Thorne, 2008: Recent Changes in Surface Humidity: Development of the HadCRUH dataset. *J. Clim.*, **21**, 5364–5383.
- Willett, K. M., P. D. Jones, P. W. Thorne, and N. P. Gillett, 2010: A comparison of large scale changes in surface humidity over land in observations and CMIP3 general circulation models. *Environ. Res. Lett.*, **5**.
- Willett, K. M., et al., 2013: HadISDH: an updateable land surface specific humidity product for climate monitoring. *Clim. Past*, **9**, 657–677.
- Williams, C. N., M. J. Menne, and P. W. Thorne, 2012: Benchmarking the performance of pairwise homogenization of surface temperatures in the United States. *J. Geophys. Res. Atmos.*, **117**.
- Willson, R. C., and A. V. Mordvinov, 2003: Secular total solar irradiance trend during solar cycles 21–23. *Geophys. Res. Lett.*, **30**, 1199.
- Winkler, P., 2009: Revision and necessary correction of the long-term temperature series of Hohenpeissenberg, 1781–2006. *Theor. Appl. Climatol.*, **98**, 259–268.

- Wong, T., B. A. Wielicki, R. B. Lee, G. L. Smith, K. A. Bush, and J. K. Willis, 2006: Reexamination of the observed decadal variability of the earth radiation budget using altitude-corrected ERBE/ERBS nonscanner WFOV data. *J. Clim.*, **19**, 4028–4040.
- Wood, S. N., 2006: *Generalized Additive Models: An Introduction with R*. CRC/Chapman & Hall, Boca Raton, FL, USA.
- Woodruff, S. D., et al., 2011: ICOADS Release 2.5: Extensions and enhancements to the Surface Marine Meteorological Archive. *Int. J. Climatol.*, **31**, 951–967.
- Worden, H. M., et al., 2013: Decadal record of satellite carbon monoxide observations. *Atmos. Chem. Phys.*, **13**, 837–850.
- Worton, D., et al., 2007: Atmospheric trends and radiative forcings of CF4 and C2F6 inferred from firm air. *Environ. Sci. Technol.*, **41**, 2184–2189.
- Worton, D. R., et al., 2012: Evidence from firm air for recent decreases in non-methane hydrocarbons and a 20th century increase in nitrogen oxides in the northern hemisphere. *Atmos. Environ.*, **54**, 592–602.
- Wu, Z., N. E. Huang, S. R. Long, and C.-K. Peng, 2007: On the trend, detrending, and variability of nonlinear and nonstationary time series. *Proc. Natl. Acad. Sci. U.S.A.*, **104**, 14889–14894.
- Wu, Z., N. E. Huang, J. M. Wallace, B. V. Smoliak, and X. Chen, 2011: On the time-varying trend in global-mean surface temperature. *Clim. Dyn.*, **37**, 759–773.
- Xavier, P. K., V. O. John, S. A. Buehler, R. S. Ajayamohan, and S. Sijikumar, 2010: Variability of Indian summer monsoon in a new upper tropospheric humidity data set. *Geophys. Res. Lett.*, **37**, L05705.
- Xia, X., 2010a: A closer looking at dimming and brightening in China during 1961–2005. *Ann. Geophys.*, **28**, 1121–1132.
- Xia, X. G., 2010b: Spatiotemporal changes in sunshine duration and cloud amount as well as their relationship in China during 1954–2005. *J. Geophys. Res. Atmos.*, **115**, D00K06.
- Xiao, X., et al., 2010: Atmospheric three-dimensional inverse modeling of regional industrial emissions and global oceanic uptake of carbon tetrachloride. *Atmos. Chem. Phys.*, **10**, 10421–10434.
- Xie, B., Q. Zhang, and Y. Wang, 2010: Observed characteristics of hail size in four regions in China during 1980–2005. *J. Clim.*, **23**, 4973–4982.
- Xie, B. G., Q. H. Zhang, and Y. Q. Wang, 2008: Trends in hail in China during 1960–2005. *Geophys. Res. Lett.*, **35**, L13801.
- Xie, S., K. Hu, J. Hafner, H. Tokinaga, Y. Du, G. Huang, and T. Sampe, 2009: Indian Ocean capacitor effect on Indo-Western Pacific climate during the summer following El Niño. *J. Clim.*, **22**, 730–747.
- Xu, C. Y., L. B. Gong, J. Tong, and D. L. Chen, 2006a: Decreasing reference evapotranspiration in a warming climate – A case of Changjiang (Yangtze) River catchment during 1970–2000. *Adv. Atmos. Sci.*, **23**, 513–520.
- Xu, K. H., J. D. Milliman, and H. Xu, 2010: Temporal trend of precipitation and runoff in major Chinese Rivers since 1951. *Global Planet. Change*, **73**, 219–232.
- Xu, M., C. P. Chang, C. B. Fu, Y. Qi, A. Robock, D. Robinson, and H. M. Zhang, 2006b: Steady decline of east Asian monsoon winds, 1969–2000: Evidence from direct ground measurements of wind speed. *J. Geophys. Res. Atmos.*, **111**.
- Yan, Z. W., Z. Li, Q. X. Li, and P. Jones, 2010: Effects of site change and urbanisation in the Beijing temperature series 1977–2006. *Int. J. Climatol.*, **30**, 1226–1234.
- Yang, J., Q. Liu, S.-P. Xie, Z. Liu, and L. Wu, 2007: Impact of the Indian Ocean SST basin mode on the Asian summer monsoon. *Geophys. Res. Lett.*, **34**, L02708.
- Yang, X. C., Y. L. Hou, and B. D. Chen, 2011: Observed surface warming induced by urbanization in east China. *J. Geophys. Res. Atmos.*, **116**, 12.
- Yokouchi, Y., S. Taguchi, T. Saito, Y. Tohjima, H. Tanimoto, and H. Mukai, 2006: High frequency measurements of HFCs at a remote site in east Asia and their implications for Chinese emissions. *Geophys. Res. Lett.*, **33**, L21814.
- Yoon, J., W. von Hoyningen-Huene, A. A. Kokhanovsky, M. Vountas, and J. P. Burrows, 2012: Trend analysis of aerosol optical thickness and Angstrom exponent derived from the global AERONET spectral observations. *Atmos. Meas. Tech.*, **5**, 1271–1299.
- You, Q., et al., 2010: Changes in daily climate extremes in China and their connection to the large scale atmospheric circulation during 1961–2003. *Clim. Dyn.*, **36**, 2399–2417.
- Yttri, K. E., et al., 2011: Transboundary particulate matter in Europe, Status Report 2011. In: *Co-operative Programme for Monitoring and Evaluation of the Long Range Transmission of Air Pollutants (Joint CCC, MSC-W, CEIP and CIAM report 2011)*. NILU - Chemical Coordinating Centre - CCC. http://emep.int/publ/common_publications.html
- Yu, B., and F. W. Zwiers, 2010: Changes in equatorial atmospheric zonal circulations in recent decades. *Geophys. Res. Lett.*, **37**, L05701.
- Yu, L., and R. Weller, 2007: Objectively analyzed air-sea heat fluxes for the global ice-free oceans (1981–2005). *Bull. Am. Meteor. Soc.*, **88**, 527–539.
- Yuan, X., and C. Li, 2008: Climate modes in southern high latitudes and their impacts on Antarctic sea ice. *J. Geophys. Res. Oceans*, **113**, C06S91.
- Yurganov, L., W. McMillan, E. Grechko, and A. Dzhola, 2010: Analysis of global and regional CO burdens measured from space between 2000 and 2009 and validated by ground-based solar tracking spectrometers. *Atmos. Chem. Phys.*, **10**, 3479–3494.
- Zebiak, S. E., 1993: Air-sea interaction in the equatorial Atlantic region. *J. Clim.*, **6**, 1567–1568.
- Zerefos, C. S., et al., 2009: Solar dimming and brightening over Thessaloniki, Greece, and Beijing, China. *Tellus B*, **61**, 657–665.
- Zhang, A. Y., G. Y. Ren, J. X. Zhou, Z. Y. Chu, Y. Y. Ren, and G. L. Tang, 2010: On the urbanization effect on surface air temperature trends over China. *Acta Meteorol. Sin.*, **68**, 957–966.
- Zhang, H., J. Bates, and R. Reynolds, 2006: Assessment of composite global sampling: Sea surface wind speed. *Geophys. Res. Lett.*, **33**, L17714.
- Zhang, J., and J. S. Reid, 2010: A decadal regional and global trend analysis of the aerosol optical depth using a data-assimilation grade over-water MODIS and Level 2 MISR aerosol products. *Atmos. Chem. Phys.*, **10**, 10949–10963.
- Zhang, X., J. He, J. Zhang, I. Polaykov, R. Gerdes, J. Inoue, and P. Wu, 2012a: Enhanced poleward moisture transport and amplified northern high-latitude wetting trend. *Nature Clim. Change*, **3**, 47–51.
- Zhang, X., et al., 2007a: Detection of human influence on twentieth-century precipitation trends. *Nature*, **448**, 461–464.
- Zhang, X., et al., 2011: Indices for monitoring changes in extremes based on daily temperature and precipitation data. *Wiley Interdisc. Rev. Clim. Change*, **2**, 851–870.
- Zhang, X. B., et al., 2005: Trends in Middle East climate extreme indices from 1950 to 2003. *J. Geophys. Res. Atmos.*, **110**, D22104.
- Zhang, X. D., C. H. Lu, and Z. Y. Guan, 2012b: Weakened cyclones, intensified anticyclones and recent extreme cold winter weather events in Eurasia. *Environ. Res. Lett.*, **7**, 044044.
- Zhang, X. D., J. E. Walsh, J. Zhang, U. S. Bhatt, and M. Ikeda, 2004: Climatology and interannual variability of Arctic cyclone activity: 1948–2002. *J. Clim.*, **17**, 2300–2317.
- Zhang, Y., J. M. Wallace, and D. S. Battisti, 1997: ENSO-like interdecadal variability: 1900–93. *J. Clim.*, **10**, 1004–1020.
- Zhang, Y. Q., C. M. Liu, Y. H. Tang, and Y. H. Yang, 2007b: Trends in pan evaporation and reference and actual evapotranspiration across the Tibetan Plateau. *J. Geophys. Res. Atmos.*, **112**, D12110.
- Zhao, X. P. T., A. K. Heidinger, and K. R. Knapp, 2011: Long-term trends of zonally averaged aerosol optical thickness observed from operational satellite AVHRR instrument. *Meteorol. Appl.*, **18**, 440–445.
- Zhen, L., and Y. Zhong-Wei, 2009: Homogenized daily mean/maximum/minimum temperature series for China from 1960–2008. 237–243.
- Zhou, J., and K.-K. Tung, 2012: Deducing multidecadal anthropogenic global warming trends using multiple regression Analysis. *J. Atmos. Sci.*, **70**, 3–8.
- Zhou, T., L. Zhang, and H. Li, 2008: Changes in global land monsoon area and total rainfall accumulation over the last half century. *Geophys. Res. Lett.*, **35**, L16707.
- Zhou, T. J., D. Y. Gong, J. Li, and B. Li, 2009a: Detecting and understanding the multi-decadal variability of the East Asian summer monsoon – Recent progress and state of affairs. *Meteorol. Z.*, **18**, 455–467.
- Zhou, T. J., et al., 2009b: Why the Western Pacific subtropical high has extended westward since the late 1970s. *J. Clim.*, **22**, 2199–2215.
- Zhou, Y. P., K. M. Xu, Y. C. Sud, and A. K. Betts, 2011: Recent trends of the tropical hydrological cycle inferred from Global Precipitation Climatology Project and International Satellite Cloud Climatology Project data. *J. Geophys. Res. Atmos.*, **116**, D09101.
- Zhou, Y. Q., and G. Y. Ren, 2011: Change in extreme temperature event frequency over mainland China, 1961–2008. *Clim. Res.*, **50**, 125–139.
- Ziemke, J. R., S. Chandra, and P. K. Bhartia, 2005: A 25-year data record of atmospheric ozone in the Pacific from Total Ozone Mapping Spectrometer (TOMS) cloud slicing: Implications for ozone trends in the stratosphere and troposphere. *J. Geophys. Res.*, **110**, D15105.
- Ziemke, J. R., S. Chandra, G. J. Labow, P. K. Bhartia, L. Froidevaux, and J. C. Witte, 2011: A global climatology of tropospheric and stratospheric ozone derived from Aura OMI and MLS measurements. *Atmos. Chem. Phys.*, **11**, 9237–9251.

- Zipser, E. J., C. Liu, D. J. Cecil, S. W. Nesbitt, and D. P. Yorty, 2006: Where are the most intense thunderstorms on Earth? *Bull. Am. Meteor. Soc.*, **87**, 1057–1071.
- Zolina, O., C. Simmer, K. Belyaev, A. Kapala, and S. Gulev, 2009: Improving estimates of heavy and extreme precipitation using daily records from European rain gauges. *J. Hydrometeor.*, **10**, 701–716.
- Zorita, E., T. F. Stocker, and H. von Storch, 2008: How unusual is the recent series of warm years? *Geophys. Res. Lett.*, **35**, L24706.
- Zou, C. Z., and W. H. Wang, 2010: Stability of the MSU-derived atmospheric temperature trend. *J. Atmos. Ocean Technol.*, **27**, 1960–1971.
- Zou, C. Z., and W. H. Wang, 2011: Intersatellite calibration of AMSU-A observations for weather and climate applications. *J. Geophys. Res. Atmos.*, **116**, D23113.
- Zou, C. Z., M. D. Goldberg, Z. H. Cheng, N. C. Grody, J. T. Sullivan, C. Y. Cao, and D. Tarpley, 2006a: Recalibration of microwave sounding unit for climate studies using simultaneous nadir overpasses. *J. Geophys. Res. Atmos.*, **111**, L17701.
- Zou, X., L. V. Alexander, D. Parker, and J. Caesar, 2006b: Variations in severe storms over China. *Geophys. Res. Lett.*, **33**.
- Zwiers, F. W., and V. V. Kharin, 1998: Changes in the extremes of the climate simulated by CCC GCM2 under CO₂ doubling. *J. Clim.*, **11**, 2200–2222.